Institut für Phytopathologie

der Justus-Liebig-Universität Gießen

Investigation of small RNA communication in the mutualistic interaction of *Serendipita indica* and *Arabidopsis thaliana*

INAUGURAL-DISSERTATION

zur Erlangung des Doktorgrades (Dr. rer. nat.)

im Fachbereich Agrarwissenschaften, Ökotrophologie und Umweltmanagement der Justus-Liebig-Universität Gießen

vorgelegt von

Sabrine Nasfi-Moses

aus Tunesien

Gießen, 2026

Mit Genehmigung des Fachbereichs Agrarwissenschaften,

Ökotrophologie und Umweltmanagement der

Justus-Liebig-Universität Gießen

Prüfungskommission:

1. Gutachter(in):	Prof. Dr. Karl-Heinz Kogel
2. Gutachter(in):	Prof. Dr. Patrick Schäfer
3. Gutachter(in):	Prof. Dr. Volker Wissemann
Prüfer(in):	PD Dr. habil. Oliver Roßbach
Prüfer(in):	Prof. Dr. Bork Berghoff
Vorsitzende(r):	Prof. Dr. Jan Siemens

Tag der Disputation: 29.05.2026

Table of Contents

Authors´ Declaration

Gemäß der Promotionsordnung des Fachbereichs 09, Agrarwissenschaften, Ökotrophologie und Umweltmanagement der Justus-Liebig-Universität Gießen (Ausgabe vom 29.05.2019) § 17 (2):

„Ich erkläre: Ich habe die vorgelegte Dissertation selbständig und ohne unerlaubte fremde Hilfe und nur mit den Hilfen angefertigt, die ich in der Dissertation angegeben habe.

Alle Textstellen, die wörtlich oder sinngemäß aus veröffentlichten Schriften entnommen sind, und alle Angaben, die auf mündlichen Auskünften beruhen, sind als solche kenntlich gemacht.

Bei den von mir durchgeführten und in der Dissertation erwähnten Untersuchungen habe ich die Grundsätze guter wissenschaftlicher Praxis, wie sie in der „Satzung der Justus-Liebig-Universität Gießen zur Sicherung guter wissenschaftlicher Praxis "niedergelegt sind, eingehalten."

_____

Sabrine Nasfi-Moses

Parts of this work have already been published or under consideration

1. Šečić, E., Zanini, S., Wibberg, D., Jelonek, L., Busche, T., Kalinowski, J., Nasfi, S., Thielmann, J., Imani, J., Steinbrenner, J., & Kogel, K.-H. (2021). A novel plant-fungal association reveals fundamental sRNA and gene expression reprogramming at the onset of symbiosis. *BMC Biology*, 19, 171. https://doi.org/10.1186/s12915-021-01104-2

2. Nasfi, S., Shahbazi, S., Bitterlich, K., Šečić, E., Kogel, K.-H., & Steinbrenner, J. (2024). A pipeline for validation of *Serendipita indica* effector-like sRNA suggests cross-kingdom communication in the symbiosis with *Arabidopsis*. *Journal of Experimental Botany*, erae515. https://doi.org/10.1093/jxb/erae515

3. Ruf, A., Thieron, H., Nasfi, S., Lederer, B., Fricke, S., Adeshara, T., Postma, J., Blumenkamp, P., Kwon, S., Brinkrolf, K., Feldbrügge, M., Goesmann, A., Kehr, J., Steinbrenner, J., Šečić, E., Göhre, V., Weiberg, A., Kogel, K.-H., Panstruga, R., Robatzek, S., & on behalf of the exRNA consortium. (2024). Broad-scale phenotyping in *Arabidopsis* reveals varied involvement of RNA interference across diverse plant-microbe interactions. *Plant Direct*, 8(11), e70017. https://doi.org/10.1002/pld3.70017

4. Werner, B. T., Nasfi, S., Schmitz, M. L., Makhoul, M., Steinbrenner, J., & Schäfer, P. (2025). High precision quantification of small RNA slicing activity—Native index ligation-based targeted degradome sequencing (NIL-TDS). *bioRxiv*, 2025.09.30.679503. https://doi.org/10.1101/2025.09.30.679503

5. Nasfi, S., & Kogel, K.-H. (2022). Packaged or unpackaged: Appearance and transport of extracellular noncoding RNAs in the plant apoplast. *ExRNA*, 4. https://exrna.amegroups.com/article/view/64855

6. Thieron, H., Krassini, L., Kwon, S., Fricke, S., Nasfi, S., Oberkofler, L., Ruf, A., Kehr, J., Kogel, K.-H., Weiberg, A., Feldbrügge, M., Robatzek, S., & Panstruga, R. (2024). Practical advice for extracellular vesicle isolation in plant–microbe interactions: Concerns, considerations, and conclusions. *Journal of Extracellular Vesicles*, 13, e70022. https://doi.org/10.1002/jev2.70022

7. Hossain, M., Pfafenrot, C., Nasfi, S., Sede, A., Imani, J., Šečić, E., Galli, M., Schäfer, P., Bindereif, A., Heinlein, M., Ladera-Carmona, M., & Kogel, K.-H. (2025). Designer circRNAGFP reduces GFP abundance in Arabidopsis protoplasts in a sequence-specific manner, independent of RNAi pathways. *Plant Cell Reports, 44*(6), 128. https://doi.org/10.1007/s00299-025-03512-y

8. Werner, B. T., Nasfi, S., Procida-Kowalski, T., Schmidt, R., Wilhelm, J., & Schäfer, P. (2025). Cross-kingdom degradomics identifies natural plant small RNAs with disease-protecting activity. *bioRxiv*. https://doi.org/10.1101/2025.10.06.680647

List of Figures

CHAPTER 1

CHAPTER 2

The online version of this chapter contains supplementary figures available at https://doi.org/10.1186/s12915-021-01104-2.

CHAPTER 3

The online version of this chapter contains supplementary figures available at https://onlinelibrary.wiley.com/doi/10.1002/pld3.70017

CHAPTER 5

CHAPTER 10

List of Tables

Abbreviations

A	-	Adenine
AGO	-	Argonaute
AMF	-	Arbuscular mycorrhizal fungi
amiRNA	-	Artificial microRNA
At	-	*Arabidopsis thaliana*
***At*sRNA**	-	*Arabidopsis thaliana* small RNA
AWF	-	Apoplastic washing fluid
Bd	-	*Brachypodium distachyon*
***Bd*sRNA**	-	*Brachypodium distachyon*-derived sRNA
C	-	Cytosine
circRNA	-	Circular RNA
ck	-	Cross-kingdom
ck-sRNA	-	Cross-kingdom sRNA
CM	-	Complete Media
DAMP	-	Danger-associated molecular pattern
DCL	-	Dicer-like
DEG	-	Differentially expressed gene
dpi	-	days post-infection/inoculation
dsRNA	-	Double-stranded RNA
ETI	-	Effector-triggered immunity
EVs	-	Extracellular vesicles
G	-	Guanosine
GFP	-	Green fluorescent protein
HIGS	-	Host Induced Gene Silencing
HEN1	-	Hua Enhancer 1
Hptr	-	hours post transformation
HYL-1	-	Hyponastic Leaves 1
IP	-	Immunoprecipitation

MAMP	-	Microbe-associated molecular pattern
ncRNA	-	non-coding RNA
miRNA	-	MicroRNA
mRNA	-	Messenger RNA
NIL-TDS	-	Native Index Ligation-based Target Degradome Sequencing
NGS	-	Next Generation Sequencing
NLR	-	Nucleotide-binding Leucine-rich Repeat Protein
nt	-	Nucleotide
NTA	-	Nanoparticle tracking analysis
PARE	-	Parallel Analysis of RNA Ends
PAMP	-	Pathogen Associated Molecular Pattern
PAZ	-	Piwi-Argonaute-Zwille domain
PIWI	-	P-element-induced wimpy testis domain
PRR	-	Pattern recognition receptor
PTGS	-	Post-transcriptional gene silencing
PTI	-	Pattern-triggered immunity
RBPs	-	RNA binding proteins
RFP	-	Red fluorescent protein
RISC	-	RNA-induced silencing complex
RLM-RACE	-	RNA ligase mediated rapid amplification of cDNA ends
RNAi	-	RNA interference
ROS	-	Reactive Oxygen Species
RT	-	Reverse transcription
SE	-	Serrate
Si	-	*Serendipita indica*
***Si*sRNA**	-	*Serendipita indica* small RNA
siRNA	-	small interfering RNA
SIGS	-	Spray Induced Gene Silencing
SL	-	Stem loop

sRNA	-	small RNA
TEM	-	Transmission Electron Microscopy
TGS	-	Transcriptional gene silencing
U	-	Uracil
UBQ	-	Ubiquitin

Summary

Interactions between plants and their symbiotic partners are characterised by complex molecular mechanisms that promote symbiont and plant growth, nutrient uptake, and stress tolerance. Despite the established role of small RNAs (sRNAs) in regulating gene expression in eukaryotes, further investigation is required to understand their contribution to this beneficial exchange. In this work, we investigated whether the beneficial endophyte *Serendipita indica* (*Si*), with its large host range, uses sRNA-mediated cross-kingdom (ck) communication with plant hosts.

Sequencing of sRNA from *S.indica* cultivated in axenic culture and during its interaction with *Brachypodium distachyon* provided first evidence of ckRNA communication between plants and their mutualistic fungi and identified putative *S.indica* sRNAs (*Si*sRNA).

To explore the molecular basis of ck-RNA interference (RNAi) in mutualism, we developed a pipeline to investigate the role of *Si*sRNAs during *S. indica* colonisation of *Arabidopsis thaliana (At)*. The expression of *Si*sRNAs was validated in *Si*-colonised *At* roots. *Si*sRNAs were overexpressed in a protoplast transient system, and their accumulation was confirmed. The potential of *Si*sRNAs to induce post-transcriptional gene silencing (PTGS) of predicted *At* target genes was investigated, and downregulation of genes involved in cell wall organisation, hormone signalling, and immunity was observed.

Immunoprecipitation (IP) of Argonaute 1 (AGO1) from *Si*-colonised *At* roots, followed by western-blot analysis and stem-loop PCR, confirmed the translocation of *Si*sRNAs into *At* roots and their loading into the plant RNAi machinery. Additionally, sRNA sequencing of AGO1- and AGO2-bound sRNA recovered after IP identified 18 to 26 nt *Si*sRNAs being loaded into AGO1 and AGO2 in *Si*-colonised *At* roots with diverse 5´-ends.

The role of Arabidopsis RNAi machinery in regulating symbiosis and colonisation was examined by analysing *S. indica* growth on Arabidopsis DICER-LIKE (DCL) and AGO mutants, as well as AGO expression profiling of *At* Col-0 *S. indica* colonised roots. The results demonstrated that AGO2 and AGO10, but not AGO1, function as positive regulators, suggesting specialised and potentially redundant functions of AGO proteins in mutualistic interactions.

S.indica extracellular vesicles (EV)-like particles were isolated from *S.indica* liquid cultures. EV-like structures with cup-shaped morphology were observed, and *Si*sRNAs previously associated with the *Si-At* interaction were detected in the vesicle fraction, suggesting a possible role for *S.indica* EVs in RNA transport, but further investigations are needed.

Taken together, this work reveals that mutualistic fungi can use sRNAs to regulate host gene expression by exploiting plant RNAi machinery and provides genomic and molecular hints for ck-RNA communication in mutualistic symbioses.

Zusammenfassung

Interaktionen zwischen Pflanzen und ihren symbiotischen Partnern sind durch komplexe molekulare Mechanismen gekennzeichnet, die das Wachstum von Symbionten und Pflanzen, die Nährstoffaufnahme sowie die Stresstoleranz fördern. Trotz der etablierten Rolle kleiner RNAs (small RNAs, sRNAs) bei der Regulierung der Genexpression in Eukaryoten sind weitere Untersuchungen erforderlich, um ihren Beitrag zu diesem vorteilhaften Austausch zu verstehen. In dieser Arbeit untersuchten wir, ob der nützliche Endophyt *Serendipita indica* (*Si*) mit seinem großen Wirtsspektrum eine sRNA-vermittelte cross-kingdom (ck) Kommunikation mit Pflanzenwirten nutzt.

Die Sequenzierung von sRNA aus *S. indica*, die in axenischer Kultur als auch während ihrer Interaktion mit *Brachypodium distachyon* kultiviert wurden, lieferte erste Hinweise auf eine ckRNA-Kommunikation zwischen Pflanzen und ihren mutualistischen Pilzen und identifizierte putative *S. indica* sRNAs (*Si*sRNA).

Zur Untersuchung der molekularen Grundlagen der ck-RNA-Interferenz (RNAi) im Mutualismus entwickelten wir eine Pipeline zur Analyse der Rolle von *Si*sRNAs während der Kolonisation von *Arabidopsis thaliana* (*At*) durch *S. indica*. Die Expression der *Si*sRNAs wurde in *Si*-kolonisierten *At*-Wurzeln validiert. *Si*sRNAs wurden in einem transienten Protoplastensystem überexprimiert, und ihre Akkumulation wurde bestätigt. Das Potenzial von *Si*sRNAs zur induction einer posttranskriptionelle Gen-Silencing (Post transcriptional gene silencing, PTGS) vorhergesagter *At*-Zielgenen wurde untersucht, wobei eine Herunterregulation von Genen beobachtet wurde, die an der Zellwandorganisation, der Hormonsignalisierung und der Immunität beteiligt sind.

Die Immunpräzipitation (Immunoprecipitation, IP) von Argonaute 1 (AGO1) aus *Si*-kolonisierten *At*-Wurzeln, gefolgt von Western-Blot-Analysen und Stem-Loop-PCR, bestätigte die Translokation von *Si*sRNAs in *At*-Wurzeln sowie deren Beladung in die pflanzliche RNAi-Maschinerie. Zusätzlich identifizierte die sRNA-Sequenzierung von AGO1- und AGO2-gebundener sRNA, die nach IP gewonnen wurde, 18 bis 26 nt *Si*sRNAs, die in *Si*-kolonisierten *At*-Wurzeln mit unterschiedlichen 5'-Enden in AGO1 und AGO2 geladen wurden.

Die Rolle des Arabidopsis-RNAi-Maschinerie bei der Regulation von Symbiose und Kolonisation wurde durch die Analyse des Wachstums von *S. indica* auf Arabidopsis-DICER-LIKE (DCL)- und AGO-Mutanten sowie durch die Expressionsanalysen von AGOs in *Si*-kolonisierten *At* Col-0 Wurzeln untersucht. Die Ergebnisse zeigten, dass AGO2 und AGO10, jedoch nicht AGO1, als positive Regulatoren fungieren, was auf spezialisierte und potenziell redundante Funktionen von AGO-Proteinen in mutualistischen Interaktionen hindeutet.

Extrazelluläre Vesikel (EV)-like Partikel von *S.indica* wurden aus flüssigen *S.indica*-Kulturen isoliert. EV-like Strukturen mit becherförmiger Morphologie wurden beobachtet, und *Si*RNAs, die zuvor mit der *Si–At*-Interaktion in Verbindung gebracht wurden, konnten in der Vesikelfraktion nachgewiesen werden, was auf eine mögliche Rolle von *S.indica*-EVs beim RNA-Transport hindeutet, weitere Untersuchungen sind jedoch erforderlich.

Zusammenfassend zeigt diese Arbeit, dass mutualistische Pilze sRNAs nutzen können, um die Genexpression des Wirts durch Ausnutzung der pflanzlichen RNAi-Maschinerie zu regulieren, und liefert genomische und molekulare Hinweise für eine ck-RNA-Kommunikation in mutualistischen Symbiosen.

“Die Wissenschaft fängt eigentlich da an, interessant zu werden, wo sie aufhört”

Justus von Liebig (1803 – 1873)

CHAPTER 1 - Introduction

1.1 Feeding a growing population in a resource-limited world

To feed a growing population projected to reach 10.3 billion people by 2080 (*World Population Prospects*, 2024.), sustainable agriculture is essential.

Approaches such as integrated pest management (Oerke, 2006), genetic engineering (e.g., CRISPR technology (Gong et al., 2025)) and biologicals (e.g., RNA-based products (Bramlett et al., 2020)), can contribute to higher crop yields and resilience while reducing environmental impact. When used with precision agriculture techniques, these approaches help farmers to maximise productivity without over-exploiting limited resources, ensuring food security for future generations.

1.2 RNAi approach: a pathway to sustainable agriculture

RNA interference (RNAi) was first discovered in the late 1990s in the nematode *Caenorhabditis elegans* (Fire et al., 1998) and later proved to be a widespread mechanism in plants (Napoli et al., 1990), insects (Bucher et al., 2002), and fungi (Romano & Macino, 1992). It is a conserved natural process where RNA molecules known as non-coding regulatory RNAs (ncRNAs) silence genes by degrading or inhibiting messenger RNA (mRNA).

Recently, RNAi has shown great promise in agriculture. For example, double-stranded RNA (dsRNA) has been used to control the Colorado potato beetle (CPB) as an effective pest management method (Palli, 2014). Another application of dsRNA targeting the *Magnaporthe oryzae* MoPMK1 gene reduced the leaf blast disease progression in the leaves of the grass model *Brachypodium distachyon* (Zheng et al., 2025).

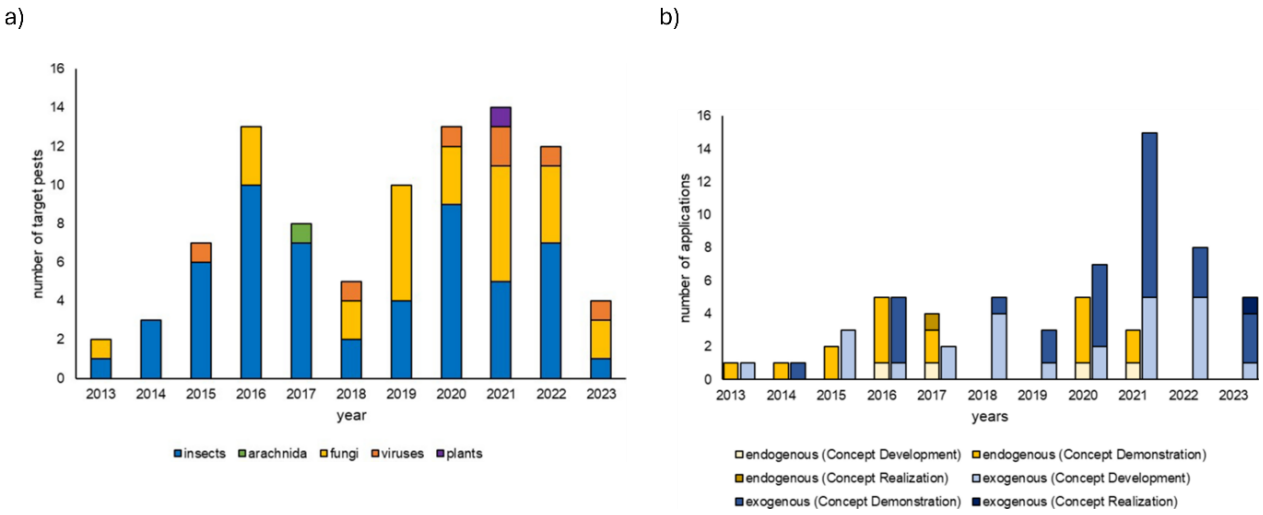

Figure 1. Trends in RNAi-based plant protection applications from 2013 to 2023. **(a)** Annual distribution of RNAi targets among microorganisms shows an increase in diversity over time. **(b)** Annual distribution of endogenous (transgenic plants) and exogenous (e.g., Spray-induced gene silencing, SIGS) RNAi applications show a growing focus on exogenous approaches. Figure taken from Germing et al., 2025.

Nevertheless, effective RNAi strategies are dependent on a fundamental understanding of the interaction between plants and microbes and the central role of small RNAs (sRNAs) as key regulatory elements.

1.3 Plant-microbe interaction: core concepts

Plants interact with a wide range of microorganisms, each capable of triggering immune responses or establishing beneficial symbiosis, ranging from defence to mutualistic cooperation with their hosts (Jones & Dangl, 2006). During pathogenic interactions, plants have evolved sophisticated defensive strategies to counteract microbial invasion (Dodds & Rathjen, 2010). In contrast, in mutualistic symbiosis, plants have evolved a win-win strategy with microorganisms, trading nutrients to support mutual growth and development (Pieterse et al., 2014; Zamioudis & Pieterse, 2012). This molecular dialogue, known as bidirectional cross-kingdom (ck) communication, involves the transfer of sRNAs and proteins, potentially through extracellular vesicles (EVs), between plants and

their interacting microbes (Rutter & Innes, 2018; Wang et al., 2016; Weiberg et al., 2013; Zeng et al., 2019).

1.3.1 Overview of plant immunity

To successfully invade their hosts, microorganisms suppress or evade the plant´s immune system using unique molecules known as Pathogen- or Microbe-Associated Molecular Patterns (PAMPs/MAMPs) or Danger-Associated Molecular Patterns (DAMPs), such as flagellin (flg22), chitin, plant elicitor peptides (PEPs), and B-glucans (Wu et al., 2014).

At this initial stage of interaction, plants rely solely on their innate immune system to recognise non-self through Pattern Recognition Receptors (PRRs), such as Receptor-like kinase (RLKs) and Receptor-like proteins (RLPs). This recognition triggers Pattern-Triggered Immunity (PTI), which involves reprogramming of defence-related genes (PRs), calcium influx, activation of Mitogen-activated protein kinases (MAPKs), production of Reactive Oxygen Species (ROS), callose deposition, and sugar efflux (Dodds & Rathjen, 2010; Jones & Dangl, 2006; Zipfel, 2009).

To counteract PTI, microorganisms release effector molecules recognised by the plant intracellular receptors, known as nucleotide-binding Leucine-rich Repeat (NLR) proteins encoded by resistance (R) genes (Win et al., 2012). NLRs are divided into “sensor NLRs”, which recognise effectors, and “helper NLRs”, which trigger immune signals. NLRs activation initiates Effector-Triggered Immunity (ETI), leading to a stronger immune response and often localised cell death to limit pathogens (Dalio et al., 2021; Nguyen et al., 2021). Together with PTI and ETI, plants use a network of hormones involving salicylic acid (SA), jasmonic acid (JA), and ethylene (ET) to coordinate their defence (Pieterse et al., 2012).

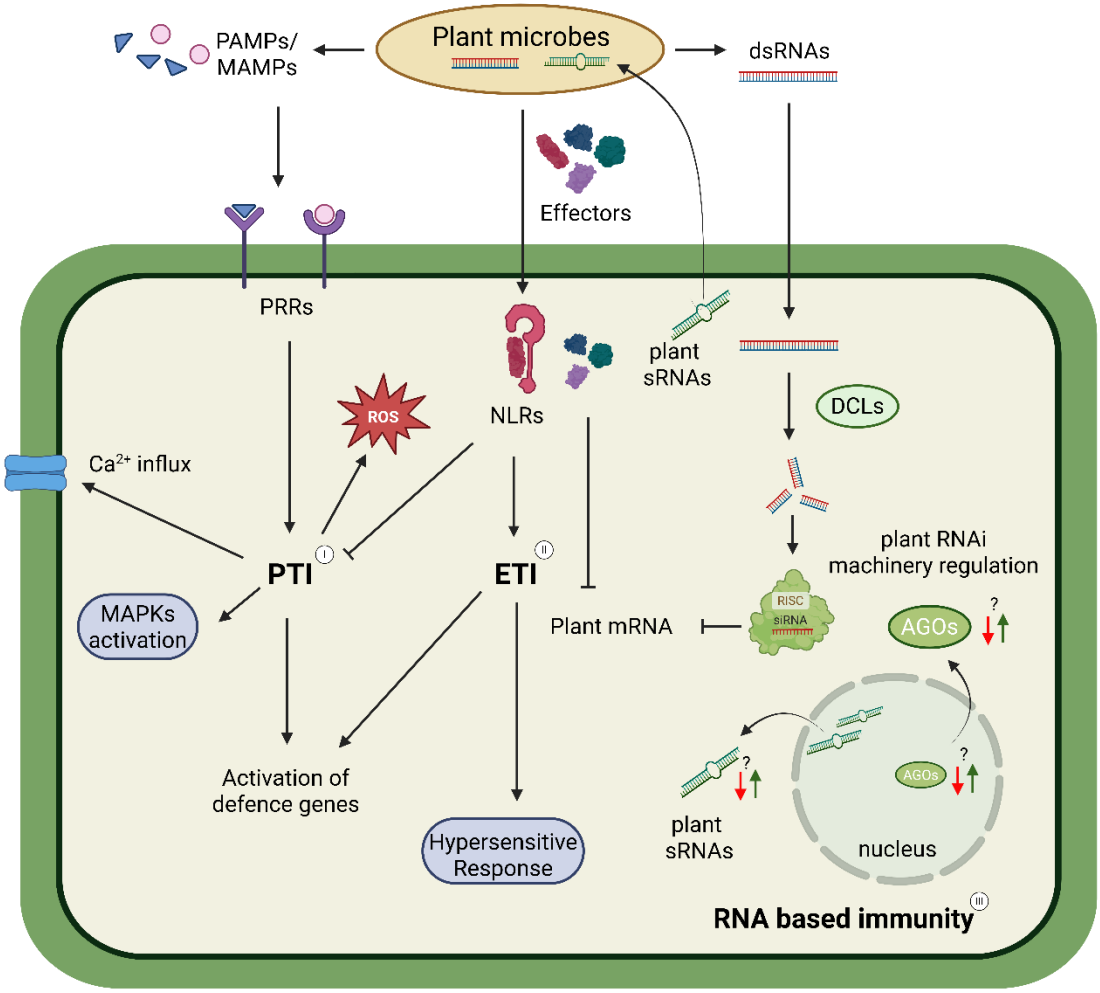

Figure 2. Overview of plant immunity in plants. (I) PRRs recognise PAMPs/MAMPs triggering PTI, leading to Ca^{2+} influx, MAPK activation, ROS production, and the activation of defence genes. (II) NLRs recognise microbial effectors, triggering ETI, which also activates defence genes and causes hypersensitive responses. (III) Microbial dsRNAs are processed by plant DCLs into sRNAs that can hijack the plant RISC, guided by AGO proteins to target the plant mRNAs. In parallel, plants regulate the expression of their own endogenous sRNAs and RNAi components contributing to RNAi-mediated defence. Together, these interconnected layers establish plant immunity as a key component of plant defence signalling. Figure created with biorender.

While the discovery of PTI, ETI, and hormonal signalling as major plant defence strategies began in the early 2000s, the role of regulatory non-coding RNAs in modulating gene expression during plant immune responses was uncovered much later.

1.3.2 Non-coding RNAs: big players in plant immunity

Non-coding RNAs (ncRNAs) are functional RNA molecules transcribed from the genome, do not code for proteins, but play a regulatory role in plant biology, immunity, and gene expression under both biotic and abiotic stresses. In plants, ncRNAs are divided into long ncRNAs (> 200 nucleotides (nt)), circular ncRNAs and small ncRNAs (sRNAs, < 200nt), which include microRNAs (miRNAs), usually 21-22 nt in length and small interfering RNAs (siRNAs), usually 21 to 24 nt in length (Bartel, 2009; Chen, 2009; Jones-Rhoades et al., 2006; Vazquez et al., 2004). miRNAs are transcribed from *MIR* genes, as primary miRNAs (pri-miRNAs) that fold into a stem-loop structure, then are cleaved into precursor miRNAs (pre-miRNAs) by Dicer-like proteins (DCLs) (Kurihara & Watanabe, 2004). In contrast, siRNAs are produced from long dsRNA molecules and can originate from endogenous or exogenous RNA sequences (viral and transgene transcripts) (Carthew & Sontheimer, 2009; Vazquez et al., 2004). Both dsRNAs and pre-miRNAs are subsequently processed in the nucleus into sRNA duplexes, comprising a guide strand and a passenger strand. In the cytoplasm, the guide strand of sRNA and miRNA duplexes binds to Argonaute (AGO) proteins, thus forming and activating the RNA-Induced Silencing Complex (RISC). Guided by sequence complementarity, sRNAs can mediate Post-Transcriptional Gene Silencing (PTGS, mainly mediated by 21-22 nt sRNAs) or Transcriptional Gene Silencing (TGS, mediated by 24 nt sRNAs) via RNA-directed DNA Methylation (RdDM) (Baulcombe, 2004; Carthew & Sontheimer, 2009).

1.3.3 Cross-kingdom RNAi and sRNA-mediated gene silencing

Only a decade ago, it was discovered that sRNAs can move between plants and their interacting microorganisms, a phenomenon known as bidirectional cross-kingdom (ck) RNAi (Wang et al., 2016; Weiberg et al., 2013). In this exchange, microorganisms use sRNAs to suppress plant immunity by hijacking the plant´s RNAi machinery. In return, plants send sRNAs to reduce pathogen virulence and/or fine-tune the expression of target genes. CkRNAi was first demonstrated in the interaction between the necrotrophic

fungus *Botrytis cinerea* (*Bc*) and the two host plants *Solanum lycopersicum* and *Arabidopsis thaliana* (*At*). It was shown that the expression of *Bc* sRNAs, *Bc*-DCL1 and *Bc*-DCL2, in Arabidopsis and tomato targeting *Bc-DCL* genes, attenuated fungal pathogenicity and growth (Weiberg et al., 2013). Later, it was shown that cotton plants produced an increasing level of miRNAs in response to infection with the fungal pathogen *Verticillium dahliae*, introducing bidirectional ck-RNAi (Zhang et al., 2016).

Table 1. Examples of cross-kingdom RNA communication studies between plants and interacting microbes between 2013 and 2025.

Plant host(s)	Microbe	Direction of RNA transfer	Key finding	Citation
Arabidopsis, tomato	*Botrytis cinerea* (pathogen)	Fungus → plant	Fungal sRNAs translocate into plant cells, are loaded into AGO1, causing silencing of immunity genes (first ckRNAi example).	(Weiberg et al., 2013)
Cotton	*Verticillium dahliae* (pathogen)	Plant → fungus	Cotton miR159 and miR166 move into Verticillium and silence fungal virulence genes.	(Zhang et al., 2016)
Arabidopsis	*Botrytis cinerea* (pathogen)	Fungus → plant	Fungal sRNA effector *Bc*-siR37 targets several plant defence genes via ckRNAi.	(Wang et al., 2017)
Arabidopsis	*Botrytis cinerea* (pathogen)	Plant → fungus (mediated by extracellular vesicles, EVs)	Arabidopsis secretes tetraspanin-EVs that deliver sRNAs into the fungus to silence virulence genes.	(Cai et al., 2018)
Barley, wheat and other cereals	*Blumeria spp*. (pathogen, Powdery mildew fungi)	Fungus → plant (predicted)	sRNA catalogue shows that many fungal sRNAs are predicted to target plant targets in cereal and powdery mildew interactions.	(Kusch et al., 2018)
Soybean	*Bradyrhizobium japonicum* (rhizobium, symbiont)	Bacterium → plant	Rhizobial tRNA fragments are loaded into the host´s AGO1 and regulate genes that control nodule initiation.	(Ren et al., 2019)
Medicago truncatula	*Rhizophagus irregularis* (Arbuscular Mycorrhiza fungus, AMF, symbiont)	Fungus → plant (predicted)	AMF sRNAs are profiled and predicted to target multiple plant transcripts, suggesting ckRNAi in symbiosis.	(Silvestri et al., 2019)
Arabidopsis and downy mildew hosts	*Hyaloperonospora spp*. (Downy mildew oomycete, pathogen)	Oomycete → plant	Oomycete sRNAs associate with plant AGO1 and act as virulence factors.	(Dunker et al., 2020)

Wheat	*Fusarium graminearum* (*Fg*, fungus, pathogen)	Plant → fungus	Spraying dsRNA targeting *Fg* AGOs and DCLs confers protection to barley leaves from *Fg* infection.	(Werner et al., 2021)
Nicotiana benthamiana (sensor line)	*Fusarium solani* strain K (FsK, beneficial fungal, endophyte)	Fungus → plant	*Fsk* triggers systemic ckRNAi and DNA methylation of the host reporter gene, indicating long-distance RdDM.	(Dalakouras et al., 2023)
Arabidopsis	*Serendipita indica* (root endophyte)	Fungus → plant	AGO1-IP and protoplast functional assays confirmed that *S. indica* sRNAs are translocated into Arabidopsis roots and can silence host genes during symbiosis.	(Nasfi et al., 2024)
Nicotiana benthamiana	*Fusarium solani* strain K (FsK, beneficial fungal, endophyte)	Fungus → plant	Endophyte-induced ckRNAi in the host requires RDR6-mediated amplification of silencing signals.	(Kellari et al., 2025)
Medicago truncatula (*Mt*)	*Rhizophagus irregularis* (AMF)	Fungus → plant	Fungal sRNA *Rir*2216 loads into plant AGO1 and cleaves *Mt*WRKY69, promoting mycorrhization.	(Silvestri et al., 2025)

1.3.4 RNA interference machinery in *Arabidopsis thaliana*

Arabidopsis thaliana (*At*), a dicotyledonous model plant, has a well-characterised RNAi machinery, making it particularly suitable for studying plant-microbe interactions. DCLs and AGOs, along with their interacting endogenous or exogenous sRNAs, are central to *At* RNAi pathway, and play a crucial role in gene regulation and the modulation of the plant immune system (Baulcombe, 2004; Bologna & Voinnet, 2014). DCLs are complex, multi-domain proteins. The DExD-box helicase-C domain helps separate dsRNA strands and facilitates their cleavage into smaller fragments. The PAZ (Piwi-Argonaute-Zwille) domain binds the dsRNA, making it ready for cleavage. Two RNase III domains responsible for cleavage of dsRNA into small RNA fragments (Margis et al., 2006).

Arabidopsis encodes four DCL proteins; each is responsible for producing sRNAs of specific sizes. DCL1 (AT1G01040) mainly generates 21-22 nt miRNAs and is involved in PTGS (Baulcombe, 2004; Henderson et al., 2006). Complete loss of DCL1 function is embryo-lethal, while partial loss causes developmental abnormalities in *At* (Schauer et al., 2002).

DCL2 (AT3G03300), DCL3 (AT3G43920) and DCL4 (AT5G20320) generate 22 nt, 24 nt and 21 nt siRNAs, respectively (Henderson et al., 2006). DCL2 processes siRNA from natural antisense transcripts and plays a role in antiviral defence (Deleris et al., 2006; Taochy et al., 2017). DCL3 is important for RdDM, producing siRNAs from dsRNAs generated by RNA-Dependent RNA (RDR) 2 (Xie et al., 2004). DCL4 is needed for the generation of trans-acting siRNAs (ta-siRNAs) (Gasciolli et al., 2005), and also plays a role in antiviral defence (Deleris et al., 2006). During the interaction of Arabidopsis and *Trichoderma atroviride*, DCL genes were differentially expressed both locally and systemically and were confirmed to function in coordination with defence hormone pathways, suggesting that they are part of the small RNA mechanism required for beneficial colonization (Rebolledo-Prudencio et al., 2022). Nevertheless, current knowledge of the role of Arabidopsis DCLs in beneficial plant–microbe interactions remains limited.

After DCLs trigger RNAi silencing, only one strand of the sRNA duplex, the guide strand, is loaded into the RISC complex by an AGO protein.

At encodes 10 AGO genes, each encoding proteins with four domains: PAZ, MID, PIWI, and an N-terminal domain, connected by two linker regions, L1 and L2. The PAZ and the MID domains bind the 3' and the 5' ends of the guide sRNA strand, respectively, while the N-domain helps interactions with other proteins and complexes of the RNAi machinery, and the PIWI (P-element induced wimpy) domain exhibits the RNase catalytic site, enabling the RNA cleavage (Fang & Qi, 2016; Vaucheret, 2008; Zhang et al., 2015).

AGOs play a major role in PTGS and are also being explored for their involvement in plant immunity, leading to different regulatory outcomes. Arabidopsis AGOs are grouped into three clades: clade I (AGO1/5/10), clade II (AGO2/3/7), and clade III (AGO4/6/8/9) (Mallory & Vaucheret, 2010; Rodríguez-Leal et al., 2016; Vaucheret, 2008). In clade I, AGO1 (AT1G48410) is broadly expressed across tissues and is one of the most studied AGOs, which binds mainly 21/22-nt sRNAs with 5'-uracil (U) (Mi et al., 2008), mediating mRNA cleavage, translational inhibition, or both (Vaucheret et al., 2004). Beyond RNAi, AGO1 is involved in plant development (Kidner & Martienssen, 2005), hormonal responses and stress regulation (Liu et al., 2018; Loreti et al., 2020), and antiviral defence and immunity (Carbonell & Carrington, 2015; Zhao et al., 2023). AGO10 (AT5G43810), a paralog of AGO1, displays a more restricted expression pattern, with weak expression in roots (Rich-Griffin et al., 2020). AGO10 binds 21 nt sRNA with a 5'-U and functions as a miRNA sequester (Mi et al., 2008). It is essential during shoot apical meristem development, as it modulates miR165/miR166 and miR172 activity (Ji et al., 2011; Zhu et al., 2011). While AGO1 is mainly involved in PTGS, AGO10 modulates gene expression by translational repression and acts as a negative regulator of AGO1 expression by binding miR168 (Brodersen et al., 2008; Mallory et al., 2009). Although several studies suggested a redundancy between AGO1 and AGO10 (Ji et al., 2011; Mallory et al., 2009), AGO10 has no confirmed role in plant defence.

Of the same clade, AGO5 (AT2G27880) primarily binds 21 nt sRNAs with 5'-cytosine (C) (Mi et al., 2008), and is predominantly expressed in reproductive tissues, suggesting its role in gametophyte development and flowering time regulation (Roussin-Léveillée et al.,

2020; Tucker et al., 2012). AGO5 also contributes to antiviral defence (Brosseau & Moffett, 2015).

AGO2 (AT1G31280), which belongs to clade II, plays a significant role in gene silencing pathways and contributes to both antibacterial and antiviral defence mechanisms (Fang & Qi, 2016; Mallory & Vaucheret, 2010; Vaucheret, 2008). Moreover, recent research suggested that AGO2 is implicated in DNA damage response and repair (Kim et al., 2025). Unlike AGO2, AGO3 binds 24 nt but similarly, with a 5'-adenosine (A), while AGO7 selectively binds miR390, forming a complex that anchors to the non-cleavable site on TAS3 transcripts, initiating the production of phased ta-siRNAs that regulate AUXIN RESPONSE FACTOR genes (Montgomery et al., 2008).

The third clade of Arabidopsis argonautes is central to maintaining genome stability. AGO4 primarily binds 24 nt sRNAs and has a major role in the RdDM pathway and TGS (Carbonell, 2017, p. 4; Gao et al., 2010). AGO4 also contributes to plant immunity and to antiviral defence (Brosseau et al., 2016).

AGO6, from the same clade as AGO4, acts redundantly in RdDM and TGS by also binding 24 nt siRNAs to guide DNA methylation (Duan et al., 2015).

1.3.5 Regulatory role of miRNAs in plant-microbe interaction

As of this writing, 430 mature miRNAs have been identified and annotated in Arabidopsis (miRBase database (v22)). These miRNAs are multifunctional, regulating gene expression and playing crucial roles in development and responses to biotic and abiotic stress. For instance, miR156, the first identified Arabidopsis microRNA, targets the SQUAMOSA promoter-binding protein-like (SPL) family, crucial for developmental timing (Reinhart et al., 2002). Shortly after, miR172 was identified, controlling flower development and timing (Aukerman & Sakai, 2003). Since then, research has increasingly focused on miRNAs in plant-microbe interactions. A key example in Arabidopsis is miR393, which accumulates after *Pseudomonas syringae* DC3000 infection and triggers PTI by suppressing auxin receptors. Its complementary strand miR393b*, loaded into AGO2, targets the Golgi SNARE MEMB12; both miR393b* overexpression and MEMB12 disruption enhance PR1 secretion and antibacterial immunity. Thus, the miR393 duplex acts via distinct AGOs: miR393 with AGO1, and miR393b* with AGO2 (Zhang et al., 2011).

The role of miRNAs in regulating plant development and immune response has also been investigated in the context of symbiotic interactions. For example, miR169 regulates *Mt*HAP2-1, an essential gene for nodule development in *Medicago truncatula* during symbiosis with nitrogen-fixing bacteria (Combier et al., 2006). Similarly, miR166 regulates *HB7*, a gene involved in root and nodule development in *Medicago truncatula* (Boualem et al., 2008). In soybean, miR1511 and miR169 regulate genes such as GmNAC1 and GmSCL6, which are critical for root development during nodulation (Subramanian et al., 2008). miR399 has been shown to regulate *PHO2*, a gene controlling phosphate uptake during arbuscular mycorrhizal symbiosis (Branscheid et al., 2010), while in tomato, miR160 regulates *ARF10* and *ARF16* genes involved in auxin signalling during mycorrhizal interactions (Wu et al., 2016). In *Oncidium* orchids, miR156, miR160, and miR166 regulate genes related to root development and growth promotion during interaction with the endophytic fungus *Serendipita indica* (Ye et al., 2014).

1.4 Plant-symbiotic interaction

1.4.1 *Serendipita indica*: a model root symbiont

Serendipita indica (*Si*; syn. *Piriformospora indica)* was first isolated from the roots of the *Prosopis juliflora* and *Zizyphus nummularia* in India´s Thar desert (Verma et al., 1998). *Si* is a root-colonising endophyte that can be axenically cultured and grows on different media (Varma et al., 2012). As a basidiomycete with a fully sequenced and annotated genome (Šečić et al., 2021; Zuccaro et al., 2011) *S. indica* colonises a broad range of plants and crop roots.

S. indica interaction with the model plant *Arabidopsis thaliana* has been widely used to dissect the stages of root colonisation. Colonisation begins with a biotrophic phase around 3 days post-inoculation, followed by localised cell death in the root cortex, where the fungus sporulates and forms chlamydospores along with inter- and intracellular hyphae (Deshmukh et al., 2006; Jacobs et al., 2011; Qiang, Weiss, et al., 2012; Schäfer et al., 2007). Furthermore, to successfully establish symbiosis, *S. indica* suppresses innate immune responses in roots (Jacobs et al., 2011; Qiang, Weiss, et al., 2012).

One of the most notable features of *S. indica* is its ability to promote plant growth (Osborne et al., 2023; Varma et al., 2012), enhance nitrate and phosphate uptake (Bajaj

et al., 2018; Ngwene et al., 2016; Scholz et al., 2023; Sharma & Varma, 2021), stimulate root and root hair formation (Jacobs et al., 2011), and promote early flowering and higher seed yield. In Arabidopsis, *Si* has been shown to alter auxin transport and signalling, thereby stimulating root development and biomass accumulation (Vadassery et al., 2008). Beyond model systems, *S. indica* has been shown to benefit a wide range of crops, including *Oryza sativa* (rice) (X. Li et al., 2023), *Hordeum vulgare* (barley) (Sepehri et al., 2021; Waller et al., 2005), *Triticum aestivum* (wheat) where it improved root development and stress resilience (Hosseini et al., 2017), *Brassica rapa* (Chinese cabbage) (Lee et al., 2011) and *Solanum lycopersicum* (tomato) where it boosts sucrose production in roots, leading to better shoot growth and energy allocation (De Rocchis et al., 2022; for review see L. Li et al., 2023). These studies demonstrate the potential of *S.indica* as a natural growth promoter in sustainable agriculture, emphasising its role in enhancing plant resilience to abiotic stresses, including salinity, drought, cold, and heavy metal toxicity (Boorboori & Zhang, 2022; Liu et al., 2021; Roylawar et al., 2021a; Saleem et al., 2022).

Furthermore, *S. indica* has been shown to enhance plant resistance to a wide range of pathogens. In *Allium cepa* (onion), *S. indica* significantly reduced symptoms of Stemphylium leaf blight disease, the most destructive foliar fungal disease of onion and other economically important crops, in greenhouse trials (Roylawar et al., 2021b). Cucumber plants colonised by *S. indica* exhibit increased tolerance to root-knot nematode (*Meloidogyne incognita*), supported by improved photosynthetic performance and activation of innate defence genes (Atia et al., 2020). In barley, *S. indica* triggers systemic induced resistance against *Blumeria graminis* (powdery mildew fungus), accompanied by transcriptomic and metabolic reprogramming in the leaves (Molitor et al., 2011). These examples highlight *S. indica*'s ability to induce plant immunity against pathogens across diverse crop species.

1.4.2 Plant response to beneficial microbes

A core principle of plant–microbe interactions is the plant's ability to distinguish between beneficial and harmful partners. Researchers showed that mutualistic microbes often initiate colonisation by evading or suppressing early immune responses, after which they activate specialised recognition systems that trigger signalling pathways distinct from those engaged by pathogens. While some molecular components, like nutrient

transporters, are used in both mutualistic and pathogenic contexts, most transcriptional and signalling responses are lifestyle-specific (Oldroyd, 2013; Plett & Martin, 2018). In arbuscular mycorrhizal fungi (AMF), lipochitooligosaccharides (LCOs), which resemble chitin-based MAMPs, carry unique lipid modifications that activate LysM receptor kinases without triggering full immune responses. This recognition induces an early calcium signalling and ROS production, followed by the activation of symbiosis-specific transcriptional regulators rather than canonical defence pathways (Feng et al., 2019). In *Glomus intraradices*, the effector SP7 interacts with the pathogenesis-related transcription factor ERF19 in the plant nucleus, thereby counteracting the plant immune program and promoting the biotrophic lifestyle of AMF in roots (Kloppholz et al., 2011). More recently, expression of RiCRN1, a crinkler effector from *Rhizophagus irregularis*, was shown to be essential for successful symbiosis progression and arbuscule formation (Voß et al., 2018). *S. indica* also deploys a sophisticated molecular toolkit to control and facilitate the host´s immunity and colonisation. In barley, *S. indica* induces systemic resistance, enhances antioxidant activity, and manipulates programmed cell death by downregulating *Hv*BI-1 gene (Deshmukh et al., 2006; Waller et al., 2005). Moreover, *S.indica* colonisation of Arabidopsis triggers an Induced Systemic Resistance (ISR) that requires jasmonic acid signalling and cytoplasmic localisation of NPR1 (Stein et al., 2008), suppresses host innate immunity (Jacobs et al., 2011), and induces ER stress leading to controlled cell death that facilitates colonisation (Qiang, Zechmann, et al., 2012). *The S.indica* effector PIIN_08944 interferes with the plant´s salicylic acid-mediated basal resistance, promoting colonisation in both *Arabidopsis thaliana* and barley (Akum et al., 2015). Furthermore, *S. indica* secretes E5'NT, an active ecto-5'-nucleotidase that modifies apoplastic metabolites, altering extracellular nucleotides to suppress plant defences and support beneficial symbiosis (Nizam et al., 2019). Meanwhile, the effector SIE141 relocates the thioredoxin-like protein CDSP32 into the nucleus, activating NPR1-mediated systemic resistance in Arabidopsis (Y. Zhang et al., 2024).

Alongside protein effectors, *S. indica* engages in cross-kingdom RNA signalling by transferring small RNAs into *Arabidopsis thaliana* and *Brachypodium distachyon*, where they downregulate host defence genes and facilitate symbiosis (Nasfi et al., 2024; Šečić

et al., 2021). Similar strategies are observed in other mutualistic interactions. For example, *Laccaria bicolor* delivers miRNA-like sRNAs into poplar to silence immune receptor transcripts (Mewalal et al., 2019), while *Sinorhizobium meliloti* exports tRNA-derived fragments that utilise plant AGO proteins to promote nodulation (Ren et al., 2019). In response, plants modulate their own pathways and receptor-like kinases to fine-tune colonisation and immune responses, and adjust their sRNA machinery to modulate colonisation responses (reviewed in Qiao et al., 2023).

1.4.3 Beneficial microorganisms in agriculture

In modern agriculture, beneficial microorganisms are increasingly recognised for their role in enhancing plant nutrient uptake, protecting against plant diseases, improving resilience to environmental stress and reducing dependence on chemicals (Compant et al., 2025; Galli et al., 2024). For example, *Bacillus subtilis* BS-58 significantly reduced infection of *Fusarium oxysporum* and *Rhizoctonia solani* in Amaranth by producing antifungal compounds that disrupted fungal growth (Pandey et al., 2023). Similarly, *B. subtilis* BS-2301 suppressed *Sclerotinia sclerotiorum* in soybeans and promoted plant growth (Ayaz et al., 2024). In another study, the combined application of *B. subtilis* and *Pseudomonas fluorescens* to tomato roots also showed synergistic effects against *Alternaria solani*, reducing disease incidence, promoting plant growth, and activating resistance genes (Jia et al., 2023).

Fungal mutualists, such as AMF fungi, also play an important role in enhancing crop performance. AMF inoculation in Alfalfa significantly improved root colonisation, boosted yield, and enhanced both nutrient and fatty acid concentrations over two consecutive years (Pellegrino et al., 2022). A two-year study using a mixture of 14 AMF species also demonstrated improved nutritional value in barley, with the effect varying depending on genotype and environmental conditions (Marrassini et al., 2025). In addition to AMF, several endophytic fungi are known for their beneficial effects and agricultural applications. For example, *Trichoderma harzianum* has been shown to improve root architecture and enhance tolerance to abiotic stresses in *Triticum aestivum L*. over a three-year study (Sharma et al., 2012). *S. indica* has also shown notable success

in greenhouses and field trials. It significantly enhanced photosynthesis and biomass in *Camellia Oleifera* (Fu et al., 2024). In addition, winter wheat plants colonised with *S. indica* in a greenhouse experiment showed an increase in biomass and reduced disease severity caused by *Blumeria graminis*, *Pseudocercosporella herpotrichoides*, and *Fusarium culmorum*. Field trials in the same study confirmed a reduced infection of the stem base by *P. herpotrichoides*, although no effect against leaf pathogens was observed (Serfling et al., 2007). Li et al. (2022) reported that in a two-year field trial with *Citrus sinensis* trees inoculated with *Serendipita indica*, sugar content in leaves and roots increased significantly, while lower H_2O_2 and superoxide levels were observed in the leaves compared to non-inoculated controls (Li et al., 2022). These studies demonstrate the considerable potential of beneficial microorganisms to enhance crop yields, particularly in environments with limited nutritional resources or in stressed conditions.

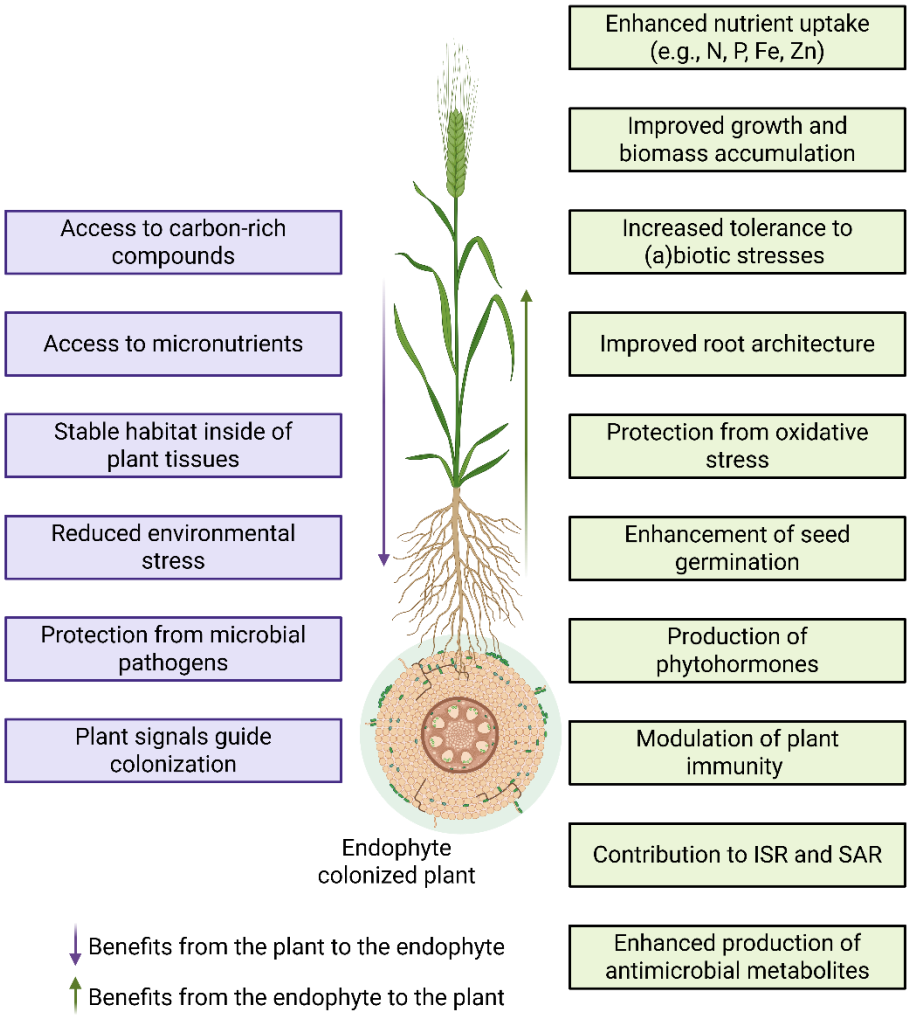

Figure 3. Bidirectional benefits in plant–endophyte interactions. Schematic representation of mutualistic exchanges between an endophyte and its host plant. The benefits provided by the plant to the endophyte are shown in the left panel in purple. The benefits provided by the endophyte to the plant are shown in the right panel in green. Figure created with Biorender.

1.5 Extracellular vesicles: mediator of cross-kingdom communication

When studying plant–microbe interactions, a fundamental question is how communication takes place, what is exchanged, and what mediates this exchange across kingdoms? Increasing evidence indicates that extracellular vesicles (EVs) are

important carriers of molecular signals that enable cross-kingdom communication. EVs are nano-sized membrane-bound particles with a lipid bilayer secreted by nearly all living cells, including plants, fungi, bacteria, animals and humans, and can deliver bioactive molecules such as proteins, lipids and various classes of RNAs between different species (Colombo et al., 2014). In plant-microbe interactions, EVs were shown to contain defence-related bioactive molecules, suggesting a role in plant immune responses (J. Zhang et al., 2024a). A seminal study by Regente et al. (2017) showed that sunflower EVs are taken up by the fungal pathogen *Sclerotinia sclerotiorum*, carrying defence-related proteins that inhibit spore germination and cause cell death, suggesting that sunflower EVs exert an antifungal effect (Regente et al., 2017). In another recent study, Cai et al. (2018) showed that EVs secreted by *Arabidopsis thaliana* are loaded with sRNAs during infection with *Botrytis cinerea*. These sRNAs are taken up by the fungus and induce the silencing of essential virulence genes, representing a form of EV-mediated cross-kingdom communication associated with Tertraspanin (TET8 and TET9) proteins (Cai et al., 2018). In the same pathosystem, RNA-binding proteins (RBPs) such us AGO1, DEAD-box RNA helicases RH11 (RNA helicase 11), RH37, RH52, Annexin1 (ANN1) and ANN2 were identified to play a role in the loading of the plant sRNA in EVs (He et al., 2021) and more recent it was shown that these Arabidopsis EVs also contains mRNAs (Wang et al., 2024). Nevertheless, whether the different RNA biotypes are located outside or encapsulated within EVs is still not fully understood, as variation in experimental conditions and the tissue used might cause a variation in the isolated EVs and their content (Cai et al., 2018; Zand Karimi et al., 2022; Zand Karimi & Innes, 2022).

On the microbial side, fungi and bacteria also produce EVs during plant colonisation. Pathogenic fungi such as *B. cinerea* (He et al., 2023a), *Fusarium oxysporum* (Bleackley et al., 2020), *Ustilago maydis* (Kwon et al., 2021) and *Zymoseptoria tritici* (Hill & Solomon, 2020) were shown to release EVs that contain proteins, lipids, and RNAs involved in virulence and the fungal immune response. These fungal EVs can act on plant receptors or penetrate plant cells, although the exact uptake pathways are still being investigated (J. Zhang et al., 2024a).

Although most EV research in plant–microbe interactions focuses on plants and pathogens, recent studies show that beneficial microbes potentially release EVs that

support plant growth and symbiosis (reviewed in J. Zhang et al., 2024). Moreover, EVs are hypothesised to play a role in arbuscular mycorrhizal symbiosis, but their exact functions and mechanisms in facilitating this interaction remain incompletely understood. Therefore, studying EVs in plant-mutualistic interactions could help develop new, green approaches for enhancing crop yield and protection (reviewed in Holland & Roth, 2023).

1.6 Research question and aims of the study

S. indica is a beneficial root endophyte with a significant potential for agricultural applications, as it enhances plant growth, stress resilience, and overall fitness of a wide range of host plants and crops. Although its beneficial effects are well documented, the molecular mechanisms underlying *S. indica*'s mutualistic interaction remain not yet fully understood, particularly regarding the role of *S.* indica's sRNAs (*Si*sRNAs) in mutualism. To address this knowledge gap, we use *Arabidopsis thaliana* as a model system to investigate whether *Si*sRNAs are transferred into Arabidopsis root cells during colonisation and function as regulators of Arabidopsis gene expression therein.

The central question of this study is whether *Si*sRNAs play a role in the establishment of mutualism and whether cross-kingdom communication occurs by triggering PTGS in host targets. To systematically address this question, this research first identifies *Si*sRNAs expressed during both axenic *S. indica* culture and *Arabidopsis* root colonisation and validates their transfer into host root cells. *Si*sRNAs with potential cross-kingdom silencing activity are distinguished from the broader fungal sRNA pool. To examine *SisRNAs*' function, we predicted their putative Arabidopsis target transcripts. Subsequently, we profiled the expression of the predicted target genes in a time-course experiment during *S. indica* colonisation. *Si*sRNAs were then overexpressed in protoplast-based assays to determine their potential to mediate PTGS and their contribution to the mutualistic interaction.

To deepen our understanding, our next logical step was to answer which RNAi component of Arabidopsis, in particular which AGO proteins, are involved in *S. indica* Arabidopsis interaction? Are *Si*sRNAs recognised and loaded by Arabidopsis AGOs? Does AGO1 mediate *Si*sRNA activity, as demonstrated in plant-pathogen systems, or do

other AGOs also contribute to their recognition? Alternatively, do *Si*sRNAs use alternative RNAi pathways?

Another objective of this study is to investigate how *Si*sRNAs are delivered and transferred into host cells. Does *S. indica* use extracellular vesicles (EVs) as carriers for sRNA transport as observed in pathogenic fungi, or alternatively, do yet unidentified pathways mediate this transfer? To explore this, EVs from *S. indica* were isolated and characterised, their content was analysed for the presence of *Si*sRNAs and compared with *Si*sRNAs detected in colonised root tissues.

Finally, to better characterise the outcomes of sRNA-target interaction in plant-microbe interaction, this thesis developed a novel methodological pipeline, Native Index Ligation-based Targeted Degradome Sequencing (NIL-TDS). This method was developed to overcome the limitations of traditional 5' RLM-RACE, which posed a challenge for our study in detecting low-abundance cleavage events in the *S. indica-Arabidopsis* system. By combining 5' RLM-RACE with Oxford Nanopore sequencing, NIL-TDS can quantitatively detect both canonical and non-canonical cleavage sites. Importantly, this method is broadly applicable to other interacting systems and can facilitate the study of sRNA–mRNA interactions beyond the *S. indica-Arabidopsis* system.

In summary, this work aims to: *i.* identify *Si*sRNA with cross-kingdom regulatory activity; *ii.* characterise their effects on Arabidopsis gene expression; *iii.* determine which components of the host RNAi machinery are involved in the *Si-At* interaction; and *iv.* investigate the mechanism of *Si*sRNA delivery into host cells.

CHAPTER 2 –

A novel plant-fungal association reveals fundamental sRNA and gene expression reprogramming at the onset of symbiosis

(Contributions as a Co-author)

Summary:

This chapter contains the publication **"A novel plant-fungal association reveals fundamental sRNA and gene expression reprogramming at the onset of symbiosis"**, accepted by BMC Biology on July 16, 2021, and published online on August 24, 2021 (DOI: 10.1186/s12915-021-01104-2).

This chapter explores the beneficial interaction between the root endophyte *Serendipita indica* (*Si*; syn. *Piriformospora indica*, Sebacinales) and the model grass *Brachypodium distachyon* (*Bd*). sRNA-mediated cross-kingdom communication is well established in plant-pathogen systems. However, knowledge of its function in mutualistic symbiosis remains limited. Gene expression regulation and sRNA profiling of early Sebacinalean symbiosis were investigated in this work. In this study, I contributed by performing stem-loop PCR to confirm the expression of *Si*- and *Bd*- derived sRNA during the interaction.

Šečić et al. BMC Biology (2021) 19:171
https://doi.org/10.1186/s12915-021-01104-2

BMC Biology

RESEARCH ARTICLE Open Access

A novel plant-fungal association reveals fundamental sRNA and gene expression reprogramming at the onset of symbiosis

Ena Šečić[1], Silvia Zanini[1], Daniel Wibberg[2], Lukas Jelonek[3], Tobias Busche[2], Jörn Kalinowski[2], Sabrine Nasfi[1], Jennifer Thielmann[1], Jafargholi Imani[1], Jens Steinbrenner[1] and Karl-Heinz Kogel[1*]

Abstract

Background: Beneficial associations between plants and microbes are widespread in nature and have been studied extensively in the microbial-dominant environment of the rhizosphere. Such associations are highly advantageous for the organisms involved, benefiting soil microbes by providing them access to plant metabolites, while plant growth and development are enhanced through the promotion of nutrient uptake and/or protection against (a)biotic stresses. While the establishment and maintenance of mutualistic associations have been shown to require genetic and epigenetic reprogramming, as well as an exchange of effector molecules between microbes and plants, whether short RNAs are able to effect such changes is currently unknown. Here, we established an interaction between the model grass species *Brachypodium distachyon* (*Bd*, Pooideae) and the beneficial fungal root endophyte *Serendipita indica* (*Si*, syn. *Piriformospora indica*, Sebacinales) to elucidate RNA interference-based regulatory changes in gene expression and small (s)RNA profiles that occurred during establishment of a Sebacinalean symbiosis.

Results: Colonization of *Bd* roots with *Si* resulted in higher grain yield, confirming the mutualistic character of this interaction. Resequencing of the *Si* genome using the Oxford Nanopore technique, followed by de novo assembly yielded in 57 contigs and 9441 predicted genes, including putative members of several families involved in sRNA production. Transcriptome analysis at an early stage of the mutualistic interaction identified 2963 differentially expressed genes (DEG) in *Si* and 317 in *Bd* line 21-3. The fungal DEGs were largely associated with carbohydrate metabolism, cell wall degradation, and nutrient uptake, while plant DEGs indicated modulation of (a)biotic stress responses and defense pathways. Additionally, 10% of the upregulated fungal DEGs encode candidate protein effectors, including six DELD proteins typical for Sebacinales. Analysis of the global changes in the sRNA profiles of both associated organisms revealed several putative endogenous plant sRNAs expressed during colonization belonging to known micro (mi)RNA families involved in growth and developmental regulation. Among *Bd*- and *Si*-generated sRNAs with putative functions in the interacting organism, we identified transcripts for proteins involved in circadian clock and flowering regulation as well as immunity as potential targets of fungal sRNAs, reflecting the beneficial activity of *Si*.

* Correspondence: Karl-Heinz.Kogel@agrar.uni-giessen.de
[1]Institute of Phytopathology, Centre for BioSystems, Land Use and Nutrition, Justus Liebig University, 35392 Giessen, Germany
Full list of author information is available at the end of the article

Conclusions: We detected beneficial effects of *Si* colonization on *Bd* growth and development, and established a novel plant-mutualist interaction model between these organisms. Together, the changes in gene expression and identification of interaction-induced sRNAs in both organisms support sRNA-based regulation of defense responses and plant development in *Bd*, as well as nutrient acquisition and cell growth in *Si*. Our data suggests that a Sebacinalean symbiosis involves reciprocal sRNA targeting of genes during the interaction.

Keywords: *Brachypodium distachyon*, Genome sequencing, Sebacinalean symbiosis, *Serendipita indica*, Small RNAs

Background

Mutualistic associations between beneficial microbes and plants are widespread and highly advantageous, especially in the microbial-dominant environment of the rhizosphere. This relationship benefits soil microbes by providing them access to plant metabolites; in return, they enhance plant growth and development by promoting nutrient uptake and/or protection against (a)biotic stresses [1, 2]. The beneficial or parasitic outcome of a plant-microbe interaction is governed by the genotype and physiological status of the host, identity of the microbe, and environmental factors such as soil type and nutrient availability [3, 4]. The establishment and maintenance of mutualistic associations (here called symbiosis) require genetic and epigenetic reprogramming and metabolome modulation by the exchange of effector molecules between the beneficial microbe and the plant [5, 6]. Beneficial microbes have a significant impact on crop production, due to their effects on plant health and yield. However, considerable gaps in knowledge prior to their establishment in agricultural practice remain, including systemic identification of microbial abundance and diversity in various ecosystems, understanding the influence of climate, soil conditions, management practices, and, lastly, elucidating the intricacies of molecular mechanisms governing establishment of colonization and nutrient acquisition [7].

Crucial for regulation of gene expression, RNA interference (RNAi) is a well-known eukaryotic gene silencing mechanism [8], mediated by small RNAs (sRNAs) of 20–24 nucleotides (nt) in size and RNAi-associated proteins, primarily from the Argonaute (AGO), Dicer-like (DCL) and RNA-dependent RNA polymerase (RdRP) families [9]. DCLs generate sRNAs from longer RNA molecules, whereas AGOs bind sRNAs within an RNA-induced silencing complex (RISC). In the context of plant-microbe interactions, microbial protein effectors are known to promote pathogen colonization by suppressing host immune responses [10] and have been described in mutualistic associations as well [5], including the Sebacinalean symbiosis [11]. Recent findings suggest that sRNAs, through RNAi-based regulatory mechanisms, also can serve as effectors of pathogenic microbes [12], whereby the sRNA is secreted to suppress translation of a host mRNA via RNAi. Conversely, plants can secrete sRNAs that target virulence-associated mRNAs in the microbe [13]. This transfer of sRNAs and subsequent gene silencing in the target organism is called cross-kingdom RNAi [12].

We studied the association of the beneficial fungus *Serendipita indica* (*Si*) with the model grass *Brachypodium distachyon* (*Bd*, purple false brome, Pooideae [14];). *Si* is an endophytic fungus belonging to the order Sebacinales that colonizes the rhizodermis and cortex of a large spectrum of plants [15]. *Si* serves as an excellent model for beneficial microbes as it (i) primes plants for disease resistance against biotrophic [16] and necrotrophic [17] fungi, oomycetes [18], and viruses [19]; (ii) enhances the tolerance of plants against abiotic stress [20]; (iii) promotes growth and yield [21]; (iv) has a sequenced 25 Mb genome [22]; and (v) is genetically transformable and culturable in axenic conditions [23]. *Si* initially undergoes a biotrophic growth phase during Arabidopsis (*Arabidopsis thaliana*) and barley (*Hordeum vulgare*) colonization, with suppression of innate immune responses [24, 25] and activation of induced systemic resistance [16]. Subsequently, *Si* colonization of barley enters a cell-death associated phase and switches to a saprophytic lifestyle [26, 27].

Bd is a temperate grass species belonging to the Pooideae subfamily and a model for genetic studies of stress resistance and yield parameters of cereals [28]. *Bd* is self-pollinating, genetically transformable, easy to cultivate, and has a sequenced genome of 272 Mb [29–31]. It shares evolutionary proximity and broad synteny with complex crop genomes, such as wheat and rice [14], and is a host for major cereal pathogens [32]. Additionally, RNAi is operational in *Bd*, with proven alteration of micro RNA (miRNA) expression patterns in response to abiotic stresses [33, 34]. In silico analyses revealed that the *Bd* genome, similar to other cereals, contains an expansion of DCL and AGO families [35].

Currently, the significance of cross-kingdom RNAi in mutualistic interactions is largely unknown. A recent in silico study predicted that the arbuscular mycorrhizal fungus *Rhizophagus irregularis* generates sRNAs, which have predicted targets in the host plant *Medicago truncatula* [36]. Moreover, tRNA-derived sRNA fragments from rhizobial bacteria were shown to regulate host nodulation-associated genes by utilizing the host's RNAi machinery [37]. To investigate the role of sRNAs in

another agronomically relevant mutualistic interaction, we established a protocol for *Si* colonization of the model Pooideae *Bd*. Additionally, integrative high-throughput sequencing and transcriptome analysis assessed symbiosis-associated changes in the mRNA and sRNA expression patterns of both organisms. We discuss here possible sRNA-based regulation that might be critical for the establishment of the Sebacinalean symbiosis.

Results

Brachypodium distachyon Bd21-3 forms a mutualistic interaction with *Serendipita indica*

To investigate whether *Bd* can develop a beneficial interaction with *Si*, we established an inoculation protocol using one-week-old seedlings of *Bd* line Bd21-3, with dip-inoculation in 5×10^5 chlamydospores ml^{-1} for 3 h. Comparison of grain production in fully mature, colonized vs. non-colonized plants grown in soil showed that *Si* increased the number of filled grains/plant by 49.9% (Fig. 1a, Additional file 1), and total grain weight/plant increased by 38.1% (Fig. 1b, Additional file 1). Consistent with the observation that *Si*-colonized Bd21-3 plants flower several days earlier than control plants, they exhibited a 32.2% increase in the number of spikelets at 2 months after inoculation (Fig. 1c, Additional file 1). Concordantly, growth and biomass analyses of Bd21-3 seedlings revealed a significant 8.6% increase in shoot length (Fig. 1d) upon *Si* colonization.

Further analysis of Bd21-3 seedlings indicated that *Si* colonization increased lateral root growth, as early as 4 days post inoculation (4 DPI, Additional file 2: Figure S1a). By 25 DPI, roots showed a more extensively branched structure (Additional file 2: Figure S1b). Microscopy of *Si*-inoculated Bd21-3 roots confirmed root surface colonization and proliferation of fungal spores after staining with chitin-specific WGA-AF 488 at 4 DPI (Fig. 2a–d) and further on at 7 DPI and 14 DPI (Additional file 2: Figure S2). Inter- and intracellular colonization of Bd21-3 cells in the root differentiation zone also was visible after WGA-AF 488 and propidium iodide staining (Fig. 2e–h). These results suggest that establishment of a mutualistic symbiosis correlates with observable phenotypic changes by 4 DPI; thus, this time point was used to further investigate the Bd21-3-*Si* system.

Resequencing of the *Si* genome

To improve *Si* assembly, the genome was resequenced using MinION (25,167 reads, 324 Mb) and MiSeq (18,225,814 reads, 5.46 Gb); together they yielded approx. 6.0 Gb of sequence information. *De novo* assembly of the Nanopore sequence reads generated 57 contigs, accounting for a total length of 24.7 Mb and a N50 of 1.3 Mb. The draft genome sequence features GC content of 50.8%, similar to the first genome version with 2,359 contigs and GC content of 50.7% [22]. Analyses using the eukaryotic gene prediction tool Genemark-ES 4.33 [38] revealed 9441 predicted genes (75% of the genome; 59,045 exons), 9498 intergenic regions (25% of the genome), and a gene density of 380.68 genes/Mbp (Additional file 2: Table S1). Annotation of the *Si* genes using a GenDB version designed to process eukaryotic genomes possessing multi-exon genes [39, 40] revealed that 4756 have a predicted function. Comparison of predicted genes from the resequenced *Si* genome (Si-2020) vs. the 2011 assembly [22] indicated that the vast majority are shared (90.3%), with 915 genes unique to the Si-2020 genome (Additional file 2: Figure S3). There is a reduction in gene model numbers relative to the 2011 assembly, which can be attributed to improved gene prediction tools for eukaryotic organisms and a considerably reduced number of contigs. Additionally, *Si* shares 2585 genes with another member of the Sebacinales, *Serendipita vermifera*, while 156 genes are shared only with the ectomycorrhizal fungus *Laccaria bicolor* and 2729 genes are common in all three species (Additional file 2: Figure S4).

Establishment of the *Si-Bd* symbiosis is associated with extensive transcriptional reprogramming

To assess how the symbiotic interaction affects gene expression in both organisms, mRNA was sequenced and analyzed (Additional file 2: Table S2) from the roots of *Si*-colonized Bd21-3 seedlings (sample Bd-Si) and mock-treated plants (Bd-C) at 4 DPI, and from 4-week-old axenic *Si* cultures (Si-ax). Comparison of reads between Bd-Si and Si-ax identified 2963 differentially expressed fungal genes (DEGs, DESeq2: Wald test, Benjamini-Hochberg (BH) adjustment, padj < 0.05), which accounts for 31.4% of the 9441 predicted *Si* genes. Comparison of reads from Bd-Si and Bd-C revealed 317 plant DEGs (0.66% out of approximately 47,917 protein-coding transcripts disclosed in the JGI v1.1 annotation, padj < 0.05). The interaction-responsive DEGs in *Si* and Bd21-3, split into up- and downregulated groups are shown in Fig. 3.

All significant DEGs were submitted to gene ontology term analysis against the reference background for *Bd* and a customized *Si*-specific background. The resulting enriched terms relate to metabolic, mainly redox processes and catalytic activity functions (Additional file 2: Table S3). Of the 25 highly downregulated *Si* DEGs, many encode proteins associated with metabolic reprogramming networks involved in nutrient exchange and adaptation to nutrient availability (Table 1). By contrast, highly upregulated *Si* DEGs encode for proteins involved in fungal catalytic and hydrolytic processes. This suggests that by 4 DPI, *Si* has entered a saprophytic-like

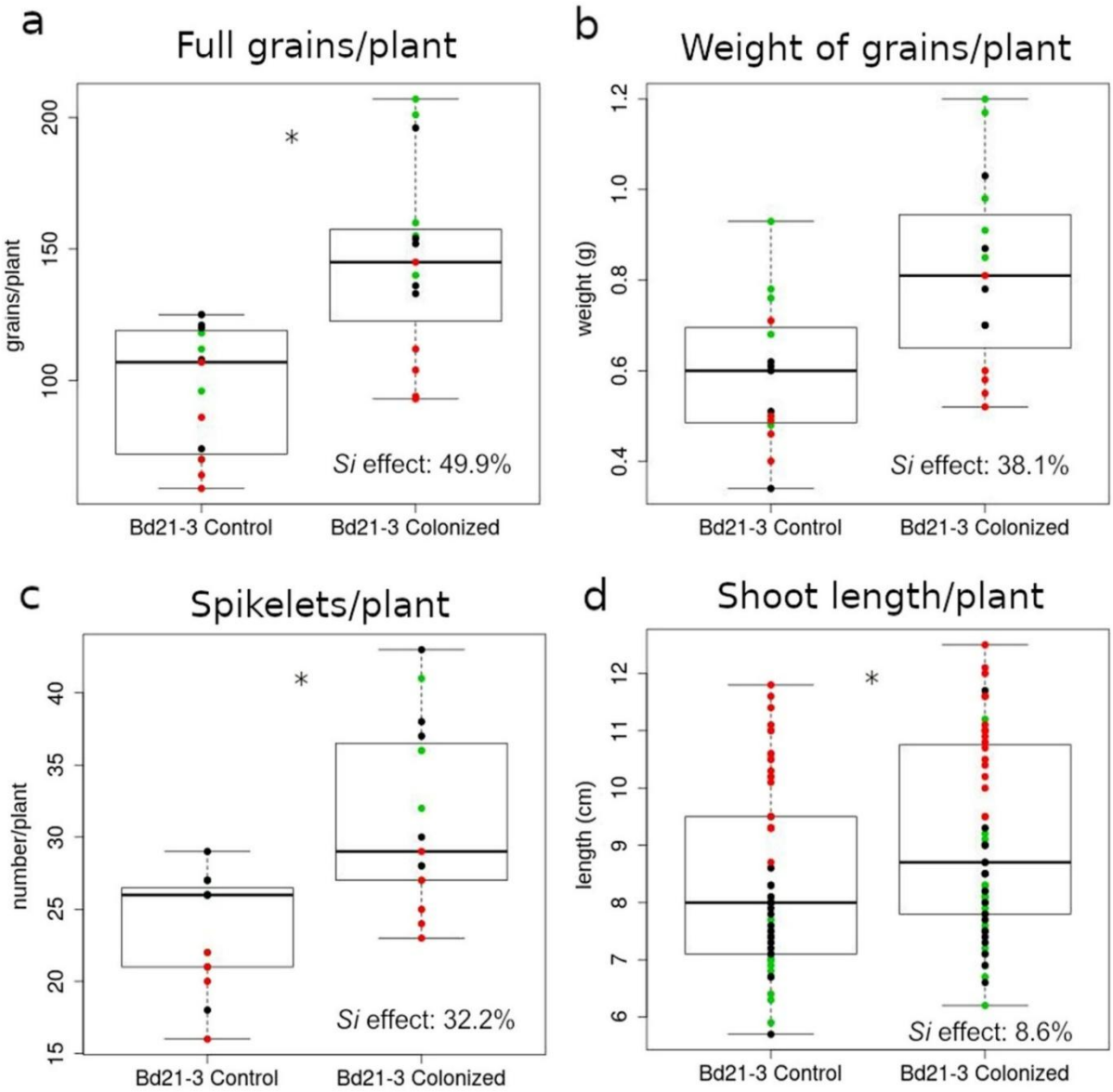

Fig. 1 Root colonization by *Serendipita indica* (*Si*) increases growth and yield of *Brachypodium distachyon* (*Bd*) Bd21-3. **a** Number of full grains produced by non-colonized (control) vs. *Si*-colonized plants. Sample size $n = 5$. **b** Total grain weight of control vs. colonized plants. Sample size $n = 5$. **c** Number of spikelets of control vs. colonized plants. Sample size $n = 5$. **d** Shoot length of control vs. colonized plants. Sample size $n = 20$. The results are from three independent biological replicates that are represented by green, black, and red dots on the scatter graph, individual data values for 1a–c in Additional File 1. For **a** and **b**, 1-week-old seedlings were inoculated with 5×10^5 chlamydospores per ml and grown for approximately 3 months in F-E type LD 80 soil; for **c**, spikelets were counted on 2-month-old plants; for **d**, seedlings were grown for 3 weeks on a vermiculite:oil dri mixture (semi-sterile conditions). The significance threshold for *p* values, corrected for multiple testing (Benjamini-Hochberg) was set at 0.05 (*≤ 0.05) and the *Si* effect was calculated as ((Mean_Si-Mean_Control)/Mean_Control) × 10^2)

growth phase similar to that detected in barley roots [22]. To investigate whether any *Si* DEG encodes effector proteins, a computational pipeline [41] was used to mine 982 genes identified in the Si-2020 genome that encode signal peptide-containing proteins, resulting in 480 putative protein effector genes. In total, 174 (36%) of these were significantly upregulated during colonization of Bd21-3 (Additional file 2: Table S4), including six DELD family proteins [22]. In Bd21-3, many of the highly downregulated interaction-responsive DEGs encode transcription factors or proteins associated with stress responses or circadian clock regulation. Those showing high levels of upregulation include genes linked to immune responses and hormone

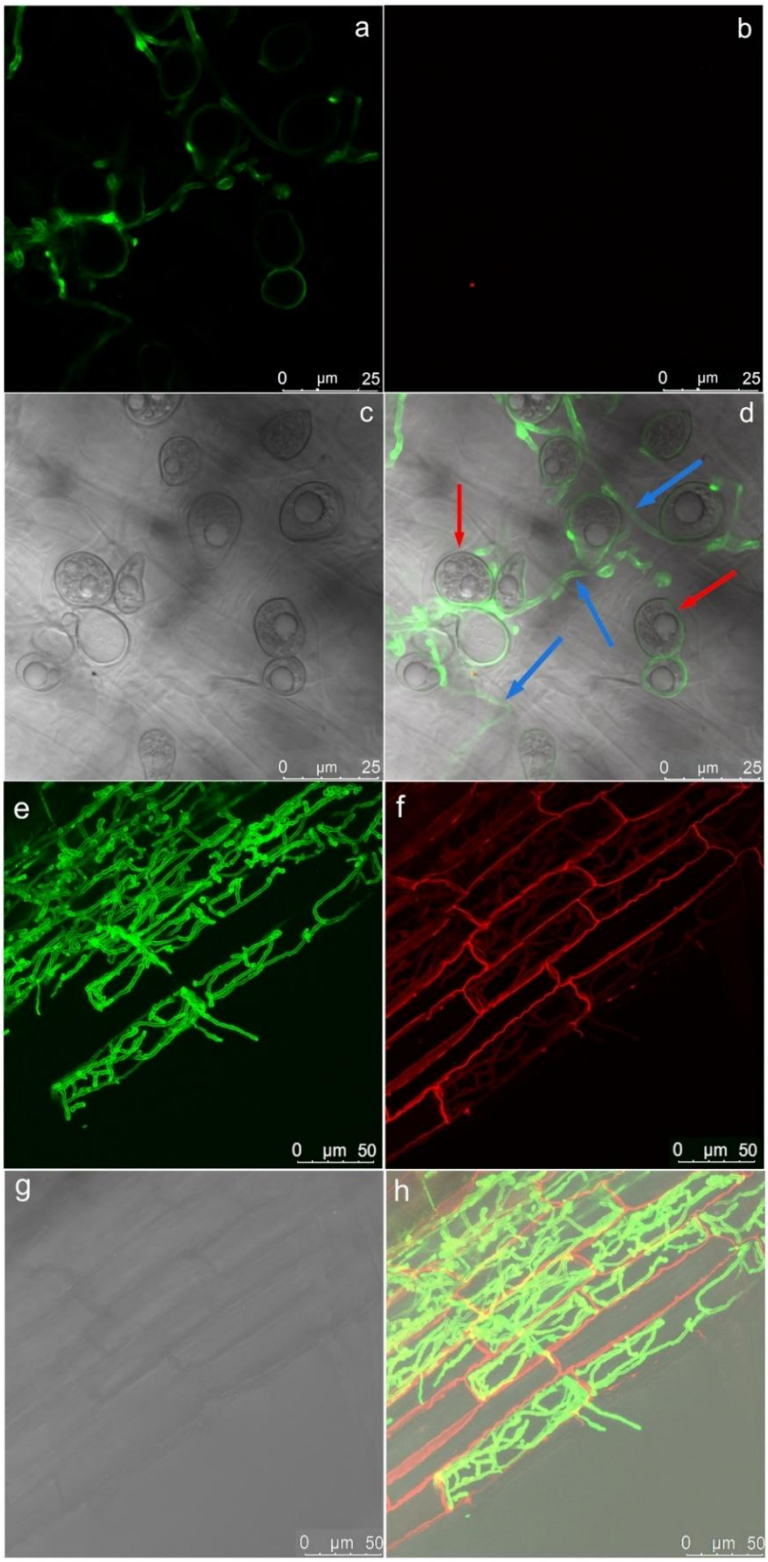

Fig. 2 (See legend on next page.)

(See figure on previous page.)
Fig. 2 Colonization pattern of *Serendipita indica* (*Si*) on *Brachypodium distachyon* Bd21-3 roots. **a**–**d** Colonization at 4 DPI. **a** Fluorescence microscopy showing WGA-AF488 staining of *Si* cell walls (λexc494 nm, λem515). **b** Fluorescence control (λexc631 nm, λem642). **c** Bright-field microscopy to visualize *Si* chlamydospores. **d** Overlay showing *Si* chlamydospores (red arrows), which have germinated and formed a hyphal network on the root surface (blue arrows). **e**–**h** Rhizodermal root colonization by *Si* at 4 DPI. **e** Fluorescence microscopy showing WGA-AF488 staining of *Si* cell walls (λexc494 nm, λem515). **f** Fluorescence microscopy to visualize propidium iodide staining of root cell walls (λexc535 nm, λem617). **g** Bright-field microscopy to visualize root cells. **h** Overlay showing extensive inter- and intracellular fungal growth on Bd21-3 roots. Imaging was done with a LEICA S8 confocal microscope (e-h: maximum projection; *z*-stack). For **a**–**d**, 1-week-old seedlings were inoculated with 5×10^5 chlamydospores per ml and subsequently grown on a plastic mesh over 0.5X MS; for **e**–**h**, *Si*-inoculated seedlings were grown on vermiculite:oil dri mix before harvesting at 4 DPI

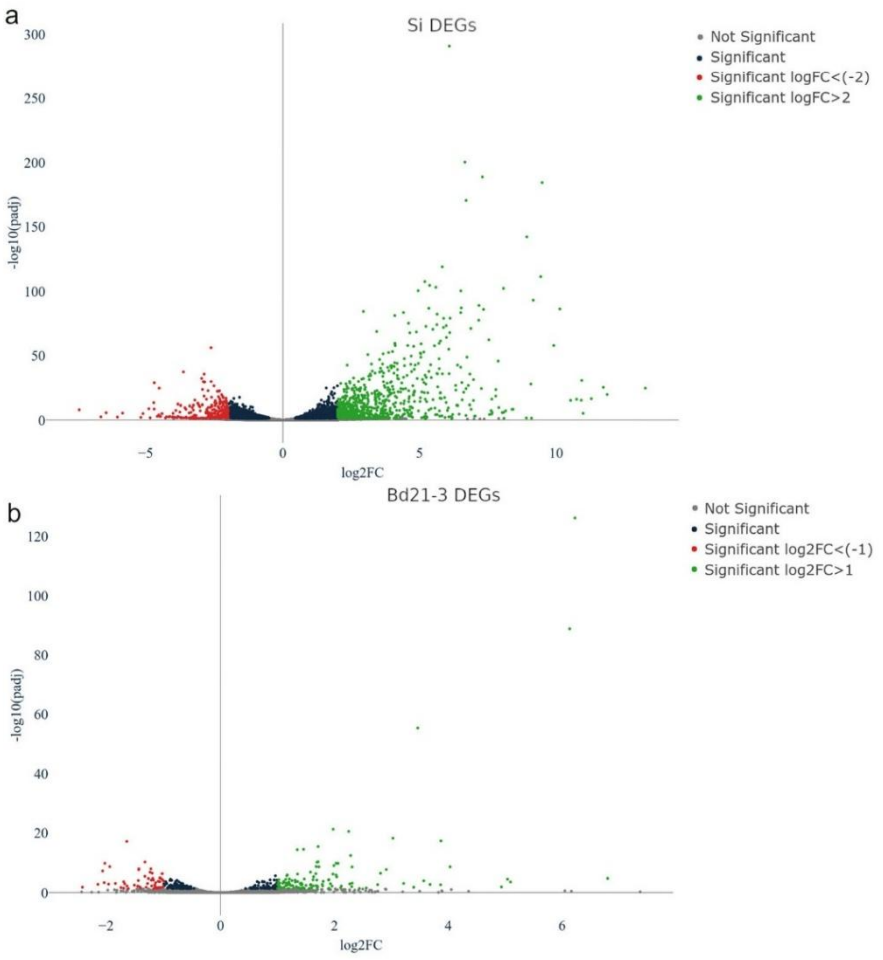

Fig. 3 Volcano plots of colonization-associated, differentially expressed genes (DEGs). **a** *Serendipita indica* (*Si*) DEGs identified by comparing reads from colonized roots (Bd-Si) vs. axenic mycelium (Si-ax). **b** *Brachypodium distachyon* Bd21-3 DEGs identified by comparing colonized (Bd-Si) vs. mock-treated (Bd-C) roots. *X*-axis displays the $\log_2$ FoldChange and *Y*-axis displays the negative $\log_{10}$ of adjusted *p* values from DE analysis. The magnitude of up- or downregulation for the DEGs (represented by individual dots) is indicated by different colors, as designated in the legend for each plot

Table 1 Top 25 *Serendipita indica* (*Si*) differentially expressed genes (DEGs) during colonization (4 DPI)

Gene	Description	log2FC
1937_g (PIIN_04746)	Related to mismatch base pair and cruciform DNA recognition protein HMP1	− 5.84
465_g (PIIN_02587)	Related to phenylalanine ammonia-lyase	− 5.1
281_g (PIIN_04449)	Probable succinate-fumarate transporter	− 4.7
1121_g (PIIN_02682)	Related to ADY2-protein essential for the acetate permease activity	− 4.68
7809_g (PIIN_07312)	Related to RTM1 protein	− 4.52
2544_g (PIIN_02778)	Probable ADH1-alcohol dehydrogenase I	− 4.42
4482_g (PIIN_08427)	Related to mixed-linked glucanase precursor MLG1	− 4.23
4969_g (PIIN_02119)	Related to meiotic nuclear division protein 1 homolog	− 3.54
1859_g (PIIN_00204)	Probable thioredoxin	− 3.45
5786_g (PIIN_00305)	Probable DHA14-like major facilitator; ABC transporter	− 3.41
4465_g (PIIN_06089)	Putative mitochondrial carnitine O-acetyltransferase	− 3.36
1392_g (PIIN_11719)	Putative alkaline ceramidase 3	− 3.22
8569_g (PIIN_01532)	Related to Ca^{2+}-transport (H^+/Ca^{2+} exchange) protein	− 3.21
2933_g (PIIN_07440)	Related to monocarboxylate transporter 2	− 3.21
758_g (PIIN_02772)	Probable TOM40-mitochondrial import receptor MOM38	− 3.19
2855_g (PIIN_07067)	Related to l-asparaginase	− 3.18
5713_g (PIIN_07616)	Related to MFS transporter	− 3.17
3225_g (PIIN_08230)	Related to RSB1-integral membrane transporter	− 3.11
8602_g (PIIN_08742)	Putative maintenance of mitochondrial morphology protein 1	− 3.09
917_g (PIIN_03155)	Related to YTP1	− 3.05
6928_g (PIIN_00312)	Related to nitrogen metabolic regulation protein	− 2.96
6930_g (PIIN_00314)	Probable malate synthase	− 2.94
4348_g (PIIN_03103)	Putative ubiquitin-conjugating enzyme D4	− 2.9
6400_g (PIIN_07801)	Probable acyl-CoA dehydrogenase short-branched chain precursor	− 2.9
5097_g (PIIN_04235)	Related to acyl-CoA dehydrogenase	− 2.88
5186_g (PIIN_09750)	Probable pectate lyase	11.93
8239_g (PIIN_02110)	Related to family 61 glucanase	11.29
3289_g (PIIN_05863)	Endo-1,4-beta-xylanase	10.75
7464_g (PIIN_04708)	Alpha-L-arabinofuranosidase	10.14
5322_g (PIIN_05889)	Endo-1,4-beta-xylanase	10.14
1898_g (PIIN_08141)	Glutathione S-transferase	9.1
5131_g (PIIN_02752)	Cellulose 1,4-beta-cellobiosidase	8.93
3537_g (PIIN_10118)	Carboxylic ester hydrolase	8.83
6726_g (PIIN_08399)	Probable alpha-galactosidase B	8.29
4844_g (PIIN_06890)	Endo-1,4-beta-xylanase A	7.9
8585_g (PIIN_01553)	Probable beta-glucosidase	7.88
3597_g (PIIN_06117)	Related to endoglucanase B	7.78
5420_g (PIIN_07414)	Related to NACHT/WD40 domain-containing protein	7.64
1875_g (PIIN_06862)	Rhamnogalacturonan acetylesterase	7.62
6520_g (PIIN_06360)	Endo-1,4-beta-xylanase C	7.53
3290_g (PIIN_05862)	Probable endo-1,4-beta-xylanase A	7.42
3615_g (PIIN_11270)	Probable feruloyl esterase C	7.37
5971_g (PIIN_04536)	Probable gEgh 16 protein	7.3
8031_g (PIIN_01484)	Related to CEL1 protein precursor	7.2

Table 1 Top 25 *Serendipita indica* (*Si*) differentially expressed genes (DEGs) during colonization (4 DPI) *(Continued)*

Gene	Description	log2FC
6665_g (PIIN_03039)	Probable beta-glucoside glucohydrolase	7.15
720_g (PIIN_06594)	Cellulose 1,4-beta-cellobiosidase	7.08
3514_g (PIIN_09664)	Glucose oxidase	7.01
290_g (PIIN_04439)	Related to peroxisomal short-chain alcohol dehydrogenase	6.97
6967_g (PIIN_00353)	Exocellobiohydrolase 3	6.7
1893_g (PIIN_08147)	Probable glutathione S-transferase	6.57

DEGs are calculated as: colonized root vs. *Si* axenic culture exhibiting significant (padj. < 0.05) down- or up-regulation, $\log_2$ FC (fold change) during colonization

signaling networks (Table 2 and Additional file 2: Table S3). In order to further validate our sequencing data, we confirmed the expression of five *Si* and five Bd21-3 DEGs from Tables 1 and 2 by RT-qPCR. Generally, the qPCR results show a similar fold change for the selected genes between the colonized root and the respective controls, compared to the mRNA-seq results (Additional file 2: Figure S5). Together, these results show that both organisms utilize a complex enzymatic arsenal to establish and control the symbiosis.

Prediction of *Si* RNAi genes

Since RNAi-mediated gene silencing has been documented in most but not all fungi [42], we assessed whether the Si-2020 genome encodes RNAi-related proteins with conserved domain architecture and homology to RNAi components in the model filamentous fungus *Neurospora crassa* [43]. Genes encoding predicted DCLs (G4U2H0, G4TBW9) with typical domains (dsRNA-binding, RNase III and helicase, [44]), QDE2-like proteins with PIWI domains typical of AGOs (G4TEK0, G4TLO4, [45]), an AGO-like protein (G4T5G9), and RdRPs (G4TNU7, G4TQP0) were identified and were expressed in axenic culture and Bd21-3-associated *Si* samples (Additional file 2: Table S5). Thus, the *Si* genome is predicted to contain genes encoding critical components of the RNAi machinery. Based on these new data, and the earlier discovery that AGO and DCL families are expanded in the *Bd* genome [35], we decided to sequence the sRNAs of both organisms, in order to assess the role of RNAi-based regulation and communication in symbiosis.

sRNA profiles undergo a substantial change at the onset of the *Si-Bd* symbiosis

To evaluate how the mutualistic interaction affects the sRNA profiles in the colonized root and respective *Si* and *Bd* controls, reads from Bd-C, Bd-Si, and Si-ax sRNA data sets were subjected to consecutive filtering steps (Additional file 2: Figure S6). This greatly reduced the number of raw reads to be analyzed and allowed us to distinguish between sRNAs with potential targets in the interacting organism (putative ck-sRNAs) and sRNAs with potential functions in the same organism (putative endogenous sRNAs) (Additional file 2: Table S6).

Analysis of sRNAs from the Bd-Si dataset revealed that the total number of putative ck-sRNAs exceeds that of endogenous sRNAs in both *Si* (786,732 vs. 261,478) and Bd21-3 (17 million vs. 1.6 million), but the converse is true for unique sRNAs (36,163 endogenous vs. 35,895 putative ck-sRNAs in *Si* and 483,352 endogenous vs. 286,198 putative ck-sRNAs in Bd21-3).

Size distribution profiles of *Si* and Bd21-3 sRNAs

Size distribution of sRNA reads from Bd21-3 and *Si* during colonization, and the respective controls was then assessed. For putative endogenous Bd21-3 sRNAs, peaks at 21 and 24 nt were identified, with the 24 nt sRNAs exhibiting greater diversity than those of 21 nt (Fig. 4a, b). These sizes are consistent with the expected peaks of RNAi-associated sRNAs in plants [46]. For putative endogenous *Si* sRNAs, a bimodal size distribution pattern was observed in the total fractions, with the first peak at 26 nt and second at 29–30 nt (Fig. 4c, d). A smaller peak of 21 nt long molecules was observed in the Bd-Si but not Si-ax samples, indicating that colonization affects the relative size distribution of *Si* sRNAs. Since previously identified ck-sRNAs range from 20 to 24 nt [12, 13], the size distribution of putative ck-sRNAs and corresponding reads in the control samples was assessed over a narrower window. Contrary to endogenous sRNAs, ck-sRNAs displayed no prominent peaks in the 20–24 nt window (Additional file 2: Figure S7).

Before sRNAs can guide RNAi-mediated gene silencing, they must be loaded onto AGO proteins and assembled into a RISC. Previously, Arabidopsis AGO proteins were shown to preferentially recruit sRNAs with specific 5′ termini [47]. Hence, we analyzed the 5′ terminal nt composition of Bd-C, Si-ax, and Bd-Si sRNAs. For unique putative endogenous and ck-sRNAs, the 5′ nt composition was relatively consistent except for the 24 nt Bd21-3 sRNAs, which exhibited a strong bias towards 5′ A (Additional file 2: Figure S8, Figure S9). The total sRNA

Table 2 Top 25 *Brachypodium distachyon* (*Bd*) differentially expressed genes (DEGs) during root colonization (4 DPI)

Gene	Description	log2FC
BdiBd21-3.2G0197800	MYB-related transcription factor	− 2.41
BdiBd21-3.5G0123400	ABA/WDS induced protein	− 2.14
BdiBd21-3.3G0280400	Putative glycosyltransferase family 28	− 2.06
BdiBd21-3.3G0558500	Putative steroid 17-alpha-monooxygenase	− 2.03
BdiBd21-3.3G0660200	AP2 domain-containing protein	− 2.02
BdiBd21-3.1G0813200	GRAS transcription factor	− 1.96
BdiBd21-3.3G0264400	Homologous to barley constans-like protein CO8	− 1.94
BdiBd21-3.4G0000100	Fantastic four meristem regulator FAF	− 1.84
BdiBd21-3.1G0416000	Hydrophobic Protein RCI2	− 1.69
BdiBd21-3.1G0002200	Ca2+-independent phospholipase A2	− 1.67
BdiBd21-3.1G0887100	Putative pseudo-response regulator 7	− 1.64
BdiBd21-3.4G0311800	Dirigent-like protein	− 1.6
BdiBd21-3.1G0815300	SPX domain-containing protein 3	− 1.43
BdiBd21-3.1G0972800	Cold regulated protein 27	− 1.42
BdiBd21-3.4G0303000	Putative protein kinase	− 1.32
BdiBd21-3.2G0034900	Putative sulfoquinovosyltransferase SQD2	− 1.21
BdiBd21-3.1G0281100	SPX – domain containing protein 3	− 1.23
BdiBd21-3.1G0554700	Anthranilate O-methyltransferase	− 1.18
BdiBd21-3.1G0584400	Peroxidase	− 1.17
BdiBd21-3.5G0205300	Putative calmodulin-dependent protein kinase	− 1.15
BdiBd21-3.2G0749200	Probable lipid transfer LTP2	− 1.13
BdiBd21-3.5G0303700	Wound-induced protein	− 1.1
BdiBd21-3.5G0024800	Heat shock protein 90-1	− 1.07
BdiBd21-3.1G0399200	bZIP transcription factor	− 1
BdiBd21-3.1G0557300	BURP domain protein	− 0.93
BdiBd21-3.3G0203000	Cupin-domain protein	6.13
BdiBd21-3.1G0469800	Glutathione S-Transferase	5.09
BdiBd21-3.4G0405200	Protein Hothead/ FAD binding	4.93
BdiBd21-3.3G0354800	Cytochrome P450 76C1	4.03
BdiBd21-3.3G0136300	Proprotein convertase subtilisin/kexin	3.87
BdiBd21-3.4G0068000	Pathogenesis-related protein Bet v I family	3.86
BdiBd21-3.1G0662500	LRR receptor-like serine/theronine protein kinase	3.57
BdiBd21-3.4G0556000	Alcohol dehydrogenase	3.39
BdiBd21-3.1G0772700	Pathogenesis-related protein 1 (PR1)	3.21
BdiBd21-3.4G0393500	Putative chalcone synthase	2.44
BdiBd21-3.3G0195800	Tryptophan decarboxylase	2.3
BdiBd21-3.4G0171000	Multicopper oxidase	2.28
BdiBd21-3.3G0639500	Glycosyl hydrolase protein/Chitinase-related	2.12
BdiBd21-3.1G0129100	Potato inhibitor I family	2.06
BdiBd21-3.2G0160100	Pipecolate/sarcosine oxidase	2.04
BdiBd21-3.4G0189100	Putative LRR protein kinase	1.99
BdiBd21-3.2G0418600	WRKY transcription factor	1.9
BdiBd21-3.4G0073800	Thaumatin family protein	1.8
BdiBd21-3.2G0545400	LRR protein	1.79

Table 2 Top 25 *Brachypodium distachyon* (*Bd*) differentially expressed genes (DEGs) during root colonization (4 DPI) *(Continued)*

Gene	Description	log2FC
BdiBd21-3.4G0121800	Tryptophan biosynthesis protein	1.71
BdiBd21-3.4G0397700	Serine/threonine protein kinase	1.7
BdiBd21-3.4G0026800	Putative protein kinase	1.69
BdiBd21-3.2G0468100	Peroxidase	1.68
BdiBd21-3.2G0600500	Wall-associated receptor kinase	1.6
BdiBd21-3.2G0233800	PGP-like phosphoglycoprotein auxin transporter	1.58

DEGs are calculated as: colonized root vs. mock-inoculated root exhibiting significant (padj. < 0.05) down- or upregulation, $\log_2$ FC (fold change) during colonization

fractions exhibited somewhat greater variability in 5′ nt composition. Of the total Bd21-3 endogenous sRNAs, 24 nt molecules from colonized and non-colonized tissue showed a strong bias towards 5′ A, while 21 nt molecules were biased towards a terminal U (Additional file 2: Figure S10), and 20 nt ck-sRNAs had a higher percentage of 5′ Cs (Additional file 2: Figure S11). Of the total endogenous *Si* sRNAs, those from colonized samples generally had a stronger bias towards 5′ A than sRNA reads from Si-ax, especially at 26 nt and 21 nt (Additional file 2: Figure S10). A slightly higher percentage of 5′ As also was detected in total putative ck-sRNAs of 21 nt (Additional file 2: Figure S11).

Differentially expressed *Si* and Bd21-3 sRNAs

Analysis of unique plant sRNAs in Bd-C vs. Bd-Si revealed that 63% of the putative endogenous sRNAs were exclusively present in Bd-C, 30% were exclusively in Bd-Si and 7% were present in both (Fig. 5). For the reads from the putative ck-sRNA pipeline, 76% of the reads were exclusively present in Bd-C, 13% were exclusive to Bd-Si, and 11% were found in both. Comparison between the unique fungal sRNAs in Si-ax and Bd-Si indicated that 98.1% of the putative endogenous sRNAs were exclusively present in axenic culture, 0.98% were exclusively found in Bd-Si, and 0.92% were in both. Similarly, from the putative ck-sRNA pipeline, 98.2% of

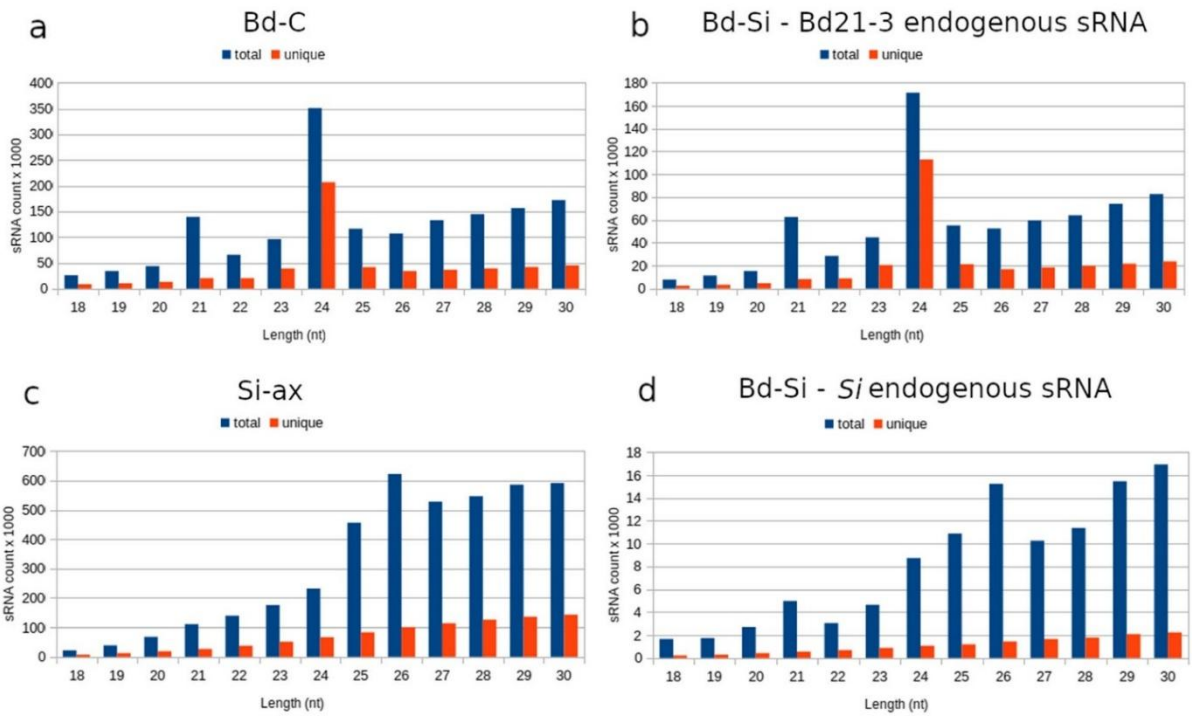

Fig. 4 Size distribution of total and unique putative endogenous sRNAs. **a** Bd-C (mock-treated), **b** Bd-Si (colonized root), **c** Si-ax (axenic mycelium), and **d** Bd-Si (colonized root). All datasets represent three biological replicates and corresponding two technical replicates, merged together. sRNA length is displayed on the *X*-axis (nt) and number of total/unique sRNA counts on the *Y*-axis ($\times 10^3$)

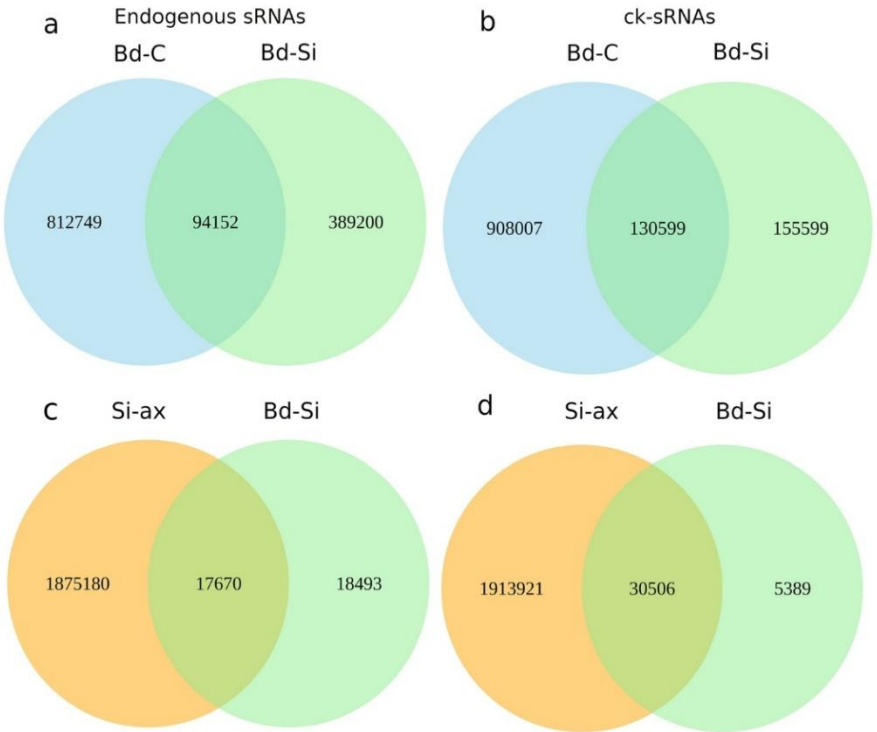

Fig. 5 Venn diagrams showing the sample-exclusive or communal presence of unique putative endogenous or ck-sRNAs. **a** putative endogenous sRNAs in Bd-C (mock-treated) vs. Bd-Si (colonized root), **b** sRNA reads in Bd-C vs. putative ck-sRNAs in Bd-Si, **c** putative endogenous sRNAs in Si-ax (axenic mycelium) vs. Bd-Si (colonized root), and **d** sRNA reads in Si-ax vs. putative ck-RNAs in Bd-Si

the sRNA reads were exclusive to the Si-ax sample, 0.3 % were exclusive to Bd-Si, and 1.5% were present in both. Considering only the *Si* sRNAs in the Bd-Si sample, 51.1% of the putative endogenous ones and 15% of the putative ck-sRNAs are exclusively present in the colonized sample. Among Bd21-3 sRNAs in the Bd-Si sample, there are 80.5% putative endogenous sRNAs and 54.3% ck-sRNAs exclusive for the colonized root. These data show that colonization induces many novel putative endogenous and ck-sRNAs in Bd21-3, and a smaller amount in *Si*, due to fungal quantity in the colonized roots.

Identification of Bd21-3 miRNAs during the *Bd-Si* interaction

Using the ShortStack analysis tool, we identified Bd21-3 loci that correspond to putative endogenous sRNAs expressed during *Si* colonization. The DicerCall function indicated loci whose predominant sRNAs are 20–24 nt. Comparison of these sRNAs with miRBase identified 16 sRNA-generating loci that correlate to known miRNAs (Table 3). These miRNAs belong to highly conserved plant miRNA families that regulate growth and development [33, 34]. We conducted the same analysis with *Si* sRNAs, but no predicted miRNA-like RNAs were identified in the colonized sample, possibly due to a lack of data about the fungal sRNA-generating loci.

In silico target prediction of putative *Si* and Bd21-3 ck-sRNAs

Since most examples of sRNA-based communication in plant-microbe interactions have the commonality of 21 nt long sRNAs that silence transcripts in the target organism [12, 13, 48], we predicted the targets of 21 nt colonization-induced *Si* and *Bd* putative ck-sRNAs and assessed their expression after colonization. Of 16,003 unique Bd21-3 targets predicted for 412 induced 21 nt *Si* sRNAs, 49 were confirmed as downregulated at 4DPI. This represents 15.4% of all significantly changed genes in Bd21-3 during *Si* colonization. Some 89% of these transcripts are predicted as targets of *Si* sRNAs that are expressed exclusively in colonized tissue or with $\log_2$FC > 1. A representative set of sRNA-mRNA duplexes, chosen based on target identity and expression of target and sRNA, indicates that putative ck-sRNA targets in Bd21-3 are associated with transcription factor families, signaling pathways, and basal plant defense (Table 4, Additional file 2: Table S7).

To assess whether Bd21-3 generates ck-sRNAs that potentially target *Si* genes, we searched for predicted targets of 329 Bd21-3 sRNAs (21 nt long) induced in *Si*-

Table 3 Predicted miRNA-generating loci identified in Bd21-3 roots colonized by *Serendipita indica*

Locus	Predominant sRNA	Known miRNA
Bd1:31073434-31073613	UCGGACCAGGCUUCAUUCCCC	bdi-MIR166b
Bd2:10327043-10327213	CUGCACUGCCUCUUCCCUGGC	bdi-MIR408
Bd2:3991996-3992115	UGACAGAAGAGAGUGAGCAC	bdi-MIR156e
Bd2:3992232-3992320	UGACAGAAGAGAGUGAGCAC	bdi-MIR156f
Bd2:3992444-3992557	UUGACAGAAGAGAGUGAGCAC	bdi-MIR156g
Bd2:5570263-5570488	CUUGGAUUGAAGGGAGCUCU	bdi-MIR159a
Bd3:1968409-1968509	UCGCUUGGUGCAGAUCGGGAC	bdi-MIR168
Bd3:33173606-33173746	UCGGACCAGGCUUCAUUCCCC	bdi-MIR166c
Bd3:39150748-39150893	GCUCACUUCUCUCUCUGUCACC	bdi-MIR156b
Bd3:4482899-4483000	UUGACAGAAGAGAGUGAGCAC	bdi-MIR156c
Bd3:44836298-44836372	AGAAGAGAGAGAGUACAGCCU	bdi-MIR529
Bd3:7316295-7316393	GGGCAACUCCUCCGUUGGCAGA	bdi-MIR399d
Bd4:1654850-1654943	UGAAGCUGCCAGCAUGAUCUGA	bdi-MIR167e
Bd4:4893304-4893422	CGGAGGUCAGGAAUUCUACUGAUU	bdi-MIR9481b
Bd4:6029321-6029440	UCUCGGACCAGGCUUCAUUCC	bdi-MIR166f
Bd5:18466111-18466202	UGACAGAAGAGAGUGAGCAC	bdi-MIR156d

Table 4 Examples of deduced duplexes of *Serendipita indica* sRNAs and their downregulated targets in *Brachypodium distachyon*

sRNA name	sRNA Expression	Target transcript	Description	Transcript expression
*Sis*RNA 1	NA	BdiBd21-3.1G0887100.1	Homologous to Arabidopsis pseudo-response regulator 3 and 7	− 1.63
		BdiBd21-3.2G0440200.1	Serine-carboxypeptidase-like 26-related	− 0.81
*Sis*RNA 2	NA	BdiBd21-3.1G0399200.1	bZIP transcription factor	− 1.00
*Sis*RNA 3	NA	BdiBd21-3.2G0288400.1	LURP1-related	− 1.20
*Sis*RNA 4	NA	BdiBd21-3.1G0475100.1	Zinc-finger of the FCS-type	− 1.00
*Sis*RNA 5	0.13	BdiBd21-3.1G0047100.1	Nitrogen metabolic regulation protein NMR-related	− 0.78
*Sis*RNA 6	1.35	BdiBd21-3.3G0750900.1	Peroxygenase	− 0.77
*Sis*RNA 7	NA	BdiBd21-3.1G0917100.1	Enolase	− 0.52
*Sis*RNA 8	NA	BdiBd21-3.4G0303000.1	Protein kinase domain protein	− 1.31
*Sis*RNA 9	NA	BdiBd21-3.1G0759800.1	Carboxyl-esterase 15 related	− 0.86
*Sis*RNA 10	NA	BdiBd21-3.1G0813200.1	GRAS transcription factor	− 1.95
*Sis*RNA 11	NA	BdiBd21-3.1G1017200.1	Expansin-like related	− 0.84
*Sis*RNA 12	NA	BdiBd21-3.3G0134800.1	Copper transport protein ATOX1-related	− 1.11
*Sis*RNA 13	1.95	BdiBd21-3.2G0288400.1	LURP1-related	− 1.20
*Sis*RNA 14	NA	BdiBd21-3.1G0917100.1	Enolase	− 0.52
*Sis*RNA 15	NA	BdiBd21-3.4G0303000.1	Protein kinase domain protein	− 1.31
	NA	BdiBd21-3.1G0411900.1	Serine-type carboxypeptidase activity (Blast2GO)	− 0.82
*Sis*RNA 16	NA	BdiBd21-3.4G0507800.1	MYB transcrition factor	− 0.70
*Sis*RNA 17	NA	BdiBd21-3.1G0411900.1	Serine-type carboxypeptidase activity (Blast2GO)	− 0.82
*Sis*RNA 18	NA	BdiBd21-3.2G0269000.1	Mannose-binding lectin family	− 0.85
*Sis*RNA 19	NA	BdiBd21-3.3G0264400.1	Homologous to barley CONSTANS-like protein CO8	− 1.93
*Sis*RNA 20	NA	BdiBd21-3.5G0237900.1	Aquaporin transporter	− 1.02

sRNA expression was calculated as $\log_2$(colonized/control) from normalized reads, NA (not available) stands for sRNAs expressed exclusively in the colonized sample; transcript expression is indicated as the $\log_2$(colonized/control) FC

colonized roots. Of 3,019 predicted unique *Si* targets, 358 were confirmed as downregulated after colonization. This represents 12% of all significantly changed *Si* genes. 35% of the 358 *Si* transcripts are predicted to be targeted by Bd21-3 sRNAs exclusive to colonized tissue and an additional 27.6 % are targeted by sRNAs that are highly upregulated in colonized tissue ($log_2FC > 1$). A set of sRNA-mRNA duplexes, selected with the same criteria as for the *Si* sRNA – Bd21-3 targets (Table 4), shows that predicted Bd21-3 ck-sRNAs have putative targets in *Si* which include proteins associated with nutrient acquisition, development of cell walls, hyphal networks, pathogenic fungal activities, fungal starvation, and signaling (Table 5, Additional file 2: Table S7). In order to confirm the expression of some of these sRNAs, we conducted stem-loop PCR and sRNA-specific sequencing on 10 *Si* and 10 Bd21-3-originating sRNAs from our Bd-Si sample and Table S7. All *Si* and all Bd21-3 sRNAs were amplified in the stem-loop PCR. To verify the nature of the amplification products, a subset of four *Si*sRNAs and three *Bd*sRNAs were cloned and sent for Sanger sequencing, confirming the expected sRNA sequences (Additional file 2: Figure S12, original gel pictures in Additional file 3 and Additional File 4, sequencing results in Additional file 2: Table S8). Thus, predicted targets of putative ck-sRNAs within this system imply another layer of expression control within the mutualistic interaction.

Discussion

We established and studied the interaction between *Brachypodium distachyon*—a model Pooideae plant with shared synteny to major cereal crops—and *Serendipita indica*—a beneficial endophyte with an exceptionally large host range. This particular combination of traits adorning the *Bd-Si* interaction has great translational value towards filling in the gaps in knowledge about plant symbioses, especially their transcriptomic and sRNA expression profiles and the significance of RNAi. We show that *Si* colonizes *Bd*, resulting in shoot growth promotion, earlier flowering, and improved grain development. In comparison, earlier studies characterizing

Table 5 Examples of deduced duplexes of *Brachypodium distachyon* sRNAs and their downregulated targets in *Serendipita indica*

sRNA	sRNA expression	Transcript	Description of target transcript	Transcript expression
*Bd*sRNA 1	NA	CCA68723	Related to phenylalanine ammonia-lyase	− 5.1
*Bd*sRNA 2	1.43	CCA69635	Probable acetyl-CoA synthetase	− 2.19
*Bd*sRNA 3	0.04	CCA72153	Putative mitochondrial carnitine O-acetyltransferase	− 2.94
*Bd*sRNA 4	0.58	CCA68099	Probable protein required for hyphal anastomosis HAM2	− 1.38
*Bd*sRNA 5	0.59	CCA69082	Related to serine/threonine-protein kinase	− 1.65
*Bd*sRNA 6	0.039	CCA67801	Probable isocitrate lyase	− 2.34
*Bd*sRNA 7	4.37	CCA68918	Probable ADH1-alcohol dehydrogenase I	− 4.42
*Bd*sRNA 8	NA	CCA77975	Related to peroxisomal membrane protein 4	− 2.39
		CCA68099	Probable protein required for hyphal anastomosis HAM2	− 1.38
*Bd*sRNA 9	0.029	CCA73455	Related to phosphoprotein phosphatase 2C	− 0.89
*Bd*sRNA 10	1.39	CCA72944	Protein TOXD	− 2.73
		CCA72668	Hypothetical protein	− 1.68
		CCA74115	Probable nucleolar rRNA processing protein GAR1	− 0.93
*Bd*sRNA 11	0.19	CCA77931	Related to iron transport protein	− 2.4
*Bd*sRNA 12	0.48	CCA68412	Related to ECM32-DNA dependent ATPase/DNA helicase B	− 1.96
*Bd*sRNA 13	1.06	CCA75416	Related to estradiol 17 beta-dehydrogenase 4	− 2.12
*Bd*sRNA 14	NA	CCA73650	Related to chitinase	− 1.37
*Bd*sRNA 15	0.49	CCA77900	Related to LSB5-possible role in the regulation of actin cytoskeletal organization	− 1.27
*Bd*sRNA 16	0.62	CCA69912	Related to acyl-CoA dehydrogenase	− 2.28
*Bd*sRNA 17	0.88	CCA70015	Related to CAT1	− 1.84
*Bd*sRNA 18	NA	CCA68373	Probable subtilisin-like serine protease	− 0.91
*Bd*sRNA 19	1.38	CCA72980	Hypothetical protein	− 2.59
		CCA67021	Probable VID27-involved in vacuole import and degradation	− 0.93
*Bd*sRNA 20	0.1	CCA73174	Related to ECM4-involved in cell wall biogenesis and architecture	− 2.48

sRNA expression was calculated as log_2(colonized/control) from normalized reads, NA stands for sRNAs expressed exclusively in the colonized sample; transcript expression is indicated as the log_2(colonized/control) FC

the interaction between *Si* and barley have demonstrated that fungal hyphae establish an interface with the root cell plasma membrane at an early colonization stage, followed by expansion of an extracellular hyphal network, intercellular growth, and intracellular penetration of cortical and rhizodermal cells [26]. Around 3 to 5 DPI, *Si* starts the switch from a biotrophic to a saprophytic lifestyle [26, 27]. Although this change involves intracellular hyphae extensively colonizing dead host cells and gradual digestion of cortical cell walls, the plant still benefits from the fungal presence. Consistent with these findings, our microscopic analyses confirmed proliferation of *Si* chlamydospores and both inter- and intracellular colonization of Bd21-3 cells in the root differentiation zone from 4 to 14 DPI. Detection of proliferating hyphae that were not wrapped in plasma membrane further suggests that *Si* is colonizing dead surface plant root cells at 4 DPI [25, 26].

Transcriptional changes detected during the *Bd-Si* interaction

To investigate colonization of Bd21-3 by *Si*, we analyzed *Si* DEGs in colonized vs. axenic mycelium samples. Gene ontology analysis indicated enrichment in genes involved in various metabolic and catalytic processes. DEGs with the greatest changes in expression play roles in plant cell wall degradation, carbohydrate metabolism and nutrient acquisition. These changes in nutritional reprogramming are to be expected, considering the different nutritional content that *Si* has accessible in planta vs. axenic CM plates and a more detailed look into the roles of the changed genes unveils a typical switch of fungal lifestyle. Examples of upregulated *Si* genes involved in cell wall degradation include a probable *Pectate lyase*, *Endo-1,4-beta-xylanases*, *Cellulose 1,4-beta-cellobiosidase*, and *Rhamnogalacturonan acetylesterase*. The genes encoding these hydrolytic enzymes, which have undergone expansion in the *Si* genome [49], are similar to those upregulated in *Si* during saprophytic growth on autoclaved barley roots at 3 DPI and 5 DPI [22]. *PiAMT1*, encoding a high affinity ammonium transporter also was upregulated (logFC = 3.35; padj < 0.0001). Other upregulated genes encode enzymes involved in carbohydrate metabolism, including probable glucosidases, glucanase, and galactosidase. These proteins may modulate glucose concentration, which then regulates expression of some cell-wall degrading enzymes [22, 50]. Some of the 174 putative effector protein-encoding genes also are differentially expressed during *Si* colonization of barley and Arabidopsis [22, 27]. Six of these proteins (Additional file 2: Table S4) contain the *Si*-specific DELD domain, which suggests that *Si* utilizes a common protein effector arsenal to colonize various hosts. Considering highly downregulated *Si* DEGs, several encoded proteins are associated with adaption to nutrient availability (*Accumulation of dyads protein 2*, *ADY2*; *Succinate-fumarate transporter*) and nutrient acquisition (*Acyl-CoA dehydrogenase*; *Carnitine acetyltransferase*, *CRAT*; *Phenylalanine ammonia-lyase*, *PAL* [51, 52];). Their reduced expression suggests ample nutrient availability at 4 DPI. Given the similarities in the *Si* transcriptome during colonization of *Bd* and barley, we propose that these fungal-plant interactions follow a pattern, and that by 4 DPI, a network of plant-endophyte communication cues has initiated a tightly controlled transcriptional program, leading to a shift from biotrophic to saprophytic growth.

Roots of Bd21-3 plants also displayed substantial transcriptional reprogramming following *Si* colonization. Gene ontology term analysis indicated enrichment in genes involved in catalytic and oxidoreduction-associated processes. Bd21-3 DEGs exhibiting the greatest changes in expression between colonized and non-colonized plants are related to stress-response, defense, and plant development. Of the downregulated Bd21-3 genes, several encode proteins commonly associated with stress responses, including a peroxidase, a wound-induced protein, and a putative protein kinase. Additionally, members of the *Heat-shock protein* gene family [53] are commonly induced in *Bd* during abiotic stress and members of the *Abscisic acid/water deficit stress (ABA/WDS)-induced protein* and the *Rare cold inducible (RCI2)* gene families enhance abiotic stress tolerance in various plant species [54, 55]. Circadian clock and flowering regulation genes such as *Pseudo-response regulator 7* (*PRR7*), *Cold regulated protein 27* and *Constans-like protein* (*CO8*), also are downregulated during *Si* colonization. While members of the PRR and CO protein families work together to control flowering time [56, 57], any influence on early flowering in *Si*-colonized Bd21-3 is unclear. Circadian clock-associated genes also regulate lateral root development in Arabidopsis [58]; whether *Si*-induced changes in their expression influence root growth is unknown. Other downregulated development-associated DEGs include *Fantastic four meristem regulator* (*FAF*), which regulates shoot and root development [59], and putative *Sulfoquinovosyltransferase* (*SQD2*), which modulates seed setting and tiller development in rice [60]. Finally, several downregulated DEGs encode transcription factors, including MYB-related, GRAS, and bZIP.

In comparison, many of the upregulated Bd21-3 DEGs are associated with immune responses. Examples include genes encoding leucine-rich repeat (LRR) protein, a WRKY transcription factor, and thaumatin family protein. Increased expression of the defense gene *Pathogenesis-related protein 1* (*PR1*) was similarly and transiently reported in *Si*-colonized Arabidopsis roots [61]. Upregulation of *Glutathione S-transferase* (*GST*) is consistent

with the increased antioxidant capacity of *Si*-colonized plants, which provides protection against attack by necrotrophic pathogens [21, 62]. The upregulation of genes in other hormonal networks (*PGP-like Phosphoglycoprotein auxin transporter*) and redox processes (*Multicopper oxidase*) further suggests that *Si* colonization affects a range of signaling pathways.

Bd miRNAs detected in the Bd-Si sample

The role of miRNAs as regulators of gene expression in the Sebacinalean symbiosis is largely unexplored. One report showed that *Si* induces growth promotion-associated miRNAs in *Oncidium* orchid roots [63]. Analysis of putative endogenous Bd21-3 sRNAs expressed during *Si* colonization identified 16 miRNAs. Some of them have known targets in transcription factors associated with plant growth and development. For example, the bdi-MIR166 family targets mRNAs encoding *Homeobox domain-leucine zipper* transcription factors [64]. In Arabidopsis, repression of these transcription factors by the miR165/166 family modulates root growth, maintenance of the shoot apical meristem, and development of leaf polarity [65]. Plant-specific transcription factors encoded by *Squamosa promoter-binding protein-like* (*SPL*) genes are the presumed targets of bdi-MIR156 and bdi-MIR529 [66]. In Arabidopsis, miR156-mediated downregulation of SPLs modulates developmental timing, lateral root development, branching, and leaf morphology [65]. Members of the *MYB* superfamily of transcription factors, which regulate many aspects of development, are the predicted targets of bdi-MIR159 [34]. Interestingly, miRNAs belonging to the miR159 and miR166 families in cotton are known ck-sRNAs that target virulence genes in *Verticillium dahliae* [13].

Other miRNAs identified in Bd21-3 include bdi-MIR168, predicted to target *AGO1* [64], and two miRNAs that regulate nutrition: bdi-MIR399, which is upregulated in *Bd* by phosphate starvation [64, 67], whereas bdi-MIR408 influences copper levels [34, 68]. Additionally, bdi-MIR408 (*Bd*sRNA 10) has predicted ck targets in three *Si* transcripts: *CCA72944*, *CCA72668*, and *CCA74115*. Since various targets were predicted for bdi-MIR167 [34, 68] and no target was predicted for bdi-MIR9481, their endogenous functions in *Bd* are unclear. Interestingly, the miRNA families identified in our analysis, except bdi-MIR9481, also were detected in *Si*-colonized *Oncidium* [63]. Thus, this group of miRNAs may play an important role in reprogramming plant cells during Sebacinalean symbiosis establishment.

Putative *Si* and Bd21-3 ck-sRNAs and their predicted targets

To date, cross-kingdom RNAi has been demonstrated in pathogenic plant-fungal interactions [12, 13, 69], and while there are promising indications for its presence during plant-mycorrhiza interactions [36], whether it occurs in *Si*-plant associations is unknown. To investigate this possibility, we predicted targets for 21 nt putative ck-sRNAs from *Si* and Bd21-3 and confirmed their downregulation during colonization. This analysis uncovered 358 downregulated *Si* transcripts that are the predicted targets of 228 unique Bd21-3 sRNAs. Cross-kingdom RNAi-mediated downregulation of these targets might allow Bd21-3 to modulate *Si* growth during colonization. For example, *PAL*, *Acetyl-CoA synthetase*, *Carnitine acetyl transferase*, *Isocitrate lyase*, and *Acyl-CoA dehydrogenase*, which are targeted by *Bd*sRNA 1, *Bd*sRNA 2, *Bd*sRNA 3, *Bd*sRNA 6, and *Bd*sRNA 16 (Table 5), are involved in fungal nutrient acquisition [22, 55, 70, 71]. Genes with important homologs in pathogenic fungi also are predicted targets, including *Subtilisin-like serine protease* (*Bd*sRNA 18) [72], *Alcohol dehydrogenase 1* (*Bd*sRNA 7) [73], and *Phosphoprotein phosphatase 2C* (*Bd*sRNA 9) [74]. Targeting of *Hyphal anastomosis-2* (*HAM-2*) by *Bd*sRNA 8 and *Bd*sRNA 4 may provide another mechanism for controlling fungal growth, as HAM-2 is required for hyphal fusion in *N. crassa* [75]. Similarly, targeting of *Chitinase* (*Bd*sRNA 14) may help control *Si* growth.

Concurrently, we identified 49 downregulated Bd21-3 mRNAs that are the predicted targets of 63 unique *Si*-generated ck-sRNAs. Downregulation of these target genes via cross-kingdom RNAi might facilitate *Si* growth during colonization. For example, *Mannose-binding lectin* (targeted by *Sis*RNA 18) belongs to a family of defense-related genes whose products trigger immune responses following pathogen recognition [76]. *Sis*RNA 8 and *Sis*RNA 15 target a protein kinase domain/LRR gene (*BdiBd21-3.4G0303000.1*) that may belong to the LRR receptor kinase family, which regulates defense and developmental-related processes [77]. Transcripts encoding serine-carboxypeptidase-like (SCPL) proteins *BdiBd21-3.2G0440200.1* and *BdiBd21-3.1G0411900.1* (targeted by *Sis*RNA 1 and *Sis*RNA 15) are associated with defense against (a)biotic stresses in monocots [78]. Members of various transcription factors families also were identified as predicted targets (*MYB* by *Sis*RNA 16, *bZIP* by *Sis*RNA 2, and *GRAS* by *Sis*RNA 10). These families are associated with (a)biotic stress responses, as well as plant growth and development [79–81]. Lastly, transcripts for proteins involved in circadian clock and flowering regulation (*BdiBd21-3.1G0887100.1* and *BdiBd21-3.3G0264400.1* [56];) are the presumed targets of *Sis*RNA 1 and *Sis*RNA 19. Together, these findings suggest that *Si*-derived ck-sRNAs may promote fungal colonization by targeting signaling processes associated with plant development and responses to (a)biotic stresses.

In combination with earlier studies on *Bd* RNAi proteins [35] and *Bd* interaction with the pathogen *Magnaporthe oryzae* [82], the in silico analyses presented here suggest that *Si* and *Bd* contain functional RNAi components and that both organisms generate ck-sRNAs, which potentially modulate this mutualistic interaction. However, further studies are necessary to validate cross-kingdom RNAi in a Sebacinalean symbiosis. Namely, degradome analysis is needed to confirm target degradation and evidence that Bd21-3 and *Si* AGOs associate with sRNAs expressed by the interacting organism is necessary for confirmation of cross-kingdom RNAi.

Conclusions

We report that Bd21-3 and *Si* form a mutualistic symbiosis with a promoting effect on plant yield and development, accompanied by changes in gene expression in both organisms, including putative protein *Si* effectors and RNAi-related genes. sRNA profiles of both organisms also changed, indicating that this model system will provide important insights into the multiple layers of regulation and interaction between beneficial fungi and cereal hosts. Within the broader scope of plant-mutualist interactions, we show that detection of putative RNAi-involved sRNAs in an interaction highly benefits from simultaneous transcriptome analysis and indicate an involvement of sRNA-based regulation in defense responses, nutritional reprogramming, and colonization maintenance. Alongside other experimental approaches in plant-microbe interactions (eg. sRNA uptake studies [83]), developing a deeper understanding of the communication mechanisms that modulate mutualistic interactions is highly relevant for establishing robust growth promotion and protection strategies in crops.

Methods

Bd and *Si* cultivation and inoculation

The seeds of *Brachypodium distachyon* (*Bd*) line Bd21-3 (gift from R. Sibout, INRA Versailles, France) were surface sterilized (3% active chlorine, sodium hypochlorite solution) for 15 min, washed three times, and placed on half-strength MS [84] medium in dark at 4 °C for 2 days and then 7 days at 24 °C and 16 h light/8 h dark cycle (47 μmol m^{-2} s^{-1} photon flux density). *Serendipita indica* (*Si*) (IPAZ-11827, Institute of Phytopathology, Giessen, Germany) was grown on complete media plates (CM [85]) at 23 °C in dark for 4–5 weeks.

For inoculation, *Si* mycelium was collected in 0.002% aqueous Tween 20 solution, filtered (Miracloth, Calbiochem), and pelleted by centrifugation (10 min/4000 rpm/20 °C) twice. Chlamydospore concentration of 5 × 10^5 conidia ml^{-1} in 0.002% Tween 20 solution was used to inoculate 7-day-old plant seedlings for 2–3 h. Control plants were mock treated with the 0.002% Tween 20 solution for the same time. Grain yield analyses were done on mature plants grown on soil (F-E type LD 80, Fruhstorfer Erde, Germany) under 16 h light (160 μmol m^{-2} s^{-1}, 22 °C) and 8 h dark (18 °C) conditions at 60% relative humidity for 1 month, and then greenhouse conditions until seed maturity. Number of spikelets was assessed after 2 months. Shoot biomass was assessed 3 weeks after inoculation of seedlings grown on a mixture (2:1, v/v) of vermiculite (Deutsche Vermiculite GmbH) and oil dri (oil binder Typ III R Coarse grain, Damolin, Mettmann, Germany) under comparable conditions as for grain yield, and fertilized every 3 days with an aqueous solution of Wuxal Super NPK-8/8/6 (1:10^3 v/v; Haug, Düsseldorf, Germany). Samples for RNA-seq, RT-qPCR, stem-loop PCR, and microscopy were also grown under these conditions. To assess growth promotion in *Si* inoculated *Bd* relative to the control, we used the pairwise *t* test or the Mann-Whitney-Wilcoxon test on each of the three repetitions of experiments, after checking for normality and homogenous variances. Benjamini-Hochberg correction for multiple testing was used to correct the *p* values and the significance asterisks were assigned to the average p-value as follows: * for $p \leq 0.05$, ** for $p \leq 0.001$, and *** for $p \leq 0.0001$.

Microscopy

Following *Si* inoculation, one-week-old seedlings were grown on plastic mesh (~ 90 μm) placed over half-strength MS medium or on vermiculite/oil dri prior to assessing root colonization. *Si* was visualized with the chitin-specific dye WGA-AF 488 (wheat germ agglutinin; Molecular Probes, Karlsruhe, Germany), as described in Deshmukh *et al.* (2006) [26], with boiling in KOH (10%) for 30 s, prior to incubation in phosphate-buffered saline (PBS, pH 7.4). Root cells were visualized by incubating with propidium iodide (10 μg ml^{-1}) for 10 min and washing with sterile water. Confocal laser scanning microscopy was done (TCS SP8 microscope, Leica, Bensheim, Germany) and the Leica LAS X software was utilized for visualization and maximum (*z*-stack) projections.

Resequencing, assembly, and annotation of the *Si* genome

The MasterPure Yeast DNA Purification Kit (Epicentre, Illumina) was used to extract genomic DNA from 4-week-old axenic *Si* cultures. The *Si* genome was resequenced, assembled [86], and annotated as described [87], whereby a MinION sequencing library

was prepared using the Nanopore Rapid DNA Sequencing kit. Sequencing was performed on an Oxford Nanopore MinION Mk1b sequencer using a R9.5 flow cell. Additionally, sequencing of an Illumina Nextra XT library was performed on the MiSeq platform (Illumina; 2 × 300 bp paired-end sequencing, v3 chemistry). Adapters and low-quality reads were removed by an in-house software pipeline prior to polishing [88]. MinKNOW (v1.13.1, Oxford Nanopore Technologies) was used to control the run with the 48 h sequencing run protocol, and base calling was performed offline using albacore (v2.3.1, Oxford Nanopore Technologies). The assembly was performed using Canu v1.6 ([89], default settings). The resulting contigs were polished with Illumina short read data using Pilon [90] for eight iterative cycles. BWA-MEM [91] was used for read mapping in the first four iterations and Bowtie2 v2.3.2 [92] in the second set. Gene prediction was performed with GeneMark-ES 4.3.3. ([38], default settings). Predicted genes were functionally annotated using a modified version of the genome annotation platform GenDB 2.0 [39] for eukaryotic genomes [40]. RNAi-associated proteins were predicted by searching the proteome [22] for typical domain structure and highest homology to *Neurospora crassa* RNAi proteins (NC12 genome assembly [93]). A modified version of the pipeline from Rafiqi et al. (2013) [41] was used to predict protein effectors. After identifying proteins with signal peptides (signalp-4.1 [94]), those predicted as transmembrane helix proteins (tmhmm [95]), mitochondrial proteins (target-1.1 [96]), and cell wall hydrolysis-associated proteins were removed. For comparative analysis of the *Si* (Si-2020 and DSM11827 ASM31354 v.1 [22]), *Serendipita vermifera* [97] and *Laccaria bicolor* [98] genomes, software platform EDGAR 2.3 [99] was used.

RNA extraction, library preparation, and mRNA/sRNA sequencing

Roots inoculated with *Si* (Bd-Si) or mock-inoculated (Bd-C), as described above, were grown for 4 days and pooled (three roots per sample). *Si* mycelium and spores were collected from 4-week-old axenic cultures grown on CM medium. All samples in triplicates were shock frozen, stored at − 80 °C, and ground in liquid N_2. Total RNA was isolated using the ZymoBIOMICS RNA Mini Kit (Zymo Research, USA), quantified with DropSense16/Xpose (BIOKÉ, Netherlands), and analyzed with an Agilent 2100 Bioanalyzer Nano Chip (Agilent, Germany). RNA Clean and Concentrator 25 and 5 kits (Zymo Research) were utilized to separate total RNA into fractions: 17–200 nt and > 200 nt. 1.5 μg of the larger fractions were processed for mRNA library preparation (TruSeq Stranded mRNA protocol, Illumina, USA). Fragment Analyzer Automated CE System (Advanced Analytical Technologies, Austria) determined the quality of the generated polyA mRNA libraries. Quantity and quality of the smaller RNA fractions were assessed with the Qubit fluorometer (Invitrogen, Germany) and Agilent 2100 Bioanalyzer Pico Chip. sRNA library preparation was done with 50 ng of RNA (TruSeq Small RNA Library Prep, Illumina) and size selection with the BluePippin (Sage Science, USA) for fragments between 140 and 160 nt (15–35 nt without adapters) applied. Sequencing was accomplished on the Illumina HiSeq 1500.

Transcriptome analysis

Raw reads from mRNA sequencing [100] were submitted to quality check using FastQC [101] and aligned to the Bd21-3 v1.1 (DOE-JGI, http://phytozome.jgi.doe.gov/ [102]) or resequenced *Si* (Si-2020) genomes with HISA T2 [103]. An intron length of 20–2000 nt was allowed for *Si* [104] and 20–10,000 nt for Bd21-3 [105]. The reads were counted using HTSeq-count [106], differential gene expression was performed with DESeq2 [107], and gene enrichment analysis with AgriGO v.2 [108], with reference Bd21 setting for Bd21-3 (Bd 21 synonyms) and a customized background for *Si*. Volcano plots were generated using plotly [109] and ggplot2 [110] R [111] libraries. Gene descriptions were obtained from the organism annotations or Blast2GO [112].

sRNA analysis and prediction of putative endogenous and ck-sRNAs

Raw reads from sRNA sequencing [113] were submitted to FastQC [101] and adapter trimming [114]. Bowtie [115] was used for alignment as detailed in Additional file 2: Fig. S6. The resequenced *Si* genome was used for alignments of fungal origin. tRNA/rRNA sequences were downloaded from RNAcentral ([116], EMBL-EBI). Putative endogenous sRNA reads were submitted to ShortStack [117]. For filtering putative ck-sRNAs, a previously established pipeline [118] was utilized. Reads were normalized to the total number of mapped reads for a single genome and reads per million (RPM) and $\log_2$ (colonized/mock-treated) values calculated. Thus, a sRNA read was selected as a putative ck-sRNA if it was present exclusively or at a higher quantity (i.e., induced) in the colonized vs. control sample. Putative ck-sRNAs were submitted to psRNAtarget [119]. Since the separation of sRNA and mRNA fractions from each biological sample was facilitated, we checked for downregulation of mRNAs corresponding to predicted sRNA target genes within the DEGs. Transcriptomes used for these predictions were Bd 21-3 v1.1 (DOE-JGI, http://phytozome.jgi.doe.gov/ [102]) and *Si* DSM11827 ASM31354 v.1 [22].

Venn diagrams were generated using the VennDiagram R package [120].

Quantitative real-time PCR and stem-loop PCR for validation of sequencing results

To validate gene expression detected in the sequencing, we used quantitative real-time PCR (qRT-PCR). RNA extraction from mock treated and *Si* inoculated Bd21-3 roots, as well as *Si* axenic cultures, under the same conditions as explained above for the sequencing, was done with TRIzol (Thermo Fisher Scientific, Waltham, MA, USA), cDNA synthesized using qScriptTM cDNA kit (Quantabio, Beverly, MA, USA) and 10 ng of cDNA used as template in the QuantStudio 5 Real-Time PCR system (Applied Biosystems), with SYBR® green JumpStart Taq ReadyMix (Sigma-Aldrich, St. Louis, MO, USA). Each sample had three technical replicates. Primers used for these amplifications are listed in Table S9 (Additional file 2: Table S9). Transcript levels were calculated using the 2−ΔΔCt method [121], relatively to *BdUbi4-3* for Bd21-3 and *Si ITS* sequence for *Si*.

For the identification of sRNAs in the interaction of *Si* with Bd21-3 stem-loop RT-PCR was employed [122]. cDNA was synthesized from DNase I-treated total RNA extracted from *Si* axenic culture or inoculated Bd21-3 roots. The folding of the hairpin primer was performed according to Kramer (2011) [123]. For each stem-loop reaction, six hairpin primers were multiplexed in a 20-μL reaction using the Revertaid RT enzyme according to the manufacturer's instructions (Thermo Scientific). For primer annealing, the reaction was incubated for 30 min at 16 °C followed by an extension step at 42 °C for 30 min. The reaction was stopped at 85 °C for 5 min. cDNA was stored at − 80 °C until further use. Endpoint PCR was performed using an universal stem-loop primer and specific sRNA primer (Additional file 2: Table S10) under the following conditions: initial denaturation at 95 °C for 5 min followed by 35 cycles: 95 °C for 30 s, primer annealing at 60 °C for 30 s, and extension at 72 °C for 30 s. PCR products were separated by gel electrophoresis on a 2% (*w*/*v*) agarose gel. To obtain sequence information of the amplified sRNAs of the stem-loop reaction, PCR products were purified and cloned into the pGEM®-T Easy Vector Systems (Promega, Madison, WI, USA) following the manufacturer's instructions. From each cloned sRNA, six colonies were further analyzed by Sanger sequencing using a M13 reverse primer.

Abbreviations

AGO: Argonaute; *Bd*: *Brachypodium distachyon*; Bd-C: Mock-inoculated *Bd* root sample; Bd-Si: *Si*-inoculated *Bd* root sample; *Bd*sRNA: *Brachypodium distachyon*-derived sRNA; ck-sRNA: Cross-kingdom sRNA; DCL: Dicer-like; DEG: Differentially expressed gene; DPI: Day(s) post inoculation; FC: Fold change; miRNA: MicroRNA; nt: Nucleotide; RdRP: RNA-dependent RNA polymerase; RNAi: RNA interference; *Si*: *Serendipita indica*; Si-ax: *Si* axenic culture sample; *Si*sRNA: *Serendipita indica*-derived sRNA; sRNA: Small RNA

Supplementary Information

The online version contains supplementary material available at https://doi.org/10.1186/s12915-021-01104-2.

Additional file 1. Supporting individual data values displayed in Figure 1a-c and Additional File 2: Figure S5.

Additional file 2: Fig. S1. *Serendipita indica* (*Si*) colonization has an effect on *Brachypodium distachyon* (*Bd*) root structure. **Fig. S2.** Progress of *Serendipita indica* (*Si*) spore proliferation during colonization of *Brachypodium distachyon* Bd21-3. **Fig. S3.** Comparison of the resequenced *Serendipita indica* (*Si*) genome to the 2011 assembly. **Fig.S4.** Comparison of the resequenced *Serendipita indica* (*Si*) genome to *Serendipita vermifera* and *Laccaria bicolor*. **Fig. S5**. qRT-PCR confirmation of DEGs identified during mRNA sequencing. **Fig. S6.** Filtering pipelines applied in the analysis. **Fig. S7.** Size distribution of total and unique putative ck (cross-kingdom) -sRNAs. **Fig. S8.** Percentage distribution of the 5′ terminal nucleotide in unique putative endogenous sRNAs. **Fig. S9.** Percentage distribution of the 5′ terminal nucleotide in unique putative ck-sRNAs. **Fig. S10.** Percentage distribution of the 5′ terminal nucleotide in total putative endogenous sRNAs. **Fig. S11.** Percentage distribution of the 5′ terminal nucleotide in total putative ck-sRNAs. **Fig. S12.** Stem-loop PCR (gel electrophoresis) of some *Si* and Bd21-3 sRNAs expressed in the Bd-Si sample. **Table S1.** Quantification of identified features in the resequenced genome of *Serendipita indica* (*Si*). **Table S2.** Total reads from the Bd-C (mock-treated), Bd-Si (colonized root) and Si-ax (axenic culture) samples and their alignment rate (HISAT2) to the corresponding genomes. **Table S3.** Significant gene ontology terms of molecular function in the differentially expressed genes (DEGs) datasets. **Table S4.** Predicted protein effectors identified in the resequenced *Serendipita indica* (*Si*) genome. **Table S5.** Candidate RNAi machinery proteins predicted from the resequenced *Serendipita indica* (*Si*) genome. **Table S6.** Total and unique reads for filtered sRNAs from Bd-C (mock-treated), Bd-Si (colonized root) and Si-ax (axenic culture). **Table S7.** Sequences of putative sRNAs in Tables 4 and 5. **Table S8**. sRNA sequences after stem-loop PCR amplification. **Table S9.** Primers used for qRT-PCR (Figure S5). **Table S10.** Primers used for stem-loop PCR and sequencing (Figure S12, Table S8).

Additional file 3. Uncropped gel picture annotated in Additional file 2: Figure S12a.

Additional file 4. Uncropped gel picture annotated in Additional file 2: Figure S12b.

Acknowledgements

We thank Elke Stein, Dagmar Biedenkopf, Ute Micknass and Christina Birkenstock for technical assistance. We thank Dr. John Vogel and the DOE-JGI for permission to use the Bd21-3 genome under early access conditions. *Brachypodium distachyon* Bd21-3 is a gift of R. Sibout, INRA Versailles. We are very thankful to D'Maris Dempsey for her assistance in preparation of the manuscript.

Authors' contributions

EŠ, SZ, DW, and KHK wrote the text and drafted the figures. EŠ and SZ designed and conducted the establishment experiments, EŠ, SZ, TB, DW, LJ, and JK conducted the RNAseq and genome resequencing experiments and analyzed the data. SN and JS conducted the stem-loop PCR experiments and sequencing analysis. JI and JT performed microscopy in sterile conditions. All authors read and approved the final manuscript.

Funding

This work was supported by the Deutsche Forschungsgemeinschaft (DFG), Research Training Group (RTG) 2355, and Research Unit FOR5116 to KHK. We gratefully acknowledge the bioinformatics support of the BMBF-funded project Bielefeld-Gießen Center for Microbial Bioinformatics-BiGi (grant number 031A533) within the German Network for Bioinformatics Infrastructure (de.NBI). Open Access funding enabled and organized by Projekt DEAL.

Availability of data and materials

All data generated or analyzed during this study are included in this published article, its supplementary information files (Additional files 1, 2, 3 and 4) and publicly available repositories. mRNA and sRNA-seq of

Brachypodium distachyon roots inoculated with *Serendipita indica* datasets are available in the ArrayExpress database at EMBL-EBI (www.ebi.ac.uk/arrayexpress) under accession numbers E-MTAB-10649 and E-MTAB-10650, respectively. The genome assembly data for *Serendipita indica* resequencing study is available in the European Nucleotide Archive (ENA) at EMBL-EBI under accession numbers: assembly GCA_910890315 and study PRJEB45884 (https://www.ebi.ac.uk/ena/browser/view/PRJEB45884).
Additional publicly available datasets have been accessed from the corresponding European Nucleotide Archive accessions and EnsemblFungi: *Serendipita indica* 2011 genome (GCA_000313545.1) [22], NC12 of *Neurospora crassa* (GCA_000182925.2) [93]. *Serendipita vermifera* subsp. bescii [97] has been accessed from JGI MycoCosm (https://mycocosm.jgi.doe.gov/Sebvebe1/Sebvebe1.home.html), as was the *Laccaria bicolor* genome ([98], https://mycocosm.jgi.doe.gov/Lacbi2/Lacbi2.home.html).
The Bd21-3 v1.1 genome [102] was accessed under early access conditions and these sequence data were produced by the US Department of Energy Joint Genome Institute - DOE-JGI, http://phytozome.jgi.doe.gov/.

Declarations

Ethics approval and consent to participate
Not applicable.

Consent for publication
Not applicable.

Competing interests
The authors declare that they have no competing interests.

Author details
[1]Institute of Phytopathology, Centre for BioSystems, Land Use and Nutrition, Justus Liebig University, 35392 Giessen, Germany. [2]Center for Biotechnology - CeBiTec, Bielefeld University, 33615 Bielefeld, Germany. [3]Institute of Bioinformatics and Systems Biology, Justus Liebig University, 35392 Giessen, Germany.

Received: 17 December 2020 Accepted: 16 July 2021
Published online: 24 August 2021

References
1. Marschner P, Yang C-H, Lieberei R, Crowley DE. Soil and plant specific effects on bacterial community composition in the rhizosphere. Soil Biol Biochem. 2001;33(11):1437–45. https://doi.org/10.1016/S0038-0717(01)00052-9.
2. Lagunas B, Schäfer P, Gifford ML. Housing helpful invaders: the evolutionary and molecular architecture underlying plant root-mutualist microbe interactions. J Exp Bot. 2015;66(8):2177–86. https://doi.org/10.1093/jxb/erv038.
3. Kogel KH, Franken P, Hückelhoven R. Endophyte or parasite – what decides? Curr Opin Plant Biol. 2006;9(4):358–63. https://doi.org/10.1016/j.pbi.2006.05.001.
4. Fesel PH, Zuccaro A. Dissecting endophytic lifestyle along the parasitism/mutualism continuum in Arabidopsis. Curr Opin Microbiol. 2016;32:103–12. https://doi.org/10.1016/j.mib.2016.05.008.
5. Kloppholz S, Kuhn H, Requena N. A secreted fungal effector of *Glomus intraradices* promotes symbiotic biotrophy. Curr Biol. 2011;21(14):1204–9. https://doi.org/10.1016/j.cub.2011.06.044.
6. Doehlemann G, Requena N, Schaefer P, Brunner F, O'Connell R, Parker JE. Reprogramming of plant cells by filamentous plant-colonizing microbes. New Phytol. 2014;204(4):803–14. https://doi.org/10.1111/nph.12938.
7. Vishwakarma K, Kumar N, Shandilya C, Mohapatra S, Bhayana S, Varma A. Revisiting plant–microbe interactions and microbial consortia application for enhancing sustainable agriculture: a review. Front Microbiol. 2020;11:3195.
8. Baulcombe D. RNA silencing in plants. Nature. 2004;431(7006):356–63. https://doi.org/10.1038/nature02874.
9. Fang X, Qi Y. RNAi in plants: an Argonaute-centered view. Plant Cell. 2016;28(2):272–85. https://doi.org/10.1105/tpc.15.00920.
10. Uhse S, Djamei A. Effectors of plant-colonizing fungi and beyond. PLOS Pathog. 2018;14(6):e1006992. https://doi.org/10.1371/journal.ppat.1006992.
11. Akum FN, Steinbrenner J, Biedenkopf D, Imani J, Kogel KH. The *Piriformospora indica* effector PIIN_08944 promotes the mutualistic Sebacinalean symbiosis. Front Plant Sci. 2015;6:1–12.
12. Weiberg A, Wang M, Lin F-M, Zhao H, Zhang Z, Kaloshian I, et al. Fungal small RNAs suppress plant immunity by hijacking host RNA interference pathways. Science (80-). 2013;342(6154):118–23.
13. Zhang T, Zhao YL, Zhao JH, Wang S, Jin Y, Chen ZQ, et al. Cotton plants export microRNAs to inhibit virulence gene expression in a fungal pathogen. Nat Plants. 2016;2(10):1–6.
14. Kellogg EA. *Brachypodium distachyon* as a genetic model system. Annu Rev Genet. 2015;49(1):1–20. https://doi.org/10.1146/annurev-genet-112414-055135.
15. Qiang X, Weiss M, Kogel KH, Schäfer P. *Piriformospora indica*-a mutualistic basidiomycete with an exceptionally large plant host range. Mol Plant Pathol. 2012;13(5):508–18. https://doi.org/10.1111/j.1364-3703.2011.00764.x.
16. Stein E, Molitor A, Kogel KH, Waller F. Systemic resistance in Arabidopsis conferred by the mycorrhizal fungus *Piriformospora indica* requires jasmonic acid signaling and the cytoplasmic function of NPR1. Plant Cell Physiol. 2008;49(11):1747–51. https://doi.org/10.1093/pcp/pcn147.
17. Deshmukh SD, Kogel KH. *Piriformospora indica* protects barley from root rot caused by *Fusarium graminearum*. J Plant Dis Prot. 2007;114(6):263–8. https://doi.org/10.1007/BF03356227.
18. Trzewik A, Maciorowski R, Klocke E, Orlikowska T. The influence of *Piriformospora indica* on the resistance of two rhododendron cultivars to *Phytophthora cinnamomi* and *P. plurivora*. Biol Control. 2020;140:104121.
19. Fakhro A, Andrade-Linares DR, von Bargen S, Bandte M, Büttner C, Grosch R, et al. Impact of *Piriformospora indica* on tomato growth and on interaction with fungal and viral pathogens. Mycorrhiza. 2010;20(3):191–200. https://doi.org/10.1007/s00572-009-0279-5.
20. Baltruschat H, Fodor J, Harrach BD, Niemczyk E, Barna B, Gullner G, et al. Salt tolerance of barley induced by the root endophyte *Piriformospora indica* is associated with a strong increase in antioxidants. New Phytol. 2008;180(2):501–10. https://doi.org/10.1111/j.1469-8137.2008.02583.x.
21. Waller F, Achatz B, Baltruschat H, Fodor J, Becker K, Fischer M, et al. The endophytic fungus *Piriformospora indica* reprograms barley to salt-stress tolerance, disease resistance, and higher yield. Proc Natl Acad Sci U S A. 2005;102(38):13386–91. https://doi.org/10.1073/pnas.0504423102.
22. Zuccaro A, Lahrmann U, Güldener U, Langen G, Pfiffi S, Biedenkopf D, et al. Endophytic life strategies decoded by genome and transcriptome analyses of the mutualistic root symbiont *Piriformospora indica*. PLoS Pathog. 2011;7(10) Serendipita indica genome assembly. 2011. GCA accession number: GCA_000313545.1 (https://www.ebi.ac.uk/ena/browser/view/GCA_000313545.1).
23. Zuccaro A, Basiewicz M, Zurawska M, Biedenkopf D, Kogel KH. Karyotype analysis, genome organization, and stable genetic transformation of the root colonizing fungus *Piriformospora indica*. Fungal Genet Biol. 2009;46(8):543–50. https://doi.org/10.1016/j.fgb.2009.03.009.
24. Schäfer P, Pfiffi S, Voll LM, Zajic D, Chandler PM, Waller F, et al. Manipulation of plant innate immunity and gibberellin as factor of compatibility in the mutualistic association of barley roots with *Piriformospora indica*. Plant J. 2009;59(3):461–74. https://doi.org/10.1111/j.1365-313X.2009.03887.x.
25. Jacobs S, Zechmann B, Molitor A, Trujillo M, Petutschnig E, Likpa V, et al. Broad-spectrum suppression of innate immunity is required for colonization of Arabidopsis roots by the fungus *Piriformospora indica*. Plant Physiol. 2011;156(2):726–40. https://doi.org/10.1104/pp.111.176446.
26. Deshmukh S, Hückelhoven R, Schäfer P, Imani J, Sharma M, Weiss M, et al. The root endophytic fungus *Piriformospora indica* requires host cell death for proliferation during mutualistic symbiosis with barley. Proc Natl Acad Sci U S A. 2006;103(49):18450–7. https://doi.org/10.1073/pnas.0605697103.
27. Lahrmann U, Ding Y, Banhara A, Rath M, Hajirezaei MR, Döhlemann S, et al. Host-related metabolic cues affect colonization strategies of a root endophyte. Proc Natl Acad Sci U S A. 2013;110(34):13965–70. https://doi.org/10.1073/pnas.1301653110.
28. Scholthof K-BG, Irigoyen S, Catalan P, Mandadi KK. Brachypodium: a monocot grass model genus for plant biology. Plant Cell. 2018;30(8):1673–94. https://doi.org/10.1105/tpc.18.00083.
29. Vogel J, Hill T. High-efficiency Agrobacterium-mediated transformation of *Brachypodium distachyon* inbred line Bd21-3. Plant Cell Rep. 2008;27(3):471–8. https://doi.org/10.1007/s00299-007-0472-y.
30. Vogel JP, Garvin DF, Mockler TC, Schmutz J, Rokhsar D, Bevan MW, et al. Genome sequencing and analysis of the model grass *Brachypodium distachyon*. Nature. 2010;463(7282):763–8.
31. Hsia MM, O'Malley R, Cartwright A, Nieu R, Gordon SP, Kelly S, et al. Sequencing and functional validation of the JGI *Brachypodium distachyon* T-DNA collection. Plant J. 2017;91(3):361–70. https://doi.org/10.1111/tpj.13582.

32. Fitzgerald TL, Powell JJ, Schneebeli K, Hsia MM, Gardiner DM, Bragg JN, et al. Brachypodium as an emerging model for cereal-pathogen interactions. Ann Bot. 2015;115(5):717–31. https://doi.org/10.1093/aob/mcv010.
33. Zhang J, Xu Y, Huan Q, Chong K. Deep sequencing of Brachypodium small RNAs at the global genome level identifies microRNAs involved in cold stress response. BMC Genomics. 2009;10(1):449. https://doi.org/10.1186/1471-2164-10-449.
34. Bertolini E, Verelst W, Horner DS, Gianfranceschi L, Piccolo V, Inzé D, et al. Addressing the role of microRNAs in reprogramming leaf growth during drought stress in *Brachypodium distachyon*. Mol Plant. 2013;6(2):423–43. https://doi.org/10.1093/mp/sss160.
35. Šečić E, Zanini S, Kogel KH. Further elucidation of the Argonaute and Dicer protein families in the model grass species *Brachypodium distachyon*. Front Plant Sci. 2019;10:1332. https://doi.org/10.3389/fpls.2019.01332.
36. Silvestri A, Fiorilli V, Miozzi L, Accotto GP, Turina M, Lanfranco L. In silico analysis of fungal small RNA accumulation reveals putative plant mRNA targets in the symbiosis between an arbuscular mycorrhizal fungus and its host plant. BMC Genomics. 2019;20(1):1–18.
37. Ren B, Wang X, Duan J, Ma J. Rhizobial tRNA-derived small RNAs are signal molecules regulating plant nodulation. Science (80-). 2019;365:919–22.
38. Ter-Hovhannisyan V, Lomsadze A, Chernoff YO, Borodovsky M. Gene prediction in novel fungal genomes using an *ab initio* algorithm with unsupervised training. Genome Res. 2008;18(12):1979–90. https://doi.org/10.1101/gr.081612.108.
39. Meyer F, Goesmann A, McHardy AC, Bartels D, Bekel T, Clausen J, et al. GenDB--an open source genome annotation system for prokaryote genomes. Nucleic Acids Res. 2003;31(8):2187–95. https://doi.org/10.1093/nar/gkg312.
40. Rupp O, Becker J, Brinkrolf K, Timmermann C, Borth N, Pühler A, et al. Construction of a public CHO cell line transcript database using versatile bioinformatics analysis pipelines. PLoS One. 2014;9(1):e85568. https://doi.org/10.1371/journal.pone.0085568.
41. Rafiqi M, Jelonek L, Akum NF, Zhang F, Kogel KH. Effector candidates in the secretome of *Piriformospora indica*, a ubiquitous plant-associated fungus. Front Plant Sci. 2013;4:228.
42. Billmyre RB, Calo S, Feretzaki M, Wang X, Heitman J. RNAi function, diversity, and loss in the fungal kingdom. Chromosome Res. 2013;21(6–7):561–72. https://doi.org/10.1007/s10577-013-9388-2.
43. Dang Y, Yang Q, Xue Z, Liu Y. RNA interference in fungi: pathways, functions, and applications. Eukaryot Cell. 2011;10(9):1148 LP–1155.
44. Lau P-W, Guiley KZ, De N, Potter CS, Carragher B, MacRae IJ. The molecular architecture of human Dicer. Nat Struct Mol Biol. 2012;19(4):436–40. https://doi.org/10.1038/nsmb.2268.
45. Cenik ES, Zamore PD. Argonaute proteins. Curr Biol. 2011;21(12):R446–9. https://doi.org/10.1016/j.cub.2011.05.020.
46. Meyers BC, Axtell MJ. MicroRNAs in plants: key findings from the early years. Plant Cell. 2019;31(6):1206–7. https://doi.org/10.1105/tpc.19.00310.
47. Mi S, Cai T, Hu Y, Chen Y, Hodges E, Ni F, et al. Sorting of small RNAs into Arabidopsis Argonaute complexes is directed by the 5′ terminal nucleotide. Cell. 2008;133(1):116–27. https://doi.org/10.1016/j.cell.2008.02.034.
48. Cai Q, Qiao L, Wang M, He B, Lin F-M, Palmquist J, et al. Plants send small RNAs in extracellular vesicles to fungal pathogen to silence virulence genes. Science (80-). 2018;360:eaar4142.
49. Lahrmann U, Strehmel N, Langen G, Frerigmann H, Leson L, Ding Y, et al. Mutualistic root endophytism is not associated with the reduction of saprotrophic traits and requires a noncompromised plant innate immunity. New Phytol. 2015;207(3):841–57. https://doi.org/10.1111/nph.13411.
50. Tonukari NJ, Scott-Craig JS, Waltonb JD. The *Cochliobolus carbonum* SNF1 gene is required for cell wall–degrading enzyme expression and virulence on maize. Plant Cell. 2000;12(2):237–47.
51. Zhou H, Lorenz MC. Carnitine acetyltransferases are required for growth on non-fermentable carbon sources but not for pathogenesis in *Candida albicans*. Microbiology. 2008;154(2):500–9. https://doi.org/10.1099/mic.0.2007/014555-0.
52. Hyun MW, Yun YH, Kim JY, Kim SH. Fungal and plant phenylalanine ammonia-lyase. Mycobiology. 2011;39(4):257–65. https://doi.org/10.5941/MYCO.2011.39.4.257.
53. Zhang M, Shen Z, Meng G, Lu Y, Wang Y. Genome-wide analysis of the *Brachypodium distachyon* (L.) P. Beauv. Hsp90 gene family reveals molecular evolution and expression profiling under drought and salt stresses. PLoS One. 2017;12(12):e0189187. https://doi.org/10.1371/journal.pone.0189187.
54. Brunetti SC, Arseneault MKM, Gulick PJ. Characterization of the Esi3/RCI2/PMP3 gene family in the Triticeae. BMC Genomics. 2018;19(1):898. https://doi.org/10.1186/s12864-018-5311-8.
55. Liang Y, Jiang Y, Du M, Li B, Chen L, Chen M, et al. ZmASR3 from the maize ASR gene family positively regulates drought tolerance in transgenic Arabidopsis. Int J Mol Sci. 2019;20(9):2278. https://doi.org/10.3390/ijms20092278.
56. Hayama R, Sarid-Krebs L, Richter R, Fernández V, Jang S, Coupland G. PSEUDO RESPONSE REGULATORs stabilize CONSTANS protein to promote flowering in response to day length. EMBO J. 2017;36(7):904–18. https://doi.org/10.15252/embj.201693907.
57. Li Y, Xu M. CCT family genes in cereal crops: A current overview. Crop J. 2017;5(6):449–58. https://doi.org/10.1016/j.cj.2017.07.001.
58. Voß U, Wilson MH, Kenobi K, Gould PD, Robertson FC, Peer WA, et al. The circadian clock rephases during lateral root organ initiation in *Arabidopsis thaliana*. Nat Commun. 2015;6(1):7641. https://doi.org/10.1038/ncomms8641.
59. Wahl V, Brand LH, Guo Y-L, Schmid M. The FANTASTIC FOUR proteins influence shoot meristem size in *Arabidopsis thaliana*. BMC Plant Biol. 2010;10(1):285. https://doi.org/10.1186/1471-2229-10-285.
60. Zhan X, Shen Q, Wang X, Hong Y. The Sulfoquinovosyltransferase-like enzyme SQD2.2 is involved in flavonoid glycosylation, regulating sugar metabolism and seed setting in rice. Sci Rep. 2017;7(1):4685.
61. Pedrotti L, Mueller MJ, Waller F. *Piriformospora indica* root colonization triggers local and systemic root responses and inhibits secondary colonization of distal roots. PLoS One. 2013;8(7):e69352. https://doi.org/10.1371/journal.pone.0069352.
62. Harrach B, Baltruschat H, Barna B, Fodor J, Kogel KH. The mutualistic fungus *Piriformospora indica* protects barley roots from a loss of antioxidant capacity caused by the necrotrophic pathogen *Fusarium culmorum*. Mol Plant Microbe Interact. 2013;26(5):599–605. https://doi.org/10.1094/MPMI-09-12-0216-R.
63. Ye W, Shen C-H, Lin Y, Chen P-J, Xu X, Oelmüller R, et al. Growth promotion-related miRNAs in Oncidium orchid roots colonized by the endophytic fungus *Piriformospora indica*. PLoS One. 2014;9(1):e84920. https://doi.org/10.1371/journal.pone.0084920.
64. Jeong D-H, Schmidt SA, Rymarquis LA, Park S, Ganssmann M, German MA, et al. Parallel analysis of RNA ends enhances global investigation of microRNAs and target RNAs of *Brachypodium distachyon*. Genome Biol. 2013;14(12):R145. https://doi.org/10.1186/gb-2013-14-12-r145.
65. Šečić E, Kogel KH, Ladera-Carmona MJ. Biotic stress-associated microRNA families in plants. J Plant Physiol. 2021;263:153451. https://doi.org/10.1016/j.jplph.2021.153451.
66. Morea E, Silva E, Silva G, Valente G, Barrera C, Vincentz M, et al. Functional and evolutionary analyses of the miR156 and miR529 families in land plants. BMC Plant Biol. 2016;16:40.
67. Hackenberg M, Shi B-J, Gustafson P, Langridge P. Characterization of phosphorus-regulated miR399 and miR827 and their isomirs in barley under phosphorus-sufficient and phosphorus-deficient conditions. BMC Plant Biol. 2013;13(1):214. https://doi.org/10.1186/1471-2229-13-214.
68. Baev V, Milev I, Naydenov M, Apostolova E, Minkov G, Minkov I, et al. Implementation of a de novo genome-wide computational approach for updating Brachypodium miRNAs. Genomics. 2011;97(5):282–93. https://doi.org/10.1016/j.ygeno.2011.02.008.
69. Wang B, Sun Y, Song N, Zhao M, Liu R, Feng H, et al. *Puccinia striiformis* f. sp. tritici microRNA-like RNA 1 (Pst-milR1), an important pathogenicity factor of Pst, impairs wheat resistance to Pst by suppressing the wheat pathogenesis-related 2 gene. New Phytol. 2017;215(1):338–50. https://doi.org/10.1111/nph.14577.
70. Lammers PJ, Jun J, Abubaker J, Arreola R, Gopalan A, Bago B, et al. The glyoxylate cycle in an arbuscular mycorrhizal fungus. Carbon flux and gene expression. Plant Physiol. 2001;127(3):1287–98. https://doi.org/10.1104/pp.010375.
71. Hynes MJ, Murray SL, Andrianopoulos A, Davis MA. Role of carnitine acetyltransferases in acetyl coenzyme A metabolism in *Aspergillus nidulans*. Eukaryot Cell. 2011;10(4):547–55. https://doi.org/10.1128/EC.00295-10.
72. Li J, Yu L, Yang J, Dong L, Tian B, Yu Z, et al. New insights into the evolution of subtilisin-like serine protease genes in Pezizomycotina. BMC Evol Biol. 2010;10(1):68. https://doi.org/10.1186/1471-2148-10-68.
73. Corrales Escobosa AR, Rangel Porras RA, Meza Carmen V, Gonzalez Hernandez GA, Torres Guzman JC, Wrobel K, et al. *Fusarium oxysporum* Adh1 has dual fermentative and oxidative functions and is involved in

fungal virulence in tomato plants. Fungal Genet Biol. 2011;48(9):886–95. https://doi.org/10.1016/j.fgb.2011.06.004.
74. Jiang J, Yun Y, Yang Q, Shim W-B, Wang Z, Ma Z. A type 2C protein phosphatase FgPtc3 is involved in cell wall integrity, lipid metabolism, and virulence in *Fusarium graminearum*. PLoS One. 2011;6(9):e25311. https://doi.org/10.1371/journal.pone.0025311.
75. Xiang Q, Rasmussen C, Glass NL. The ham-2 locus, encoding a putative transmembrane protein, is required for hyphal fusion in *Neurospora crassa*. Genetics. 2002;160(1):169–80. https://doi.org/10.1093/genetics/160.1.169.
76. Lannoo N, Van Damme EJM. Lectin domains at the frontiers of plant defense. Front Plant Sci. 2014;5:397.
77. Torii KU. Leucine-rich repeat receptor kinases in plants: structure, function, and signal transduction pathways. Int Rev Cytol. 2004;234:1–46. https://doi.org/10.1016/S0074-7696(04)34001-5.
78. Mugford ST, Osbourn A. Evolution of serine carboxypeptidase-like acyltransferases in the monocots. Plant Signal Behav. 2010;5(2):193–5. https://doi.org/10.4161/psb.5.2.11093.
79. Corrêa LGG, Riaño-Pachón DM, Schrago CG, dos Santos RV, Mueller-Roeber B, Vincentz M. The role of bZIP transcription factors in green plant evolution: adaptive features emerging from four founder genes. PLoS One. 2008;3(8):e2944. https://doi.org/10.1371/journal.pone.0002944.
80. Hirsch S, Oldroyd GED. GRAS-domain transcription factors that regulate plant development. Plant Signal Behav. 2009;4(8):698–700. https://doi.org/10.4161/psb.4.8.9176.
81. Ambawat S, Sharma P, Yadav NR, Yadav RC. MYB transcription factor genes as regulators for plant responses: an overview. Physiol Mol Biol Plants. 2013;19(3):307–21. https://doi.org/10.1007/s12298-013-0179-1.
82. Zanini S, Šečić E, Busche T, Galli M, Zheng Y, Kalinowski J, et al. Comparative analysis of transcriptome and sRNAs expression patterns in the *Brachypodium distachyon- Magnaporthe oryzae* pathosystems. Int J Mol Sci. 2021;22(2). https://doi.org/10.3390/ijms22020650.
83. Šečić E, Kogel KH. Requirements for fungal uptake of dsRNA and gene silencing in RNAi-based crop protection strategies. Curr Opin Biotech. 2021;70:136–42. https://doi.org/10.1016/j.copbio.2021.04.001.
84. Murashige T, Skoog F. A revised medium for rapid growth and bio assays with tobacco tissue cultures. Physiol Plant. 1962;15(3):473–97. https://doi.org/10.1111/j.1399-3054.1962.tb08052.x.
85. Pontecorvo G, Roper JA, Hemmons LM, Macdonald KD, Bufton AW. The genetics of *Aspergillus nidulans*. Ad Genet. 1953;5:141–238. https://doi.org/10.1016/S0065-2660(08)60408-3.
86. Resequencing and genome assembly of *Serendipita indica* (syn. *Piriformospora indica*). European Nucleotide Archive. 2021. https://www.ebi.ac.uk/ena/browser/view/PRJEB45884
87. Wibberg D, Stadler M, Lambert C, Bunk B, Spröer C, Rückert C, et al. High quality genome sequences of thirteen Hypoxylaceae (Ascomycota) strengthen the phylogenetic family backbone and enable the discovery of new taxa. Fungal Divers. 2021;106:7–28.
88. Wibberg D, Andersson L, Tzelepis G, Rupp O, Blom J, Jelonek L, et al. Genome analysis of the sugar beet pathogen *Rhizoctonia solani* AG2-2IIIB revealed high numbers in secreted proteins and cell wall degrading enzymes. BMC Genomics. 2016;17(1):245. https://doi.org/10.1186/s12864-016-2561-1.
89. Koren S, Walenz BP, Berlin K, Miller JR, Bergman NH, Phillippy AM. Canu: scalable and accurate long-read assembly via adaptive k-mer weighting and repeat separation. Genome Res. 2017;27(5):722–36. https://doi.org/10.1101/gr.215087.116.
90. Walker BJ, Abeel T, Shea T, Priest M, Abouelliel A, Sakthikumar S, et al. Pilon: an integrated tool for comprehensive microbial variant detection and genome assembly improvement. PLoS One. 2014;9(11):e112963. https://doi.org/10.1371/journal.pone.0112963.
91. Li H. Aligning sequence reads, clone sequences and assembly contigs with BWA-MEM. ArXiv. 2013;1303.3997:1–3.
92. Langmead B, Salzberg SL. Fast gapped-read alignment with Bowtie 2. Nat Methods. 2012;9(4):357–9. https://doi.org/10.1038/nmeth.1923.
93. Galagan JE, Calvo SE, Borkovich KA, Selker EU, Read ND, Jaffe D, et al. The genome sequence of the filamentous fungus *Neurospora crassa*. Nature. 2003;422(6934):859–68 NC12 genome assembly. 2014. GCA accession number: GCA_000182925.2 (https://www.ebi.ac.uk/ena/browser/view/GCA_000182925.2).
94. Petersen TN, Brunak S, von Heijne G, Nielsen H. SignalP 4.0: discriminating signal peptides from transmembrane regions. Nat Methods. 2011;8(10):785–6. https://doi.org/10.1038/nmeth.1701.
95. Krogh A, Larsson B, von Heijne G, Sonnhammer ELL. Predicting transmembrane protein topology with a hidden markov model: application to complete genomes. J Mol Biol. 2001;305(3):567–80. https://doi.org/10.1006/jmbi.2000.4315.
96. Emanuelsson O, Nielsen H, Brunak S, von Heijne G. Predicting subcellular localization of proteins based on their N-terminal amino acid sequence. J Mol Biol. 2000;300(4):1005–16. https://doi.org/10.1006/jmbi.2000.3903.
97. Ray P, Chi M-H, Guo Y, Chen C, Adam C, Kuo A, et al. Genome sequence of the plant growth promoting fungus *Serendipita vermifera* subsp. bescii: The First Native Strain from North America. Phytobiomes J. 2018;2(2):62–3 *Serendipita vermifera* ssp. bescii NFPB0129 v1.0. (https://mycocosm.jgi.doe.gov/Sebvebe1/Sebvebe1.home.html).
98. Martin F, Aerts A, Ahrén D, Brun A, Danchin EGJ, Duchaussoy F, et al. The genome of *Laccaria bicolor* provides insights into mycorrhizal symbiosis. Nature. 2008;452(7183):88–92 *Laccaria bicolor* v2.0. (https://mycocosm.jgi.doe.gov/Lacbi2/Lacbi2.home.html).
99. Blom J, Kreis J, Spänig S, Juhre T, Bertelli C, Ernst C, et al. EDGAR 2.0: an enhanced software platform for comparative gene content analyses. Nucleic Acids Res. 2016;44(W1):W22–8. https://doi.org/10.1093/nar/gkw255.
100. mRNA-seq of *Brachypodium distachyon* roots inoculated with *Serendipita indica* (syn. *Piriformospora indica*). ArrayExpress database at EMBL-EBI. 2021. https://www.ebi.ac.uk/arrayexpress/experiments/E-MTAB-10649
101. Andrews S, Krueger F, Segonds-Pichon A, Biggins L, Krueger C, Wingett S. FastQC: a quality control tool for high throughput sequence data. Babraham; 2016. http://www.bioinformatics.babraham.ac.uk/projects/fastqc [Accessed 1 Feb 2019]
102. *Brachypodium distachyon* Bd21-3 v1.1 DOE-JGI, http://phytozome.jgi.doe.gov/
103. Kim D, Paggi JM, Park C, Bennett C, Salzberg SL. Graph-based genome alignment and genotyping with HISAT2 and HISAT-genotype. Nat Biotechnol. 2019;37(8):907–15. https://doi.org/10.1038/s41587-019-0201-4.
104. Kupfer DM, Drabenstot SD, Buchanan KL, Lai H, Zhu H, Dyer DW, et al. Introns and splicing elements of five diverse fungi. Eukaryot Cell. 2004;3(5):1088–100. https://doi.org/10.1128/EC.3.5.1088-1100.2004.
105. Walters B, Lum G, Sablok G, Min XJ. Genome-wide landscape of alternative splicing events in *Brachypodium distachyon*. DNA Res. 2013;20(2):163–71. https://doi.org/10.1093/dnares/dss041.
106. Anders S, Pyl PT, Huber W. HTSeq--a Python framework to work with high-throughput sequencing data. Bioinformatics. 2015;31(2):166–9. https://doi.org/10.1093/bioinformatics/btu638.
107. Love MI, Huber W, Anders S. Moderated estimation of fold change and dispersion for RNA-seq data with DESeq2. Genome Biol. 2014;15(12):550. https://doi.org/10.1186/s13059-014-0550-8.
108. Du Z, Zhou X, Ling Y, Zhang Z, Su Z. agriGO: a GO analysis toolkit for the agricultural community. Nucleic Acids Res. 2010 Jul;38(suppl_2):W64–70. https://doi.org/10.1093/nar/gkq310.
109. Sievert C. Interactive web-based data visualization with R, plotly, and shiny: Chapman and Hall/CRC; 2020. Available from: https://plotly-r.com. https://doi.org/10.1201/9780429447273.
110. Wickham H. ggplot2: Elegant graphics for data analysis. New York: Springer-Verlag; 2016. Available from: http://ggplot2.org
111. R Core Team. R: A language and environment for statistical computing. Vienna; 2017. Available from: https://www.r-project.org/
112. Götz S, García-Gómez JM, Terol J, Williams TD, Nagaraj SH, Nueda MJ, et al. High-throughput functional annotation and data mining with the Blast2GO suite. Nucleic Acids Res. 2008;36(10):3420–35. https://doi.org/10.1093/nar/gkn176.
113. sRNA-seq of *Brachypodium distachyon* roots inoculated with *Serendipita indica* (syn. *Piriformospora indica*). ArrayExpress database at EMBL-EBI. 2021. https://www.ebi.ac.uk/arrayexpress/experiments/E-MTAB-10650
114. Martin M. Cutadapt removes adapter sequences from high-throughput sequencing reads. EMBnet.journal. 2011;17(1):10–12. Next Gener Seq Data Anal - 1014806/ej171200.
115. Langmead B, Trapnell C, Pop M, Salzberg SL. Ultrafast and memory-efficient alignment of short DNA sequences to the human genome. Genome Biol. 2009;10(3):R25. https://doi.org/10.1186/gb-2009-10-3-r25.
116. The RNAcentral Consortium, Petrov AI, Kay SJE, Kalvari I, Howe KL, Gray KA, et al. RNAcentral: a comprehensive database of non-coding RNA sequences. Nucleic Acids Res. 2017;45(D1):D128–34. https://doi.org/10.1093/nar/gkw1008.
117. Johnson NR, Yeoh JM, Coruh C, Axtell MJ. Improved placement of multi-mapping small RNAs. G3 (Bethesda). 2016;6(7):2103–11.

118. Zanini S, Šečić E, Jelonek L, Kogel KH. A bioinformatics pipeline for the analysis and target prediction of RNA effectors in bidirectional communication during plant–microbe interactions. Front Plant Sci. 2018;9. https://doi.org/10.3389/fpls.2018.01212.
119. Dai X, Zhao PX. psRNATarget: a plant small RNA target analysis server. Nucleic Acids Res. 2011;39(suppl_2):W155–9. https://doi.org/10.1093/nar/gkr319.
120. Chen H, Boutros PC. VennDiagram: a package for the generation of highly-customizable Venn and Euler diagrams in R. BMC Bioinformatics. 2011;12(1):35. https://doi.org/10.1186/1471-2105-12-35.
121. Livak KJ, Schmittgen TD. Analysis of relative gene expression data using real-time quantitative PCR and the 2−ΔΔCT Method. Methods. 2001;25(4):402–8. https://doi.org/10.1006/meth.2001.1262.
122. Chen C, Ridzon DA, Broomer AJ, Zhou Z, Lee DH, Nguyen JT, et al. Real-time quantification of microRNAs by stem–loop RT–PCR. Nucleic Acids Res. 2005;33(20):e179. https://doi.org/10.1093/nar/gni178.
123. Kramer MF. Stem-Loop RT-qPCR for miRNAs. Curr Protoc Mol Biol. 2011;95:15.10.1.

Publisher's Note

Conclusion:

This study established a mutualistic interaction model between *Serendipita indica* (*Si*) and *Brachypodium distachyon* (*Bd*), demonstrating that *Si* colonisation promotes *Bd* growth, increases grain yield, and accelerates flowering. Transcriptome and sRNA profiling of *Bd-colonised* roots revealed active, mutual regulatory changes, suggesting that ck-RNAi may contribute to the mutualistic outcome. At the transcript level, *Si* colonisation induced significant changes in *Bd* gene expression, particularly in genes associated with biotic stress responses and immunity. In parallel, *Si* showed transcriptional shifts in pathways related to carbohydrate metabolism, cell wall organisation, and nutrient acquisition, indicating its metabolic adaptation to the host environment. sRNA analysis in *Bd*-colonised roots identified putative endogenous plant sRNAs belonging to known miRNA families involved in growth and development. Additionally, we identified putative *Si*-derived ck-sRNAs with predicted targets in *Bd* involved in immunity, circadian rhythm, and flowering time regulation. These findings suggest that *Si* manipulates the host physiology to establish mutualism. To further support the functional relevance of *Si*sRNAs, *in silico* analysis of re-sequenced *Si* genome indicates that *Si* encodes RNAi components, supporting its ability to generate functional regulatory sRNAs.

Taken together, our findings support an sRNA-mediated ck-RNAi in mutualistic interactions.

CHAPTER 3 –

A pipeline for validation of *Serendipita indica* effector-like sRNA suggests cross-kingdom communication in the symbiosis with Arabidopsis

(Contribution as first author)

Summary:

This chapter contains the publication "**A pipeline for validation of *Serendipita indica* effector-like sRNA suggests cross-kingdom communication in the symbiosis with Arabidopsis"** accepted by the Journal of Experimental Botany on December 19, 2024, and published online on December 26, 2024 (DOI:10.1093/jxb/erae515).

One of the main advantages of *Serendipita indica* as an endophytic fungus is its broad host range. In this study, we extended our investigation of *Si*-host interaction to the dicotyledon model plant *Arabidopsis thaliana* and established a functional protoplast assay to validate the gene silencing activity of effector-like *Si*sRNAs and investigate their potential role in ckRNAi

SOCIETY FOR EXPERIMENTAL BIOLOGY

Journal of Experimental Botany
https://doi.org/10.1093/jxb/erae515 Advance Access Publication 26 December 2024

RESEARCH PAPER

A pipeline for validation of *Serendipita indica* effector-like sRNA suggests cross-kingdom communication in the symbiosis with Arabidopsis

Sabrine Nasfi[1], Saba Shahbazi[1], Katharina Bitterlich[1], Ena Šečić[1], Karl-Heinz Kogel[1,2,*], and Jens Steinbrenner[1]

[1] Institute of Phytopathology, Research Centre for BioSystems, Land Use and Nutrition, Justus-Liebig-University Giessen, Heinrich-Buff-Ring 26, D-35392 Giessen, Germany
[2] Institut de Biologie Moléculaire des Plantes, CNRS, Université de Strasbourg, 12 rue du Général Zimmer, 67084 Strasbourg, France

* Correspondence: karl-heinz.kogel@agrar.uni-giessen.de

Received 13 May 2024; Editorial decision 17 December 2024; Accepted 19 December 2024

Editor: Miriam Gifford, University of Warwick, UK

Abstract

Bidirectional communication between pathogenic microbes and their plant hosts via small RNA (sRNA)-mediated cross-kingdom RNAi (ckRNAi) is a key element for successful host colonization. Whether mutualistic fungi of the *Serendipitaceae* family, known for their extremely broad host range, use sRNAs to colonize plant roots is still under debate. To address this question, we developed a pipeline to validate the accumulation, translocation, and activity of fungal sRNAs in post-transcriptional silencing of *Arabidopsis thaliana* genes. Using stem–loop quantitative reverse transcription–PCR, we detected the expression of a specific set of *Serendipita indica* (*Si*) sRNAs, targeting host genes involved in cell wall organization, hormonal signalling regulation, immunity, and gene regulation. To confirm the gene silencing activity of these sRNAs in plant cells, *Si*sRNAs were transiently expressed in protoplasts. Stem–loop PCR confirmed sRNA expression and accumulation, while qPCR validated post-transcriptional gene silencing of their predicted target genes. Furthermore, Arabidopsis ARGONAUTE 1 immunoprecipitation revealed the loading of fungal *Si*sRNAs into the plant RNAi machinery, suggesting the translocation of *Si*sRNA from the fungus into root cells. In conclusion, this study provides a blueprint for rapid selection and analysis of sRNA effectors and further supports the model of cross-kingdom communication in the Sebacinoid symbiosis.

Keywords: AGO1-IP, Arabidopsis roots, cross-kingdom communication, mutualism, *Piriformospora*, 5′-RLM-RACE, RNA interference, *Serendipita indica*, small RNA, symbiosis.

Introduction

RNAi is a regulatory process in most eukaryotes in which gene expression is silenced at the transcriptional or post-transcriptional level through the action of small RNA (sRNA). This process is associated with the control of genome stability, developmental processes, and responses to biotic and abiotic stresses (Zhan and Meyers, 2023). Two main

Abbreviations: AGO, ARGONAUTE; *At*, *Arabidopsis thaliana*; dpi, days post-inoculation; hptr, hours post-transformation; IP, immunoprecipitation; PTGS, post-transcriptional gene silencing; RISC, RNA-Induced Silencing Complex; *Si*, *Serendipita indica*; sRNA, small RNA.

types of sRNAs predominate in plants. miRNAs are typically 21 and 22 nucleotides (nt) in length and are processed from primary miRNAs (pri-miRNAs) containing a stem–loop structure encoded by miRNA (*MIR*) genes (Reinhart *et al.*, 2002; Meyers and Axtell, 2019). In contrast siRNAs are RNA molecules of 20–24 nt in length produced from longer endogenous RNA templates or from exogenous RNA sequences (e.g. viruses or transgenes). In plants and fungi, both miRNA and siRNA precursors are processed by RNase III-like endonucleases named DICER-like (DCL) proteins. One strand of these sRNA duplexes is then bound by ARGONAUTE (AGO) proteins and incorporated into the RNA-Induced Silencing Complex (RISC), where they target complementary mRNA transcripts to induce post-transcriptional gene silencing (PTGS) (Iwakawa and Tomari, 2022). Plant sRNAs can also move from cell to cell via plasmodesmata and systemically through the phloem, acting in a cell non-autonomous manner. Additionally, they can translocate between interacting organisms (Zhan and Meyers, 2023). For example, sRNAs are transferred bidirectionally between plant hosts and pathogenic microbes to modulate defence and virulence, a phenomenon called cross-kingdom RNAi (ckRNAi) (for reviews, see Wang *et al.*, 2017; Göhre and Weiberg, 2023; Mahanty *et al.*, 2023). ckRNAi in plant–pathogen interactions was discovered in 2013 when the necrotrophic fungus *Botrytis cinerea* was shown to induce silencing of host defence genes in *Solanum lycopersicum* and *Arabidopsis thaliana* (*At*) (Weiberg *et al.*, 2013). Since then, several studies have supported the existence of ckRNAi and also showed that the exchange of sRNA effectors can be bidirectional (Zhang *et al.*, 2016; Cai *et al.*, 2018).

Already in 2006, Huang and colleagues reported reduced nematode infectivity when root-knot nematodes (RKNs) fed on roots of Arabidopsis plants expressing dsRNA targeting the *16D10* gene, which encodes a conserved secreted RKN root growth-stimulating peptide known to be involved in parasitism (Huang *et al.*, 2006). Later, it was shown that sRNAs can indeed move from a plant to an attacking pathogen in the interaction of barley and wheat with the powdery mildew fungus (*Blumeria graminis*) (Nowara *et al.*, 2010). Transient transformation of leaf epidermal cells with a plasmid overexpressing dsRNA directed against the fungal effector *AVRA10* enhanced resistance to *B. graminis* in the absence of the powdery resistance gene *Mla10*, a technique termed host-induced gene silencing (HIGS). Since then, numerous reports have shown that HIGS is an efficient strategy for pest and disease control in crops (Koch *et al.*, 2013; Cai *et al.*, 2018; Liu *et al.*, 2020; Sang and Kim, 2020; Zand Karimi and Innes, 2022).

Although ckRNAi and related artificial processes such as HIGS were discovered in plants >18 years ago, the molecular mechanisms are still not fully understood. For instance, the bidirectional transfer of RNAs in extracellular vesicles is still a topic of debate (Rutter and Innes, 2018; He *et al.*, 2021a, b; Nasfi and Kogel, 2022), and only in recent years have a growing number of studies shed light on ckRNAi in plant–symbiont interactions (Qiao *et al.*, 2023).

ckRNAi in mycorrhizal symbioses seems to include miRNAs. For example, Pmic_miR-8, an miRNA from the ectomycorrhizal fungus *Pisolithus microcarpus*, enhanced the colonization of its host *Eucalyptus grandis*, indicating its role in the beneficial ectomycorrhizal symbiosis (Wong-Bajracharya *et al.*, 2022). Moreover, sRNA Rir2216 from the arbuscular mycorrhiza fungus (AMF) *Rhizophagus irregularis* targets the WRKY transcription factor MtWRKY69 in its host *Medicago truncatula*. Consistent with ckRNAi, Rir2216 was loaded into an MtAGO1 silencing complex, leading to the cleavage of a host target transcript encoding MtWRKY69 (Silvestri *et al.*, 2024). Moreover, tRNA-derived sRNA fragments (tRFs) identified in root nodule symbioses between soybean and the bacterial symbiont *Bradyrhizobium japonicum* have been shown to hijack *Glycine max* AGO1. These tRFs act as positive regulators of rhizobial infection and nodule formation (Ren *et al.*, 2019), further emphasizing the existence of ckRNAi in mutualistic plant–microbe interactions.

Understanding ckRNAi depends on the identification and functional validation of translocated sRNA (sRNA effectors), which requires tools to study the mode of action of numerous sRNAs derived from extensive sRNA sequencing data. In this context, we present a pipeline for validation of sRNA effectors by studying the interaction between the mutualistic basidiomycete fungus *Serendipita indica* (*Si*) and the dicot model plant *At*. The fungus was originally isolated from the roots of the shrubs *Prosopis juliflora* and *Ziziphus nummularia* in the Indian Thar desert (Verma *et al.*, 1998). Its beneficial activity includes plant growth promotion, enhanced plant resistance, enhanced nitrate and phosphate delivery, promotion of adventitious root and root hair formation, early flowering, support of higher seed yield, alteration in secondary metabolites, and hardening of tissue-cultured plants (Zuccaro *et al.*, 2011; Qiang *et al.*, 2012; Glaeser *et al.*, 2016; Weiß *et al.*, 2016; Xu *et al.*, 2018; Verma *et al.*, 2022; Galli *et al.*, 2024). Moreover, the fungus transfers protein effectors to host cells to exploit the host's metabolism and promote microbial colonization (Akum *et al.*, 2015; Osborne *et al.*, 2023). To further explore the molecular basis of the mutualistic interaction formed by *Si* with a wide range of plants (Sebacinalean symbiosis), we recently demonstrated the global change in sRNA profiles in the interaction of the beneficial fungus and the grass model *Brachypodium distachyon* (*Bd*) (Šečić *et al.*, 2021). Among *Bd*- and *Si*-generated sRNAs with putative functions in the interacting organism, we found proteins involved in cell wall organization, hormonal signalling regulation, and immunity as potential targets of putative fungal effector sRNAs.

Building upon the findings from our prior work, we have selected a set of fungal sRNAs with interesting predicted *At* targets to further investigate their activity in the *Si–At* interaction. We developed a functional protoplast assay to validate

these potential fungal effector sRNAs and assessed their gene silencing activity. Using stem–loop quantitative reverse transcription–PCR (RT–qPCR), we confirmed sRNA transformation and accumulation in plant protoplasts and recorded the down-regulation of predicted host target genes via qPCR. Additionally, we investigated the capability of *Si*sRNA candidates in mediating the degradation of host mRNA by 5′-RNA ligation-mediated (RLM)-RACE. Finally, *At*AGO1 immunoprecipitation assay confirmed the loading of fungal *Si*sRNAs into the plant's RNAi machinery. The data support the existence of naturally occurring ckRNAi between the beneficial fungus *Serendipita indica* and *Arabidopsis thaliana*.

Materials and methods

*Si*sRNA selection and Arabidopsis target prediction

The *Si*sRNAs selected from Šečić *et al.* (2021) and their predicted *At* target genes are summarized and detailed in Supplementary Table S1 and Supplementary Dataset S1.

Plants, fungi, and plant inoculation

For interaction studies of *At* roots and *Si* (IPAZ-11827, Institute of Phytopathology, Giessen, Germany), *At* plants of ecotype Columbia-0 (Col-0) were grown on vertical square Petri dishes on an ATS medium (Lincoln *et al.*, 1990) without sucrose and supplemented with 4.5 g l^{-1} Gelrite (Duchefa #G1101) in a 22 °C day/18 °C night cycle (8 h of light). Roots of 14-day-old plants were inoculated with 1 ml of a suspension of 500 000 *Si* chlamydospores ml^{-1} in aqueous 0.002% Tween-20 per Petri dish as described in Jacobs *et al.* (2011). For the protoplast experiment, *At* plants were cultivated in a 4:1 ratio of T-type soil (F.-E. Typ Nullerde, Hawita) and crystal quartz sand mixture for 4–5 weeks in a growth chamber in a 19 °C day/18 °C night (9 h of light, 150 µmol photons m^{-2} s^{-1}), and a constant relative humidity of 60%. *Si* was grown in axenic culture on complete medium (Pontecorvo *et al.*, 1953) for 4 weeks in daylight under sterile conditions with shaking at 100 rpm.

Plasmid construct

Digestion–ligation of the AtMIR390a distal stem–loop

The Arabidopsis MIR390a distal stem–loop, containing a *ccd*B cassette flanked by two *Bsa*I sites (*At*MIR390a-B/c), was excised from the pMDC32B-*At*MIR390a-B/c vector (Plasmid #51776, https://www.addgene.org, Carbonell *et al.*, 2014) using *Eco*RI and *Hin*dIII Fast digest restriction enzymes (Thermo Fisher Scientific, FD0274 & FD0505). The pUC18 vector backbone (plasmid #50004) was similarly digested with the same enzymes. The *At*MIR390a-B/c fragment was then ligated into the pUC18 vector backbone using T4 DNA Ligase (Thermo Fischer Scientific, EL0011) generating the pUC18-*At*MIR390a-B/c protoplast expression vector for MIR390a-based 21 or 22 nt sRNAs. Digestion was carried out at 37 °C for 1 h, followed by enzyme inactivation at 80 °C for 10 min. The ligation was performed overnight at 16 °C.

Digestion ligation of the red fluorescent protein cassette

The red fluorescent protein (RFP) cassette was excised from the pBeaconRFP_GR vector (https://gatewayvectors.vib.be/index.php/ID:3_20, Bargmann and Birnbaum, 2009) using *Nde*I restriction enzyme (NEB, R0111S). The pUC18-*At*MIR390a-B/c vector, which contains an *Nde*I restriction site, was similarly digested. The RFP cassette was then ligated into the *Nde*I site of the pUC18-*At*MIR390a-B/c vector using T4 DNA ligase.

Site-directed mutagenesis

Before cloning 75-mer oligonucleotides, a third *Bsa*I site in the pUC18 backbone, which would interfere with the Golden Gate cloning of artificial miRNAs (amiRNAs) and *Si*sRNA, was removed by site-directed mutagenesis. This was achieved using Phusion High-Fidelity DNA polymerase (Thermo Fisher Scientific, F553S), the fast digest *Dpn*I endonuclease (Thermo Fisher Scientific, FD1703), and custom-designed site-directed mutagenesis primers (pUC18-Mut-Fwd and pUC18-Mut-Rev) following the manufacturer's protocol.

Direct cloning of amiRNAs and SisRNAs

The 75-mer oligonucleotides comprising the 21 nt sequences of amiRNAs and *Si*sRNAs were designed using the P-SAMS web-tool (http://p-sams.carringtonlab.org/) as described by Fahlgren *et al.* (2016), Carbonell *et al.* (2014), and Carbonell (2017a, 2019). Forward and reverse 75-mer oligonucleotides were diluted to 100 µM and annealed using a thermocycler under the following conditions: 5 min at 94 °C, followed by cooling at 0.05 °C s^{-1} to 20 °C. Prior to cloning, the annealed 75-mer oligonucleotides were further diluted to 0.15 µM. These oligonucleotides were then cloned into the *Bsa*I sites of the pUC18-*At*MIR390a-B/c vector using the Golden Gate strategy. A single digestion–ligation reaction was performed with *BsaI-HF®v2* (NEB, R3733) and T4 DNA ligase (Thermo Fischer Scientific, EL0011), replacing the ccdB cassette, allowing for the selection of 75-mer-positive clones.

An *in silico* cloning design was performed using Snapgene software (www.snapgene.com). The cloning strategy workflow is outlined in Supplementary Fig. S1A, while Supplementary Fig. S1B presents the final pUC18-*At*MIR390a-RFP-amiRNA/*Si*sRNA vector map. The content of the 75-mer oligonucleotides is illustrated in Supplementary Fig. S2. The designed amiRNAs, including their 5′-nucleotide sequences, predicted targets, target aligned fragments, expectation values, and mode of regulation, are detailed in Supplementary Table S2. Similarly, the same information for the selected putative *Si*sRNAs cloned into the expression vector for PTGS analysis are listed in Supplementary Table S3. An alignment of amiRNAs and *Si*sRNA with their predicted *At* targets, as generated by the psRNATarget web-tool, is shown in Supplementary Fig. S3A, while Supplementary Fig. S3B provides a color-coded heatmap visualizing the sRNA–mRNA pair alignment created using RStudio. The forward and reverse 75-mer oligonucleotides for amiRNAs and *Si*sRNAs are listed in Supplementary Table S4.

Protoplast transformation

Protoplasts were isolated using the 'Tape–Arabidopsis Sandwich' method (Wu *et al.*, 2009). Transformation was performed using the polyethylene glycol (PEG) method, following the transient expression of recombinant genes using the Arabidopsis mesophyll protoplast (TEAMP) approach (Yoo *et al.*, 2007), with minor modifications (WI incubation solution was replaced by the W5 solution). Since transformation efficiency was crucial for all subsequent experiments, we optimized the transformation by varying (i) protoplast concentration (10×10^4 and 5×10^4 protoplasts ml^{-1}), (ii) plasmid pUC18-*At*MIR390a-RFP-sRNA concentration (20, 30, and 40 µg), and (ii) incubation time (24 h and 48 h). High transformation efficiency was achieved with 5×10^4 protoplasts ml^{-1}, 30 µg of plasmid, and 24 h incubation time, comparable with the efficiencies reported for *At* leaf protoplasts (Yoo *et al.*, 2007). Total cell numbers were counted using a Fuchs–Rosenthal counting chamber under an optical microscope. Protoplast transformation was checked using an epifluorescence microscope (TCS SP2 Leica), and images were acquired with Leica Application Suite (LAS) software. All counts were

performed in triplicate. Transformed protoplasts were harvested by centrifugation at 100 *g* for 2 min, the supernatant was removed, and protoplasts were snap-frozen in liquid nitrogen and stored at –80 °C for further studies.

RNA extraction and quality analysis

Total RNA was extracted from protoplasts using the QuickRNA™ Miniprep kit (Zymo Research, R1050) with an on-column DNase I treatment. Total RNAs from *Si–At* interaction grown on ATS plates and from *Si* mycellium grown in axenic culture were extracted using Direct-zol RNA Miniprep (Zymo Research, R2051) with an on-column DNase I treatment. RNA concentration was measured using a NanoDrop ND-1000 Spectrophotometer (Thermo Fisher Scientific, USA), and RNA purity was determined by assessing $A_{260}/_{280}$ and $A_{260}/_{230}$ ratios. The quality of the RNA extracted from transformed protoplasts was further checked using the Agilent 2100 Bioanalyzer Nano Chip (Agilent, Germany).

Stem–loop end-point PCR

Designed amiRNA and *Sis*RNA sequences were used as templates to design specific stem–loop primers matching the corresponding sRNA over 6 nt at the 3′ end. Hairpin primers and forward primers were designed using the tool published in Adhikari *et al.* (2013) based on Varkonyi-Gasic and Hellens (2011). Stem–loop PCR was performed as described by Werner *et al.* (2021), either in duplexed stem–loop (cDNA generated from two sRNA hairpin primers simultaneously in one reaction) or multiplexed stem–loop (cDNA generated from multiple hairpin sRNA primers simultaneously in one reaction). End-point PCR was used to assess the expression of amiRNAs and *Sis*RNAs. The PCR program was optimized as follows: initial denaturation at 95 °C for 5 min; followed by 40 cycles of 95 °C for 30 s, 60 °C for 30 s, 72 °C for 30 s; with a final extension at 72 °C for 5 min and a hold at 4 °C. PCR products were separated and visualized in 2% TBE–agarose gels. Stem–loop PCR primers are listed in Supplementary Table S5.

Stem–loop RT–qPCR

For the *Sis*RNA expression level analysis, cDNA was reverse transcribed from RNA extracted from *At* roots, either inoculated with *Si* or mock treated (non-inoculated), using hairpin primers in multiplexed stem–loop to target respective *Sis*RNAs, as well as two endogenous housekeeping miRNAs, *At*miR159a and *At*miR166a. To assess *Sis*RNA and amiRNA accumulation in protoplasts, cDNA was reverse transcribed using RNA extracted from transformed and control (non-transformed) protoplasts, using hairpin primers in duplexed stem–loop to target the respective amiRNAs or *Sis*RNAs, with *At*miR159a serving as the endogenous miRNA control. Amplification efficiencies were evaluated by generating stem–loop cDNA using RNA extracted from *Si* axenic culture or from *At* mock-treated roots (non-inoculated). A four-step, 10-fold dilution series of cDNA (ranging from 15 ng μl^{-1} to 15 pg μl^{-1}) was used. All *Sis*RNA amplifications showed efficiencies between 80% and 110% with an R^2 value between 1 and 0.991, except for *Sis*RNA154, with an efficiency of 122%. stem–loop RT–qPCR was performed with 5 ng of cDNA on the QuantStudio 5 Real-Time PCR system (Applied Biosystems). A 2 µl aliquot of ROX (CRX reference dye, Promega, C5411) was added to 1 ml of SybrGreen as a passive reference dye that allows fluorescent normalization for qPCR data. The PCR conditions were 95 °C for 5 min, followed by 40 cycles of 95 °C for 15 s, 60 °C for 30 s, and 72 °C for 30 s, and then by a melting curve analysis. Each sample had three technical replicates. Specific forward and universal reverse stem–loop primers were used for the amplification of amiRNAs or *Sis*RNAs, and relative abundance was calculated using the ΔΔCt method (Livak and Schmittgen, 2001), normalized against the geometric mean (Vandesompele *et al.*, 2002) of *At*miR159a and/or *At*miR166a.

PTGS detection by qPCR

The standard curve method was used to test the efficiency of the qPCR transcript primers using a serial dilution of an *At* cDNA library along with three different primer concentrations (0.4, 0.2, and 0.1 µM for each primer) and 5 µl of SybrGreen (Sigma-Aldrich). The total volume of 10 µl and three technical replicates are considered for each reaction. Prior to master mix preparation, 2 µl of ROX (CRX reference dye, Promega, C5411) were added to 1 ml of SybrGreen as a passive reference dye that allows fluorescent normalization for qPCR data. For cDNA synthesis, 500 ng of RNA samples from both transformed and control *At* protoplasts were used. qPCR was performed using the QuantStudio 5 real-time PCR system (Applied Biosystems) as described before. Fold changes in expression were calculated using the ΔΔCt method (Livak and Schmittgen, 2001), normalized against the endogenous housekeeping gene *Ubiquitin* (*UBC21, AT5G25760*). Standard errors were calculated for all mean values. All qPCR primers are listed in Supplementary Table S6.

5′-RLM-RACE

5′-RLM-RACE was performed using the FirstChoice® RLM-RACE kit (Thermo Fisher Scientific) following the manufacturer's protocol and omitting the dephosphorylation and decapping steps. A 1 µg aliquot of RNA isolated from *At* transformed and control protoplasts was used as a template and ligated to the 5′-RACE adapter using T4 RNA ligase (10 U μl^{-1}) (Thermo Fisher Scientific). The ligation reaction was used entirely to generate the first cDNA strand. Two rounds of nested hot-start touch-down PCR were performed using outer (first) and inner (second) 5′-RLM-RACE universal primers in combination consecutively with gene-specific outer and gene-specific inner primers. PCR products were evaluated in a 1.5% agarose gel, and bands of the expected size were excised. These products were cleaned with the Wizard® SV Gel and PCR Clean-Up System (Promega) and cloned with the pGEM®-T Vector Systems (Promega). For each band, six clones were selected for sequencing by LGC Genomics (Berlin, Germany). The oligonucleotides used are listed in Supplementary Table S7.

Arabidopsis root transcript analysis

Arabidopsis Col-0 plants were grown on ATS plates and inoculated with *Si* chlamydospores as described above. *At* mock-treated roots (non-inoculated) were treated with water containing 0.002% Tween-20. Inoculated roots were harvested at 3 and 7 days post-inoculation (dpi), ground using a tissue lyser, and RNA was extracted using Trizol and the Zymo Quick-RNA™ Miniprep kit (Zymo research R2070), with a subsequent in-column DNase digestion. cDNA was sythesized from 500 ng of RNA using Revert Aid Reverse transcriptase. Gene transcription levels were quantified by qPCR using SYBR Green JumpStart Taq ReadyMix (Sigma Aldrich, 1003444642) with a QuantStudio5 Real-Time PCR System (Applied Biosystems). A 2 µl aliquot of ROX (CRX reference dye, Promega, C5411) was added to 1 ml of SybrGreen as a passive reference dye that allows fluorescent normalization for qPCR data. PCR conditions were as previously described. Gene expression levels were normalized to the geometric mean of two endogenous housekeeping genes (Vandesompele *et al.*, 2002), *Ubiquitin* (*UBC21, AT5G25760*) and *Elongation Factor-1 alpha* (*EF1α, AT5G60390*). Fold changes in expression were calculated using the ΔΔCt method (Livak and Schmittgen, 2001). Roots from two ATS plates were considered as one biological replicate. The results of two biological replicates are included in the data analysis. All qPCR primers are listed in Supplementary Table S6.

T-vector cloning and sequencing

Stem–loop PCR and 5′-RLM-RACE PCR amplification products were purified using the Wizard® SV Gel and PCR Clean-Up System (Promega). Cloning of the different PCR products was performed as described in the pGEM®-TVector system according to the manufacturer's instructions (Promega). Sequencing was performed at LGC Genomics and analysed using the Snapgene tool (GSL Biotech, available at snapgene.com). All PCR primers are presented in Supplementary Table S8.

AGO immunoprecipitation

*At*AGO1 co-immunoprecipitation (Co-IP) was performed following Dunker *et al.* (2021) with modifications. A 5 g aliquot of *Si* mycelium or *At* roots, inoculated or not with *Si*, was ground to a fine powder using a pre-cooled mortar and pestle. To each sample, 20 ml of immunoprecipitation extraction buffer was added, then centrifuged at 3200 *g* for 15 min at 4 °C to remove root debris. The supernatants were filtered through double-layered Miracloth and 200 µl of crude extract (CE, supernatant before antibodies) was collected for western blot analysis. To the remaining supernatant, 5 µl of anti-AGO1 polyclonal antibody (Agrisera, catalogue no. AS09527), and 200 µl of protein A agarose beads (Roche, Ref: 11719408001) were added, and the mixture was incubated for 2 h at 4 °C on a rotation wheel. After centrifugation at 200 *g* for 30 s, 200 µl of the supernatant (SN, after antibodies) was collected for further western blot analysis. The remaining supernatants were discarded, and the pelleted beads were washed three times with ice-cold IP wash buffer. The washed beads were resuspended in 1 ml of wash buffer, with 30% used for western blot analysis (IP fraction) and 70% for sRNA recovery.

sRNA recovery from the IP fraction

IP fractions were pelleted and resuspended in 300 µl of IP wash buffer with 150 µl of RNA release buffer. Samples were incubated for 15 min at 300 rpm at 65 °C. A 450 µl aliquot of water-saturated phenol was added, and samples were vortexed for 2 min then centrifuged at 10 000 *g* at room temperature for 8 min. The upper aqueous phase containing the sRNAs was transferred into a low binding RNA tube. Then 450 µl of chloroform/isoamyl alcohol (24:1) (Carl Roth, Germany) was added to the RNA samples. The step was repeated twice. For RNA precipitation, 0.1× volume of 3 M sodium acetate, 2.5× volume of 96% ethanol, and 20 µg of RNA grade glycogen (Thermo Fisher Scientific, R0551) were added to the RNA samples and left overnight at –20 °C. Samples were pelleted at 20 000 *g* for 30 min at 4 °C and washed with 500 µl of 80% ethanol. RNA was pelleted at 20 000 *g* for 20 min at 4 °C, ethanol was removed, and pellets were air-dried until ethanol was completely evaporated. The RNA pellets were resuspended in 8 µl of diethylpyrocarbonate (DEPC)-treated water and stored at –80 °C.

Western blot analysis

Western blot analysis was performed using a 5.5% stacking gel and a 12% resolving gel. For each sample, 20 µl of total protein, crude extract before antibodies (CE), supernatant after pelleting agarose beads (SN), and *At*AGO1 Co-IP fraction (IP) were loaded after boiling at 95 °C for 5 min. Proteins were transferred to a polyvinylidene fluoride (PVDF) blotting membrane (Carl Roth, Germany). The membrane was blocked with 5% (w/v) milk powder (Carl Roth, Germany) in phosphate-buffered saline with Tween-20 (PBS-T) for 1 h at room temperature, then probed overnight at 4 °C on a shaker with anti-AGO1 primary antibody (1:4000 dilution) (Agrisera, AS09 527). After washing, the membrane was incubated for 2 h at room temperature with mouse anti-rabbit horseradish peroxidase (HRP)-conjugated (Santa Cruz-2357) secondary antibody. For the membrane development, chemiluminescent substrates were applied according to the manufacturer's recommendation, and images were captured using the Bio-rad ChemiDoc MP imaging system.

Statistical analysis

For qPCR gene expression data in *Si–At* interaction and in transformed protoplasts, measurements were compared with *At* non-inoculated roots and non-transformed protoplasts, respectively. Expression values were analysed using the ΔΔCt method (Livak and Schmittgen, 2001), normalized against *UBC21* and/or *EF1α* as housekeeping genes, and visualized as a fold change of the expression level. For stem–loop qPCR for the *Sis*RNA expression level in *Si–At* interaction, and for *Sis*RNA and amiRNA accumulation in transformed protoplasts, *At*miR159a and/or *At*miR166a were used as endogenous housekeeping miRNAs and expressed as $\log_2$ fold change of the expression level. Significance was assessed either by a two-sided unpaired Student's *t*-test or by a two-sided Welch's *t*-test (α=0.05, ⋆P<0.05, ⋆⋆P<0.01, ⋆⋆⋆P<0.001).

Results

We developed a pipeline for the validation of sRNA-mediated gene silencing activities in the mutualistic interaction of *Si* and *At*, comprising (i) prediction of Arabidopsis target genes for fungal sRNAs (*Sis*RNAs, using psRNATarget), (ii) detection of *Sis*RNA expression in axenic culture and *Si*-colonized *At* roots (*Si–At* interaction), (iii) validation of gene silencing activity of *Sis*RNAs in *At* protoplasts, and (iv) detection of the association of *Sis*RNAs with the *At*AGO1 protein (Fig. 1).

Effector-like *Sis*RNA candidates are present in axenic cultures of *Serendipita indica*

From the dataset of 412 putative *Sis*RNAs identified by sRNA sequencing in our previous study in the *Si–Bd* symbiosis (Šečić *et al.*, 2021), we selected a set of 14 potential *Sis*RNA effector candidates of 21 nt on the basis that they (i) showed a higher expression level in colonized *Bd* roots, (ii) covered all four 5′-terminal nucleotides, and (iii) had interesting Arabidopsis predicted targets involved in cell wall organization, regulation of hormone signalling, immunity, and gene regulation. Using multiplexed (cDNA generated from multiple hairpin sRNA primers simultaneously in one reaction) stem–loop PCR followed by gel electrophoresis, we detected all 14 *Sis*RNAs in 4-week-old axenic *Si* cultures (Fig. 2). Next, we cloned a random subset of six out of 14 *Sis*RNAs (*Sis*RNA21, SisRNA23, *Sis*RNA24, *Sis*RNA28, *Sis*RNA154, and *Sis*RNA296) and subjected them to Sanger sequencing, which further confirmed the expected *Sis*RNA sequences.

Effector-like *Sis*RNA candidates are detected in colonized *A. thaliana* roots

Next, we analysed the presence of the 14 *Sis*RNAs identified in axenic culture in *Si*-colonized *At* roots. Roots of 14-day-old seedlings were inoculated with chlamydospores and harvested at 3, 7, and 14 dpi. Root colonization was confirmed after 7

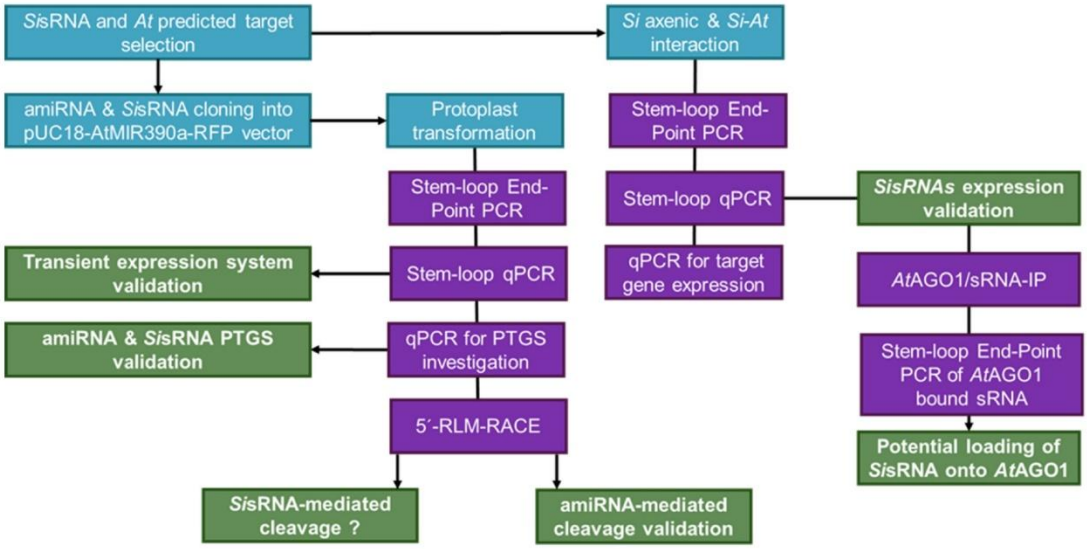

Fig. 1. Schematic flowchart showing the methods and outputs in this study. The blue colour indicates the different input material, and purple indicates the wet-lab steps. Green represents the validated outputs of the study. For details see also the Materials and methods. amiRNAs, artificial miRNA; *At*, *Arabidopsis thaliana*; PTGS, post-transcriptional gene silencing; *Si*, *Serendipita indica*; sRNA-IP, small RNA immunoprecipitation.

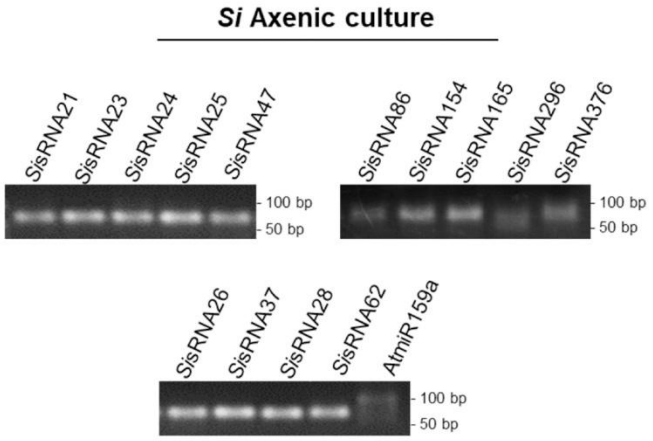

Fig. 2. Gel electrophoresis of stem–loop PCR products of potential *Sis*RNA effector candidates in *Serendipita indica*. Multiplexed stem–loop PCR confirmed the presence of *Sis*RNAs in a 4-week-old *Si* axenic culture. A PCR product of the expected size of 62 bp (sum of the 21 bp of the sRNA sequence, loop region, plus the forward primer and the reverse primer length) is visualized in a 2% agarose gel. The plant *At*miR159a of 21 nt served as a negative control. A shorter and weaker band of *Sis*RNA296 was detected possibly due to a lower abundance of the sRNA in the sample. A weak and unspecific amplification was detected for the *At*miR159a due to the multiplexing of hairpin primers or a possible partial complementarity of the hairpin primer to a non-target sequence.

dpi by confocal laser scanning microscopy using the chitin-specific dye wheat germ agglutinin linked to Alexa Fluor 488 (WGA–AF-488) (Fig. 3A) and by PCR using internal transcribed spacer (*Si-ITS*) primers and *Si*-specific *Ubiquitin* (*Si-Ubi*) primers (Supplementary Fig. S4). Multiplexed stem–loop PCR of total RNA extracted from *Si*-colonized *At* roots at different time points detected 13 of 14 *Sis*RNAs (Fig. 3B). Bands for *Sis*RNA21 and *Sis*RNA24 did not consistently show up at all three time points, probably because of the limitations associated with multiplexing the hairpin cDNA primers (Kramer, 2011;Varkonyi-Gasic and Hellens, 2011; Colombo *et al.*, 2013). Consistent with this notion, the expression of *Sis*RNA21 and *Sis*RNA24 was detected at 7 dpi using stem–loop PCR with less multiplexing (using four hairpin cDNA primers instead of 10 simultaneously in one reaction) (Supplementary Fig. S5). A random subset of the detected *Sis*RNAs (*Sis*RNA21, *Sis*RNA24, *Sis*RNA28, and *Sis*RNA154) were cloned and submitted for Sanger sequencing, confirming the expected *Sis*RNA sequences in *Si*-colonized *At* roots.

To assess the abundance and expression of *Sis*RNAs during the interaction with *At* roots, we selected *Sis*RNA21, *Sis*RNA24, *Sis*RNA28, and *Sis*RNA154, which were confirmed to be expressed in axenic culture and during *Si–At* interaction. Using stem–loop RT–qPCR, we detected all four *Sis*RNAs in inoculated *At* roots, while they could not be found in non-inoculated roots, indicating high abundance (Fig. 3C). These findings are consistent with the previous identification of these *Sis*RNAs in the *Si–Bd* interaction (Šečić *et al.*, 2021) (Supplementary Table S1).

amiRNAs mediate PTGS in transformed Arabidopsis protoplasts

To validate sRNA–mRNA interactions, we developed a protoplast-based sRNA expression system. Arabidopsis protoplasts are a reproducible and cost-effective model system to validate the expression and the potential silencing activity of

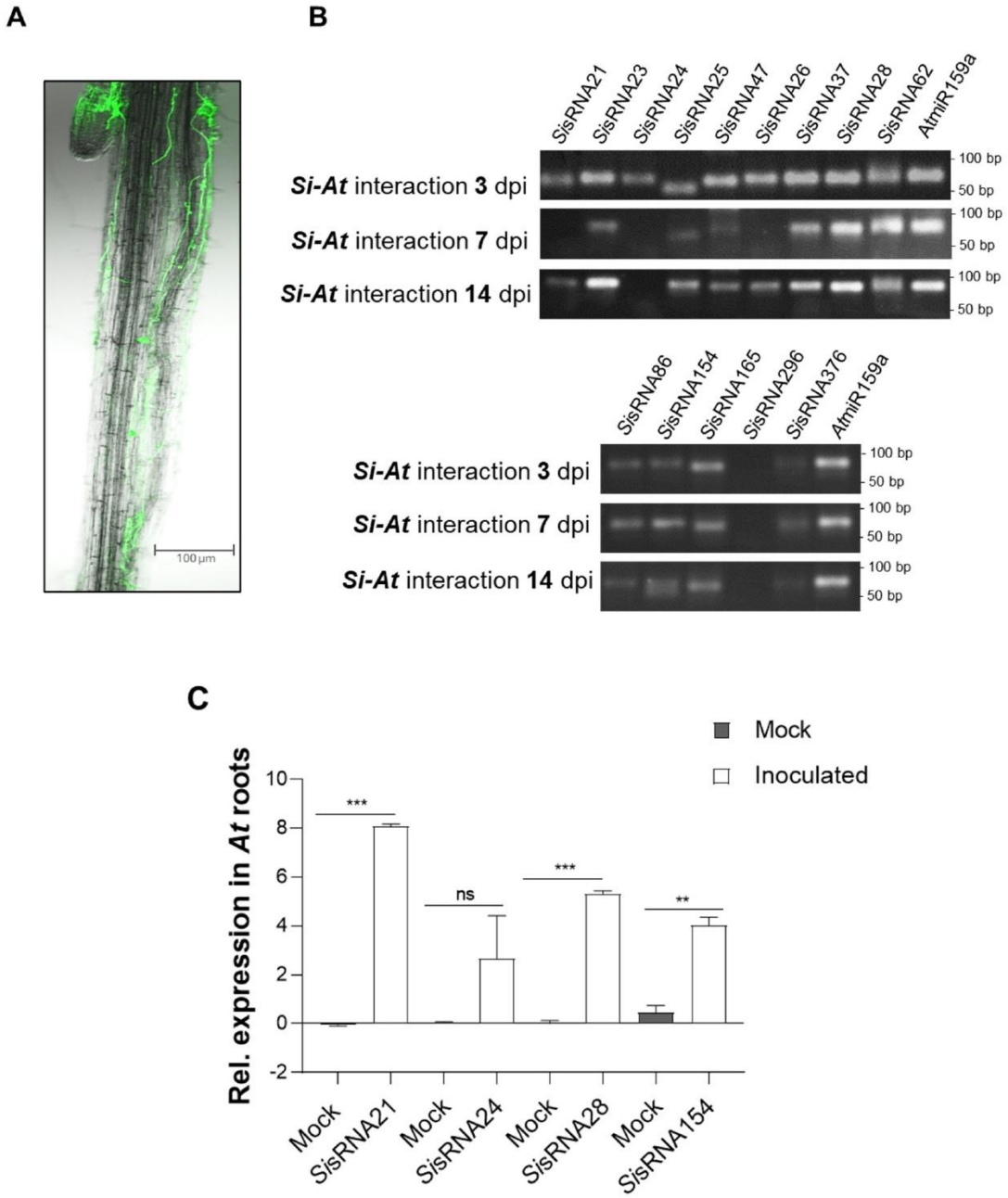

Fig. 3. Detection of putative effector-like *Sis*RNAs in Arabidopsis roots colonized by *Serendipita indica*. (A) Root colonization pattern at 7 days post-inoculation (dpi). Fluorescence microscopy (λexc494 nm, λem515) shows green chitin-specific WGA-AF488 staining of hyphal walls in the root maturation zone. (B) Detection of *Sis*RNAs in roots at 3, 7, and 14 dpi using multiplexed stem–loop PCR. Agarose gel analysis of *Sis*RNAs of the expected size of 62 bp. Plant *At*miR159a was used as a positive control for a plant-expressed sRNA. A shorter band of the *Sis*RNA25 was detected at 3 dpi, probably due to a lower abundance of the sRNA in the samples at that time point. (C) Relative expression of four *Sis*RNAs in Arabidopsis roots inoculated with *Si* at 7 dpi. The relative amounts of *Sis*RNA21, *Sis*RNA24, *Sis*RNA28, and *Sis*RNA154 during interaction with *At* were normalized to *At*miR159a and *At*miR166a. Values represent the mean ±SE of two independent biological replicates. Asterisks indicate significant differences at $^{*}P \leq 0.05$, $^{**}P \leq 0.01$, and $^{***}P \leq 0.001$ based on Student's *t*-test. ns=not significant.

*Sis*RNA on predicted *At* target genes. To confirm the reliability of the system, we first used amiRNAs. amiRNAs are designed following the P.SAMS software (Fahlgren *et al.*, 2016). The software identifies 21 nt sequences from the input transcript based on high sequence complementarity to the target mRNA with a target prediction score of 0 (also called expectation value, with an expectation value of 0 being the highest level of sequence complementarity and 5 being the

lowest), filters out off-targets using TargetFinder, and then designs the guide amiRNA following certain rules such as having a 5′-U nucleotide, a C at position 19, and a mismatch or a bulge at position 21. The use of amiRNAs allowed the amiRNA–mRNA binding to be manipulated, as they are artificially designed to have almost complete complementarity with the mRNA target gene, unlike naturally occurring *Si*sRNAs, which have varying degrees of mismatch with their predicted target genes. To this end, we designed four amiRNAs of 21 nt, namely amir21, amir24, amir154, and amir296, that almost fully match the predicted target genes *AT5G25350*, *AT2G39020*, *AT4G32160*, and *AT2G45240*, respectively, and exhibit a U at their 5′ end. Target genes were chosen based on their functions with *AT5G25350* (*EIN3-BINDING F BOX PROTEIN 2*), a negative regulator of the ethylene-activated signalling pathway, *AT2G39020* (*GCN5-RELATED N-ACETYLTRANSFERASE 8*) potentially involved in development and stress response pathways, *AT4G32160* [*Phox* (*PX*) *DOMAIN-CONTAINING PROTEIN EREL1*] predicted to be involved in membrane trafficking, and *AT2G45240* (*METHIONINE AMINOPEPTIDASE 1A*) involved in post-translational modification of proteins.

Information on the amiRNAs is summarized in Supplementary Table S2, including their 5′-terminal nucleotides, their predicted *At* target genes, their target aligned fragment, and their target prediction expectation values, indicating the degree of mismatches between the amiRNAs and the *At* target sequence. Alignment of the designed amiRNAs to their predicted target fragment is illustrated in Supplementary Fig. S3A and B. Subsequently, the four amiRNAs were cloned into the pUC18-*At*MIR390a-B/c-RFP vector and transformed into *At* protoplasts, reaching a transformation efficiency of 65–90% (calculated as the ratio between the red fluorescing protoplasts and the total number of viable protoplasts; Supplementary Fig. S6). The four amiRNAs were successfully expressed in protoplasts as detected by duplexed stem–loop PCR (Fig. 4A). Amplification products were cloned into the pGEM-T® cloning vector, and sequencing confirmed amiRNAs sequences.

Next, we quantified amiRNA accumulation in protoplasts using stem–loop RT–qPCR. All four amiRNAs were successfully detected in transformed protoplasts, while they could not be found in non-transformed protoplasts, indicating a high accumulation (Fig. 4B).

Target gene down-regulation in protoplasts was further assessed by qPCR 24 hours post-transformation (hptr), revealing reductions of 68% for *AT5G25350*, 43% for *AT2G39020*, 50% for *AT4G32160*, and 65% for *AT2G45240* (Fig. 5).

5′-RLM-RACE reveals canonical cleavage in protoplasts transformed with amiRNA

We selected amir296 and its predicted target gene *AT2G45240* to investigate the canonical PTGS cleavage site by 5′-RLM-RACE (Llave *et al.*, 2002; Ueno *et al.*, 2022). Samples were obtained from transformed protoplasts at 24 hptr, from control protoplasts (without amiRNA construct), and from non-treated protoplasts. A distinct band of ~383 bp was amplified from protoplasts expressing amir296, consistent with the expected size of the canonical cleavage product predicted to be targeted by amir296. Unexpectedly, weaker DNA fragments of a similar size were detected in both control and non-treated protoplasts (Fig. 6A). Cloning and subsequent sequencing of the amplicons confirmed that all sequences aligned with the *AT2G45240* sequence, and 50% of the obtained sequences from protoplasts transformed with pUC18-*At*MIR390a-RFP-amir296 (three of six clones) exhibited the canonical cleavage site between nucleotides 10 and 11 of amir296. In contrast, PCR products from control and non-treated protoplasts contained an *AT2G45240* fragment, but did not correspond to a canonical cleavage site, suggesting a possible cleavage by an endogenous miRNA near the amir296-binding site or RNA degradation (Fig. 6B).

Effector-like *Si*sRNA candidates mediate PTGS in transformed Arabidopsis protoplasts

Next, we transiently transformed protoplasts with *Si*sRNAs to demonstrate their gene silencing activity. *At* protoplasts were transformed with the pUC18-*At*MIR390a-RFP expression construct containing *Si*sRNA21, *Si*sRNA24, *Si*sRNA28, and *Si*sRNA154, respectively (confirmed in axenic culture and *Si*–*At* interaction). Duplexed stem–loop PCR confirmed the expression and amplification of the four *Si*sRNAs (Fig. 7). The amplification products were cloned into the pGEM-T® cloning vector, and sequencing confirmed their identity. Validation of *Si*sRNA accumulation was performed using stem–loop RT–qPCR for *Si*sRNA28 and *Si*sRNA154 to further confirm the success of the protoplast transformation system (Supplementary Fig. S7).

Next, we investigated the ability of the expressed *Si*sRNAs to induce PTGS of predicted target genes in protoplasts. From 199 Arabidopsis target genes of *Si*sRNA21, *Si*sRNA24, *Si*sRNA28, and *Si*sRNA154 predicted using psRNATarget (Supplementary Dataset S1), we selected 13 genes for further analysis, prioritizing those with intriguing descriptions and with a potential involvement in mutualistic interaction and plant immunity. *Si*sRNA24 was predicted to target five *At* genes: *AT1G57590* (*PECTIN ACETYLESTERASE 2*), involved in cell wall organization, *AT1G63180* (*UDP-D-GALACTOSE 4-EPIMERASE 3*), involved in pollen development, *AT1G65090* (*SEED LIPID DROPLET PROTEIN1*), involved in lipid droplet–plasma membrane tethering, *AT4G15765* [*FAD/NAD(P)-BINDING OXIDOREDUCTASE FAMILY PROTEIN*], involved in jasmonic acid-mediated signalling, and *AT5G16680* (*Protein PARALOG OF AIPP2, PAIPP2, PHD2*), involved in regulation of gene expression (Supplementary Dataset S1;

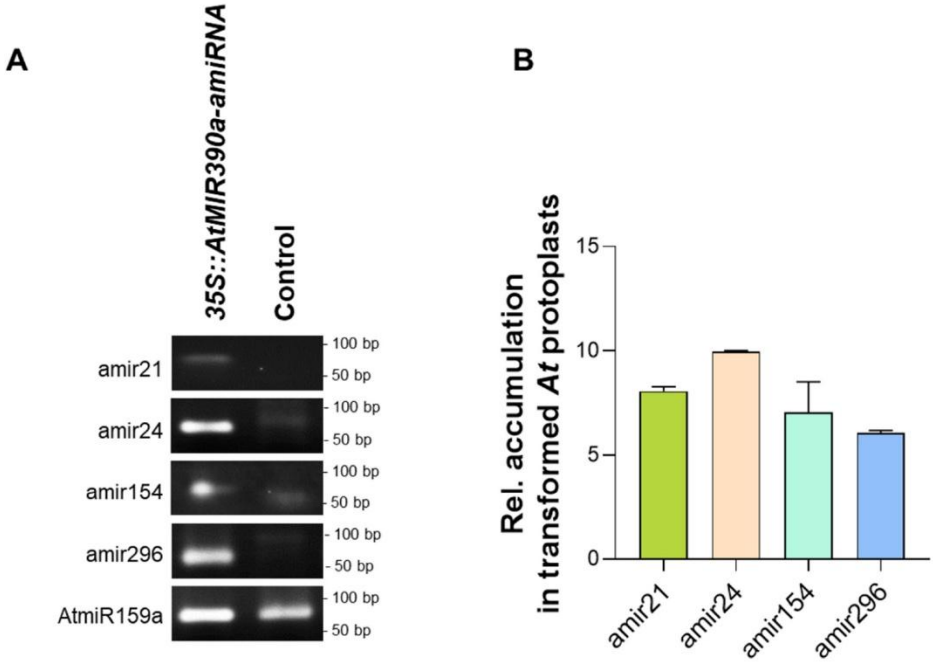

Fig. 4. Expression and accumulation of amiRNAs in transformed Arabidopsis protoplasts. (A) Agarose gel analysis confirming expression of all four amiRNAs (amir21, amir24, amir154, and amir296) in transformed protoplasts 24 hours post-transformation (hptr), but not in control protoplasts, using duplexed stem–loop PCR. No amplification or only weak bands of primer dimers were seen in the control protoplast (without construct) samples, probably due to the high number of cycles in the stem–loop PCR. Plant *At*miR159a of 21 nt was used as a positive control. (B) Relative accumulation of the four amiRNAs in transformed Arabidopsis protoplasts at 24 hptr. The relative amounts of amir21, amir24, amir154, and amir296 were normalized to *At*miR159a. Values represent the mean ±SE of three technical replicates from one biological replicate.

Supplementary Table S3). Expression of *Si*sRNA24, which carries a U at the 5′-terminus, and thus a preference for AGO1 (Mi *et al.*, 2008; Montgomery *et al.*, 2008; Takeda *et al.*, 2008), significantly reduced the mRNA abundance of *AT1G63180*, *AT1G65090*, *AT4G15765*, and *AT5G16680* in protoplasts 24 hptr by 63, 56, 45, and 73%, respectively (Fig. 8A). Similarly, *Si*sRNA154, also with 5′-U, is predicted to target *AT2G47600* (*MAGNESIUM/PROTON EXCHANGER*) involved in magnesium, iron, and zinc ion transport, and *AT4G32160* [*Phox* (*PX*) *DOMAIN-CONTAINING PROTEIN EREL1*], involved in signal transduction. Expression of *Si*sRNA154 significantly down-regulated the accumulation of *AT2G47600* mRNA by 37%, but not of *AT4G32160* (Fig. 8B). *Si*sRNA28 has a 5′-A, therefore a loading preference for AGO2 and AGO4 (Mi *et al.*, 2008; Montgomery *et al.*, 2008; Takeda *et al.*, 2008). Expression of *Si*sRNA28 in protoplasts did not result in down-regulation of any of the three predicted target genes, namely *AT1G05180* (*AUXIN RESISTANT 1*), involved in auxin-activated signalling pathway and response to cytokinin, *AT5G55930* (*ARABIDOPSIS THALIANA OLIGOPEPTIDE TRANSPORTER 1*), an oligopeptide transporter, and *AT3G06670* (*PLATINUM SENSITIVE 2 LIKE*) with a regulatory function in non-coding RNA processing (Fig. 8C). Finally, expression of *Si*sRNA21 with 5′-C and thus a preference for AGO5 (Mi *et al.*, 2008; Montgomery *et al.*, 2008; Takeda *et al.*, 2008) resulted in down-regulation of predicted target transcripts *AT5G25350* (*EIN3-BINDING F BOX PROTEIN 2*), a negative regulator of the ethylene-activated signalling pathway, and of *AT5G37600* (*ARABIDOPSIS GLUTAMINE SYNTHASE 1*), involved in nitrate assimilation, by 51% and 16%, respectively (Fig. 8D).

5′-RLM-RACE reveals non-canonical cleavage of Arabidopsis target genes in protoplasts expressing *Si*sRNAs with preference for AGO1

We selected *Si*sRNA24 to study the cleavage pattern of the down-regulated target transcripts *AT1G65090* and *AT4G15765* using 5′-RLM-RACE. For the predicted target gene *AT1G65090*, no band corresponding to an expected canonical cleavage product was detected. For the target gene *AT4G15765*, we detected a single band of 300 bp in protoplasts expressing *Si*sRNA24, which was shorter than the expected size (443 bp), while double bands were observed for the control protoplasts (Supplementary Fig. S8A). PCR amplicons from both transformed and control protoplasts were cloned into the pGEM-T® cloning vector and sequenced. Sequence analysis confirmed the alignment of the 300 bp RLM-RACE product with *AT4G15765*. However, it did not confirm the 5′ end position, between nucleotides 10 and 11, predicted for

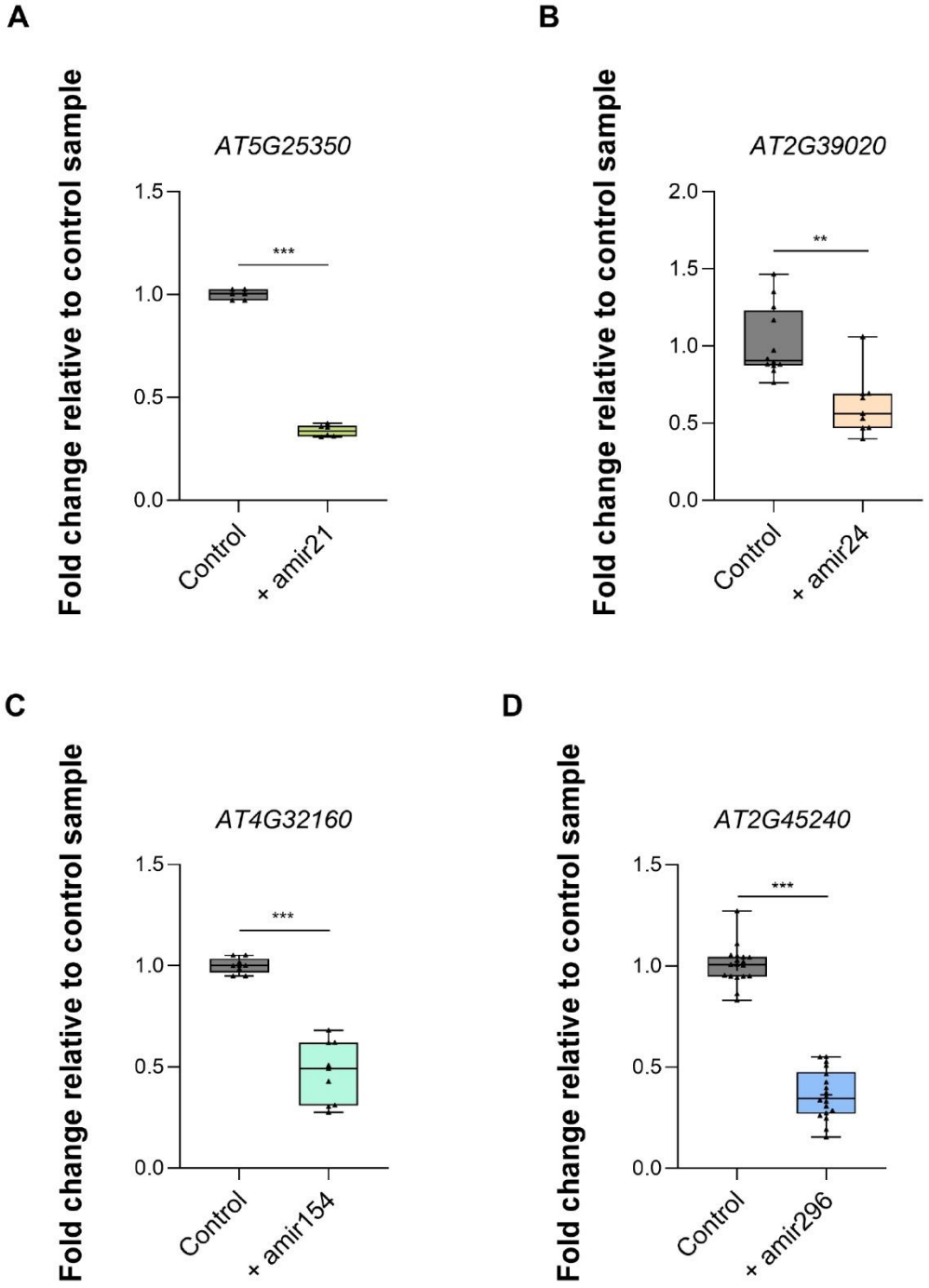

Fig. 5. qPCR analysis of target gene silencing in Arabidopsis protoplasts 24 hptr with amiRNAs. The mRNA transcript levels of the target genes (A) *AT5G25350*, (B) *AT2G39020*, (C) *AT4G32160*, and (D) *AT2G45240* in transformed protoplasts (+) expressing amir21, amir24, amir154, or amir296 were normalized against the housekeeping gene *Ubiquitin* (*UBC21*, *AT5G25760*) and displayed as fold change relative to control protoplasts (without amiRNA construct). Data are the average of 2–3 biological replicates ±SD. Asterisks indicate a difference at **P*≤0.05, ***P*≤0.01, and ****P*≤0.001 according to Student's *t*-test. ns=not significant.

*Sis*RNA24-guided canonical cleavage (Supplementary Fig. S8B). The absence of cleavage and/or a canonical cleavage product does not exclude the potential of *Sis*RNA24 in mediating predicted *At* gene silencing, as many previous studies have highlighted the challenge of identifying sRNA cleavage sites in plants (Brousse *et al.*, 2014; Werner *et al.*, 2021).

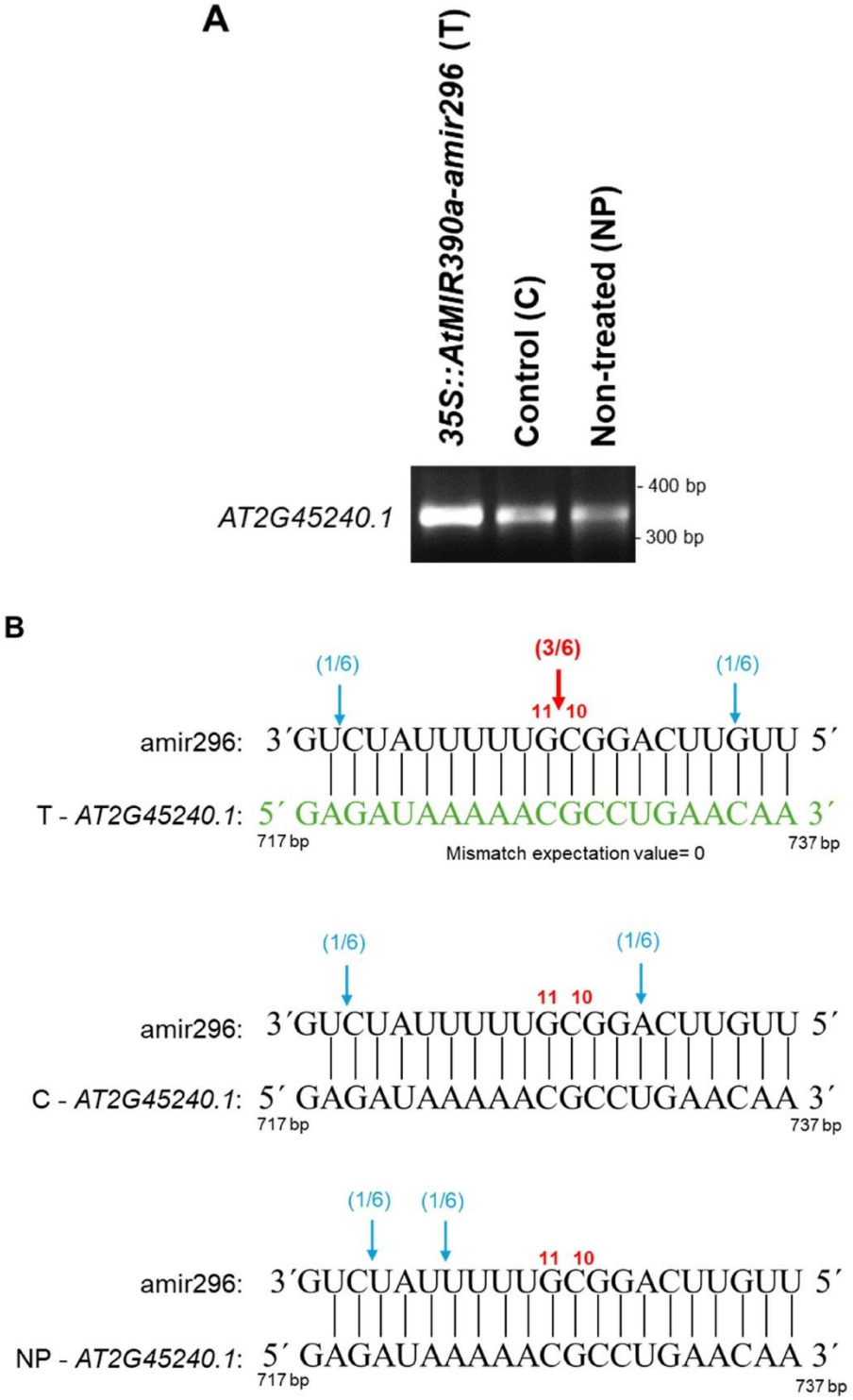

Fig. 6. Identification of 5′-RLM-RACE target sites in *AT2G45240* mRNA following amir296 expression in Arabidopsis protoplasts. (A) PCR products of the second nested 5′-RLM-RACE-PCR visualized in an ethidium bromide–agarose gel. RNA was extracted from protoplasts transformed with amir296 (T) and from corresponding control protoplasts (C) and untreated protoplasts (NP). (B) Mapping of *AT2G45240* target cleavage products by 5′-RLM-RACE. The predicted base pairing between amir296 and *AT2G45240* is shown in green. The red arrow indicates the detected canonical cleavage site, and the blue arrows indicate non-canonical cleavage occurring probably due to RNA degradation or a non-identified *At* miRNA action nearby. The proportion of cloned 5′-RLM-RACE products at the different cleavage sites is shown in parentheses. For protoplasts transformed with amir296, three colonies have the 5′ end at the expected position, opposite to nucleotides 10–11 of amir296, which is not the case for control and untreated protoplasts. A mismatch expectation value (also called target predicted score) of 0 indicates an almost full complementarity between amir296 and the target gene *AT2G45240* (expectation values range between 0 and 5, with 0 being the highest level of sequence complementarity and 5 being the lowest).

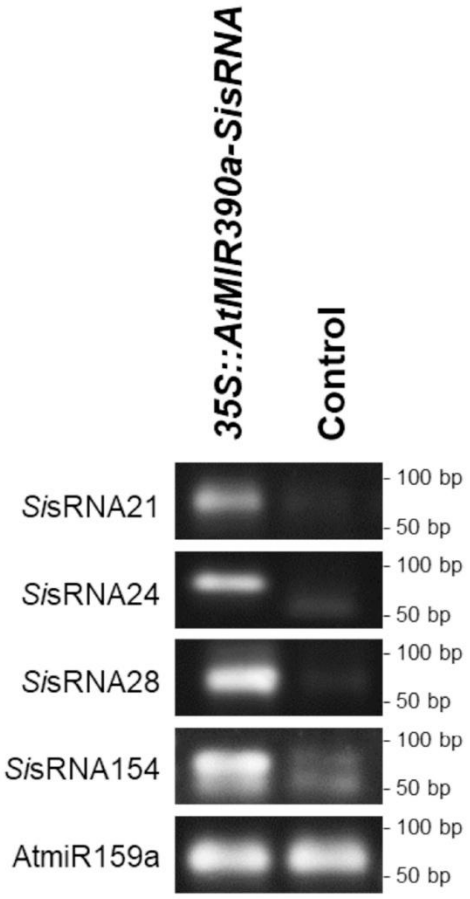

Fig. 7. Duplexed stem–loop PCR confirming expression of *Si*sRNAs in Arabidopsis protoplasts. Agarose gel analysis of stem–loop PCR detected expression of all four *Si*sRNAs in transformed protoplasts at 24 hptr, but not in control protoplasts (without *Si*sRNA construct). No amplification or weak bands of primer dimers were seen in the control protoplasts (without construct) samples, probably due to the high number of cycles in the stem–loop PCR. Plant *At*miR159a of 21 nt was used as a positive control.

Si–At interaction induces changes in predicted Arabidopsis target genes

To assess how the symbiotic interaction modulates gene expression in *At* roots, we examined the expression levels of the 15 predicted *At* target genes analysed for silencing in protoplasts transformed with amiRNAs and *Si*sRNAs. We performed RT–qPCR on inoculated and mock-treated (non-inoculated) *At* roots at 3 and 7 dpi, and found dynamic, time-dependent changes in gene expression, with distinct expression patterns observed at 3 and 7 dpi. A general trend of down-regulation was observed at 7 dpi for the majority of the target genes analysed. The differential expression patterns in the *Si–At* interaction are shown in Fig. 9.

Effector-like *Si*sRNA candidates are loaded onto Arabidopsis AGO1

To further substantiate the hypothesis that *Si*sRNAs are loaded into the *At* RISC during the *Si–At* interaction, we conducted *At*AGO1–sRNA Co-IP using samples of *Si*-colonized roots, followed by stem–loop PCR analysis (Carbonell, 2017b; Dunker *et al.*, 2021). To exclude the possibility that the *At*-specific anti-AGO1 antibody would cross-react with fungal AGOs, we first performed an *At*AGO1–sRNA Co-IP followed by western blot analysis using a 4-week-old axenic culture. No binding of the *At*AGO1-specific antibody was detected in the crude extract either in the supernatant or in the IP fraction in comparison with the total loaded proteins from *Si* axenic culture, confirming the specificity of the plant anti-AGO1 antibody (Supplementary Fig. S9A). In line with this, no *Si*sRNAs could be detected by stem–loop PCR using *Si*sRNA-specific stem–loop primers (Supplementary Fig. S9B). Similarly, western blot analysis of *At*AGO1-IP of samples from *Si*-colonized *At* roots and *At* mock-treated roots was performed. AGO1 accumulation was observed in crude extracts and IP fractions, with a stronger signal in the IP fraction than in the supernatant from the *Si–At* sample (Fig. 10A, B).

Next, we recovered the *At*AGO1-bound sRNA from the Co-IP sample of *Si*-colonized roots (*Si–At*). Stem–loop PCR was performed and detected the *At*AGO1-bound *At*miR159a and a band of the expected size for *Si*sRNA21, *Si*sRNA23, *Si*sRNA24, and *Si*sRNA28 (Fig. 11), whereas *At*miR393a*, which is known to preferably bind *At*AGO2 (Mi *et al.*, 2008), was undetectable. Stem–loop PCR products from the *Si–At* Co-IP fraction were cloned and sequenced. The sequencing results confirmed the presence of plant *At*miR159a as well as *Si*sRNA24 and *Si*sRNA28, with the exact same sequences detected from axenic culture and *Si*-colonized *At* roots, confirming the success of the pull-down. In addition, two *Si*sRNAs with almost identical sequences to *Si*sRNA21 and *Si*sRNA23 were also co-immunoprecipitated (Supplementary Table S9). Such mismatches may be caused by the processing steps of the sRNAs until the loading into the AGO1, which may result in sequence variations compared with the total RNAseq performed in our previous work (Šečić *et al.*, 2021). Nevertheless, these results show that detected *Si*sRNAs are bound to *At*AGO1, supporting the notion that *Si*sRNAs are transferred into *At* root cells during root colonization and loaded into the plant RNAi machinery.

A systematic overview of the investigated *Si*sRNAs and their experimental results is provided in Supplementary Table S10. In conclusion, this study provides a blueprint for rapid selection and analysis of sRNA effectors and further supports the model of cross-kingdom communication in Sebacinalean symbiosis.

Discussion

In this work, we developed an experimental pipeline (Fig. 1) for the analysis of putative fungal sRNA effectors and investigated their role in host target gene silencing. We have previously reported the identification and analysis of fungal *Si*sRNAs

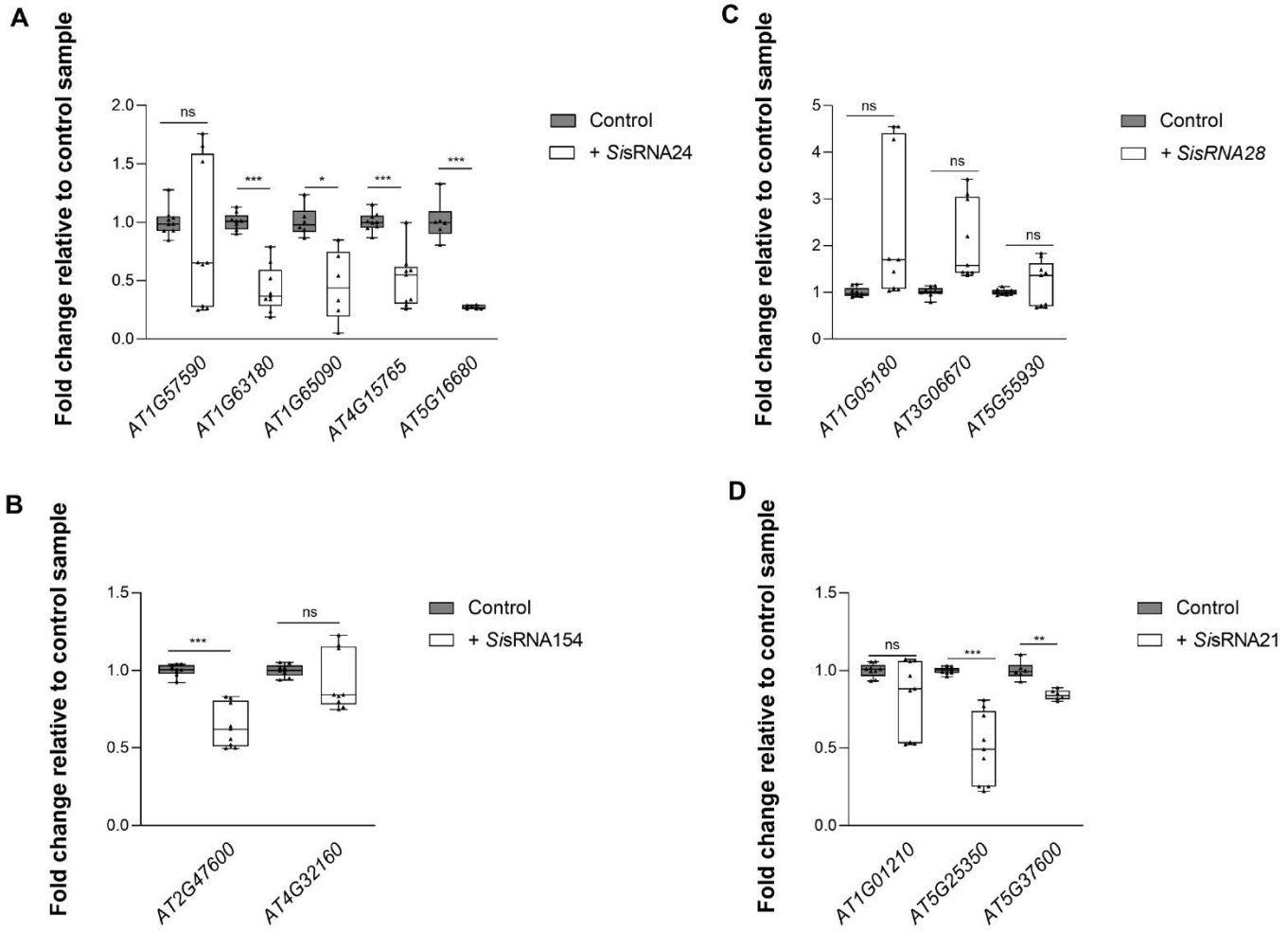

Fig. 8. qPCR analysis of target gene silencing in Arabidopsis protoplasts 24 hptr with *Sis*RNAs versus control protoplasts (without *Sis*RNA construct). The mRNA transcript levels of target genes in transformed protoplasts (+) expressing (A) *Sis*RNA24, (B) *Sis*RNA154, (C) *Sis*RNA28, and (D) *Sis*RNA21 normalized against the housekeeping gene *Ubiquitin* (*UBC21*, *AT5G25760*) are displayed as fold change relative to control protoplasts (without *Sis*RNA construct). Data are the average of 2–3 biological replicates ±SD. Asterisks indicate a difference at **P*≤0.05, ***P*≤0.01, and ****P*≤0.001 according to Student's *t*-test. ns=not significant.

induced in the interaction of the beneficial root endophyte *S. indica* with *B. distachyon* (Šečić *et al.*, 2021). To bridge the gap between the large amount of bioinformatic data available from this previous study and the functional validation of the *Sis*RNAs, we established a rapid and reproducible roadmap for the validation of *Sis*RNAs using an Arabidopsis protoplast system. First, we validated the effectiveness of our pipeline by expressing amiRNAs and *Sis*RNA in protoplasts and confirmed their accumulation and their potential to induce PTGS of predicted *At* target genes. Moreover, we confirmed the accumulation of the selected *Sis*RNAs in *Si*-colonized roots, where fungal colonization induced transcriptional changes in some of the investigated *At* genes. Second, using IP pull-down assay, we showed that *Sis*RNAs are loaded into the plant RNAi machinery, suggesting the translocation of *Sis*RNAs into host cells. Following that, we detected *Sis*RNA24 and *Sis*RNA28 bound to *At*AGO1, supporting the ckRNAi hypothesis.

To test the functionality of the selected *Sis*RNAs in the Sebacinoid symbiosis, we generated a construct to express sRNAs in *At* protoplasts based on the pUC18 backbone vector and the *At*MIR390a distal stem–loop, which can generate 21 nt amiRNAs or *Sis*RNAs. The *At*MIR390a precursor belongs to the MIR390 family, which is highly conserved and precisely produced and processed in several plant species (Axtell *et al.*, 2006; Cuperus *et al.*, 2011). Carbonell *et al.* (2014) tested the functionality of the *At*MIR390a-based amiRNA vector in repressing target gene accumulation in *At* plants. Using the plant vector pMDC32B-*At*MIR390a-B/c enables the directed cloning of amiRNAs and their stable expression in dicotyledonous plants. Although MIR390 associates preferably with AGO7, the association of *At*MIR390a-derived amiRNAs that have a 5′-U can be directed to AGO1 (Montgomery *et al.*, 2008; Cuperus *et al.*, 2010; Carbonell *et al.*, 2014; Carbonell, 2017b). Conventionally, sRNA–AGO1-mediated cleavage results in a

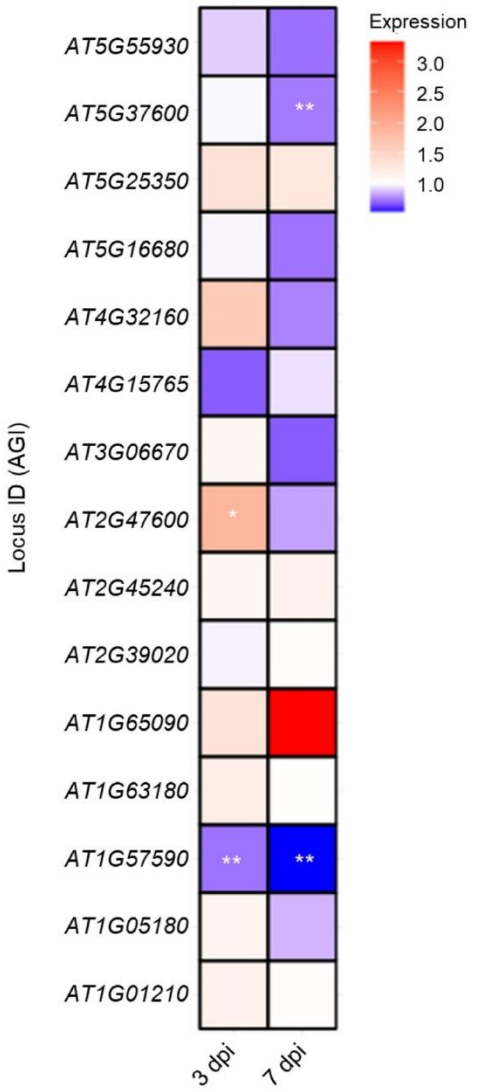

Fig. 9. Expression analysis of predicted Arabidopsis target genes under *Serendipita indica* colonization. The heat map shows transcript abundance as fold change of *At* genes assessed at 3 and 7 days post-inoculation (dpi) of root colonization. Colour intensity within each cell corresponds to the change in gene expression relative to non-inoculated samples, with red indicating up-regulation and blue indicating down-regulation. Data represent the mean of two independent biological replicates. Asterisks indicate significant differences at *$P \leq 0.05$, **$P \leq 0.01$, and ***$P \leq 0.001$ based on Student's *t*-test.

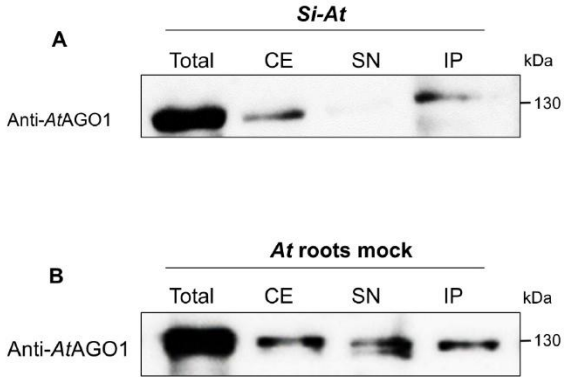

Fig. 10. Quality control of AGO1 co-immunoprecipitation by western blot analysis. Four sample fractions of the AGO1 Co-IP experiment were analysed: total protein before centrifugation and debris removal; crude extract (CE) after centrifugation and debris removal; supernatant (SN) after incubation with anti-*At*AGO1 and agarose beads; and IP fraction (resuspended IP pellet). The four fractions were analysed in *Si*-colonized roots (A) and mock-treated *At* roots (B). Both panels show the detection of *At*AGO1 using anti-*At*AGO1-specific antibody at the expected size of ~130 kDa. Of note, AGO1 signals were stronger in IP fractions than in SN. The broad-range pre-stained protein marker was used as a protein size marker.

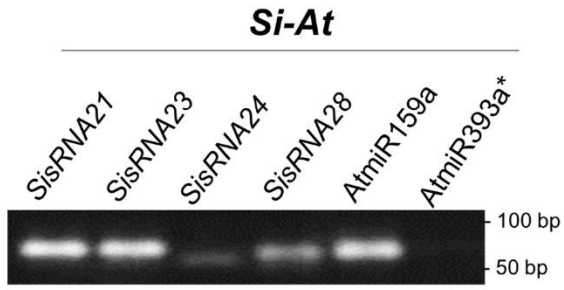

Fig. 11. *Si*sRNAs co-immunopurified with *At*AGO1 in samples from *Si*-colonized Arabidopsis roots. Stem–loop PCR confirms the presence of *Si*sRNA21, *Si*sRNA23, *Si*sRNA24, and *Si*sRNA28, as well as AGO1-bound *At*miR159a, but not AGO2-bound *At*miR393a* in AGO1 Co-IP samples from *Si*-colonized *At* roots harvested at 7 days post-inoculation.

canonical cut between nucleotides 10 and 11 of the sRNA at the corresponding mRNA site. This cleavage is a confirmation of sRNA loading into AGO1, formation of the RISC, and the processing of the mRNA transcript (Addo-Quaye *et al.*, 2009; Huntzinger and Izaurralde, 2011). In our approach, we combined the advantages of plant expression vectors and the protoplast transient expression system, both considered valuable tools, to study gene silencing and the molecular mechanisms of RNAi in plants (Tyurin *et al.*, 2020). *At* protoplasts offer some significant advantages for studying and validating sRNA functionalities. As *At* is a well-characterized model organism with a well-characterized RNAi machinery, *At* protoplasts enable detailed mechanistic studies of sRNA processing and AGO loading. Moreover, using *At* protoplasts allows the study of the *Si*sRNA–*At* predicted target interaction within a native biological and a genetically compatible context as compared with alternative—often used—transient transformation systems such as, for example, *Nicotiana benthamiana* protoplasts, which would require heterologous expression of both *Si*sRNAs and their predicted targets, thus complicating experiments and introducing new variabilities. While the most appropriate transformation system would be the use of *At* root protoplasts, their isolation is challenging due to the complexity of root cell walls, resulting in low cell yield and viability (Pasternak *et al.*, 2021). Moreover, root protoplasting results in a mixture of protoplasts derived

from different cell types, while *Si* only colonizes rhizodermis and cortex cells (Jacobs *et al.*, 2011). Overall the *At* protoplast system offers better regulatory control and biological relevance, particularly for exploring root symbiosis, as demonstrated in previous studies involving *S. indica* (Osborne *et al.*, 2023).

To confirm the robustness of the protoplast transformation system, we first used amiRNAs with an almost perfect match to a predicted plant target gene. When expressed in *At* protoplasts, all four amiRNAs, namely amir21, amir24, amir154, and amir296 (Supplementary Table S2), induced a significant reduction in abundance of their corresponding target genes (Fig. 5), confirming their silencing activity in the protoplast system. amiRNAs used in our pipeline are algorithmically designed to exhibit a 5′-U, thereby enabling their loading into the AGO1 protein (Carbonell, 2017c). Consequently, they can enter the RISC and induce a down-regulation of the target gene. Accordingly, amir296, which mediated a 65% reduction of its predicted target *AT2G45240* (*METHIONINE AMINOPEPTIDASE 1A, MAP1A*), can direct a canonical cleavage, as detected by 5′-RLM-RACE between position 10 and 11 of amir296, confirming an *At*AGO1-mediated slicing of *AT2G45240* mRNA (Fig. 6).

We also confirmed by stem–loop PCR the expression and accumulation of the putative *Si*sRNA24 effector, exhibiting a 5′-U. Four of five predicted targets of *Si*sRNA24 showed a significantly reduced abundance in the transformed protoplasts (Fig. 8A). Moreover, *Si*sRNA154, which also has a 5′-U, directed down-regulation of *AT2G47600*, one of the two *At* predicted target genes (Fig. 8B).

An important factor to consider when studying PTGS mediated by putative sRNA effectors is the degree of mismatch. Expressed as 'Expectation value' or 'Target predicted score', it reports on the mismatch score between the predicted target mRNA and the sRNA. Previous studies have demonstrated that the number and position of mismatches between the sRNA and the corresponding target mRNA can significantly impact their binding affinity, eventually weakening the interaction and resulting in either non-significant or no down-regulation (Rhoades *et al.*, 2002; Ossowski *et al.*, 2008; Carbonell *et al.*, 2015). Studies have shown that mismatches within the sRNA seed region spanning nucleotides 2–12/13 are possible, but they may reduce the sRNA activity, whereas mismatches at position 1 or between nucleotides 14 and 21 are more tolerable (Mallory *et al.*, 2004; Carbonell, 2017a). Moreover, mismatches can also lead to a different mode of sRNA action. A mismatch can trigger a deadenylation pathway or a translational repression pathway instead of an mRNA degradation pathway, leading to a decrease in protein synthesis instead of mRNA degradation (Baulcombe, 2004; Carthew and Sontheimer, 2009). We hypothesize that a high abundance level of a target mRNA may lead to less detectable down-regulation, as its accessibility for the sRNA may have an impact on the silencing process and the detection of a canonical cleavage. It is also conceivable that the presence of other endogenous miRNAs, which may bind near or at the same mRNA-binding site, might disrupt sRNA–mRNA binding, modulate the regulatory outcome, and affect the gene expression pattern.

Further analysis of the molecular cleavage pattern of *Si*sRNA24 by 5′-RLM-RACE identified non-canonical cut sites in the target gene *AT4G15765*. This finding may be explained by the low abundance of the cleaved product, falling below the detection threshold of the RLM-RACE method. This low abundance would make the detection of a precise canonical cleavage challenging. Alternatively, it might also be possible that the cleavage site within the target mRNA is located at a different position. Hence, non-canonical cleavage sites of sRNA may be further investigated as several studies speculate that PTGS can still be induced through sRNA or phasiRNA directing non-canonical cleavage (Brousse *et al.*, 2014; Ivanova *et al.*, 2022). High-throughput sequencing of samples from the *Si–At* interaction, including transcriptional analysis and degradome sequencing, is needed to better understand *Si*sRNA-mediated target cleavage.

In our study, the Arabidopsis target *AT5G25350* is predicted to be targeted by both amir21 and *Si*sRNA21. When expressing amir21 (with 5′-U and an expectation value of 0), the mRNA abundance of *AT5G25350* declined to 68% (Fig. 5A). However, when expressing *Si*sRNA21 (with a 5′-C and an expectation value of 5), we observed down-regulation of 51% of the same target gene (Fig. 8D). Another example is the predicted gene *AT4G32160* targeted by amir154 and *Si*sRNA154, both with a 5′-U. The mRNA abundance of *AT4G32160* in protoplasts expressing amir154 (with an expectation value of 0) resulted in a reduction of 50% (Fig. 5C), but protoplasts expressing *Si*sRNA154 (with an expectation value of 4.5) did not show a reduction of *AT4G32160* transcript (Fig. 8B; overview in Supplementary Fig. S10). These results raise the possibility that amiRNAs are more prone to mediate target gene silencing, but further studies with additional amiRNAs and putative sRNAs are required to confirm these observations.

Analysis of host gene expression in response to *Si* colonization, together with PTGS induced by *Si*sRNAs in protoplasts, revealed significant patterns. *AT1G57590* encodes a pectin acetyl esterase (*PAE2*) that modifies pectin in plant cell walls, affecting their rigidity, porosity, and interactions with microbes. The gene was significantly down-regulated in *At* roots upon *Si* colonization at 3 and 7 dpi (Fig. 9). This finding suggests that the fungus manipulates cell wall properties to facilitate its colonization by increasing cell wall permeability. Single-cell RNA sequencing of *At* root showed that *PAE2* is highly expressed in the root rhizodermis (Rich-Griffin *et al.*, 2020), the primary tissue colonized by *Si* (Jacobs *et al.*, 2011). Interestingly, and in clear contrast, *PAE2* is up-regulated in *At* Col-0 leaves during infection by the necrotrophic pathogen *Botrytis cinerea* (Windram *et al.*, 2012) and by biotrophic *Pseudomonas syringae* pv. tomato DC3000 (Zhang *et al.*, 2007), suggesting an ambivalent role in plant–microbe interactions and in plant defence.

Although *Si*sRNA24 targets *PAE2*, no down-regulation was observed in transformed protoplasts (Fig. 8A), which could be

attributed to the low expression of *PAE2* in leaves (Schmid *et al.*, 2005) or to the importance of tissue-specific signalling in plant–mutual interactions, warranting further investigation.

Two other interesting genes are *AT5G37600*, encoding GLUTAMINE SYNTHASE 1 (GS1), a cytosolic enzyme involved in nitrogen assimilation by converting ammonium to glutamine, and *AT2G47600* encoding MAGNESIUM/PROTON EXCHANGER (*ATMHX*). Nitrogen metabolism and magnesium and iron transport are crucial for plant growth and the uptake of essential nutrients by the plant. Both proteins are associated with immune responses, particularly in the regulation of mutualistic interactions. *GS1* was down-regulated at 7 dpi upon *Si* colonization (Fig. 9), suggesting that the plant is potentially modulating its nitrogen assimilation pathways in response to the fungal endophyte. *ATMHX* was also down-regulated at 7 dpi upon *Si* colonization (Fig. 9). Overall, the reduced nitrogen assimilation and magnesium/iron transport activity may reflect a shift in resource allocation that reduces nitrogen uptake and manipulates the nutrient transport to favour *Si* colonization. Additionally, or alternatively, the down-regulation of these genes suggests that *Si* modifies related signalling pathways. This supports the hypothesis presented by Scholz *et al.* (2023), suggesting that *Si* supports nitrogen-starved *At* seedlings by supplying nitrogen metabolites, thereby moderating metabolic nitrogen deficiency responses and reprogramming the expression of nitrogen metabolism-related genes. Of note, both *GS1* and *ATMHX* were confirmed to be down-regulated in protoplasts transformed with *Si*sRNA21 and *Si*sRNA24. In contrast, they are up-regulated in response to infection by *B. cinerea* and *P. syringae* (Zhang *et al.*, 2007; Windram *et al.*, 2012), suggesting a broader role in plant immune responses and mutualism. Moreover, both *GS1* and *ATMHX* are highly expressed in mock-treated *At* leaves and roots, particularly in the pericycle, cortex, and rhizodermis (Schmid *et al.*, 2005; Rich-Griffin *et al.*, 2020). Overall, these previous reports along with our findings strongly suggest the hypothesis that *Si* uses sRNAs to manipulate host nitrogen metabolism. Together, the data suggest that down-regulation of specific Arabidopsis genes during the Sebacinalean symbiosis does not seem to be a random event, but an effective mechanism by which the fungus manipulates the fitness of the host plant. By silencing host genes, *Si* creates a favourable environment for its colonization and nutrient acquisition, a phenomenon well documented in the literature (Qiang *et al.*, 2012; Hua *et al.*, 2017).

Hence, our data are consistent with the model that ckRNAi has evolved as an efficient mechanism in symbiosis of a plant and a fungus, striking a balance between host resistance and symbiotic benefits. Further investigation into these processes will provide deeper insights into the evolutionary advantages of ckRNAi in plant–microbe interactions.

We further evaluated ckRNAi by *At*AGO1–sRNA Co-IP on samples from *Si*-colonized *At* roots. Western blot analysis showed the enrichment of the *At*AGO1 in the IP fraction (Fig. 10). *Si*sRNA24 and *Si*sRNA28 were subsequently shown by stem–loop PCR to co-precipitate with *At*AGO1 (Fig. 11), providing strong evidence for the translocation of *Si*sRNAs and their incorporation into the RNAi machinery of *At*. Importantly, the identification in the *At*AGO1-IP of two *Si*sRNAs exhibiting nucleotide variations at their 3′ terminus to the previously identified *Si*sRNA (*Si*sRNA21 and *Si*sRNA23) suggests alternative *Si*sRNA variants. The presence of such variants highlights the complexity of the sRNA-mediated regulatory networks during *Si–At* root colonization. AGO-IP is a straightforward method to experimentally validate the loading of sRNAs into AGO proteins and to identify biologically functional sRNAs and miRNAs. However, the possibility of post-cell lysis association of sRNAs with AGOs cannot be excluded. Although testing for sRNA binding during sample lysis is not a common practice in AGO-IP workflows, it can rule out post-lysis AGO1–sRNA artifacts, as shown in Brosnan *et al.* (2019). Importantly, the absence of *At*miR393a*—preferentially loaded into AGO2—in our AGO1–sRNA Co-IP further supports that the detected AGO1-specific miRNAs and *Si*sRNAs were loaded *in vivo*. Moreover, independent confirmation of sRNA–mRNA binding and target down-regulation, as used in our pipeline, strengthens the evidence that *Si*sRNAs are incorporated into the RISC, rather than being the result of post-lysis artifacts.

In conclusion, we have developed a transient protoplast expression system to investigate the potential role of putative effector-like *Si*sRNA candidates in regulating target gene expression in *At*. This validation tool will not only help to understand the underlying molecular mechanism of *Si*sRNA-mediated PTGS but will also allow us to examine ckRNAi in mutualistic plant–fungal association. By studying *Si*sRNA-mediated PTGS, we have gained first insights that the endophytic fungus *Si* uses effector-like sRNAs to establish its mutualistic symbiosis with plants by modulating nitrogen metabolism and magnesium and iron transport as one strategy. Further studies will show whether *Si* utilizes its sRNAs to modulate the plant immune system, and additional genes may be identified as differentially regulated in symbiotic versus parasitic interactions.

Finally, amiRNAs are effective tools for fine-tuning gene expression in plants with a high silencing efficacy and thus are especially interesting for RNAi-mediated crop improvement strategies.

Supplementary data

The following supplementary data are available at *JXB* online.

Table S1. Information summary of the 14 *Si*sRNAs selected for this study.

Table S2. Sequences of amiRNAs cloned in the pUC18-*At*MIR390a-B/c-RFP construct and expressed in *At* protoplasts for PTGS validation.

Table S3. Sequences of *Si*sRNAs cloned in the pUC18-*At*MIR390a-B/c-RFP construct and expressed in *At* protoplasts for PTGS validation.

Table S4. Seventy five-mer oligonucleotides used for cloning *Si*sRNAs and amiRNAs into the pUC18-AtMIR390a-RFP vector.

Table S5. Primers used in stem–loop end-point and stem–loop qPCR.

Table S6. Primers used for gene expression analysis in qPCR.

Table S7. Primers used for RLM-RACE.

Table S8. PCR primers.

Table S9. Sequences of *Si*sRNAs detected in *Si* axenic and *Si–At* interaction compared with the respective stem–loop PCR amplicons detected from *Si–At* Co-IP.

Table S10. Summary of the selected *Si*sRNAs used in this study.

Fig. S1. Cloning strategy workflow and final vector map

Fig. S2. Description of the 75-mer oligonucleotides for amiRNA and *Si*sRNA direct cloning in pUC18-AtMIR390a-B/c-RFP vector.

Fig. S3. Visualization of sRNA–mRNA predicted alignment.

Fig. S4. Expression of *S. indica*-specific genes in Arabidopsis roots inoculated with *S. indica,* as analysed by RT–PCR.

Fig. S5. Detection of *Si*sRNA21, *Si*sRNA24, and *Si*sRNA296 by multiplexed stem–loop PCR in Arabidopsis roots 7 d after inoculation with *S. indica*.

Fig. S6. Expression of amiRNAs or *Si*sRNAs in Arabidopsis leaf protoplasts.

Fig. S7. Relative accumulation of two *Si*sRNAs in transformed Arabidopsis protoplasts 24 hptr.

Fig. S8. 5′-RLM-RACE for two Arabidopsis target genes of *Si*sRNA24 in Arabidopsis protoplasts.

Fig. S9. *At*AGO1/sRNA co-immunoprecipitation from *Si* axenic culture to show the specificity of the Arabidopsis AGO1 antibody.

Fig. S10. Comparison of target down-regulation by putative and artificial sRNA after their transient expression in Arabidopsis protoplasts.

Dataset S1. Information on *At* predicted targets of SisRNAs used in this study.

Acknowledgements

The authors gratefully thank R. Eichmann for critically reading and correcting the manuscript. We also thank M. Ladera-Carmona and B.T. Werner for their comments and suggestions, and Christina Neumann for the technical support.

Author contributions

SN and JS: conceived the study; SN and K-HK: wrote the paper; JS and EŠ: generated prediction of Arabidopsis targets from sRNAseq data; SN, KB, and SS: conducted the functional experiments. All authors read and approved the final manuscript.

Conflict of interest

The authors declare that they have no competing interests.

Funding

The work was supported by the German Research Foundation (DFG) in the DFG research unit RU 5116 on exRNA coordinated by KHK (individual grant number KO 1208/32-1 to KHK). SN was supported by the Dr Ernst-Leopold Klipstein-Stiftung, Paderborn, Giessen.

Data availability

All data associated with this paper are provided within the figures and supplementary data.

References

Addo-Quaye C, Snyder JA, Park YB, Li Y-F, Sunkar R, Axtell MJ. 2009. Sliced microRNA targets and precise loop-first processing of MIR319 hairpins revealed by analysis of the *Physcomitrella patens* degradome. RNA **15**, 2112–2121. doi: 10.1261/rna.1774909

Adhikari S, Turner M, Subramanian S. 2013. Hairpin priming is better suited than in vitro polyadenylation to generate cDNA for plant miRNA qPCR. Molecular Plant **6**, 229–231. doi: 10.1093/mp/sss106

Akum FN, Steinbrenner J, Biedenkopf D, Imani J, Kogel K-H. 2015. The *Piriformospora indica* effector PIIN_08944 promotes the mutualistic Sebacinalean symbiosis. Frontiers in Plant Science **6**, 906. doi: 10.3389/fpls.2015.00906

Axtell MJ, Jan C, Rajagopalan R, Bartel DP. 2006. A two-hit trigger for siRNA biogenesis in plants. Cell **127**, 565–577. doi: 10.1016/j.cell.2006.09.032

Bargmann BOR, Birnbaum KD. 2009. Positive fluorescent selection permits precise, rapid, and in-depth overexpression analysis in plant protoplasts. Plant Physiology **149**, 1231–1239. doi: 10.1104/pp.108.133975

Baulcombe D. 2004. RNA silencing in plants. Nature **431**, 356–363. doi: 10.1038/nature02874

Brosnan CA, Sarazin A, Lim P, Bologna NG, Hirsch-Hoffmann M, Voinnet O. 2019. Genome-scale, single-cell-type resolution of microRNA activities within a whole plant organ. The EMBO Journal **38**, e100754.

Brousse C, Liu Q, Beauclair L, Deremetz A, Axtell MJ, Bouché N. 2014. A non-canonical plant microRNA target site. Nucleic Acids Research **42**, 5270–5279. doi: 10.1093/nar/gku157

Cai Q, Qiao L, Wang M, He B, Lin F-M, Palmquist J, Huang S-D, Jin H. 2018. Plants send small RNAs in extracellular vesicles to fungal pathogen to silence virulence genes. Science **360**, 1126–1129. doi: 10.1126/science.aar4142

Carbonell A. 2017a. Artificial small RNA-based strategies for effective and specific gene silencing in plants. In: Dalmay T, ed. Plant gene silencing: mechanisms and applications. Wallingford, UK: CABI Publishing, 110–127. doi: 10.1079/9781780647678.0110

Carbonell A. 2017b. Immunoprecipitation and high-throughput sequencing of ARGONAUTE-bound target RNAs from plants. Methods in Molecular Biology **1640**, 93–112. doi: 10.1007/978-1-4939-7165-7_6

Carbonell A. 2017c. Plant ARGONAUTEs: features, functions, and unknowns. Methods in Molecular Biology **1640**, 1–21. doi: 10.1007/978-1-4939-7165-7_1

Carbonell A. 2019. Design and high-throughput generation of artificial small RNA constructs for plants. Methods in Molecular Biology **1932**, 247–260. doi: 10.1007/978-1-4939-9042-9_19

Carbonell A, Fahlgren N, Mitchell S, Cox K Jr, Mockler T, Carrington J. 2015. Highly specific gene silencing in a monocot species by artificial microRNAs derived from chimeric MIRNA precursors. The Plant Journal **82**, 1061–1075. doi: 10.1111/tpj.12835.

Carbonell A, Takeda A, Fahlgren N, Johnson SC, Cuperus JT, Carrington JC. 2014. New generation of artificial MicroRNA and synthetic

trans-acting small interfering RNA vectors for efficient gene silencing in Arabidopsis. Plant Physiology **165**, 15–29. doi: 10.1104/pp.113.234989

Carthew RW, Sontheimer EJ. 2009. Origins and mechanisms of miRNAs and siRNAs. Cell **136**, 642–655. doi: 10.1016/j.cell.2009.01.035

Colombo S, Nielsen HM, Foged C. 2013. Evaluation of carrier-mediated siRNA delivery: lessons for the design of a stem–loop qPCR-based approach for quantification of intracellular full-length siRNA. Journal of Controlled Release **166**, 220–226. doi: 10.1016/j.jconrel.2013.01.006

Cuperus JT, Carbonell A, Fahlgren N, Garcia-Ruiz H, Burke RT, Takeda A, Sullivan CM, Gilbert SD, Montgomery TA, Carrington JC. 2010. Unique functionality of 22 nt miRNAs in triggering RDR6-dependent siRNA biogenesis from target transcripts in Arabidopsis. Nature Structural & Molecular Biology **17**, 997–1003. doi: 10.1038/nsmb.1866

Cuperus JT, Fahlgren N, Carrington JC. 2011. Evolution and functional diversification of MIRNA genes. The Plant Cell **23**, 431–442. doi: 10.1105/tpc.110.082784

Dunker F, Lederer B, Weiberg A. 2021. Plant ARGONAUTE protein immunopurification for pathogen cross kingdom small RNA analysis. Bio-Protocol **11**, e3911. doi: 10.21769/BioProtoc.3911

Fahlgren N, Hill ST, Carrington JC, Carbonell A. 2016. P-SAMS: a web site for plant artificial microRNA and synthetic trans-acting small interfering RNA design. Bioinformatics **32**, 157–158. doi: 10.1093/bioinformatics/btv534

Galli M, Feldmann F, Vogler UK, Kogel K-H. 2024. Can biocontrol be the game-changer in integrated pest management? A review of definitions, methods and strategies. Journal of Plant Diseases and Protection **131**, 265–291. doi: 10.1007/s41348-024-00878-1

Glaeser SP, Imani J, Alabid I, *et al*. 2016. Non-pathogenic *Rhizobium radiobacter* F4 deploys plant beneficial activity independent of its host *Piriformospora indica*. The ISME Journal **10**, 871–884. doi: 10.1038/ismej.2015.163

Göhre V, Weiberg A. 2023. RNA dialogues in fungal–plant relationships. In Scott B, Mesarich C, eds. Plant relationships: fungal–plant interactions. Cham: Springer International Publishing. pp. 31–51. doi: 10.1007/978-3-031-16503-0_2

He B, Cai Q, Qiao L, Huang C-Y, Wang S, Miao W, Ha T, Wang Y, Jin H. 2021a. RNA-binding proteins contribute to small RNA loading in plant extracellular vesicles. Nature Plants **7**, 342–352. doi: 10.1038/s41477-021-00863-8

He B, Hamby R, Jin H. 2021b. Plant extracellular vesicles: Trojan horses of cross-kingdom warfare. FASEB Bioadvances **3**, 657–664. doi: 10.1096/fba.2021-00040

Hua MDS, Senthil Kumar R, Shyur LF, Cheng Y-B, Tian Z, Oelmüller R, Yeh K-W. 2017. Metabolomic compounds identified in *Piriformospora indica*-colonized Chinese cabbage roots delineate symbiotic functions of the interaction. Scientific Reports **7**, 9291. doi: 10.1038/s41598-017-08715-2

Huang G, Allen R, Davis EL, Baum TJ, Hussey RS. 2006. Engineering broad root-knot resistance in transgenic plants by RNAi silencing of a conserved and essential root-knot nematode parasitism gene. Proceedings of the National Academy of Sciences, USA **103**, 14302–14306. doi: 10.1073/pnas.0604698103

Huntzinger E, Izaurralde E. 2011. Gene silencing by microRNAs: contributions of translational repression and mRNA decay. Nature Reviews. Genetics **12**, 99–110. doi: 10.1038/nrg2936

Ivanova Z, Minkov G, Gisel A, Yahubyan G, Minkov I, Toneva V, Baev V. 2022. The multiverse of plant small RNAs: how can we explore it? International Journal of Molecular Sciences **23**, 3979. doi: 10.3390/ijms23073979

Iwakawa H, Tomari Y. 2022. Life of RISC: formation, action, and degradation of RNA-induced silencing complex. Molecular Cell **82**, 30–43. doi: 10.1016/j.molcel.2021.11.026

Jacobs S, Zechmann B, Molitor A, Trujillo M, Petutschnig E, Lipka V, Kogel K-H, Schäfer P. 2011. Broad-spectrum suppression of innate immunity is required for colonization of Arabidopsis roots by the fungus *Piriformospora indica*. Plant Physiology **156**, 726–740. doi: 10.1104/pp.111.176446

Koch A, Kumar N, Weber L, Keller H, Imani J, Kogel K-H. 2013. Host-induced gene silencing of cytochrome P450 lanosterol C14α-demethylase-encoding genes confers strong resistance to Fusarium species. Proceedings of the National Academy of Sciences, USA **110**, 19324–19329. doi: 10.1073/pnas.1306373110

Kramer MF. 2011. Stem–loop RT–qPCR for miRNAs. Current Protocols in Molecular Biology Chapter 15, Unit 15.10. doi: 10.1002/0471142727.mb1510s95

Lincoln C, Britton JH, Estelle M. 1990. Growth and development of the *axr1* mutants of Arabidopsis. The Plant Cell **2**, 1071–1080.

Liu S, Jaouannet M, Dempsey DA, Imani J, Coustau C, Kogel K-H. 2020. RNA-based technologies for insect control in plant production. Biotechnology Advances **39**, 107463. doi: 10.1016/j.biotechadv.2019.107463

Livak KJ, Schmittgen TD. 2001. Analysis of relative gene expression data using real-time quantitative PCR and the $2^{-\Delta\Delta CT}$ method.Methods **25**, 402–408. doi: 10.1006/meth.2001.1262

Llave C, Xie Z, Kasschau KD, Carrington JC. 2002. Cleavage of Scarecrow-like mRNA targets directed by a class of Arabidopsis miRNA. Science **297**, 2053–2056. doi: 10.1126/science.1076311

Mahanty B, Mishra R, Joshi RK. 2023. Cross-kingdom small RNA communication between plants and fungal phytopathogens—recent updates and prospects for future agriculture. RNA Biology **20**, 109–119. doi: 10.1080/15476286.2023.2195731

Mallory AC, Reinhart BJ, Jones-Rhoades MW, Tang G, Zamore PD, Barton MK, Bartel DP. 2004. MicroRNA control of PHABULOSA in leaf development: importance of pairing to the microRNA 5′ region. The EMBO Journal **23**, 3356–3364. doi: 10.1038/sj.emboj.7600340

Meyers BC, Axtell MJ. 2019. MicroRNAs in plants: key findings from the early years. The Plant Cell **31**, 1206–1207. doi: 10.1105/tpc.19.00310

Mi S, Cai T, Hu Y, *et al*. 2008. Sorting of small RNAs into Arabidopsis argonaute complexes is directed by the 5′ terminal nucleotide. Cell **133**, 116–127. doi: 10.1016/j.cell.2008.02.034

Montgomery TA, Howell MD, Cuperus JT, Li D, Hansen JE, Alexander AL, Chapman EJ, Fahlgren N, Allen E, Carrington JC. 2008. Specificity of ARGONAUTE7–miR390 interaction and dual functionality in TAS3 trans-acting siRNA formation. Cell **133**, 128–141. doi: 10.1016/j.cell.2008.02.033

Nasfi S, Kogel K-H. 2022. Packaged or unpackaged: appearance and transport of extracellular noncoding RNAs in the plant apoplast. ExRNA **5**, 13–13. https://exrna.amegroups.com/article/view/64855

Nowara D, Gay A, Lacomme C, Shaw J, Ridout C, Douchkov D, Hensel G, Kumlehn J, Schweizer P. 2010. HIGS: host-induced gene silencing in the obligate biotrophic fungal pathogen *Blumeria graminis*. The Plant Cell **22**, 3130–3141. doi: 10.1105/tpc.110.077040

Osborne R, Rehneke L, Lehmann S, *et al*. 2023. Symbiont–host interactome mapping reveals effector-targeted modulation of hormone networks and activation of growth promotion. Nature Communications **14**, 4065. doi: 10.1038/s41467-023-39885-5

Ossowski S, Schwab R, Weigel D. 2008. Gene silencing in plants using artificial microRNAs and other small RNAs. The Plant Journal **53**, 674–690. doi: 10.1111/j.1365-313X.2007.03328.x

Pasternak T, Paponov IA, Kondratenko S. 2021. Optimizing protocols for Arabidopsis shoot and root protoplast cultivation. Plants **10**, 375. doi: 10.3390/plants10020375

Pontecorvo G, Roper JA, Chemmons LM, Macdonald KD, Bufton AWJ. 1953. The genetics of Aspergillus nidulans. Advances in Genetics **5**, 141–238. doi: 10.1016/S0065-2660(08)60408-3

Qiang X, Weiss M, Kogel K-H, Schäfer P. 2012. *Piriformospora indica*—a mutualistic basidiomycete with an exceptionally large plant host range. Molecular Plant Pathology **13**, 508–518. doi: 10.1111/j.1364-3703.2011.00764.x

Qiao SA, Gao Z, Roth R. 2023. A perspective on cross-kingdom RNA interference in mutualistic symbioses. New Phytologist **240**, 68–79. doi: 10.1111/nph.19122

Reinhart BJ, Weinstein EG, Rhoades MW, Bartel B, Bartel DP. 2002. MicroRNAs in plants. Genes & Development **16**, 1616–1626. doi: 10.1101/gad.1004402

Ren B, Wang X, Duan J, Ma J. 2019. Rhizobial tRNA-derived small RNAs are signal molecules regulating plant nodulation. Science **365**, 919–922. doi: 10.1126/science.aav8907

Rhoades MW, Reinhart BJ, Lim LP, Burge CB, Bartel B, Bartel DP. 2002. Prediction of plant microRNA targets. Cell **110**, 513–520. doi: 10.1016/S0092-8674(02)00863-2

Rich-Griffin C, Eichmann R, Reitz MU, *et al*. 2020. Regulation of cell type-specific immunity networks in Arabidopsis roots. The Plant Cell **32**, 2742–2762. doi: 10.1105/tpc.20.00154

Rutter BD, Innes RW. 2018. Extracellular vesicles as key mediators of plant–microbe interactions. Current Opinion in Plant Biology **44**, 16–22. doi: 10.1016/j.pbi.2018.01.008

Sang H, Kim J-I. 2020. Advanced strategies to control plant pathogenic fungi by host-induced gene silencing (HIGS) and spray-induced gene silencing (SIGS). Plant Biotechnology Reports **14**, 1–8. doi: 10.1007/s11816-019-00588-3

Schmid M, Davison TS, Henz SR, Pape UJ, Demar M, Vingron M, Schölkopf B, Weigel D, Lohmann JU. 2005. A gene expression map of *Arabidopsis thaliana* development. Nature Genetics **37**, 501–506. doi: 10.1038/ng1543

Scholz SS, Barth E, Clément G, *et al*. 2023. The root-colonizing endophyte *Piriformospora indica* supports nitrogen-starved *Arabidopsis thaliana* seedlings with nitrogen metabolites. International Journal of Molecular Sciences **24**, 15372. doi: 10.3390/ijms242015372

Šečić E, Zanini S, Wibberg D, *et al*. 2021. A novel plant–fungal association reveals fundamental sRNA and gene expression reprogramming at the onset of symbiosis. BMC Biology **19**, 171. doi: 10.1186/s12915-021-01104-2

Silvestri A, Ledford WC, Fiorilli V, *et al*. 2024. A fungal sRNA silences a host plant transcription factor to promote arbuscular mycorrhizal symbiosis. New Phytologist. doi: 10.1111/nph.20273

Takeda A, Iwasaki S, Watanabe T, Utsumi M, Watanabe Y. 2008. The mechanism selecting the guide strand from small RNA duplexes is different among argonaute proteins. Plant and Cell Physiology **49**, 493–500. doi: 10.1093/pcp/pcn043

Tyurin AA, Suhorukova AV, Kabardaeva KV, Goldenkova-Pavlova IV. 2020. Transient gene expression is an effective experimental tool for the research into the fine mechanisms of plant gene function: advantages, limitations, and solutions. Plants **9**, 1187. doi: 10.3390/plants9091187

Ueno D, Yamasaki S, Kato K. 2022. Methods for detecting RNA degradation intermediates in plants. Plant Science **318**, 111241. doi: 10.1016/j.plantsci.2022.111241

Vandesompele J, De Preter K, Pattyn F, Poppe B, Van Roy N, De Paepe A, Speleman F. 2002. Accurate normalization of real-time quantitative RT–PCR data by geometric averaging of multiple internal control genes. Genome Biology **3**, RESEARCH0034. doi: 10.1186/gb-2002-3-7-research0034

Varkonyi-Gasic E, Hellens RP. 2011. Quantitative stem–loop RT–PCR for detection of microRNAs. Methods in Molecular Biology **744**, 145–157. doi: 10.1007/978-1-61779-123-9_10

Verma N, Narayan OP, Prasad D, Jogawat A, Panwar SL, Dua M, Johri AK. 2022. Functional characterization of a high-affinity iron transporter (PiFTR) from the endophytic fungus *Piriformospora indica* and its role in plant growth and development. Environmental Microbiology **24**, 689–706. doi: 10.1111/1462-2920.15659

Verma S, Varma A, Rexer K-H, Hassel A, Kost G, Sarbhoy A, Bisen P, Bütehorn B, Franken P. 1998. *Piriformospora indica*, gen. Et sp. Nov., a new root-colonizing fungus. Mycologia **90**, 896–903. doi: 10.1080/00275514.1998.12026983

Wang M, Thomas N, Jin H. 2017. Cross-kingdom RNA trafficking and environmental RNAi for powerful innovative pre- and post-harvest plant protection. Current Opinion in Plant Biology **38**, 133–141. doi: 10.1016/j.pbi.2017.05.003

Weiberg A, Wang M, Lin F-M, Zhao H, Zhang Z, Kaloshian I, Huang H-D, Jin H. 2013. Fungal small RNAs suppress plant immunity by hijacking host RNA interference pathways. Science **342**, 118–123. doi: 10.1126/science.1239705

Weiß M, Waller F, Zuccaro A, Selosse M-A. 2016. Sebacinales—one thousand and one interactions with land plants. New Phytologist **211**, 20–40. doi: 10.1111/nph.13977

Werner BT, Koch A, Šečić E, Engelhardt J, Jelonek L, Steinbrenner J, Kogel K-H. 2021. *Fusarium graminearum* DICER-like-dependent sRNAs are required for the suppression of host immune genes and full virulence. PLoS One **16**, e0252365. doi: 10.1371/journal.pone.0252365

Windram O, Madhou P, McHattie S, *et al*. 2012. Arabidopsis defense against *Botrytis cinerea*: chronology and regulation deciphered by high-resolution temporal transcriptomic analysis. The Plant Cell **24**, 3530–3557. doi: 10.1105/tpc.112.102046

Wong-Bajracharya J, Singan VR, Monti R, Plett KL, Ng V, Grigoriev IV, Martin FM, Anderson IC, Plett JM. 2022. The ectomycorrhizal fungus *Pisolithus microcarpus* encodes a microRNA involved in cross-kingdom gene silencing during symbiosis. Proceedings of the National Academy of Sciences, USA **119**, e2103527119. doi: 10.1073/pnas.2103527119

Wu F-H, Shen S-C, Lee L-Y, Lee S-H, Chan M-T, Lin C-S. 2009. Tape–Arabidopsis Sandwich—a simpler Arabidopsis protoplast isolation method. Plant Methods **5**, 16. doi: 10.1186/1746-4811-5-16

Xu L, Wu C, Oelmüller R, Zhang W. 2018. Role of phytohormones in *Piriformospora indica*-induced growth promotion and stress tolerance in plants: more questions than answers. Frontiers in Microbiology **9**, 1646. https://www.frontiersin.org/articles/10.3389/fmicb.2018.01646

Yoo S-D, Cho Y-H, Sheen J. 2007. Arabidopsis mesophyll protoplasts: a versatile cell system for transient gene expression analysis. Nature Protocols **2**, 1565–1572. doi: 10.1038/nprot.2007.199

Zand Karimi H, Innes RW. 2022. Molecular mechanisms underlying host-induced gene silencing. The Plant Cell **34**, 3183–3199. doi: 10.1093/plcell/koac165

Zhan J, Meyers BC. 2023. Plant small RNAs: their biogenesis, regulatory roles, and functions. Annual Review of Plant Biology **74**, 21–51. doi: 10.1146/annurev-arplant-070122-035226

Zhang T, Zhao Y-L, Zhao J-H, Wang S, Jin Y, Chen Z-Q, Fang Y-Y, Hua C-L, Ding S-W, Guo H-S. 2016. Cotton plants export microRNAs to inhibit virulence gene expression in a fungal pathogen. Nature Plants **2**, 16153. doi: 10.1038/nplants.2016.153

Zhang Z, Li Q, Li Z, Staswick PE, Wang M, Zhu Y, He Z. 2007. Dual regulation role of GH3.5 in salicylic acid and auxin signaling during *Arabidopsis–Pseudomonas syringae* interaction. Plant Physiology **145**, 450–464. doi: 10.1104/pp.107.106021

Zuccaro A, Lahrmann U, Güldener U, *et al*. 2011. Endophytic life strategies decoded by genome and transcriptome analyses of the mutualistic root symbiont *Piriformospora indica*. PLoS Pathogens **7**, e1002290. doi: 10.1371/journal.ppat.1002290

Conclusion:

In this study, we developed a pipeline to functionally validate *Si*sRNA effectors, focusing on their role in host gene silencing during interaction with *At*. Using an Arabidopsis protoplast-based system, we confirmed the accumulation of selected *Si*sRNAs and demonstrated that some *Si*sRNAs, such as *Si*sRNA24, trigger significant post-transcriptional gene silencing (PTGS). Importantly, we showed that these *Si*sRNAs are loaded into the plant RNAi machinery and bind to AGO1, providing direct evidence for ckRNAi. Furthermore, our analysis of Arabidopsis gene expression revealed that *Si* modulates key genes involved in plant cell wall modification, nitrogen assimilation, and nutrient transport, processes that likely contribute to and facilitate *Si*-roots colonisation.

Overall, this work provides a robust framework for further functional studies of fungal sRNA effectors and their role in beneficial plant-microbe interactions.

CHAPTER 4 –

Broad-scale phenotyping in Arabidopsis reveals varied involvement of RNA interference across diverse plant-microbe interactions

(Equal Contribution as first Author)

Summary:

This chapter contains the publication "**Broad-scale phenotyping in Arabidopsis reveals varied involvement of RNA interference across diverse plant-microbe interactions"**, accepted by Plant Direct Journal on October 1, 2024, and published online on November 15, 2024 (DOI:10.1002/pld3.70017).

RNAi, mediated by DICER-LIKE (DCL) and ARGONAUTE (AGO) proteins, plays a central role in plant immunity, particularly during plant-pathogen interaction. However, its role in mutualistic interactions, such as with *Si*, remains underexplored.

This study aims to investigate how *Si* colonisation of *Arabidopsis thaliana* influences the regulation of AGO and DCL proteins, and how the plant dynamically tunes its defence mechanisms in response to the nature of microbial interactions.

Received: 25 June 2024 | Revised: 11 September 2024 | Accepted: 1 October 2024

DOI: 10.1002/pld3.70017

RESEARCH ARTICLE

American Society of Plant Biologists | SEB | WILEY

Broad-scale phenotyping in Arabidopsis reveals varied involvement of RNA interference across diverse plant-microbe interactions

Alessa Ruf[1] | Hannah Thieron[2] | Sabrine Nasfi[3] | Bernhard Lederer[1] | Sebastian Fricke[4] | Trusha Adeshara[5] | Johannes Postma[5] | Patrick Blumenkamp[6] | Seomun Kwon[5] | Karina Brinkrolf[6] | Michael Feldbrügge[5] | Alexander Goesmann[6] | Julia Kehr[4] | Jens Steinbrenner[3] | Ena Šečić[3] | Vera Göhre[5,7] | Arne Weiberg[1] | Karl-Heinz Kogel[3,8] | Ralph Panstruga[2] | Silke Robatzek[1] | on behalf of the exRNA consortium

[1]LMU Munich Biocenter, Planegg, Germany

[2]Unit for Plant Molecular Cell Biology, Institute for Biology I, RWTH Aachen University, Aachen, Germany

[3]Institute of Phytopathology, Centre for BioSystems, Land Use and Nutrition, Justus Liebig University, Giessen, Germany

[4]Institute of Plant Science and Microbiology, Molecular Plant Genetics, Universität, Hamburg, Germany

[5]Institute for Microbiology, Cluster of Excellence on Plant Sciences, Heinrich-Heine University Düsseldorf, Düsseldorf, Germany

[6]Bioinformatics and Systems Biology, Justus Liebig University Giessen, Germany

[7]Hochschule Darmstadt, Darmstadt, Germany

[8]Institut de biologie moléculaire des plantes, CNRS, Université de Strasbourg, Strasbourg, France

Correspondence
Silke Robatzek, LMU Munich Biocenter, Großhadener Strasse 4, 82152 Planegg, Germany.
Email: robatzek@bio.lmu.de

Abstract

RNA interference (RNAi) is a crucial mechanism in immunity against infectious microbes through the action of DICER-LIKE (DCL) and ARGONAUTE (AGO) proteins. In the case of the taxonomically diverse fungal pathogen *Botrytis cinerea* and the oomycete *Hyaloperonospora arabidopsidis*, plant DCL and AGO proteins have proven roles as negative regulators of immunity, suggesting functional specialization of these proteins. To address this aspect in a broader taxonomic context, we characterized the colonization pattern of an informative set of *DCL* and *AGO* loss-of-function mutants in *Arabidopsis thaliana* upon infection with a panel of pathogenic microbes with different lifestyles, and a fungal mutualist. Our results revealed that, depending on the interacting pathogen, AGO1 acts as a positive or negative regulator of immunity, while AGO4 functions as a positive regulator. Additionally, AGO2 and AGO10 positively modulated the colonization by a fungal mutualist. Therefore, analyzing the role of RNAi across a broader range of plant-microbe interactions has identified previously unknown functions for AGO proteins. For some pathogen interactions, however, all tested mutants exhibited wild-type-like infection phenotypes, suggesting that the roles of AGO and DCL proteins in these interactions may be more complex to elucidate.

Alessa Ruf, Hannah Thieron, and Sabrine Nasfi contributed equally to the study.

Funding information
Deutsche Forschungsgemeinschaft (DFG), Grant/Award Numbers: FE448/15-1, GO 2037/8-1, GO 2064/4-1, KE 856/8-1, KO 1208/32-1, PA 861/22-1, RO 3550/16-1, WE 5707/2-1; Dr. Ernst-Leopold Klipstein Foundation

KEYWORDS
AGO, Argonaute, DCL, Dicer-like, RNAi

1 | INTRODUCTION

RNA interference (RNAi) is a conserved mechanism that regulates gene expression via small (s)RNAs (Huang et al., 2019; Tang et al., 2022), which can be classified into micro (mi)RNAs (20–22 nt) and small interfering (si)RNAs (21–24 nt). In the interaction with infectious agents, host sRNAs target foreign genes to mediate defense, e.g., against viruses (Obbard et al., 2008; Zhan & Meyers, 2023). Host sRNAs also fine-tune the expression of host immune-responsive genes, thereby orchestrating the outcome of infection against various pathogens (Šečić, Kogel, & Ladera-Carmona, 2021). For example, in the genetic model *Arabidopsis thaliana*, miRNA393 enhances resistance to *P. syringae pv. tomato* strain DC3000 (*Pto* DC3000) by regulating pattern-triggered immunity (PTI) through auxin signaling suppression (Navarro et al., 2006). During seedling development, miR172 inhibits the expression of FLAGELLIN SENSING2 (FLS2), a well-studied pattern recognition receptor (PRR) that confers PTI against flagellated bacteria (Zou et al., 2018). This suggests a role of miR172 in coordinating plant immunity and development.

The core mechanism of RNAi involves the production of dsRNAs, which are processed into sRNA duplexes by DICER-LIKE (DCL) proteins. These sRNAs are subsequently loaded into RNA-induced silencing complexes (RISCs) (Iwakawa & Tomari, 2022; Martín-Merchán et al., 2023). To amplify RNAi, RNA-dependent RNA polymerases use single-stranded sRNA to generate long dsRNAs, which are processed by DCL2/DCL4 into secondary-phased siRNAs (Curaba & Chen, 2008; Martín-Merchán et al., 2023). *A. thaliana* encodes four DCL proteins, each producing specifically sized sRNAs (Martín-Merchán et al., 2023), suggesting specific functions. A partial *DCL1* loss-of-function mutant in *A. thaliana* showed enhanced susceptibility to *Pto* DC3000 and *Botrytis cinerea* infection (Navarro et al., 2006; Weiberg et al., 2013), but also displayed developmental abnormalities. DCL2 and DCL4 mediate antiviral immunity (Taochy et al., 2017; Z. Wang et al., 2018) (Azevedo et al., 2010; Bouché et al., 2006; Deleris et al., 2006). DCL4 is also crucial for anti-fungal defense since *dcl4* mutants showed increased susceptibility to the vascular fungus *Verticillium dahliae* (Ellendorff et al., 2009).

ARGONAUTE (AGO) proteins are key components of RISCs, bind single-stranded sRNAs, and guide them to sequence-complementary RNA and DNA targets (Fang & Qi, 2016). Ten AGO proteins have been identified in *A. thaliana* that can be classified into three clades: i) AGO1/5/10 (clade I), ii) AGO2/3/7 (clade II), and iii) AGO4/6/8/9 (clade III) (Martín-Merchán et al., 2023). They feature different subcellular localization patterns and sRNA binding preferences. The expression patterns of *AGO* genes do not seem to correlate with their clade assignment and function. The members of clade I and clade III, *AGO1* and *AGO4*, are ubiquitously expressed across tissues and during various developmental stages of *A. thaliana* (Jullien et al., 2022). The expression of *AGO2* and *AGO3* is induced in response to diverse abiotic and biotic stresses (Martín-Merchán et al., 2023). For example, *AGO2* expression is upregulated during *Pto* DC3000 infection (Zhang et al., 2011).

Several studies have examined the roles of AGO proteins in plant immunity against eukaryotic and prokaryotic microbes. For example, specific partial loss-of-function mutants in *AGO1* are compromised in microbe-associated molecular pattern (MAMP)-induced immunity against *Pto* DC3000 (Li et al., 2010). Since infection with the fungal pathogen *Sclerotinia sclerotiorum* showed more severe necrotic disease symptoms in *ago1* mutants (Cao et al., 2020), the study suggests that AGO1 is a positive regulator of PTI and enhances resistance against *S. sclerotiorum*. However, AGO1 has also been described to negatively regulate plant immunity against the fungal pathogens *B. cinerea*, *V. dahliae*, *V. longisporum* and *Botryosphaeria dothidea*, as well as the oomycete *H. arabidopsidis* (Dunker et al., 2020; Ellendorff et al., 2009; Shen et al., 2014; Weiberg et al., 2013; Yu et al., 2017). Yet, AGO1 had no detectable role in the outcome of infection with the fungal and oomycete pathogens *Erysiphe cruciferarum* and *Albugo laibachii*, respectively (Dunker et al., 2020). Of the other clades, Arabidopsis *ago2* mutants are more susceptible to infection by *V. dahliae*, *S. sclerotiorum*, and species of the oomycete pathogen *Phytophthora* (Cao et al., 2020; Ellendorff et al., 2009; Guo et al., 2018). Furthermore, AGO4 contributes to resistance to *Pto* DC3000 and is required for both local and *Trichoderma*-induced systemic immunity against *B. cinerea* (Agorio & Vera, 2007; López et al., 2011; Rebolledo-Prudencio et al., 2022).

AGO proteins act together with their loaded sRNAs within the RISC complex, suggesting that the above-outlined examples of immunity regulation in *A. thaliana* likely depend on the specificity of the sRNAs. Beyond the evolution of pathogen-derived molecular suppressors that interfere with host RNAi (Hou et al., 2019; Navarro et al., 2006), infectious microbes can hijack host AGO1 and incorporate microbe-derived sRNAs to facilitate infection. This cross-kingdom (ck)RNAi has been demonstrated for the interaction of *A. thaliana* with the taxonomically diverse pathogens *B. cinerea* and *H. arabidopsidis* (Dunker et al., 2020; Weiberg et al., 2013). In both cases, it is mediated by fungal- or oomycete-derived sRNAs, respectively, which are loaded into host AGO1 and thereby interfere with host RNAi pathways. Supporting this, the *B. cinerea rdr1 and dcl1/dcl2* mutants were less virulent on both *A. thaliana* and *Solanum lycopersicum* hosts, since the production of sRNAs was nearly abolished in these fungal mutants (Cheng et al., 2023; Weiberg et al., 2013). Since plants also deliver sRNAs into *B. cinerea* (Cai et al., 2018), ckRNAi occurs in both directions of the interacting organisms.

Different *B. cinerea* genotypes exhibited varied infection phenotypes (Qin et al., 2023; Weiberg et al., 2013). Hence, the contribution of RNAi to the outcome of microbial infections tends to be more complex and possibly species- or even pathotype-dependent. Therefore, it cannot always be assumed with certainty that plant mutants in the RNAi pathway exhibit phenotypes at each time point when infected with any microbe. To address this aspect in a broader taxonomic context, we characterized the expression patterns and loss-of-function mutant phenotypes of an informative set of *DCL* and *AGO* genes upon infection with a panel of pathogenic filamentous microbes and bacteria, each with different lifestyles, including mutualistic colonization. We reproduced some previously investigated phenotypes and uncovered new roles for AGO1, AGO2, AGO4, and AGO10 in certain microbial interactions, specifically, the dual role of AGO1 as both a positive and negative regulator of plant immunity. This study provides a phenotypic framework for the context-dependent regulatory function of *DCL* and *AGO* genes in plant immunity, offering insights into how plants dynamically adjust their defense strategies to different types of microbial interactions.

2 | RESULTS

We selected a set of *A. thaliana* genes and their corresponding mutants that are informative for the siRNA pathway. These include *DCL2*, *DCL3*, *DCL4* and the triple *dcl2/3/4* mutant and members of the three AGO clades (*AGO1*, *AGO10*, the *ago1-27*, *ago1-46* and *ago10-1* mutants (clade I), *AGO2* and the *ago2-1* mutant (clade II), *AGO4* and the *ago4-2* mutant (clade III) (Table S1). Exploring publicly available transcriptome data of *A. thaliana* elicited with MAMPs from fungi (ch8, nlp20), oomycete (nlp20), and bacteria (flg22, elf16, LPS, nlp20) (Bjornson et al., 2021), we noted that all tested *AGO* but not the selected *DCL* genes were responsive to the immune stimuli (Figure S1). Of the *AGO* genes, *AGO2* showed upregulation in response to all MAMPs, while *AGO1*, *AGO4*, and *AGO10* were downregulated in response to bacterial MAMPs. This suggests that *AGO* genes across the three clades could be involved in PTI regulation. The strong MAMP-induced expression of *AGO2* is consistent with its documented role in immunity against the pathogenic fungus *S. sclerotiorum* and anti-bacterial immunity against *Pto* DC3000 and its AvrRpt2-avirulent derivative (Cao et al., 2020; Zhang et al., 2011).

Since *AGO* gene expression was responsive to MAMPs derived from different microbial taxa, we selected a panel of pathogenic fungi (*Thecaphora thlaspeos*, *E. cruciferarum*, *V. longisporum*), a symbiotic fungus (*Serendipita indica*), and bacterial pathogens (*Pto* DC3000, *X. campestris* pv. *campestris*, *Xylella fastidiosa* subsp. *fastidiosa*) to study the *DCL* and *AGO* expression profiles as well as the infection phenotypes of corresponding mutants in *A. thaliana* (Table S2). We also included an oomycete pathogen (*H. arabidopsidis*), given that AGO1-dependent ckRNAi has been demonstrated to play a role in its infection outcome in *A. thaliana* (Dunker et al., 2020). The selected microbes also differ in their lifestyles, with *H. arabidopsidis* and *Pto* DC3000 infecting leaf mesophyll tissue, *E. cruciferarum* invading leaf epidermal cells, *S. indica* colonizing roots, and *V. longisporum*, *X. campestris* pv. campestris and *X. fastidiosa* infecting the plant xylem, and *T. thlaspeos* growing systemically along the vasculature in both roots and aerial tissues (Table S2). Appreciating the diverse lifestyles, we performed the infection experiments tailored to the type of plant-microbe interaction and according to well-established protocols, yet mainly at the whole plant/organ scale with in vitro and soil-grown plants. Gene expression was analyzed at different time points in the early, middle, and late infection/colonization stages depending on the interacting microbe. The infection/colonization success was measured as the ability to invade host cells (number of penetration events), as microbial biomass (number of hyphae or microbial DNA/RNA), scoring of the infection progress, or as the capacity of the microbe to multiply within host tissue (number of colony-forming units [cfu]). To minimize the putative effect of seed batches, we used an age-matched seed collection of *A. thaliana* Col-0 and the selected *dcl2/3/4* and *ago* mutants for our experiments.

2.1 | AGO1 is a regulator of immunity against some but not all filamentous pathogens

We first tested our collection of plant lines and investigated the role of *DCL* and AGO proteins in the interaction with *H. arabidopsidis*. Expression of *DCL2*, *DCL4*, and *AGO2* was upregulated at middle (4 days post inoculation [dpi]) and late (6 dpi) stages of *H. arabidopsidis* infection, while *AGO4* was downregulated at these time points (Figure 1a). This is in agreement with the changes in the expression of *AGO2* and *AGO4* in response to the oomycete MAMP nlp20 (Figure S1). No drastic changes in gene expression were observed for *AGO1* and *AGO10* (Figure 1a). In the infection experiments, *ago1-27* and *ago1-46* mutants displayed enhanced resistance to *H. arabidopsidis* at 6 dpi (Figure 1b). No altered infection was observed in *ago2-1* and *ago4-2* mutants. This outcome is consistent with a previous report showing evidence for loading pathogen-derived sRNAs into *A. thaliana* AGO1, resulting in ckRNAi to support infection (Dunker et al., 2020). Collectively, the data suggests a specific role for AGO1 in the interaction with the oomycete pathogen.

AGO1 also negatively regulates immunity against fungal pathogens including, *B. cinerea* and *V. longisporum* but not *E. cruciferarum* (Dunker et al., 2020; Shen et al., 2014; Weiberg et al., 2013). Consistent with the fact that AGO1 negatively regulates immunity against *V. longisporum* (Shen et al., 2014), *AGO1* expression was downregulated in the course of infection with this fungal pathogen (Figure S2). By contrast, *DCL3* and *DCL4* were upregulated by *V. longisporum*, suggesting a different response to this pathogen.

Next, we explored the selected *DCL* and *AGO* genes for their expression profiles in response to the challenge with *E. cruciferarum*. We found reduced *AGO1*, *AGO4*, and *AGO10* expression and upregulation of the tested *DCL* genes across the time course (Figure 2a). Fungal entry rates were slightly, yet statistically significantly, increased in *ago1-27*, but no differences were observed in any of the other tested mutants, including the allelic *ago1-46* mutant (Figure 2b). This outcome

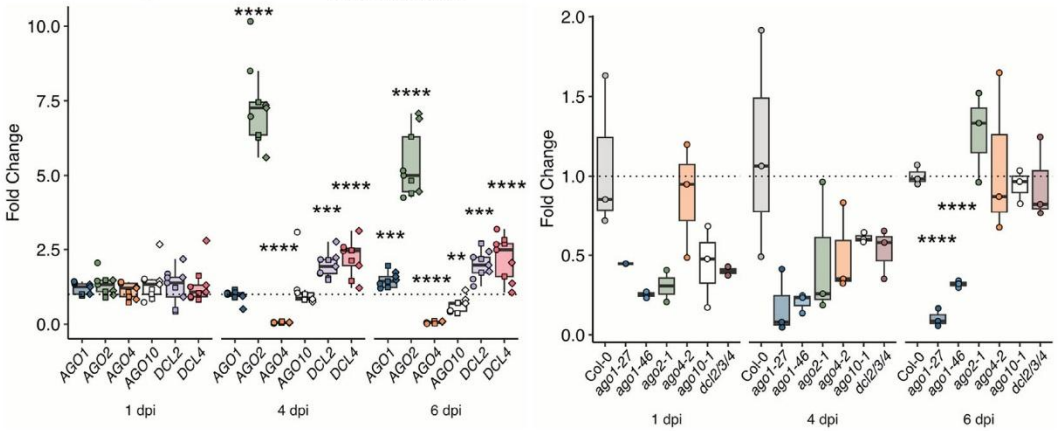

FIGURE 1 *DCL* and *AGO* gene expression patterns (a) and colonization in respective mutants (b) upon infection with *H. arabidopsidis* isolate Noco 2. (a) Samples were collected at 1 dpi (days post inoculation), 4 dpi, and 6 dpi. The RNA levels are relative to mock and normalized against *CDKA*. The results of three biological replicates are depicted. (b) Pathogen load on *ago* and *dcl* mutants was assessed by measuring relative *H. arabidopsidis* gDNA quantities with RT-qPCR at 1 dpi, 4 dpi, and 6 dpi. The result of one biological replicate is depicted. Error bars show standard deviation. Statistical significance was assessed by two-sided Welch's *t*-test ($\alpha = .05$, *p*-values * < .05, ** < .01, *** < .001, **** < .0001). Symbols indicate number of biological replicates. Circle = first, square = second, diamond = third. The dashed line indicates a fold change = 1.

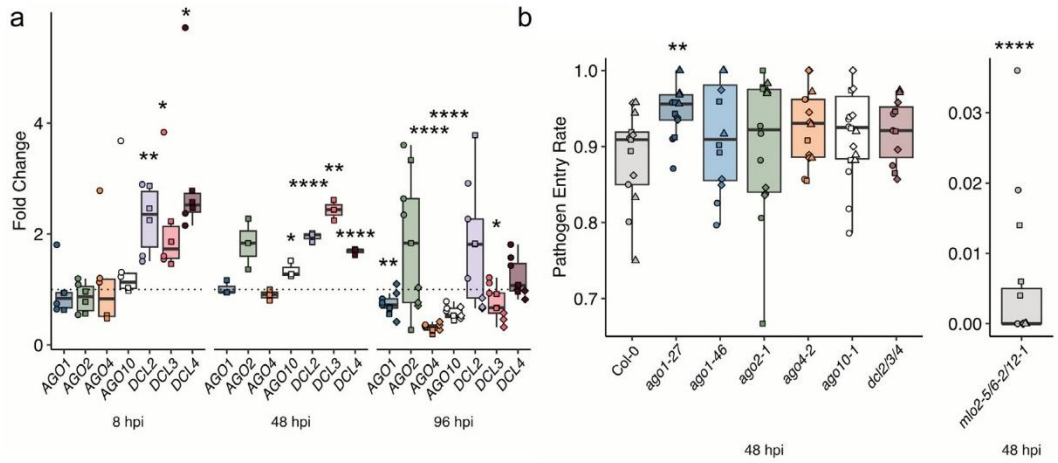

FIGURE 2 *DCL* and *AGO* gene expression patterns (a) and colonization in respective mutants (b) upon *E. cruciferarum* infection in a time course experiment. (a) Samples were collected at 8 hpi (hours post inoculation), 48 hpi, and 96 hpi. The RNA levels are relative to mock and normalized against *CDKA*. The results of three biological replicates are depicted. (b) Infection success on *ago* and *dcl* mutants was assessed by determining *E. cruciferarum* host cell entry rates at 48 hpi. The results of four biological replicates are depicted. Error bars show standard deviation. Statistical significance was assessed by two-sided Welch's *t*-test ($\alpha = .05$, *p*-values * < .05, ** < .01, *** < .001, **** < .0001). Symbols indicate number of biological replicates. Circle = first, square = second, diamond = third, triangle = fourth. The dashed line indicates a fold change = 1.

confirms previous data on unaltered *E. cruciferarum* infection in *ago1-46*. However, it contrasts the reported wild type-like phenotype in *ago1-27* (Dunker et al., 2020) possibly due to different scoring: the previous study evaluated leaf necrosis, while in our study, fungal penetration was scored. Furthermore, a clear regulation of *E. cruciferarum* penetration success by AGO1 cannot be established, since the two *ago1* mutants exhibited different infection phenotypes to this fungus (Figure 2b). We also investigated the role of AGO1 during infection with *T. thlaspeos* and observed wild-type-like colonization in *ago1-27* mutants (Figure 3). By contrast, *ago4-2* mutants showed significantly enhanced susceptibility, thereby revealing a previously unknown role for AGO4 as a positive regulator of immunity to this smut fungus.

2.2 | AGO1 is a regulator of certain but not all bacterial infections

Motivated by the previous reports on the roles of AGO1 and AGO2 in immunity against bacterial pathogens (Ren et al., 2019; Zhang et al., 2011), we examined the roles of the selected *DCL* and *AGO* genes in infection by three different bacterial pathogens. Interestingly, AGO1 might be required for immunity against *X. fastidiosa*, since it was upregulated at late infection stages (Figure 4a), and both *ago1-27* and *ago1-46* displayed enhanced susceptibility (Figure 4b). All other tested genes showed wild-type-like expression patterns, and the respective mutants supported wild-type-like infection success of *Pto* DC3000

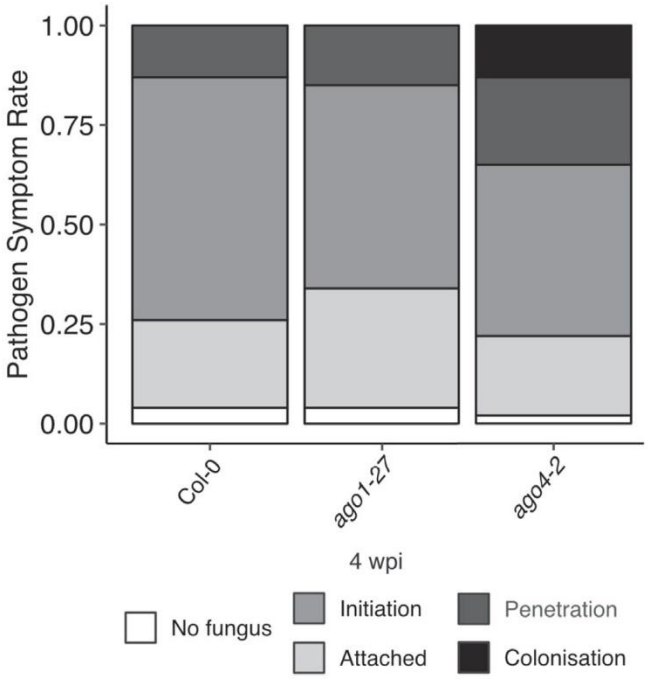

FIGURE 3 Colonization in *ago* mutants upon *T. Thlaspeos* infection. Colonization was visualized after four weeks by staining with wheat germ agglutinin (WGA, fungal hyphae) and propidium iodide (PI, plant background). In at least 150 seedlings per line, fungal progression was classified into (i) attachment of the fungus to plant tissue, (ii) initiation of penetration as indicated by bulging of the hyphal tip, (iii) penetration into the plant tissue, and (iv) colonization along the vasculature. Similar results were obtained in three independent experimental replicates.

(Figure S3A and S3B) and *X. campestris* pv. *campestris* (Figure S4A and S4B). The tested bacteria are Gram-negative γ-proteobacteria, including two belonging to the Xanthomonadaceae and colonizing xylem vessels (Table S3). However, the positive regulatory function of AGO1 appears to be specific to immunity against *X. fastidiosa*.

Previously, AGO2 and AGO4 were shown to positively regulate immunity against *Pto* DC3000 strains (Agorio & Vera, 2007; López et al., 2011; Zhang et al., 2011), which is not consistent with our findings. We neither detected any obvious induction of *AGO2* expression nor increased *Pto* DC3000 susceptibility in *ago2* and *ago4* mutants (Figure S3). It is possible that the different outcomes for these mutants might depend on the methods of bacterial inoculation, as in the previous studies, bacteria were applied by syringe-based leaf infiltration, while in this study, *Pto* DC3000 was sprayed onto the leaf surface. The two inoculation methods differ, as syringe inoculation bypasses stomatal immunity (Melotto et al., 2017).

2.3 | AGO2 and AGO10, but not AGO1, are potential regulators of fungal mutualism

Soybean AGO1 plays a positive role in the bacterial *Sinorhizobium* root-nodule symbiosis via ckRNAi (Ren et al., 2019). Furthermore, AGO1 has been speculated to regulate fungal symbiosis, supported by the prediction of plant mRNA targets of fungal sRNAs accumulating in the symbiosis between beneficial microorganisms and their hosts (Silvestri et al., 2019; Valdés-López et al., 2019; Wong-Bajracharya et al., 2022). Therefore, we next conducted colonization experiments with the mutualist basidiomycete *S. indica*, revealing *AGO4* downregulation at late time points (Figure 5a). The other tested *DCL* and *AGO* genes revealed no statistically significant changes in response to *S. indica* colonization at the investigated time points (Figure 5a). Interestingly, roots of *ago2-1* and *ago10-1* mutants showed reduced colonization by *S. indica*, whereas *ago1-27*, *ago4-2*, and *dcl2/3/4* exhibited wild type-like colonization (Figure 5b). It suggests that AGO2 and AGO10, but not AGO1, function as potential positive regulators during colonization in the mutualistic interaction of *A. thaliana* with *S. indica*, or negatively regulate immunity against this beneficial fungus. Moreover, although clade I AGO1 and AGO10 are phylogenetically related, AGO10 may have a specific function in fungal mutualism. Of note, miRNAs can be sequestered by different AGO proteins, leading to different outcomes, e.g., as shown for miRNA165/166 in flower development, which depends on their binding to AGO1 and AGO10 (Ji et al., 2011).

2.4 | AGO expression patterns do not seem to correlate with their function in immunity

We utilized heat maps to summarize our mutant infection and gene expression data. Overall, some of the most striking phenotypes were associated with *ago1*, *ago2*, and *ago10* mutants: *ago1* mutants were more susceptible to *X. fastidiosa* but more resistant to *H. arabidopsidis* while *ago2* and *ago10* were more resistant to *S. indica* (Figure 6a). Yet, despite these notable phenotypes, the overall gene expression patterns did not correlate with the mutant infection data (Figure 6b). The most striking changes in gene expression were observed for *AGO2* and *AGO4*, showing up- and down-regulation upon *H. arabidopsidis* infection, respectively (Figure 6b). *AGO4* and *AGO10* were also down-regulated in response to *E. cruciferarum*. This suggests distinct underlying mechanisms or pathways influencing the observed phenotypic outcomes.

3 | DISCUSSION

RNAi executed by DCL and AGO proteins is considered a conserved process regulating the outcome of plant-microbe interactions. Previous studies have described the roles of AGOs as positive and negative plant immunity regulators, likely linked to their binding of host or pathogen-derived sRNAs. Here, we i) confirm previous findings for AGO1 in negatively regulating immunity against *H. arabidopsidis* (Figure 1b) and ii) reveal a potential positive regulatory role of AGO1 in immunity against *X. fastidiosa* (Figure 4b). Moreover, iii) we identified clade I AGO10 and clade II AGO2 as positive modulators of *S. indica* root colonization (Figure 5b), and iv) revealed clade III AGO4

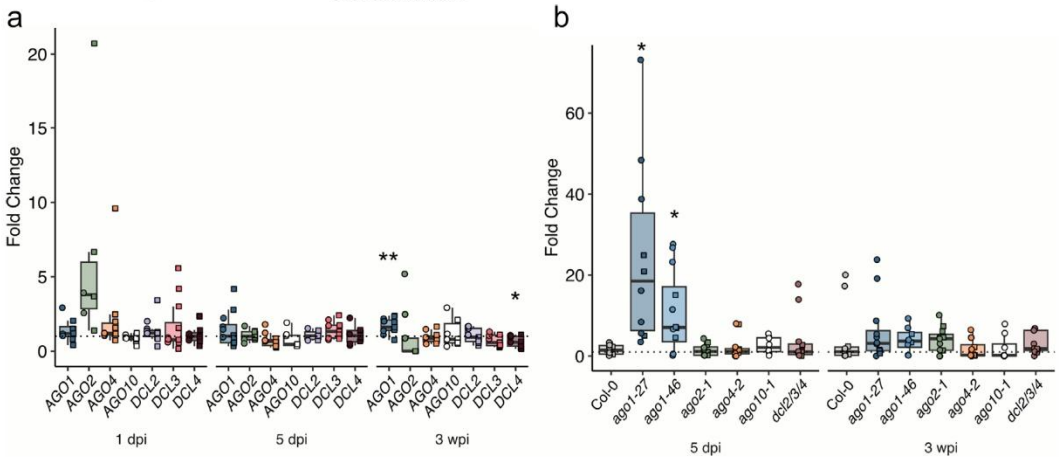

FIGURE 4 *DCL* and *AGO* gene expression patterns (a) and colonization in respective mutants (b) upon *Xylella fastidiosa subsp. fastidiosa* Temecula1 infection. (a) Samples were collected from petioles at 1 (day post-infection), 5 dpi, and 3 wpi (weeks post-infection). The RNA levels are relative to mock and normalized against *CDKA*. The results of two biological replicates are depicted. (b) Pathogen load on *ago* and *dcl* mutants was assessed by RT-qPCR at 5 dpi and 3 wpi. The results of two biological replicates are depicted. Error bars show standard deviation. Statistical significance was assessed by two-sided Welch's *t*-test ($\alpha = .05$, *p*-values * < .05, ** < .01, *** < .001, **** < .0001). Symbols indicate number of biological replicates. Circle = first, square = second, diamond = third. The dashed line indicates a fold change = 1.

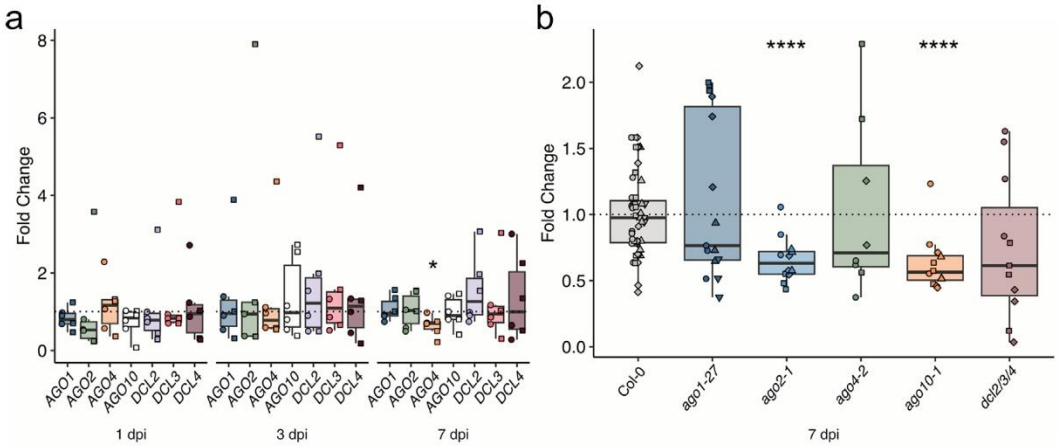

FIGURE 5 *DCL* and *AGO* expression patterns (a) and colonization in respective mutants (b) upon infection with *S. indica*. (a) Samples were collected from roots at 1 dpi (day post inoculation), 3 dpi, and 7 dpi. The RNA levels are relative to mock and normalized against *UBC21*. The results of two biological replicates are depicted. (b) Pathogen load on *ago* and *dcl* mutants was assessed by measuring relative *S. indica* gDNA quantities with RT-qPCR at 7 dpi. The results of at least three biological replicates are depicted. Error bars show standard deviation. Statistical significance was assessed by two-sided Welch's *t*-test ($\alpha = .05$, *p*-values * < .05, ** < .01, *** < .001, **** < .0001). Symbols indicate number of biological replicates. Circle = first, square = second, diamond = third. The dashed line indicates a fold change = 1.

as a positive control element of *T. thlaspeos* infection (Figure 3). Thus, our broad-scale phenotyping uncovered previously unknown positive and negative regulatory functions of different AGO proteins in the context of plant-microbe interactions (Figure 6c).

AGO1's negative adjustment of plant immunity is influenced by its role as a target for pathogen-derived sRNAs and its function in ckRNAi (Dunker et al., 2020; Weiberg et al., 2013). Therefore, it is possible that AGO1-related AGO10 and AGO2 might be hijacked by *S. indica*-secreted sRNAs, providing a possible molecular mechanism of their positive modulatory role in mutualism with this fungus. Indeed, the production of host and fungal-derived sRNAs has been revealed in the beneficial interaction of *Brachypodium distachyon* with *S. indica* (Šečić, Zanini, et al., 2021), which could result in post-transcriptional gene silencing (PTGS) of plant immunity genes and thereby facilitating *S. indica* colonization. This scenario is consistent with AGO1's role in bacterial symbiosis, binding rhizobial tRNA-derived sRNA fragments (tRFs) that promote host nodulation (Ren et al., 2019). Additionally, clade I AGOs could influence the host's transcriptional response to symbiosis, as reported for AGO5 in rhizobia-*Phaseolus vulgaris* symbiosis (del Sánchez-Correa et al., 2022).

A positive immune regulatory function of AGO proteins has been linked to its binding of host endogenous sRNAs. For example, miR393b* bound to AGO2 triggers *MEMB12* (encoding a Golgi-localized SNARE protein) cleavage, which results in increased

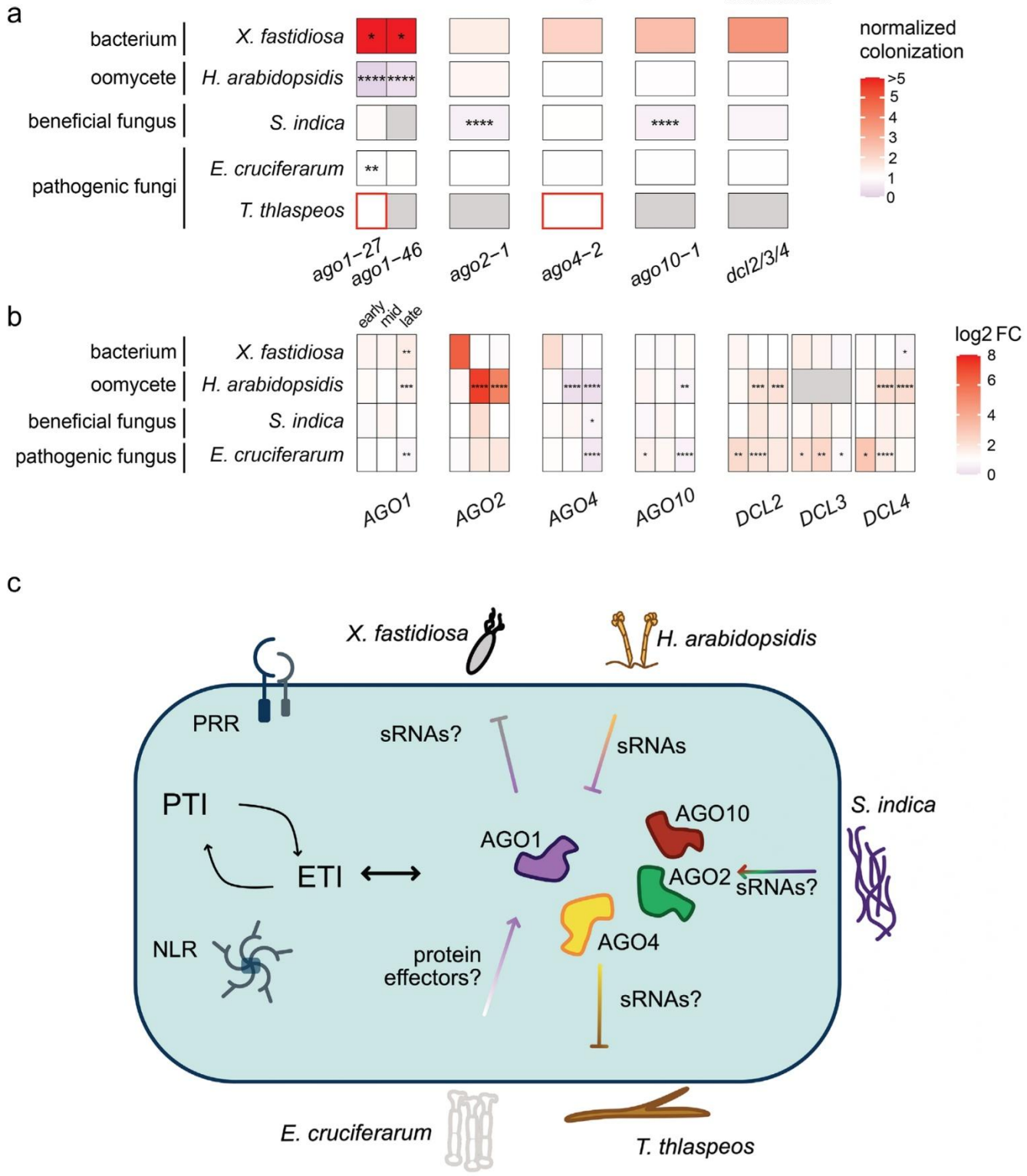

FIGURE 6 Legend on next page.

FIGURE 6 Overall results presented in heat maps and a graphical summary. (a) The heat map shows the colonization success of *S. indica*, *Xylella fastidiosa*, *T. thlaspeos*, *H. arabidopsidis*, and *E. cruciferarum* in the set of selected Arabidopsis mutants (*ago1*–27, *ago1*–46, *ago2*–1, *ago4*–2, *ago10*–1, *dcl2/3/4*) at 7 dpi, 5 dpi, 2 dpi, 6 dpi, and 2 dpi, respectively to the interacting microbe. Color intensity within each cell represents the degree of colonization success relative to wild-type Col-0 plants, with red indicating more colonization and blue indicating less colonization. Significant differences are marked with asterisks ($\alpha = .05$; adjusted *p*-values: * < .05, < .01, * < .001, **** < .0001). Non-quantifiable colonization success in *T. thlaspeos* is indicated as red boxes to indicated increased colonization. (b) Transcript abundance as log2 (fold change) of the genes of interest (*AGO1*, *AGO2*, *AGO4*, *AGO10*, *DCL2*, *DCL3*, *DCL4*) was assessed at an early, mid, or late infection stage in Col-0 for each microbe. Color intensity within each cell corresponds to the change in gene expression relative to non-inoculated samples, with red indicating upregulation and blue indicating downregulation. Significant differences are indicated with asterisks ($\alpha = .05$, adjusted *p*-values * < .05, < .01, * < .001, **** < .0001). Non-tested conditions are indicated as gray boxes. (c) Proposed model. Potential cross-talk between the plant immune system and the RNA interference pathway influenced by different microbes. Key components of the plant immune system include pattern recognition receptors (PRRs) mediating pattern-triggered immunity (PTI) and nucleotide-binding leucine-rich repeat receptors (NLRs) involved in effector-triggered immunity (ETI). Microbes such as *X. fastidiosa*, *Hyaloperonospora arabidopsidis*, *Serendipita indica*, *Tecaphora thlaspeos*, and *Erysiphe cruciferarum* may interact with the plant immune system indirectly via Argonaute (AGO) proteins. This modulation can occur bidirectionally and might be mediated by small RNAs (sRNAs) and/or effector proteins, depending on the specific microbe involved. The arrows indicate hypothesized relationships based on the presented data.

resistance due to the secretion and accumulation of the Pathogenesis-Related (PR) 1 protein (Zhang et al., 2011). A potential function of AGO1 in restricting *X. fastidiosa* infection may be related to endogenous host sRNAs associated with the control of PTI or its execution (Mitre et al., 2021; Navarro et al., 2006; Zhang et al., 2011). Given that ckRNAi functions in both directions (Cai et al., 2018), plants may also send AGO1-dependent sRNAs to alter *X. fastidiosa* growth, interfering with gene silencing in bacteria (Papenfort & Melamed, 2023).

The identification of AGO4 as a positive control element of resistance to *T. thlaspeos* expands the importance of this AGO protein beyond its requirement for immunity against *Pto* DC3000 and *B. cinerea* (Agorio & Vera, 2007; Rebolledo-Prudencio et al., 2022). Of note, upon infection with *Blumeria graminis* f.sp. *tritici*, *AGO4* was significantly downregulated in the wheat progenitor *Aegilops tauschii*, which was accompanied by a substantial reduction in AGO4a-sorted 24-nt siRNA levels, and enrichment for 'response to stress' gene functions, including receptor kinase, peroxidase, and pathogenesis-related genes, suggesting that AGO4 in some cases is a strong negative regulator of immunity (Geng et al., 2019). It further highlights the involvement of clade III AGOs-mediated TGS in the modulation of plant immunity. Interestingly, AGO1 was not required for *T. thlaspeos* infection at the early stages of colonization. Other AGOs of clade I and clade II need to be investigated to address the putative role of PTGS in this fungal interaction during the established biotrophic phase or during fungal sporulation.

The other tested interactions did not reveal obvious phenotypes. This was unexpected given the functional conservation of AGOs and the ubiquitous expression of key members like *AGO1* and *AGO4* in most tissues, including leaves, roots, and the vasculature (Martín-Merchán et al., 2023; Wook et al., 2011). The transcriptional response of *DCL* and *AGO* genes was mostly not correlated with infection phenotypes in respective mutants. Considering the different infection types, from epidermal (*E. cruciferarum*), leaf mesophyll (*H. arabidopsidis*,, *Pto* DC3000), root (*S. indica*) to vascular tissues (*V. longisporum*, *X. campestris* pv. *campestris*, *X. fastidiosa*, *T. thlaspeos*), a spatiotemporal resolution might be needed to observe changes in gene expression at the actual site of pathogen colonization (Dunker et al., 2020). We speculate that functional redundancy within the DCL and AGO family is likely accounting for wild-type-like phenotypes in some of the tested interactions. This includes the *dcl2/3/4* triple mutant, therefore suggesting potential further redundancy of these three encoded proteins with DCL1. Moreover, infection with *E. cruciferarum* and *X. campestris* pv. *campestris* did not reveal infection phenotypes in the tested mutants (Figure 2b and Figure S4B). This could suggest more functional redundancies among AGO proteins than expected.

To a large extent, the outcome of infection success is determined by the ability of the pathogen to suppress host immunity (Jones et al., 2024). This capacity is encoded in the pathogen's repertoire of diverse molecular effectors (Y. Wang et al., 2022). For example, the virulence of bacterial pathogens like *Pto* DC3000 and *X. campestris* pv. *campestris* mainly involves Type-3-secreted effector proteins (Y. Wang et al., 2022). *X. fastidiosa* lacks a Type-3 secretion system (Landa et al., 2022), and immune-suppressing protein effectors have not been described to date. Thus, the bacterium might not be able to overcome AGO1-mediated defenses. Effector proteins have also been demonstrated to improve infection of powdery mildew fungi such as *E. cruciferarum* (Bourras et al., 2018). It is, therefore, possible that protein effectors could be largely responsible for virulence in a given microbe, contrasting to the virulence mechanisms of *B. cinerea* and *H. arabidopsidis*, which at least in part rely on sRNA-like effectors (Dunker et al., 2020; Weiberg et al., 2013). Moreover, protein effectors could suppress host RNAi (Hou et al., 2019; Navarro et al., 2006). Since pathotypes of microbial subspecies encode different effector repertoires, their interaction with the host's RNAi machinery might differ (Qin et al., 2023; Weiberg et al., 2013).

To conclude, analyzing the role of RNAi in plant immunity across taxonomically diverse microbes may be more complex and might need refined experimental set-ups beyond whole plant phenotyping with improved spatiotemporal resolution. We consider three levels of functional redundancy, which complicate the phenotypic analysis: i) similar or overlapping functions of DCL and AGO clade members, ii) microbial virulence conferred by protein effectors, including iii) microbial protein effectors suppressing host RNAi. Therefore, experimental studies would benefit from using higher-order plant mutants (if not exhibiting severe

developmental phenotypes) and combinatorial analysis with different pathotypes of microbial (sub-)species, as well as microbial mutants compromised e.g. for selected protein effectors or their secretion. Taken together, this phenotypic framework will now make it possible to dissect the molecular mechanisms by which AGOs function, whether host sRNAs modulate the plant's immune system, are secreted to function in the microbe, or if microbe-derived sRNAs are delivered into the plant. Ultimately, this will allow improvement of plant protection.

4 | MATERIAL AND METHODS

4.1 | Plant materials

A. thaliana Col-0 mutants included published *ago1-27*, *ago1-46*, *ago2-1*, *ago4-2*, *ago10-1*, and *dcl2/3/4* (Table S1). Age-matched seeds were used for all experiments. The *eds1-2* mutant was used for propagation of the *E. cruciferarum* inoculum, and the *mlo2-5/6-2/12-1* mutant as an additional control for powdery mildew infection experiments (Bartsch et al., 2006; Consonni et al., 2006).

4.2 | Primers

All primers used in this study are listed in Table S3. The *CDKA* gene expression was used as a reference to assess the expression levels of the selected *AGO/DCL* genes and to quantify microbial growth *in planta* (*H. arabidopsidis*, *X. fastidiosa*) by (RT)-qPCR. For *S. indica* colonization, *UBC21* was used as a reference gene.

4.3 | Microbial infections

4.3.1 | *Hyaloperonospora arabidopsidis*

Plants for infection with *H. arabidopsidis* (GÄUM.) isolate Noco 2, *A. thaliana* plants were grown on soil under long day conditions (16 h light, 8 h dark, 60% relative humidity). Two weeks-old *A. thaliana* plants were inoculated with a final spore concentration of $2*10^4$ spores mL^{-1} as previously described (Ried et al., 2019). For biomass quantification, two leaves and two cotyledons were pooled for one technical replicate, followed by genomic DNA extraction with CTAB and RNase A treatment (Promega) (Chen & Ronald, 1999). The isolated DNAs were diluted to 5 ng/µl. *H. arabidopsidis* gDNA relative to *A. thaliana* was quantified by qPCR with Primaquant low ROX qPCR master mix (Steinbrenner Laborsysteme) according to the manufacturer's instructions (95 °C 3 min, 95 °C 20 s, 60 °C 30 s, 72 °C 40 s, 40 cycles, and subsequent melting curve analysis).

For RT-qPCR, four leaves were pooled for one technical replicate. The CTAB method was used for total RNA extraction (Bemm et al., 2016). Genomic DNA was removed by DNase I digestion (Sigma-Aldrich) following the manufacturer's instructions. For cDNA synthesis with the Maxima H Minus Reverse Transcriptase (Thermo Fisher Scientific) kit, 1 µg of total RNA from each sample was used. Relative gene expression was quantified by qPCR with the Primaquant low ROX qPCR master mix (Steinbrenner Laborsysteme), according to the manufacturer's instructions (95 °C 3 min, 95 °C 20 s, 60 °C 30 s, 72 °C 40 s, 40 cycles, melting curve analysis).

4.3.2 | *Erysiphe cruciferarum*

Plants for *E. cruciferarum* infection were grown on SoMi 513 soil (Hawita, Vechta, Germany) in 9*9 cm pots under short-day conditions with an 8-h photoperiod at 22 °C and 16 h darkness at 20 °C. *E. cruciferarum* (in-house isolate of RWTH Aachen) was cultivated selectively on *A. thaliana eds1-2* (Bartsch et al., 2006) at 20 °C with an 8-h photoperiod. Spores from three pots of plants, collected at 20–28 dpi, were used for the inoculation of 10 pots. For this, four weeks-old healthy Col-0 plants, the selected mutant lines, and the resistant *mlo2-5/6-2/12-1* triple mutant (negative control) were placed in an inoculation tower and heavily infected inoculum plants were gently agitated to release spores. To determine fungal entry rates, for one technical replicate leaves from one plant were harvested at 48 hours post inoculation (hpi) and collected in 80% EtOH for de-staining of leaf pigments. Fungal structures were stained with Coomassie staining solution (45% MeOH (v/v), 10% acetic acid (v/v), .05% Coomassie blue R-250 (w/v)). Samples were double-blinded and leaves were analyzed by light microscopy. The fungal entry rate was determined as the percentage of spores successfully developing secondary hyphae over all spores that attempted penetration, visible by the presence of an appressorium (Kusch et al., 2019). At least 100 interaction sites on leaves of three different plants per independent replicate were analyzed.

For RT-qPCR, total RNA was extracted from leaves of uninoculated Arabidopsis and leaves sampled at 8, 48, or 96 hpi with *E. cruciferarum* using TRI reagent ® (Sigma Aldrich). For one technical replicate, each one leaf of three different plants was pooled. The remaining DNA was digested using DNase I (Thermo Fisher Scientific, USA). For cDNA synthesis, 1 µg RNA was used with the High-Capacity cDNA Reverse Transcription Kit (Applied Biosystems). Relative expression of target genes was quantified by RT-qPCR (95 °C 3 min, 95 °C 10 s, 60 °C 60 s; 40 cycles; melting curve analysis) with the Takyon no ROX SYBR 2X master mix (Eurogentec).

4.3.3 | *Verticilium longisporum*

Arabidopsis mutants used for *V. longisporum (VL43)* (Zeise & Von Tiedemann, 2002)infection were grown directly on soil in a climate chamber with 22 °C/18 °C day/night cycle with 8 h of light. For infection of mutant lines, an inoculation suspension was used. This suspension was prepared by flooding a fully grown three weeks-old culture of *V. longisporum* grown on Potato Dextrose Agar (PDA) agar (Carl Roth, Art. No. X931.1) in a Petri dish at 22 °C, in the dark with 10 ml ddH_2O. The Petri dish was scraped with a small metal spatula to release conidia in suspension. The suspension was filtered through miracloth

(Calbiochem, 475,855) to exclude mycelium, and spore concentration was determined using a hemocytometer (Thoma counting chamber - Marienfeld). The final concentration of the spore suspension was adjusted to 10.000.000 spores/mL. Two weeks-old seedlings of *A. thaliana* (Col-0 and mutant lines) were infected by pipetting 1 ml of inoculation suspension directly in the soil. For one technical replicate, leaf material from one plant was harvested 1, 7, and 35 dpi and ground on liquid nitrogen. Total RNA extraction was done using TRIzol® (Invitrogen) and Zymo RNA Clean & Concentrator-25 Kit with in-column DNase I digestion. cDNA synthesis was generated using 200 ng/µL of the extracted total RNA using RevertAid Reverse transcriptase (Thermo Scientific) following manufacturer guidelines. For subsequent qPCR, the SYBR™ Green PCR Master Mix (Applied Biosystems) was used (Thermo Fisher Scientific 4,309,155). For this, 10 µl reactions were set up, consisting of 5 µl SYBR master mix, .5 µl of each primer, 3.5 µl H_20, and .5 µl cDNA, run with 3 min of 95 °C followed by 40 cycles of 95 °C for 10s, 60 °C for 1 min, and subsequent melting curve analysis, on a QuantStudio 6 Flex (Applied Biosystems).

4.3.4 | *Thecaphora thlaspeos*

One seed of an Arabidopsis line was co-germinated with 300 sterilized teliospores of *T. thlaspeos* (collection 2022, Frantzeskakis et al., 2017) in 300 µl liquid half-strength Murashige and Skoog with Nitrate (MSN) medium (Duchefa) containing 1% sucrose in a well of a 96-well plate. The infections were incubated for four weeks in a light chamber for *A. thaliana* at long-day conditions (120 µE, 12 h 21 °C light, 12 h 18 °C darkness). Seedlings were then stained with wheat germ agglutinin (WGA) and propidium iodide (PI) as previously described (Frantzeskakis et al., 2017) and scored microscopically for fungal infection stages (Zeiss Axio Immager M1). Up to 160 seedlings, each representing one biological replicate, were inspected per line and experiment.

4.3.5 | *Serendipita indica*

A. thaliana mutant lines were grown on vertical square Petri dishes on *A. thaliana* Salt medium (ATS) (Lincoln et al., 1990) without sucrose and supplemented with 4.5 g/l Gelrite (Duchefa #G1101) in a 22 °C day/18 °C night cycle (8 h of light). Spores of *S. indica* (IPAZ-11827, Institute of Phytopathology, Giessen, Germany) were freshly isolated from the plates by scraping the agar using water supplied with .002% Tween 20 added and then filtered through miracloth (Merck Millipore), centrifuged at 3.000 x g for 7 min, then resuspended in water supplied with .002% Tween 20 and adjusted to 500.000 spores mL^{-1}. Roots of 14 days-old plants were inoculated with 1 ml of a suspension of 500.000 chlamydospores mL^{-1} in water with .002% Tween 20 per Petri dish. Control plants were treated with water supplied with .002% Tween 20 (mock). Inoculated roots of different mutants are harvested after seven days, and ground for 1 min at 30 Hz with the pre-cooled Retsch Mill (Tissue Lyser II, Retsch, Qiagen). For one technical replicate, roots from one plate were pooled. For quantification of *S. indica* colonization, genomic DNA was extracted using a Qiagen DNA extraction kit (QIAGEN, 69504). Fungal colonization was quantified using internal transcribed spacer (ITS) primers (see Table S3) and SYBR Green JumpStart Taq ReadyMix (Sigma Aldrich, 1,003,444,642) with a QuantStudio5 Real-Time PCR System (Applied Biosystems). A total of 2 µl ROX (CRX reference dye, Promega, C5411) were added to 1 ml SybrGreen as a passive reference dye that allows fluorescent normalization for qPCR data. The PCR conditions were 95 °C for 5 min followed by 40 cycles of 95 °C for 15 s, 60 °C for 30 s, and 72 °C for 30 s, followed by melting curve analysis.

For *DCL* and *AGO* gene expression, Arabidopsis Col-0 plants were grown on ATS plates and inoculated with *S. indica* spores as previously described above. Control plants were treated with water containing .002% Tween 20 (mock). Inoculated roots were harvested at 1, 3, and 7 dpi, ground with the tissue lyser, and RNA was extracted using Trizol and Zymo kit (Zymo research R2070), with a subsequent in-column DNase digestion. cDNA was generated from 1 µg RNA using Revert Aid Reverse transcriptase. Gene transcription was quantified by qPCR using SYBR Green JumpStart Taq ReadyMix (Sigma Aldrich, 1,003,444,642) with QuantStudio5 Real-Time PCR System (Applied Biosystems). A total of 2 µl ROX (CRX reference dye, Promega, C5411) were added to 1 ml SybrGreen as a passive reference dye that allows fluorescent normalization for qPCR data. The PCR conditions were 95 °C for 5 min, followed by 40 cycles of 95 °C for 15 s, 60 °C for 30 s, and 72 °C for 30 s, followed by a melting curve analysis. *Ubiquitin* (*UBC21*, *AT5G25760*) was used as a housekeeping gene for all experiments. Roots from two ATS plates were harvested and considered as one technical replicate. The results of three or more biological replicates are included in the data analysis.

4.3.6 | *P. syringae* pv. *tomato* DC3000

Plants for *Pto* DC3000 infection were grown on soil with 10 h light and 55% humidity for four to five weeks. *Pto* DC3000 was routinely grown at 28 °C on King's B plates with 1% Agar. Overnight plate-grown *Pto* DC3000 cells were resuspended in 10 mM $MgCl_2$ and .04% Silwet L-77 and diluted to $OD_{600} = .02$. The *A. thaliana* plants were sprayed from below and on top with inoculum. Discs of the infected leaves (one disc per leaf, .6 cm diameter) were excised at 1 dpi and 3 dpi. For one technical replicate, four leaf discs from one plant were pooled and ground in 200 µl 10 mM $MgCl_2$. Serial dilutions were plated on King's B medium with rifampicin (50 µg mL^{-1}) and bacterial colonies were quantified after two days of incubation at 28 °C. At least four plants per genotype and time points were harvested and plated. Results of three independent rounds of infection are included.

For qRT-PCR, for one technical replicate, two inoculated or mock-treated (sprayed with buffer-only) leaves per plant were harvested at 6 hpi, 1 dpi, and 3 dpi. Leaf material was ground using a tissue lyser and RNA extractions performed with Trizol reagent

(Invitrogen, USA) according to the manufacturer's protocol and the Zymo RNA Clean & Concentrator Kit, including in-column DNase treatment. RT-qPCR was performed using the NEB Luna® Universal One-Step RT-qPCR Kit (E3005) according to the manufacturer's instructions (55 °C 10 min, 95 °C 1 min, 95 °C 10 s, 60 °C 30 s, 45 cycles, and subsequent melting curve analysis). Reactions were set-up in duplicates using 10 ng RNA in 10 µl reactions. At least four samples per time point and treatment were analyzed, two rounds of infection were included.

4.3.7 | *X. campestris* pv. *campestris*

Plants for *X. campestris* pv. *campestris* infection were grown on soil with 10 h light and 55% humidity for four to five weeks. *X. campestris* pv. campestris 8004 was routinely grown at 28 °C on NYG (Nutrient Yeast Glycerol Agar, Daniels et al., 1984) media with 1% agar. Inoculum was prepared freshly by scraping bacteria from plates and resuspended in 1x PBS for a final OD_{600} of .4. Four leaves per plant were inoculated by application of 5 µl drops of bacterial suspension onto the midvein of leaves prior to pricking with a .4 * 20 mm needle five times. Plants were covered in a plastic bag for the first two days to create optimal infection conditions with high humidity. Discs of the inoculated leaves (one disc per leaf, .6 cm diameter) were excised at 3 dpi and 5 dpi. For one technical replicate, two leaf discs of one plant were pooled and ground in 200 µl 10 mM $MgCl_2$. Serial dilutions were plated on King's B medium supplemented with rifampicin (50 µg mL^{-1}), and bacterial colonies were quantified at two days after incubation at 28 °C. Suspensions that resulted in no colonies were excluded from the analysis. At least four samples per genotype and time point were harvested and plated. Results of three independent rounds of infection are included.

For qRT-PCR, for one technical replicate, two inoculated or mock-treated leaves per plant were harvested at 1 dpi, 3 dpi, and 7 dpi. RNA extraction and qRT-PCR reactions were performed as described above for *Pto* DC3000.

4.3.8 | *X. fastidiosa* subsp. *fastidiosa*

Plants for *X. fastidiosa* subsp. *fastidiosa* infection were grown on soil with 10 h light and 55% humidity for four to five weeks. *X. fastidiosa* subsp. *fastidiosa* Temecula1 (ATCC 700964) was routinely grown at 28 °C on PD3 plates (Pierce's Disease 3, Davis, 1980) for approx. seven to ten days. The inoculum was prepared freshly by scraping bacteria from the plate and resuspending it in 1x PBS for a final OD_{600} of .5. Four leaves per plant were inoculated by application of 5 µl drops of bacterial suspension onto the midvein of leaves prior to pricking with a .4 * 20 mm needle 5 times. For one technical replicate, two petioles per plant were combined and harvested at 5 dpi and 3 weeks post-inoculation (wpi). RNA was extracted from two petioles of infected samples after disruption with a tissue lyser, using Trizol reagent (Invitrogen, USA) according to the manufacturer's protocol and Zymo RNA Clean & Concentrator Kit, including in-column DNase treatment. qRT- PCR was performed with 10 ng RNA using the NEB Luna® Universal One-Step RT-qPCR Kit (E3005), in 10 µl reactions according to manufacturer guidelines (55 °C 10 min, 95 °C 1 min, 95 °C 10 s, 60 °C 30 s, 45 cycles, and subsequent melting curve analysis) using primers for *Xf16S* and *CDKA* (see Table S3) to normalize for plant material. At least four samples per genotype and time points were analyzed. Results of two independent rounds of infections are included.

For qRT-PCR, for one technical replicate, two inoculated leaves or mock-treated leaves per plant were harvested at 1 dpi, 5 dpi, and 3 wpi. RNA extraction and qRT-PCR reactions were performed as described above for *Pto* DC3000.

4.4 | Statistical analysis

All data was analyzed using R (version 2023.06.0 + 421) and statistical analysis was performed using the stats-package (R: The R Project for Statistical Computing, n.d.). For infection data, mutant measurements were compared to respective measurements in Col-0. For RT-qPCR and qPCR data analysis, expression values were analyzed using the $2^{(-\Delta\Delta ct)}$ method (Livak & Schmittgen, 2001) and normalized against *CDKA* or *UBC21* (*S. indica*) as housekeeping genes and the average of respective mock samples. For *E. cruciferarum*, all time points were compared to T0. Significance was assessed by two-sided Welch's *t*-test ($\alpha = .05$, *p*-values * < .05, ** < .01, *** < .001, **** < .0001) using the stats-package in R. Heat maps were generated using geom_tile of the ggplot package in R depicting average of normalized colonization compared to Col-0 at selected time point or average of log2 foldchange of gene expression at early, mid or late time point. We considered tissue from independently inoculated plants as technical replicates, which were pooled in some instances. Independent biological replicates of the experiments were performed to confirm results at least twice.

4.5 | Use of public data

The heat map showing the differential expression of *DCL* and *AGO* genes (Figure S1) was generated using data from Bjornson et al., 2021 (Tables S1 and S2) with Python v3.11.4 (Van Rossum & Drake, 1995) and Seaborn v0.12.2 (Waskom, 2021).

4.6 | Accession numbers

Genes reported in this article can be found in the GenBank/RGAP databases under the following accession numbers: *AGO1 (AT1G48410), AGO2 (AT1G31280), AGO4 (AT2G27040), AGO10 (AT5G43810), DCL2 (AT3G03300), DCL3 (AT3G43920), and DCL4 (AT5G20320), CDKA (AT3G48750.1), UBC21 (AT5G25760).*

AUTHOR CONTRIBUTIONS

A.R., H.T., S.N., B.L., S.F., J.K., J.S., E.S., S.K., V.G., M.F., A.W., K.H.K., R.P., S.R. designed the methodology; A.R., H.T., S.N., B.L., S.F., T.A., J.P., E.S. performed research; A.R., H.T., S.N., B.L., S.F., V.G., P.B., K.B. analyzed data; A.G., J.K., V.G., A.W., K.H.K., R.P., S.R. conceived the project and supervised the research; A.R., H.T., S.N., S.R. wrote the manuscript with input from all authors.

ACKNOWLEDGMENTS

This work was enabled by grants within the research unit FOR5116 "exRNA" funded by the Deutsche Forschungsgemeinschaft (DFG). Individual grants of this research unit comprise DFG projects FE448/15-1 to M. F, GO 2037/8-1 to A. G, GO 2064/4-1 to V. G., KE 856/8-1 to J.K., KO 1208/32-1 to K.K., PA 861/22-1 to R. P, RO 3550/16-1 to S.R. and WE 5707/2-1 to A.W. S.N. was supported by a Dr. Ernst-Leopold Klipstein Foundation grant. We thank Elif Olkun for technical support. Open Access funding enabled and organized by Projekt DEAL.

CONFLICT OF INTEREST STATEMENT

The authors declare no conflict of interest.

PEER REVIEW

The peer review history forthis article is available in the Supporting Information for this article.

DATA AVAILABILITY STATEMENT

The data that support the findings of this study are available from the corresponding author upon reasonable request.

ORCID

Alessa Ruf https://orcid.org/0000-0003-0919-9717
Sabrine Nasfi https://orcid.org/0000-0001-5916-0824
Johannes Postma https://orcid.org/0009-0002-0565-4487
Patrick Blumenkamp https://orcid.org/0000-0002-7013-9601
Alexander Goesmann https://orcid.org/0000-0002-7086-2568
Julia Kehr https://orcid.org/0000-0003-3617-9981
Jens Steinbrenner https://orcid.org/0000-0003-1008-2268
Arne Weiberg https://orcid.org/0000-0003-4300-4864
Karl-Heinz Kogel https://orcid.org/0000-0003-1226-003X
Ralph Panstruga https://orcid.org/0000-0002-3756-8957
Silke Robatzek https://orcid.org/0000-0002-9788-322X

REFERENCES

Agorio, A., & Vera, P. (2007). ARGONAUTE4 is required for resistance to *Pseudomonas syringae* in Arabidopsis. *The Plant Cell*, *19*(11), 3778–3790. https://doi.org/10.1105/tpc.107.054494

Azevedo, J., Garcia, D., Pontier, D., Ohnesorge, S., Yu, A., Garcia, S., Braun, L., Bergdoll, M., Hakimi, M. A., Lagrange, T., & Voinnet, O. (2010). Argonaute quenching and global changes in Dicer homeostasis caused by a pathogen-encoded GW repeat protein. *Genes & Development*, *24*(9), 904–915. https://doi.org/10.1101/gad.1908710

Bartsch, M., Gobbato, E., Bednarek, P., Debey, S., Schultze, J. L., Bautor, J., & Parker, J. E. (2006). Salicylic acid–independent ENHANCED DISEASE SUSCEPTIBILITY1 signaling in Arabidopsis immunity and cell death is regulated by the monooxygenase FMO1 and the Nudix hydrolase NUDT7. *The Plant Cell*, *18*(4), 1038–1051. https://doi.org/10.1105/tpc.105.039982

Bemm, F., Becker, D., Larisch, C., Kreuzer, I., Escalante-Perez, M., Schulze, W. X., Ankenbrand, M., de Weyer, A.-L. V., Krol, E., Al-Rasheid, K. A., Mithöfer, A., Weber, A. P., Schultz, J., & Hedrich, R. (2016). Venus flytrap carnivorous lifestyle builds on herbivore defense strategies. *Genome Research*, *26*(6), 812–825. https://doi.org/10.1101/gr.202200.115

Bjornson, M., Pimprikar, P., Nürnberger, T., & Zipfel, C. (2021). The transcriptional landscape of *Arabidopsis thaliana* pattern-triggered immunity. *Nature Plants*, *7*(5), 579–586. https://doi.org/10.1038/s41477-021-00874-5

Bouché, N., Lauressergues, D., Gasciolli, V., & Vaucheret, H. (2006). An antagonistic function for Arabidopsis DCL2 in development and a new function for DCL4 in generating viral siRNAs. *The EMBO Journal*, *25*(14), 3347–3356. https://doi.org/10.1038/sj.emboj.7601217

Bourras, S., Praz, C. R., Spanu, P. D., & Keller, B. (2018). Cereal powdery mildew effectors: A complex toolbox for an obligate pathogen. *Current Opinion in Microbiology*, *46*, 26–33. https://doi.org/10.1016/j.mib.2018.01.018

Cai, Q., Qiao, L., Wang, M., He, B., Lin, F.-M., Palmquist, J., Huang, S.-D., & Jin, H. (2018). Plants send small RNAs in extracellular vesicles to fungal pathogen to silence virulence genes. *Science*, *360*(6393), 1126–1129. https://doi.org/10.1126/science.aar4142

Cao, J.-Y., Xu, Y.-P., & Cai, X.-Z. (2020). Integrated miRNAome and transcriptome analysis reveals Argonaute 2-mediated defense responses against the devastating Phytopathogen *Sclerotinia sclerotiorum*. *Frontiers in Plant Science*, *11*, 500. https://doi.org/10.3389/fpls.2020.00500

Chen, D.-H., & Ronald, P. C. (1999). A rapid DNA minipreparation method suitable for AFLP and other PCR applications. *Plant Molecular Biology Reporter*, *17*(1), 53–57. https://doi.org/10.1023/a:1007585532036

Cheng, A.-P., Lederer, B., Oberkofler, L., Huang, L., Johnson, N. R., Platten, F., Dunker, F., Tisserant, C., & Weiberg, A. (2023). A fungal RNA-dependent RNA polymerase is a novel player in plant infection and cross-kingdom RNA interference. *PLOS Pathogens*, *19*(12), e1011885. https://doi.org/10.1371/journal.ppat.1011885

Consonni, C., Humphry, M. E., Hartmann, H. A., Livaja, M., Durner, J., Westphal, L., Vogel, J., Lipka, V., Kemmerling, B., Schulze-Lefert, P., Somerville, S. C., & Panstruga, R. (2006). Conserved requirement for a plant host cell protein in powdery mildew pathogenesis. *Nature Genetics*, *38*(6), 716–720. https://doi.org/10.1038/ng1806

Curaba, J., & Chen, X. (2008). Biochemical activities of Arabidopsis RNA-dependent RNA polymerase 6 *. *Journal of Biological Chemistry*, *283*(6), 3059–3066. https://doi.org/10.1074/jbc.M708983200

Daniels, M. J., Barber, C. E., Turner, P. C., Cleary, W. G., & Sawczyc, M. K. (1984). Isolation of mutants of *Xanthomonas campestris* pv. Campestris showing altered pathogenicity. *Microbiology*, *130*(9), 2447–2455. https://doi.org/10.1099/00221287-130-9-2447

Davis, M. J. (1980). Isolation media for the Pierce's disease bacterium. *Phytopathology*, *70*(5), 425. https://doi.org/10.1094/Phyto-70-425

Deleris, A., Gallego-Bartolome, J., Bao, J., Kasschau, K. D., Carrington, J. C., & Voinnet, O. (2006). Hierarchical action and inhibition of plant Dicer-like proteins in antiviral defense. *Science*, *313*(5783), 68–71. https://doi.org/10.1126/science.1128214

Dunker, F., Trutzenberg, A., Rothenpieler, J. S., Kuhn, S., Pröls, R., Schreiber, T., Tissier, A., Kemen, A., Kemen, E., Hückelhoven, R., & Weiberg, A. (2020). Oomycete small RNAs bind to the plant RNA-induced silencing complex for virulence. *eLife*, *9*, e56096. https://doi.org/10.7554/eLife.56096

Ellendorff, U., Fradin, E. F., de Jonge, R., & Thomma, B. P. H. J. (2009). RNA silencing is required for Arabidopsis defence against Verticillium

wilt disease. *Journal of Experimental Botany*, *60*(2), 591–602. https://doi.org/10.1093/jxb/ern306

Fang, X., & Qi, Y. (2016). RNAi in plants: An Argonaute-centered view. *The Plant Cell*, *28*(2), 272–285. https://doi.org/10.1105/tpc.15.00920

Frantzeskakis, L., Courville, K. J., Plücker, L., Kellner, R., Kruse, J., Brachmann, A., Feldbrügge, M., & Göhre, V. (2017). The plant-dependent life cycle of *Thecaphora thlaspeos*: A smut fungus adapted to Brassicaceae. *Molecular Plant-Microbe Interactions*, *30*(4), 271–282. https://doi.org/10.1094/MPMI-08-16-0164-R

Geng, S., Kong, X., Song, G., Jia, M., Guan, J., Wang, F., Qin, Z., Wu, L., Lan, X., Li, A., & Mao, L. (2019). DNA methylation dynamics during the interaction of wheat progenitor *Aegilops tauschii* with the obligate biotrophic fungus *Blumeria graminis* f Sp. *tritici*. *New Phytologist*, *221*(2), 1023–1035. https://doi.org/10.1111/nph.15432

Guo, N., Zhao, J., Yan, Q., Huang, J., Ma, H., Rajput, N. A., Jiang, H., Xing, H., & Dou, D. (2018). Resistance to *Phytophthora* pathogens is dependent on gene silencing pathways in plants. *Journal of Phytopathology*, *166*(6), 379–385. https://doi.org/10.1111/jph.12695

Hou, Y., Zhai, Y., Feng, L., Karimi, H. Z., Rutter, B. D., Zeng, L., Choi, D. S., Zhang, B., Gu, W., Chen, X., Ye, W., Innes, R. W., Zhai, J., & Ma, W. (2019). A *Phytophthora* effector suppresses trans-kingdom RNAi to promote disease susceptibility. *Cell Host & Microbe*, *25*(1), 153–165. e5. https://doi.org/10.1016/j.chom.2018.11.007

Huang, C.-Y., Wang, H., Hu, P., Hamby, R., & Jin, H. (2019). Small RNAs – Big players in plant-microbe interactions. *Cell Host & Microbe*, *26*(2), 173–182. https://doi.org/10.1016/j.chom.2019.07.021

Iwakawa, H.-O., & Tomari, Y. (2022). Life of RISC: Formation, action, and degradation of RNA-induced silencing complex. *Molecular Cell*, *82*(1), 30–43. https://doi.org/10.1016/j.molcel.2021.11.026

Ji, L., Liu, X., Yan, J., Wang, W., Yumul, R. E., Kim, Y. J., Dinh, T. T., Liu, J., Cui, X., Zheng, B., Agarwal, M., Liu, C., Cao, X., Tang, G., & Chen, X. (2011). ARGONAUTE10 and ARGONAUTE1 regulate the termination of floral stem cells through two MicroRNAs in Arabidopsis. *PLoS Genetics*, *7*(3), e1001358. https://doi.org/10.1371/journal.pgen.1001358

Jones, J. D. G., Staskawicz, B. J., & Dangl, J. L. (2024). The plant immune system: From discovery to deployment. *Cell*, *187*(9), 2095–2116. https://doi.org/10.1016/j.cell.2024.03.045

Jullien, P. E., Schröder, J. A., Bonnet, D. M. V., Pumplin, N., & Voinnet, O. (2022). Asymmetric expression of Argonautes in reproductive tissues. *Plant Physiology*, *188*(1), 38–43. https://doi.org/10.1093/plphys/kiab474

Kusch, S., Thiery, S., Reinstädler, A., Gruner, K., Zienkiewicz, K., Feussner, I., & Panstruga, R. (2019). Arabidopsis mlo3 mutant plants exhibit spontaneous callose deposition and signs of early leaf senescence. *Plant Molecular Biology*, *101*(1), 21–40. https://doi.org/10.1007/s11103-019-00877-z

Landa, B. B., Saponari, M., Feitosa-Junior, O. R., Giampetruzzi, A., Vieira, F. J. D., Mor, E., & Robatzek, S. (2022). Xylella fastidiosa's relationships: The bacterium, the host plants, and the plant microbiome. *New Phytologist*, *234*(5), 1598–1605. https://doi.org/10.1111/nph.18089

Li, Y., Zhang, Q., Zhang, J., Wu, L., Qi, Y., & Zhou, J.-M. (2010). Identification of MicroRNAs involved in pathogen-associated molecular pattern-triggered plant innate immunity. *Plant Physiology*, *152*(4), 2222–2231. https://doi.org/10.1104/pp.109.151803

Lincoln, C., Britton, J. H., & Estelle, M. (1990). Growth and development of the axr1 mutants of Arabidopsis. *The Plant Cell*, *2*(11), 1071–1080.

Livak, K. J., & Schmittgen, T. D. (2001). Analysis of relative gene expression data using real-time quantitative PCR and the $2^{-\Delta\Delta CT}$ method. *Methods*, *25*(4), 402–408. https://doi.org/10.1006/meth.2001.1262

López, A., Ramírez, V., García-Andrade, J., Flors, V., & Vera, P. (2011). The RNA silencing enzyme RNA polymerase V is required for plant immunity. *PLoS Genetics*, *7*(12), e1002434. https://doi.org/10.1371/journal.pgen.1002434

Martín-Merchán, A., Moro, B., Bouet, A., & Bologna, N. G. (2023). Domain organization, expression, subcellular localization, and biological roles of ARGONAUTE proteins in Arabidopsis. *Journal of Experimental Botany*, *74*(7), 2374–2388. https://doi.org/10.1093/jxb/erad030

Melotto, M., Zhang, L., Oblessuc, P. R., & He, S. Y. (2017). Stomatal defense a decade later. *Plant Physiology*, *174*(2), 561–571. https://doi.org/10.1104/pp.16.01853

Mitre, L. K., Teixeira-Silva, N. S., Rybak, K., Magalhães, D. M., de Souza-Neto, R. R., Robatzek, S., Zipfel, C., & de Souza, A. A. (2021). The Arabidopsis immune receptor EFR increases resistance to the bacterial pathogens *Xanthomonas* and *Xylella* in transgenic sweet orange. *Plant Biotechnology Journal*, *19*(7), 1294–1296. https://doi.org/10.1111/pbi.13629

Navarro, L., Dunoyer, P., Jay, F., Arnold, B., Dharmasiri, N., Estelle, M., Voinnet, O., & Jones, J. D. G. (2006). A plant miRNA contributes to antibacterial resistance by repressing auxin signaling. *Science*, *312*(5772), 436–439. https://doi.org/10.1126/science.1126088

Obbard, D. J., Gordon, K. H. J., Buck, A. H., & Jiggins, F. M. (2008). The evolution of RNAi as a defence against viruses and transposable elements. *Philosophical Transactions of the Royal Society, B: Biological Sciences*, *364*(1513), 99–115. https://doi.org/10.1098/rstb.2008.0168

Papenfort, K., & Melamed, S. (2023). Small RNAs, large networks: Post-transcriptional regulons in gram-negative bacteria. *Annual Review of Microbiology*, *77*, 23–43. https://doi.org/10.1146/annurev-micro-041320-025836

Qin, S., Veloso, J., Baak, M., Boogmans, B., Bosman, T., Puccetti, G., Shi-Kunne, X., Smit, S., Grant-Downton, R., Leisen, T., Hahn, M., & van Kan, J. A. L. (2023). Molecular characterization reveals no functional evidence for naturally occurring cross-kingdom RNA interference in the early stages of *Botrytis cinerea*–tomato interaction. *Molecular Plant Pathology*, *24*(1), 3–15. https://doi.org/10.1111/mpp.13269

R: The R Project for Statistical Computing. (n.d.). Retrieved 21 June 2024, from https://www.r-project.org/

Rebolledo-Prudencio, O. G., Estrada-Rivera, M., Dautt-Castro, M., Arteaga-Vazquez, M. A., Arenas-Huertero, C., Rosendo-Vargas, M. M., Jin, H., & Casas-Flores, S. (2022). The small RNA-mediated gene silencing machinery is required in Arabidopsis for stimulation of growth, systemic disease resistance, and suppression of the nitrile-specifier gene NSP4 by Trichoderma atroviride. *The Plant Journal*, *109*(4), 873–890. https://doi.org/10.1111/tpj.15599

Ren, B., Wang, X., Duan, J., & Ma, J. (2019). Rhizobial tRNA-derived small RNAs are signal molecules regulating plant nodulation. *Science*, *365*, 919–922. https://doi.org/10.1126/science.aav8907

Ried, M. K., Banhara, A., Hwu, F.-Y., Binder, A., Gust, A. A., Höfle, C., Hückelhoven, R., Nürnberger, T., & Parniske, M. (2019). A set of Arabidopsis genes involved in the accommodation of the downy mildew pathogen *Hyaloperonospora arabidopsidis*. *PLoS Pathogens*, *15*(7), e1007747. https://doi.org/10.1371/journal.ppat.1007747

del Sánchez-Correa, M. S., Isidra-Arellano, M. C., Pozas-Rodríguez, E. A., del Rocio Reyero-Saavedra, M., Morales-Salazar, A., del Castillo, S. M. L.-C., Sanchez-Flores, A., Jiménez-Jacinto, V., Reyes, J. L., Formey, D., & Valdés-López, O. (2022). Argonaute5 and its associated small RNAs modulate the transcriptional response during the rhizobia-Phaseolus vulgaris symbiosis. *Frontiers in Plant Science*, *13*, 1034419. https://doi.org/10.3389/fpls.2022.1034419

Šečić, E., Kogel, K.-H., & Ladera-Carmona, M. J. (2021). Biotic stress-associated microRNA families in plants. *Journal of Plant Physiology*, *263*, 153451. https://doi.org/10.1016/j.jplph.2021.153451

Šečić, E., Zanini, S., Wibberg, D., Jelonek, L., Busche, T., Kalinowski, J., Nasfi, S., Thielmann, J., Imani, J., Steinbrenner, J., & Kogel, K.-H. (2021). A novel plant-fungal association reveals fundamental sRNA and gene expression reprogramming at the onset of symbiosis. *BMC Biology*, *19*(1), 171. https://doi.org/10.1186/s12915-021-01104-2

Shen, D., Suhrkamp, I., Wang, Y., Liu, S., Menkhaus, J., Verreet, J.-A., Fan, L., & Cai, D. (2014). Identification and characterization of microRNAs in oilseed rape (*Brassica napus*) responsive to infection with the pathogenic fungus *Verticillium longisporum* using brassica AA (*Brassica rapa*) and CC (*Brassica oleracea*) as reference genomes. *New Phytologist*, *204*(3), 577–594. https://doi.org/10.1111/nph.12934

Silvestri, A., Fiorilli, V., Miozzi, L., Accotto, G. P., Turina, M., & Lanfranco, L. (2019). In silico analysis of fungal small RNA accumulation reveals putative plant mRNA targets in the symbiosis between an arbuscular mycorrhizal fungus and its host plant. *BMC Genomics*, *20*(1), 169. https://doi.org/10.1186/s12864-019-5561-0

Tang, Y., Yan, X., Gu, C., & Yuan, X. (2022). Biogenesis, trafficking, and function of small RNAs in plants. *Frontiers in Plant Science*, *13*, 825477. https://doi.org/10.3389/fpls.2022.825477

Taochy, C., Gursanscky, N. R., Cao, J., Fletcher, S. J., Dressel, U., Mitter, N., Tucker, M. R., Koltunow, A. M. G., Bowman, J. L., Vaucheret, H., & Carroll, B. J. (2017). A genetic screen for impaired systemic RNAi highlights the crucial role of DICER-LIKE 2. *Plant Physiology*, *175*(3), 1424–1437. https://doi.org/10.1104/pp.17.01181

Valdés-López, O., Formey, D., Isidra-Arellano, M. C., del Rocio Reyero-Saavedra, M., Fernandez-Göbel, T. F., & del Socorro Sánchez-Correa, M. (2019). Argonaute proteins: Why are they so important for the legume–*Rhizobia* symbiosis? *Frontiers in Plant Science*, *10*, 1177. https://doi.org/10.3389/fpls.2019.01177

Van Rossum, G., & Drake, F. L. Jr. (1995). *Python reference manual*. Centrum voor Wiskunde en Informatica Amsterdam.

Wang, Z., Hardcastle, T. J., Pastor, A. C., Yip, W. H., Tang, S., & Baulcombe, D. C. (2018). A novel DCL2-dependent miRNA pathway in tomato affects susceptibility to RNA viruses. *Genes & Development*, *32*(17–18), 1155–1160. https://doi.org/10.1101/gad.313601.118

Wang, Y., Pruitt, R. N., Nürnberger, T., & Wang, Y. (2022). Evasion of plant immunity by microbial pathogens. *Nature Reviews Microbiology*, *20*(8), 449–464. https://doi.org/10.1038/s41579-022-00710-3

Waskom, M. L. (2021). seaborn: Statistical data visualization. *Journal of Open Source Software*, *6*(60), 3021. https://doi.org/10.21105/joss.03021

Weiberg, A., Wang, M., Lin, F.-M., Zhao, H., Zhang, Z., Kaloshian, I., Huang, H.-D., & Jin, H. (2013). Fungal small RNAs suppress plant immunity by hijacking host RNA interference pathways. *Science*, *342*(6154), 118–123. https://doi.org/10.1126/science.1239705

Wong-Bajracharya, J., Singan, V. R., Monti, R., Plett, K. L., Ng, V., Grigoriev, I. V., Martin, F. M., Anderson, I. C., & Plett, J. M. (2022). The ectomycorrhizal fungus *Pisolithus microcarpus* encodes a microRNA involved in cross-kingdom gene silencing during symbiosis. *Proceedings of the National Academy of Sciences*, *119*(3), e2103527119. https://doi.org/10.1073/pnas.2103527119

Wook, K., Eamans, A. L., & Waterhouse, P. M. (2011). RNA processing activities of the Arabidopsis Argonaute protein family. In P. Grabowski (Ed.), *RNA processing*. INTECH. https://doi.org/10.5772/22686

Yu, X., Hou, Y., Chen, W., Wang, S., Wang, P., & Qu, S. (2017). *Malus hupehensis* miR168 targets to ARGONAUTE1 and contributes to the resistance against *Botryosphaeria dothidea* infection by altering defense responses. *Plant and Cell Physiology*, *58*(9), 1541–1557. https://doi.org/10.1093/pcp/pcx080

Zeise, K., & Von Tiedemann, A. (2002). Host specialization among vegetative compatibility groups of *Verticillium dahliae* in relation to *Verticillium longisporum*. *Journal of Phytopathology*, *150*(3), 112–119. https://doi.org/10.1046/j.1439-0434.2002.00730.x

Zhan, J., & Meyers, B. C. (2023). Plant small RNAs: Their biogenesis, regulatory roles, and functions. *Annual Review of Plant Biology*, *74*, 21–51. https://doi.org/10.1146/annurev-arplant-070122-035226

Zhang, X., Zhao, H., Gao, S., Wang, W.-C., Katiyar-Agarwal, S., Huang, H.-D., Raikhel, N., & Jin, H. (2011). Arabidopsis Argonaute 2 regulates innate immunity via miRNA393*—mediated silencing of a Golgi-localized SNARE gene, MEMB12. *Molecular Cell*, *42*(3), 356–366. https://doi.org/10.1016/j.molcel.2011.04.010

Zou, Y., Wang, S., Zhou, Y., Bai, J., Huang, G., Liu, X., Zhang, Y., Tang, D., & Lu, D. (2018). Transcriptional regulation of the immune receptor FLS2 controls the ontogeny of plant innate immunity. *The Plant Cell*, *30*(11), 2779–2794. https://doi.org/10.1105/tpc.18.00297

SUPPORTING INFORMATION

Additional supporting information can be found online in the Supporting Information section at the end of this article.

How to cite this article: Ruf, A., Thieron, H., Nasfi, S., Lederer, B., Fricke, S., Adeshara, T., Postma, J., Blumenkamp, P., Kwon, S., Brinkrolf, K., Feldbrügge, M., Goesmann, A., Kehr, J., Steinbrenner, J., Šečić, E., Göhre, V., Weiberg, A., Kogel, K.-H., Panstruga, R., Robatzek, S., & on behalf of the exRNA consortium (2024). Broad-scale phenotyping in Arabidopsis reveals varied involvement of RNA interference across diverse plant-microbe interactions. *Plant Direct*, *8*(11), e70017. https://doi.org/10.1002/pld3.70017

Conclusion:

In this study, we investigated the role of AGO proteins in plant-microbe interactions and identified both positive and negative regulatory functions. We found that AGO1 negatively regulates immunity against *H. arabidopsidis* while potentially enhancing resistance to *X. Fastidiosa*. In contrast, AGO10 and AGO2 appear to facilitate *S. indica* colonisation, potentially through sRNA-mediated regulation. Furthermore, AGO4 contributes to resistance against *T. thlaspeos*. Functional redundancy among AGO and DCL proteins, along with pathogen effector-mediated immune suppression, complicates the phenotypic analysis. To gain a deeper understanding of AGO functions during the interaction between *At* and *Si*, we explored higher-order AGO mutants in Chapter 5.

CHAPTER 5 –

Interaction of *Serendipita indica* small RNAs with Arabidopsis Argonautes modulates mutualistic colonisation

Authors

Sabrine Nasfi[1], Ena Šečić[1], Christina Neumann[1], Ruth Eichmann[1], Jens Steinbrenner[1,3], Karl Heinz Kogel[1,2], Patrick Schäfer[1,*]

Affiliations

[1] Institute of Phytopathology, Research Centre for BioSystems, Land Use and Nutrition, Justus Liebig University, 35392, Giessen, Germany

[2] Institut de Biologie Moléculaire des Plantes, CNRS, Université de Strasbourg, 12 rue du Général Zimmer, 67084, Strasbourg, France

[3] Andermatt Biocontrol Suisse AG, Research & Development, Stahlermatten 6, 6146 Grossdietwil, Switzerland

Abstract

Plant ARGONAUTE (AGO) proteins, key components of the RNA interference pathway, are crucial regulators of plant-microbe interaction. They facilitate small RNA transfer and activity, modulate the outcome of the interaction in a context-dependent manner and thus influence host immunity. In this study, we investigated the role of AGO proteins during the mutualistic interaction between *Arabidopsis thaliana* (*At*) and endophytic fungus *Serendipita indica* (*Si*). *Si* colonisation assays of *At* single (*ago1*, *ago2*, *ago10*) and double mutants (*ago1ago2*, *ago1ago10*) suggest that fungal accommodation in the plant

depend on multiple AGO proteins, indicating potential functional redundancy. To further explore the molecular basis of this interaction, immunoprecipitation of AGO1 and AGO2 followed by sRNA sequencing was performed. We identified *Si*-derived sRNAs (*Si*sRNAs) being loaded and translocated in Arabidopsis root cells. Our findings highlight the presence of cross-kingdom RNAi in the mutualistic Arabidopsis-*S. indica* symbiosis.

Introduction

Plants interact with a variety of microorganisms, from pathogenic invaders to beneficial symbionts. In this interaction, fungal and oomycete small RNAs (sRNAs) can hijack plant RNA silencing machinery to suppress host defences (Dunker et al., 2020; Weiberg et al., 2013) known as cross-kingdom communication. Associations with beneficial microbes, such as arbuscular mycorrhizal Fungi (AMF), rhizobia, and root colonising endophytes, can improve nutrient supply and increase nitrogen fixation in host plants (Glaeser et al., 2016; Oldroyd, 2013; Ren et al., 2019), promote plant growth and increase plant resilience to abiotic and biotic stresses (L. Li et al., 2023; Sharma & Varma, 2021). These benefits can originate from cross-kingdom communication. In an *in-silico* study, Silvestri et al. (2019) showed that *Rhizophagus irregularis* accumulates distinct sRNAs during symbiosis with *Medicago truncatula*. These sRNAs were predicted to target host transcripts involved in defence, signal transduction, and metabolism (Silvestri et al., 2019). Later on, *R. irregularis* sRNA, *Rir*2216, was demonstrated to be delivered into *M. truncatula* root cells, recruited by the host AGO1 complex, and silenced the transcription factor *Mt*WRKY69 to facilitate fungal colonisation and arbuscule formation (Silvestri et al., 2025).

Endophytic fungi employ sRNAs to modulate the colonisation of host plants. Using an artificially engineered system, *Fusarium solani* strain K (*FsK*) was transformed with a hairpin RNA construct that was processed into 21–24 nt siRNAs to silence a *Nicotiana benthamiana* reporter gene (Dalakouras et al., 2022). A follow-up study confirmed that this induced silencing is RNA-Dependent RNA polymerase (RDR) 6 dependent, highlighting a plant genetic requirement for the amplification and durability of cross-kingdom RNAi (Kellari et al., 2025).

In the *Brachypodium distachyon (Bd)–Serendipita indica (Si)* interaction, transcriptome and sRNA profiling showed that *S. indica* encodes an RNAi machinery (predicted DCLs, AGOs/Quelling Deficient-2-like proteins, and RDR proteins) that reprograms expression of thousands of *Si* genes during colonisation. The study identified unique *S. indica* cross-kingdom sRNAs (ck-*Si*sRNAs) and their corresponding downregulated *Bd* targets, suggesting ck-RNAi as a regulatory mechanism in the *Si-Bd* interaction (Šečić et al., 2021). In *Arabidopsis*, Nasfi et al. (2024) developed a pipeline for validating *Si*sRNAs. They detected *Si*sRNAs in axenic culture and during the *Si-At* interaction, overexpressed them in protoplasts, and assayed their functional activity against predicted Arabidopsis targets in cell-wall organisation, hormone signalling, immunity, and gene regulation. Importantly, using AGO1 immunoprecipitation, *Si*sRNAs were confirmed to be translocated and loaded into the *At* RNAi machinery, indicating their regulatory role in the *Si-At* interaction (Nasfi et al., 2024).

Recent studies have indicated the importance of AGO proteins in the establishment of beneficial and pathogenic symbioses. In *Phaseolus vulgaris*, AGO5 was shown to bind the endogenous miRNAs and rhizobia tRNA fragments during nodulation. The loss of AGO5 further inhibited nodule formation and altered the expression of symbiosis-related genes, identifying AGO5 as a regulator of legume–rhizobia interactions (Sánchez-Correa et al., 2022). In *Nicotiana attenuata*, AGO7 promoted AMF colonisation by regulating small RNAs involved in root signalling. Plants with depleted AGO7 showed reduced colonisation and slower growth, suggesting a role in establishing this beneficial association (Pradhan et al., 2023). In pathogenic systems, AGO1 is the canonical effector of miRNA function (Baulcombe, 2004; Vaucheret et al., 2004). In addition, AGO2 is strongly induced during bacterial and viral infections as part of the plant defence system (Jaubert et al., 2011; Zhang et al., 2011), while AGO10 modulates development by sequestering miR165/166 (Ji et al., 2011; Zhu et al., 2011).

In *Arabidopsis thaliana*, there is initial evidence for a connection between AGO proteins that facilitate mutualistic interactions. In our previous work, we demonstrated that *Arabidopsis thaliana ago2* and *ago10* mutants showed reduced colonisation by *S.indica*, while *ago1* mutant plants showed wild-type-like colonisation.

In this study, we focused on AGO1, AGO2, and AGO10, as a canonical effector, an immunity-associated AGO, and a clade I developmental AGO, respectively. By combining mutant analyses, expression profiling, and AGO immunoprecipitation coupled with sequencing, we investigated their contribution to *S. indica* colonisation and the recruitment of *Si*-derived sRNAs into the host silencing machinery. This study fills a gap in our understanding of AGO function in the establishment and function of beneficial symbioses and reveals how the host RNAi pathway may be exploited during symbioses.

Material and Methods

Plant, fungi, and plant inoculation

For interaction assays between *Arabidopsis thaliana* (Col-0) roots and *Serendipita indica* (strain IPAZ-11827, Institute of Phytopathology, Giessen, Germany), seedlings were cultivated on vertical ATS medium (Lincoln et al., 1990) plates without sucrose and with 4.5 g L^{-1} Gelrite (Duchefa, #G1101) under an 8 h light/16 h dark cycle (22 °C/18 °C). Fourteen-day-old roots were inoculated with 1 mL of *S. indica* chlamydospore suspension (5×10^5 spores mL^{-1} in 0.002% Tween-20) following the protocol of Jacobs et al. (2011). *S. indica* cultures were maintained axenically on complete medium (Pontecorvo et al., 1953) for four weeks under daylight with agitation at 100 rpm.

AGO expression profiling in *ago* mutants

For *AGO* gene expression, Col-0, *ago1*, *ago2*, *ago10*, *ago1ago2*, and *ago1ago10* Arabidopsis mutant plants were grown on ATS plates and inoculated with *S. indica* spores as previously described. Inoculated roots were harvested at 3 and 7 dpi and ground with the tissue lyser. RNA extraction, cDNA synthesis, and quantification of AGO expression were performed as previously described in Ruf, Thieron, Nasfi et al. 2024 (Ruf, Thieron, Nasfi et al., 2024). *Ubiquitin* (*UBQ5, AT3G62250*) and *Ubiquitin* (*UBC21, AT5G25760*) were used as housekeeping genes. Roots from two ATS plates were harvested and considered as one technical replicate. Results from three or more biological replicates are included in the data analysis. All primers used in this study are presented in Supplementary Table 1.

Quantification of *S. indica* colonisation in *ago* double mutants

For quantification of *S. indica* colonisation of Arabidopsis double mutant lines, *ago1ago2* and *ago1ago10*, genomic DNA was extracted using a Qiagen DNA extraction kit (QIAGEN, 69504). DNA concentration was measured using a NanoDrop ND-1000 Spectrophotometer (Thermo Fisher Scientific, USA), and quantification of *S.indica* colonisation was performed via qPCR using internal transcribed spacer (ITS) primers as previously described in Ruf, Thieron, Nasfi et al. 2024 (Ruf, Thieron, Nasfi et al., 2024). All primers used in this study are presented in Supplementary Table 1.

AGO1 immunoprecipitation and western blot

*At*AGO1-IP was performed using 5g of *At* roots inoculated with *S.indica* chlamydospores and harvested at 7 dpi and anti-AGO1 primary antibody (1:4000 dilution) (Agrisera, AS09 527) as described in Nasfi et al. 2024. For western blot, 20 µl or 10µl of total protein, crude extract before antibodies (CE), supernatant after pelleting agarose beads (SN), and *At*AGO1 Co-IP fraction (IP) were loaded after boiling at 95 °C for 5 min using 5.5% stacking gel and a 12% resolving gel and visualised (Nasfi et al., 2024).

AGO2 immunoprecipitation and western blot

HA-AGO2 Arabidopsis roots (2.5 g), inoculated or not with *S. indica*, were ground in liquid nitrogen with sterile sand. Samples were thawed on ice (~50 min) in 10 ml of IP extraction buffer, centrifuged at 3200 × g for 15 min at 4 °C, and supernatants were filtered through two layers of Miracloth. A 200 µl aliquot of the crude extract (CE; supernatant before antibodies) was mixed with SDS loading buffer, boiled at 95 °C for 5 min, and stored at −20 °C for western blot analysis. To the remaining supernatant, 400 µL of anti-HA MicroBeads (Miltenyi Biotec) was added, and the mixture was incubated for 2 h at 4 °C on a rotation wheel. After centrifugation at 500 × g for 5 min at 4 °C, 200 µL of the supernatant (SN; after antibodies) was collected for the western blot. Beads were washed four times with ice-cold IP wash buffer, resuspended in 1 ml of wash buffer, and split into 30% for western blot (IP fraction) and 70% for RNA extraction. AGO2 western blot was performed as previously described for AGO1-IP in Nasfi et al. 2024, using an HA-HRP conjugated monoclonal antibody (clone 3F10, Roche) at a 1:6000 dilution in 1% milk in 0.1% PBS-T. Membranes were incubated with the antibody solution (20 ml) overnight at 4 °C on a

rocking shaker, then washed four times for 10 min each at room temperature with 0.1% PBS-T.

sRNA recovery

Immunoprecipitated pellets were resuspended in 300 µL of IP wash buffer mixed with 150 µL of RNA release buffer and incubated at 65 °C for 15 min with gentle agitation (300 rpm). RNA was recovered by extraction with 450 µL of water-saturated phenol, followed by vortexing for 2 min and centrifugation at 10 000 x g for 8 min at room temperature. The upper phase was transferred to a low-binding tube and purified twice using 450 µL of chloroform/isoamyl alcohol (24:1). To precipitate RNA, 0.1 volume of 3 M sodium acetate, 2.5 volumes of 96% ethanol, and 20 µg of glycogen were added, and samples were incubated overnight at –20 °C. The RNA was pelleted (20 000 x g, 30 min, 4 °C), washed with 80% ethanol, centrifuged again (20 000 x g, 20 min, 4 °C), air-dried, and finally dissolved in 8 µl of DEPC-treated water before storage at –80 °C.

Stem-loop PCR

Hairpin and forward primers were generated using the tools described by Adhikari et al. (2013) and Varkonyi-Gasic and Hellens (2011) (Adhikari et al., 2013; Varkonyi-Gasic & Hellens, 2011). Stem–loop PCR was performed as described by Nasfi et al. (2024). Expression of *Si*sRNAs pulled down from AGO2-IP was verified by end-point PCR under the following conditions: 95 °C for 5 min; 40 cycles of 95 °C for 30 s, 60 °C for 30 s, and 72 °C for 30 s; followed by 72 °C for 5 min. PCR products were separated on 2% TBE–agarose gels. Primer sequences are listed in Supplementary Table S1.

NGS sequencing of sRNAs

Small RNA libraries from AGO1 and AGO2 IP were prepared and sequenced by two service providers. AGO1-sRNAs from a first replicate were sequenced at GenXPro GmbH (Frankfurt am Main, Germany) using the TrueQuant smallRNA Seq Kit according to the manufacturer's instructions on an Illumina NextSeq500 platform. AGO2-sRNAs from a first replicate were sequenced at BMK (Biomarker Technologies, Beijing, China) on an Illumina platform. Libraries from a second replicate of AGO1- and AGO2-sRNAs were sequenced with GenXPro GmbH as previously described.

Bioinformatics

Raw sequencing reads were subjected to quality control using FastQC v0.11.9. Adapter sequences as well as low-quality bases at the read-ends were trimmed with Cutadapt v4.1. Reads between 18 and 26 nucleotides in length were retained for further analysis. The processed reads were aligned with Bowtie v1.3.1 to several reference datasets, including the *Arabidopsis thaliana* genome (Ensembl release 50, TAIR10), the *Serendipita indica* genome (Šečić et al., 2021; GCA_910890315.1), the *S. indica* transcriptome (Serendipita_indica_dsm_11827_gca_000313545.ASM31354v1), and a custom database comprising rRNA and tRNA sequences from *A. thaliana*, *S. indica*, *Neurospora crassa*, and *Laccaria bicolor*. For the generation of the Arabidopsis sRNA pool (*At→At*), only reads that mapped with 100% identity to the *A. thaliana* genome and did not map to the *S. indica* genome, the *A. thaliana* transcriptome, or the rRNA/tRNA database were retained. Conversely, the Serendipita-derived sRNA pool (*Si*→At) was defined as reads that mapped with 100% identity to the *S. indica* genome but not to the *S. indica* transcriptome, thereby representing non-coding regions, and that did not allow perfect matches to the *A. thaliana* genome but permitted overlap with rRNA and tRNA sequences.

Protoplast transformation

Protoplasts were isolated using the Tape -Arabidopsis Sandwich method as described in (Wu et al., 2009). Design and cloning of *Si*sRNAs and protoplast transformation were performed as described in Nasfi et al., 2024 using the plasmid pUC18-*At*mir390a-RFP. 75 mer oligos used for cloning *Si*sRNAs into the pUC18-*At*mir390a-RFP are presented in Supplementary Table 2.

RNA extraction and cDNA synthesis

Total RNA from protoplasts was extracted using QuickRNA™ Miniprep kit (Zymo Research, R1050) with an on-column DNase I treatment and concentration was measured using a NanoDrop ND-1000 Spectrophotometer (Thermo Fisher Scientific, USA). cDNA for qPCR analysis was synthesised from 500 ng of RNA using Revert Aid Reverse transcriptase.

qPCR for PTGS

The standard curve method was used to test the efficiency of the qPCR transcript primers (0.4 µM) using non transformed *At* protoplasts and 5 µl of SybrGreen (Sigma-Aldrich). The total volume of 10 µl and three technical replicates are considered for each reaction. Prior to master mix preparation, 2 µl of ROX (CRX reference dye, Promega, C5411) were added to 1 ml of SybrGreen as a passive reference dye that allows fluorescent normalisation for qPCR data. qPCR was performed using the QuantStudio 5 real-time PCR system (Applied Biosystems) as described in Nasfi et al. 2024. The PCR conditions were 95 °C for 5 min, followed by 40 cycles of 95 °C for 15 s, 60 °C for 30 s, and 72 °C for 30 s, and then by a melting curve analysis. Fold changes in expression were calculated using the ΔΔCt method(Livak & Schmittgen, 2001) and normalised to the geometric mean of two endogenous housekeeping genes, Ubiquitin (*UBQ5, AT3G62250*) and Elongation Factor-1 alpha (*ef1α, AT5G60390*) and Ct values of target genes were normalised to the RFP Ct values. Standard errors were calculated for all mean values. All primers are listed in Supplementary Table S1.

ago mutant lines

Seeds of AGO mutant lines, including *ago1-27*, *ago2-1*, and *ago10-1* single mutants, and the double mutants *ago1-27ago2-1* and *ago1-27ago10-1*, were kindly provided by Dr James C. Carrington's laboratory at the Donald Danforth Plant Science Centre, USA. Plants were genotyped to confirm the presence of mutations before use in colonisation experiments.

Results

Our previous findings suggested a specific role for AGO2 and AGO10, but not AGO1, in promoting Arabidopsis-*S. indica* symbiosis (Ruf, Thieron, Nasfi et al., 2024). To further investigate the functional role of AGO1, AGO2, and AGO10 in this symbiosis, the colonisation pattern of *S. indica* was examined in higher-order mutants. The *ago1ago10* mutant showed an increased *S. indica* colonisation compared to wild-type Col-0 plants at both early (3 dpi; Figure 1a) and later time points (7 dpi, Figure 1b). In contrast, the *ago1ago2* double mutant showed significantly reduced colonisation at 3 dpi (Figure 1a), with a similar trend observed at 7 dpi (Figure 1b). Taken together, these results support a

model in which AGO2 and AGO10 promote mutualistic colonisation, with AGO10 having a distinct function within clade I.

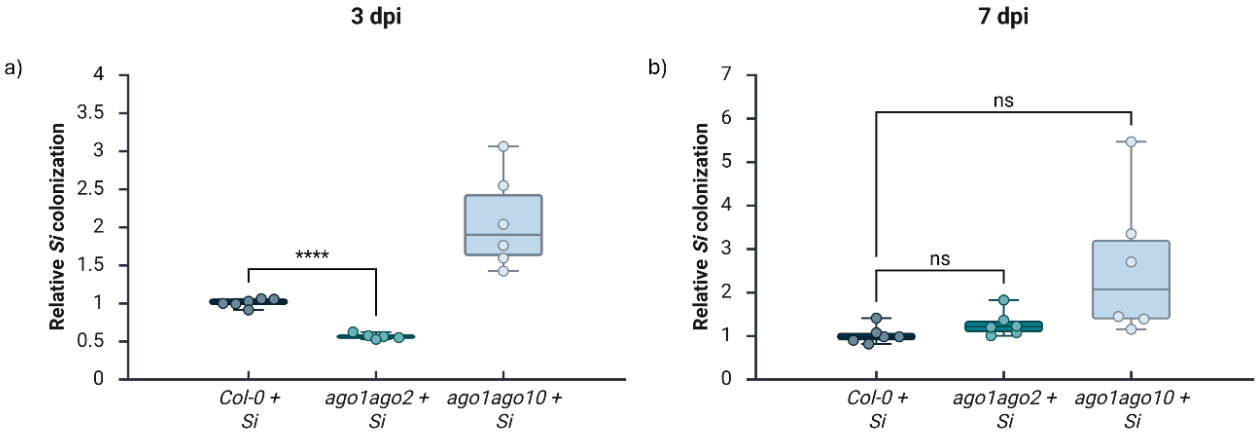

Figure 1: Quantification of *S. indica* colonisation in AGO double mutants at 3 and 7 dpi. Relative *S. indica* colonisation was quantified from genomic DNA in *ago1ago2* and *ago1ago10* compared to Col-0 at **(a)** 3 dpi and **(b)** 7 dpi. Colonisation levels were determined by qPCR using *S. indica* ITS primers and normalised to the geometric mean of two endogenous housekeeping genes, *Ubiquitin* (*UBC21, AT5G25760*) and *UBIQUITIN 5* (*UBQ5, AT3G62250*). The data represent two biological replicates. Boxplots display individual values with standard deviations. Statistical significance was assessed using a two-sided Welch's t-test (ns, not significant; α = .05 p-values * < .05, ** < .01, *** < .001, **** < .0001).

AGO's expression is dynamically regulated in response to *Si*

We previously observed that *AGO4* expression (downregulated at 7 dpi) was the only one altered following *S. indica* colonisation among all AGOs in Col-0 (Ruf, Thieron, Nasfi et al., 2024). To further investigate the role of AGOs during *S. indica* colonisation, we analysed the expression of *AGO1*, *AGO2*, and *AGO10* in the Arabidopsis single and double mutants at 3 and 7 dpi (Figure 2). *AGO1* expression showed no significant change in the *ago2* or *ago10* mutants at both time points (Figure 2a). At 3 dpi, *AGO2* levels were significantly increased in the *ago1* single and in *ago1ago10* double mutants and remained elevated in the *ago1* mutant at 7 dpi, indicating a persistent effect over time

(Figure 2b). *AGO10* expression was increased in the *ago2* but not in the *ago1ago2* double mutant (Figure 2c). These results suggest potential functional redundancy between AGO1, AGO2 and AGO10.

a)

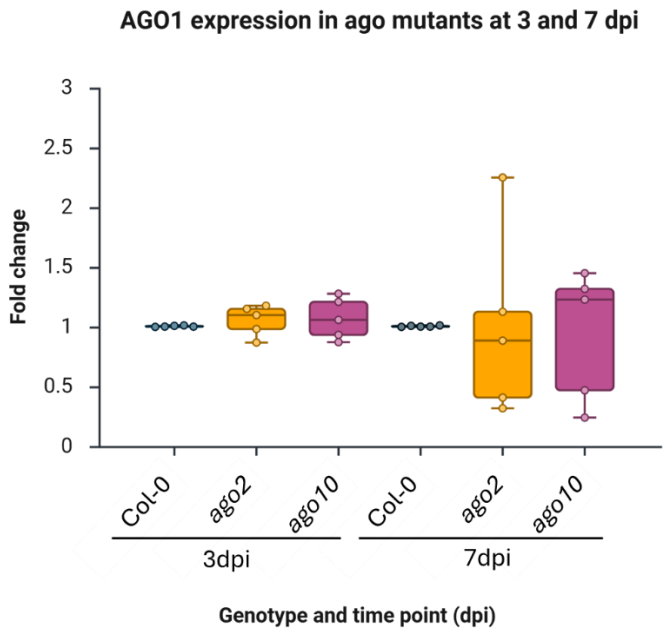

b)

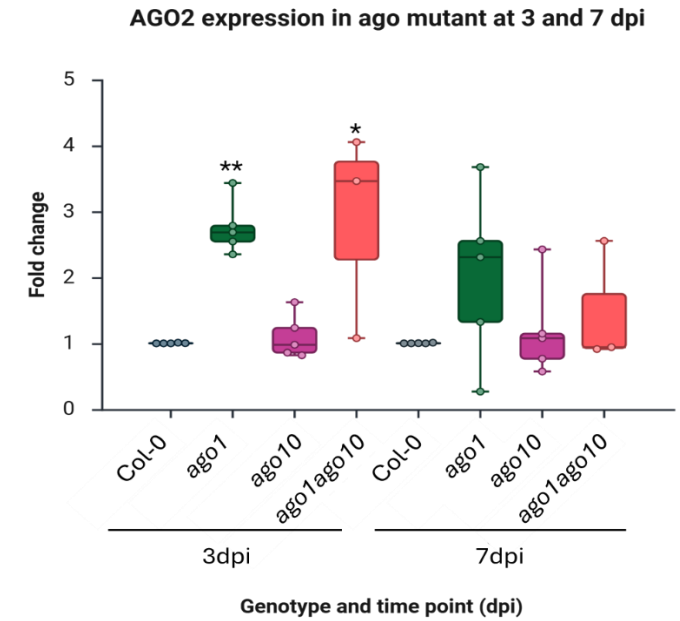

c)

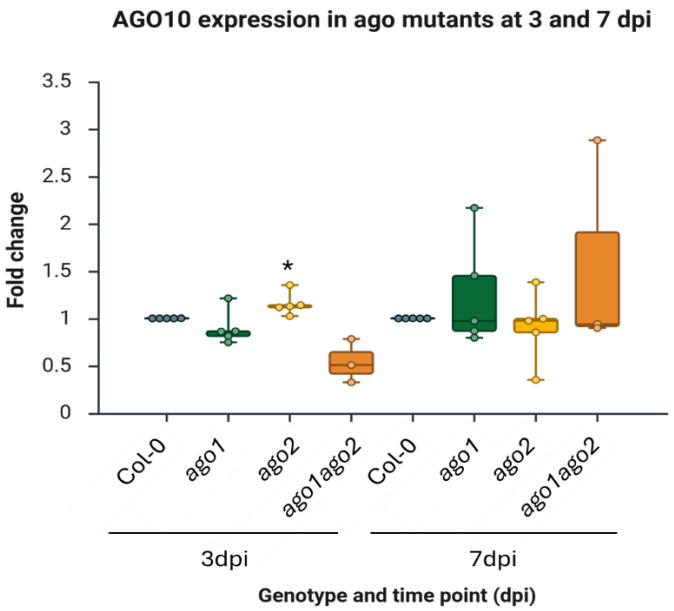

Figure 2: Relative expression of AGO genes in Arabidopsis *ago* mutants during *S. indica* colonisation. Boxplots show expression of **(a)** AGO1, **(b)** AGO2, and **(c)** AGO10 in single and double *ago* mutants at 3 dpi and 7 dpi relative to expression in Col-0. Error bars show standard deviation. The data represent three independent biological replicates. Statistical significance was assessed by two-sided Welch's t-test (* $p < 0.05$, ** $p < 0.01$, *** $p < 0.001$).

AGO1- and AGO2-IP sRNA-sequencing confirms selective loading of Arabidopsis sRNAs during colonisation

Given that mutant analysis and expression data suggested a redundant function of AGO1 and AGO2 in promoting colonisation and potentially in plant defence, we performed AGO1- and AGO2-IP of *S. indica* colonised Arabidopsis roots to identify the repertoire of *Si*sRNAs potentially involved in the *S. indica*-Arabidopsis interaction. Roots were sampled at 7 days post mock treatment or *S. indica* inoculation from two independent biological experiments, followed by sRNA sequencing. This approach enabled us to catalogue endogenous Arabidopsis sRNAs (*At*sRNAs) and potential *S. indica* cross-kingdom sRNAs (ck-*Si*sRNAs) associated with Arabidopsis AGO1 and AGO2. The success of the AGO1- and AGO2-IP was confirmed by Western blot analysis, which demonstrated a clear enrichment of AGO1 (Figure 3a) and AGO2 proteins (Figure 3b) in the IP fraction.

To validate the expression of a subset of *Si*sRNAs identified by sRNA sequencing from *S. indica* axenic culture (Šečić et al., 2021; Nasfi et al., 2024), we performed multiplexed stem-loop PCR on sRNA recovered from AGO2-IP, as previously described for sRNA recovered from AGO1-IP (Nasfi et al., 2024). Bands corresponding to *Si*sRNA24, *Si*sRNA269, *Si*sRNA28, and *Si*sRNA62 were observed (Supplementary figure 1). In addition, *At*miR393a*, with a strong bias toward AGO2, and *At*miR159a were detected. These results confirm that the sRNA recovered from the AGO2-IP contained both *Arabidopsis* and *S. indica* sRNAs, providing a strong basis for subsequent sequencing.

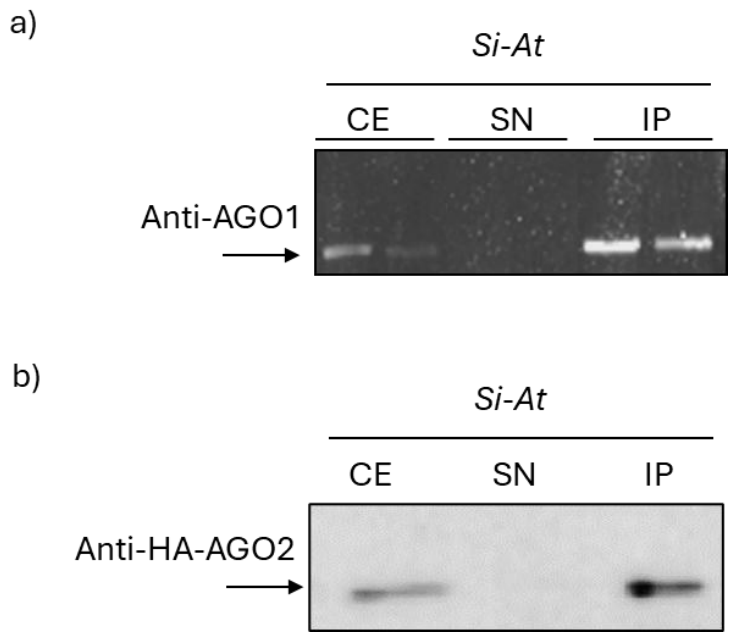

Figure 3: Quality control of AGO1- and AGO2-IP in Arabidopsis roots colonised by *S. indica*. (a) Quality control of AGO1-IP performed on *S. indica*-colonised *Arabidopsis* roots. **(b)** Quality control of AGO2-IP performed on *S. indica*-colonised *Arabidopsis* roots. Three sample fractions were analysed by Western blot: crude extract (CE) after debris removal, supernatant (SN) after incubation with anti-AGO1 and anti-HA, respectively, for AGO1 and AGO2 enrichment, and the immunoprecipitated (IP) fraction (resuspended IP pellet). AGO1 and AGO2 were detected at the expected sizes (~130 kDa) using anti-AGO1 and anti-HA antibodies, respectively. For AGO1, 20 µL or 10 µL of the samples were loaded onto the SDS-PAGE gel. AGO1 and AGO2 signals were stronger in the IP fraction compared to the SN, confirming successful enrichment. The broad-range pre-stained protein ladder was used as a size marker.

Sequencing of AGO1-bound sRNAs pulled down from mock-treated roots revealed the typical distribution of Arabidopsis sRNAs (*At*sRNAs), predominantly 21 nt (~42,000 reads) and 24 nt (~45,000 reads) in length, with a higher proportion of 5'-Uracile (U) *At*sRNAs (Figure 4a). Analysis of total *At*sRNAs from crude extracts (prior to AGO1-IP) from *S. indica*-colonised Arabidopsis roots revealed 24 nt *At*sRNAs as the most abundant, followed by 23 nt, and exhibited variable 5' nts (Figure 4b). In contrast, the AGO1-IP fraction from *S. indica*-colonised Arabidopsis roots showed a clear enrichment of 21 nt and 24 nt *At*sRNAs (75-80% of reads) with a strong bias to 5'-U, consistent with the known loading specificity of AGO1 (Figure 4c).

a)

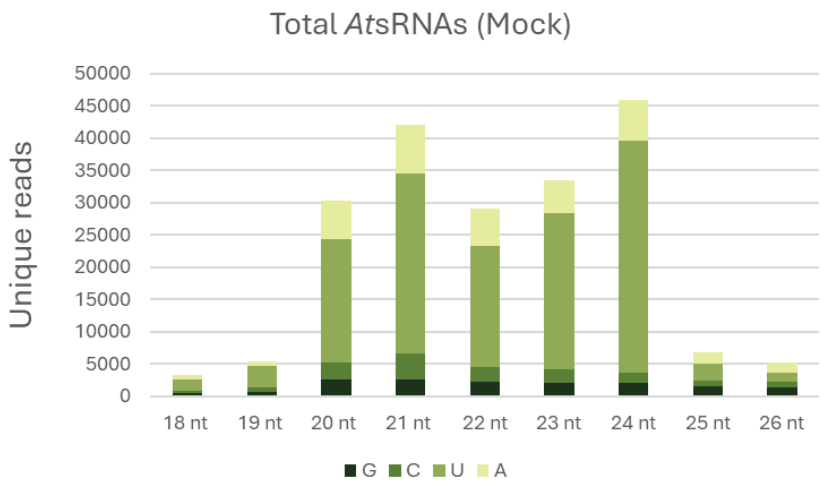

b)

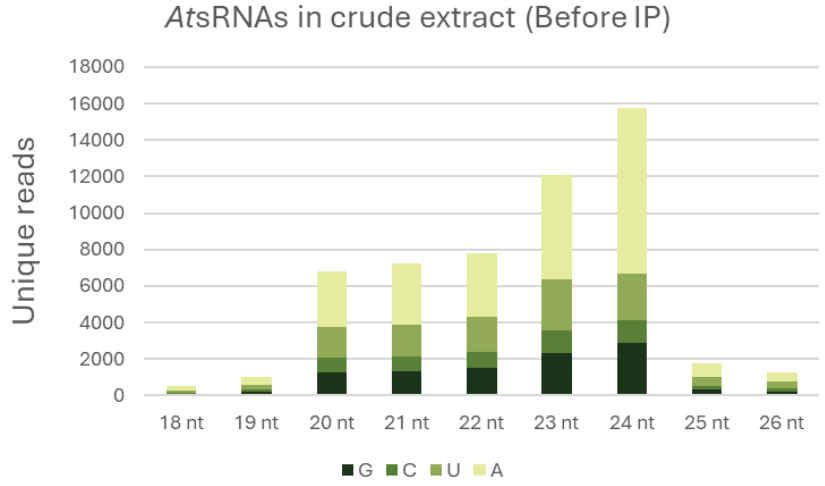

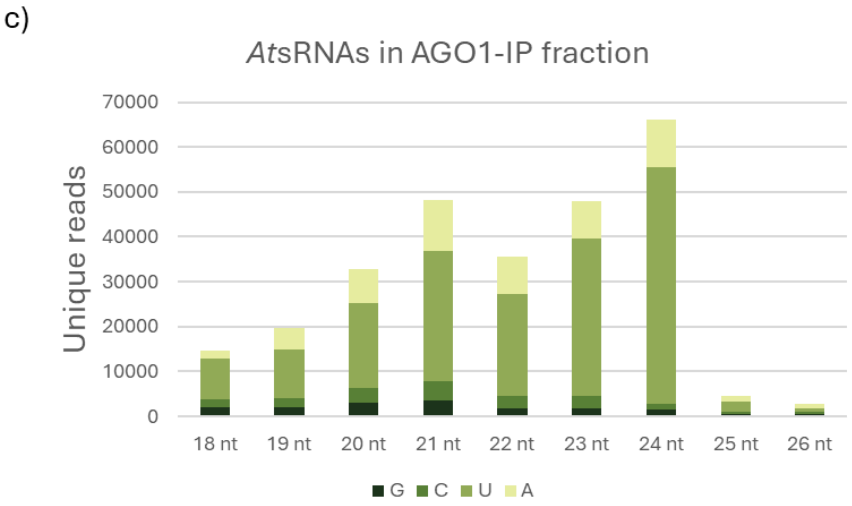

Figure 4: Distribution of Arabidopsis sRNAs in mock-treated, total fraction before IP (crude extract= input) and AGO1-IP bound *At*sRNAs during the *S. indica*–Arabidopsis interaction. (a) Total *At*sRNAs from mock-treated Arabidopsis. **(b)** total sRNAs from *S. indica*–Arabidopsis samples before AGO1-IP (crude extract). **(c)** *At*sRNAs recovered from AGO1-IP samples of two independent biological replicates. Stacked bars show the number of unique reads per sRNA length class (18–26 nt, x-axis). Colours indicate the 5' terminal nucleotide identity (G, C, U, A). All reads were aligned to the Arabidopsis genome (Ensembl release 50, TAIR10), and only Arabidopsis sRNA sequences that did not map to the *S. indica* genome, the *A. thaliana* transcriptome, or the rRNA/tRNA database were retained.

Together, these results validate the efficiency of the AGO1-IP and confirm that AGO1 preferentially associates with canonical 21 nt 5'-U *At*sRNAs during *S. indica* Arabidopsis interactions.

Next, AGO2-IP recovered sRNAs from both mock-treated and *S. indica*–colonised Arabidopsis roots were sequenced to profile AGO2-associated *At*sRNAs. In mock-treated roots, *At*sRNAs displayed the expected size distribution, with peaks at 21 nt (~22,000 reads) and 24 nt (~24,000 reads), and a clear enrichment for 5'-A *At*sRNAs (Figure 5a). Total sRNAs from crude extracts (prior to AGO2-IP) from *S. indica*-colonized Arabidopsis

roots showed an enrichment for 23 and 24 nt *At*sRNAs with a strong bias toward 5'-Adenine (A) (Figure 5b). The AGO2-IP fraction from *S. indica* Arabidopsis roots revealed a major enrichment for 21 and 24 nt *At*sRNAs with a strong bias to 5'-A, consistent with the reported loading specificity of AGO2 (Figure 5c) (Mi et al., 2008).

a)

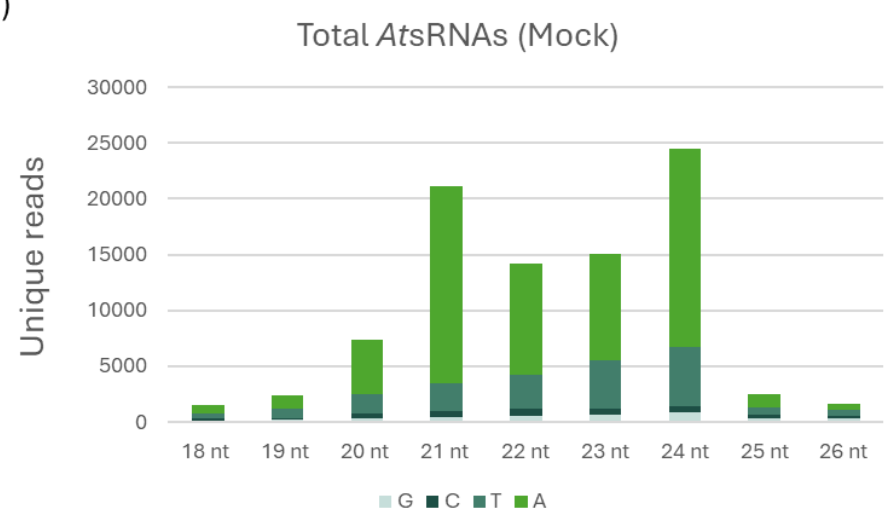

b)

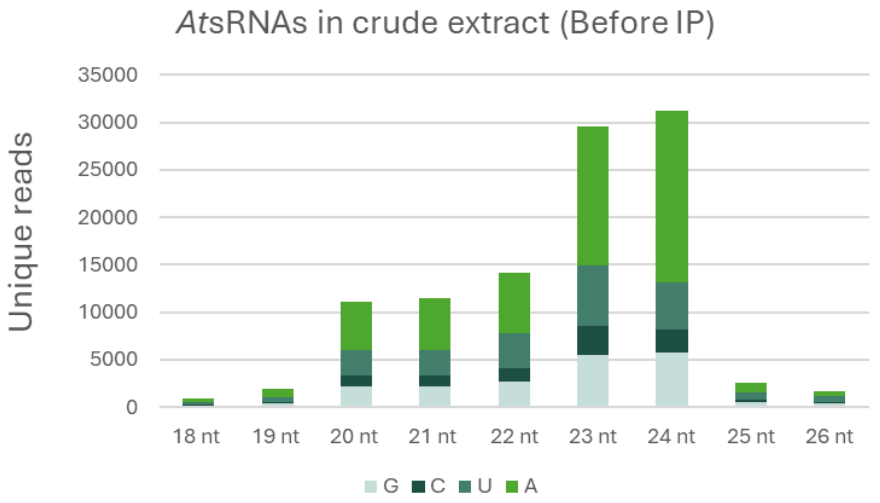

c)

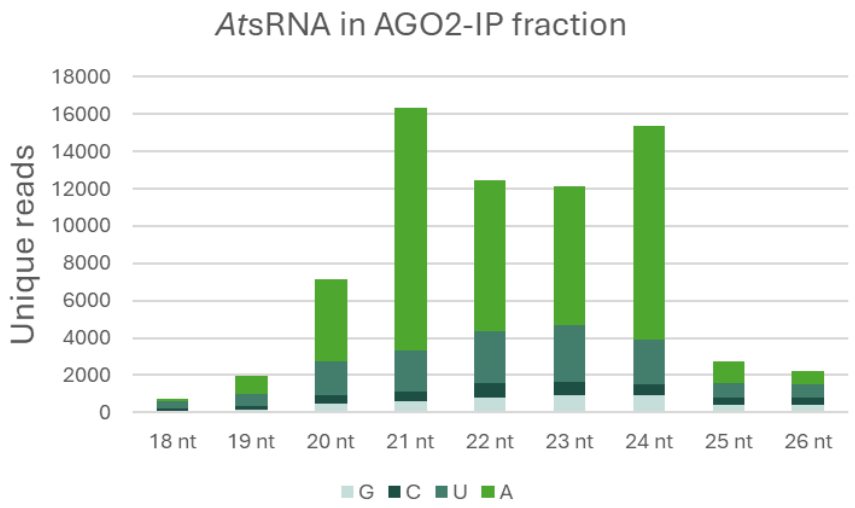

Figure 5: Distribution of Arabidopsis sRNAs in mock-treated, total fraction before IP (crude extract=input) and AGO2-IP bound *At*sRNAs during the *S. indica*–Arabidopsis interaction. (a) Total *At*sRNAs from mock-treated Arabidopsis. **(b)** Total *At*sRNAs from *S. indica*-Arabidopsis samples before AGO2-IP (crude extract). **(c)** *At*sRNAs recovered from AGO2-IP samples of two independent biological replicates. Stacked bars show the number of unique reads per small-RNA length class (18–26 nt, x-axis). Colours indicate the 5' terminal nucleotide identity (G, C, U, A). All reads were aligned to the Arabidopsis genome (Ensembl release 50, TAIR10), and only Arabidopsis sRNA sequences that did not map to the *S. indica* genome, the *A. thaliana* transcriptome, or the rRNA/tRNA database were retained.

Taken together, these results confirm that AGO2 selectively associates with 5'-A Arabidopsis sRNAs during *S. indica* colonisation, and with a broader size range (21–24 nt) compared to AGO1. The *At*sRNA analysis from AGO-IP established a reliable baseline for detecting potential *S. indica*-derived sRNAs (*Si*sRNAs) associated with AGO1 and AGO2.

To identify miRNAs from the sequenced *At*sRNAs present in AGO1- and AGO2- IP, we used ShortStack tool (Axtell, 2013). Analysis showed that some miRNAs were present in both AGO1- and AGO2- IP, while others appeared only in one AGO-IP fraction. Many of the identified miRNAs are known to be strongly expressed in Arabidopsis roots, such as miR156, miR159, miR160, miR164, miR165/166, miR167, miR168, miR171, miR319, miR393, and miR396 (Gautam et al., 2017; Xu et al., 2017). Comparing these results with

those from total *Si*-colonised roots confirmed that these miRNAs are selectively loaded into either AGO1 or AGO2 (Supplemental Table 4).

AGO-IP sRNA-sequencing reveals loading of *Si*sRNAs into Arabidopsis AGO1 and AGO2

To investigate whether *Si*sRNAs associate with Arabidopsis AGO1 and/or AGO2, we analysed reads that mapped to the *S. indica* genome (Šečić et al., 2021; GCA_910890315.1), but not to the *S. indica* transcriptome (Serendipita_indica_dsm_11827_gca_000313545.ASM31354v1), in both total fraction before IP (crude extract= input), and AGO1- (Figure 6) and AGO2-IP fractions (Fi gure 7).

For AGO1, sequencing the total input fraction revealed a broad distribution of *Si*sRNAs (18–26 nt), with the highest abundance of 20-22 nt *Si*sRNAs (Figure 6a). Their 5' nt composition was mixed, without a clear preference for any nucleotide. In turn, in the AGO1-IP fraction, around 21,000 *Si*sRNAs (unique reads) were identified. The two major peaks were at 20 and 21 nt, but no strong size preferences were detected (Figure 6b). Importantly, AGO1-bound *Si*sRNAs exhibited a slight shift towards a 5'-U bias (~40–50%), consistent with the canonical loading preference of AGO1.

a)

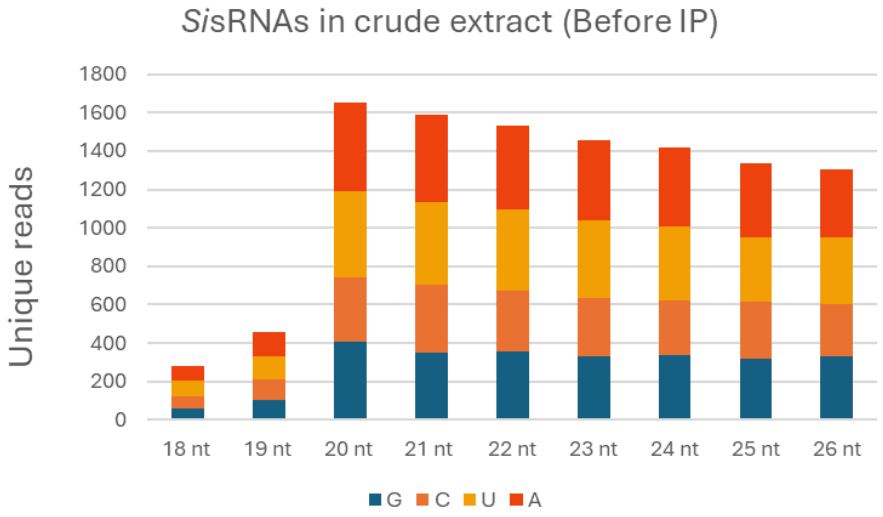

b)

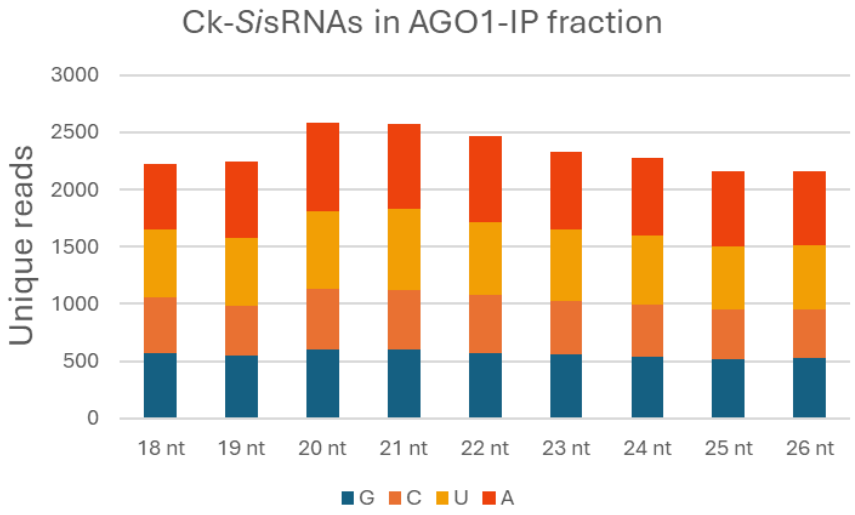

Figure 6: Distribution of *S. indica*-derived small RNAs (*Si*sRNAs) in total fraction before IP (crude extract=input) and AGO1-IP bound *Si*sRNAs. (a) Total *Si*sRNAs detected before AGO1-IP (crude extract). **(b)** *Si*sRNAs recovered from AGO1-IP from two independent biological replicates. Stacked bar plots show the number of unique reads across sRNA size classes (18–26 nt, x-axis). Colours indicate the 5' terminal nucleotide identity (G, C, U, A). Y-axes represent counts of unique sequences. Only reads aligning to the *S. indica* genome (Šečić et al., 2021; GCA_910890315.1), but not to the *S. indica* transcriptome (Serendipita_indica_dsm_11827_gca_000313545.ASM31354v1), were included in the analysis.

For AGO2, sequencing of the total input fraction revealed a broad distribution of *Si*sRNAs (18–26 nt), with no size or 5' nt preferences (Figure 7a). Similarly, in the ~ 13,000 *Si*sRNAs (unique reads) identified in the AGO2-IP fraction, no significant size or 5' nt preferences were detected, although a slight enrichment for *Si*sRNAs with 5'-A is worth mentioning (over 50% Figure 7b). These results suggest that a population of *Si*sRNAs is recruited by Arabidopsis AGO2 during colonisation and might exhibit a cross-kingdom function.

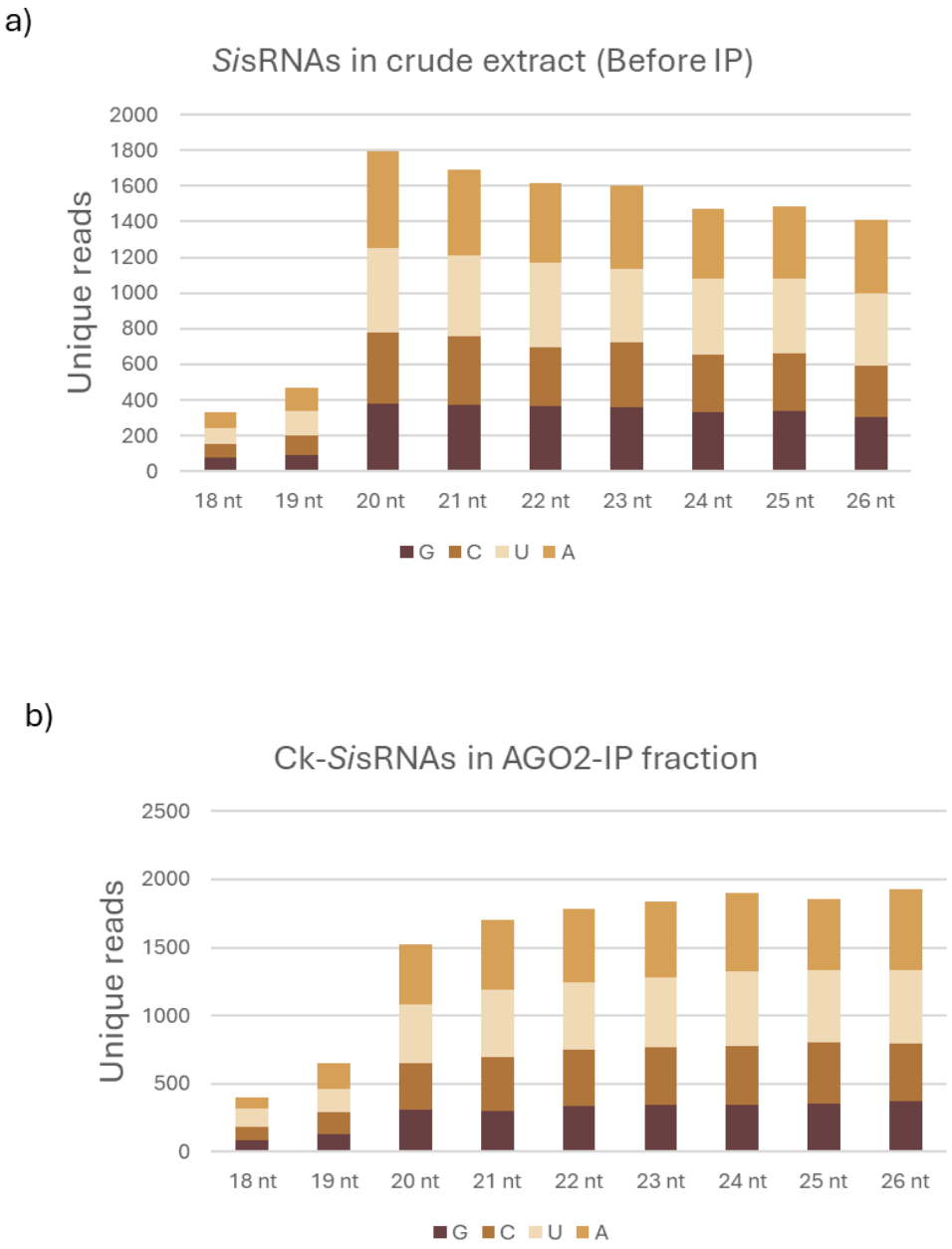

Figure 7: Distribution of *S. indica* small RNAs (*Si*sRNAs) in total fraction before IP (crude extract=input) and AGO2-IP bound *Si*sRNAs. (a) Total *Si*sRNAs detected before AGO2-IP (crude extract). **(b)** *Si*sRNAs recovered from AGO2-IP in two independent biological replicates. Stacked bar plots show the number of unique reads across sRNA size classes (18–26 nt, x-axis). Colours indicate the 5' terminal nucleotide identity (G, C, U, A). Y-axes represent counts of unique sequences. Only reads aligning to the *S. indica* genome (Šečić et al., 2021; GCA_910890315.1), but not to the *S. indica* transcriptome

(Serendipita_indica_dsm_11827_gca_000313545.ASM31354v1), were included in the analysis.

Together, these results demonstrate that, in addition to Arabidopsis sRNAs, a distinct subset of *Si*sRNAs is selectively recruited by and loaded into Arabidopsis AGO1 and AGO2.

To further investigate the functional regulatory role of *Si*sRNAs identified from AGO1- and AGO2-IP sequencing, four 21 nt *Si*sRNAs were selected: *Si*sRNA-IP-148, *Si*sRNA-IP-1603, *Si*sRNA-IP-1342 and *Si*sRNA-IP-11, respectively targeting *AT1G18890* (*CPK1*, CALCIUM-DEPENDENT PROTEIN KINASE 1) related to salt stress, *AT5G53450* (*ORG1*, OBP3-responsive gene 1) related to salicylic acid response, *AT2G41530* (*SFGH*; S-FORMYLGLUTATHIONE HYDROLASE) related to oxidative stress and glutathione activity, and *AT4G09160* (*PATL5*, PATELLIN 5) related to auxin regulation in roots, and involved in vesicle trafficking and membrane-related processes. Target gene prediction for *Si*sRNAs was performed using psRNATarget, as described by Nasfi et al. (2024), and one target gene per *Si*sRNA was selected based on functional relevance and potential roles in beneficial interactions and immunity. Supplementary Table 5 provides detailed information on these *Si*sRNAs and their predicted target genes, and Supplementary Figure 2 illustrates the alignment between the selected *Si*sRNAs and their predicted Arabidopsis target genes as displayed by the psRNATarget web tool.

The potential of selected *Si*sRNAs, identified by sequencing the IP fraction to induce PTGS of predicted target genes in Arabidopsis protoplasts, was investigated using mRNA level quantification. Overexpression of *Si*sRNA-IP-148, *Si*sRNA-IP-1603 and *Si*sRNA-IP-1342 in protoplasts did not result in downregulation of any of the three predicted target genes: *CPK1*, *ORG1*, and *SFGH* (Supplementary Figure 3). In contrast, expression of *Si*sRNA-IP-11 resulted in a 42% reduction in *PATL5* mRNA levels (Figure 8).

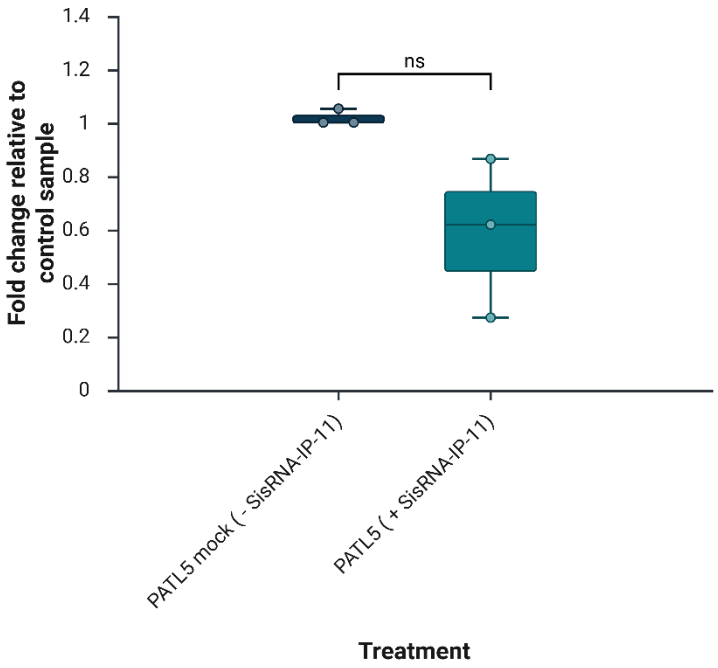

Figure 8. qPCR analysis of target gene silencing in Arabidopsis protoplasts 24hptr with *Si*sRNA-IP-11 identified from AGO1- and AGO2- IP sequencing versus control protoplasts without *Si*sRNA-IP-11 (mock). mRNA transcript level of the target gene *PATL5* was normalised to the geometric mean of two endogenous housekeeping genes, Ubiquitin (*UBQ5, AT3G62250*) and Elongation Factor-1 alpha (*ef1α, AT5G60390*) and Ct values of target genes were normalised to the RFP Ct values. *PATL5* mRNA transcript level is shown as fold change relative to mock (without the *Si*sRNA construct). Data are the average of 3 biological replicates ± SD. The Mann-Whitney U test was used for statistical analysis. ns=not significant. The graph was created with Biorender.

Discussion

In this study, we demonstrate that AGO proteins play a regulatory role in the mutualistic interaction between *Arabidopsis thaliana* and *Serendipita indica*. Analysis of higher-order *ago* mutants revealed that AGO2 and AGO10 promote *S.indica* colonisation, while AGO1 seems to restrict *S.indica* growth in the absence of AGO10 (Figure 1). This observation is consistent with previous work showing that AGO10 (also called ZWILLE/PINHEAD/AGO10 (ZLL)) act as a negative regulator of AGO1 (Mallory et al., 2009).

Interestingly, Mallory et al showed that the AGO1 PAZ domain, responsible for sRNA binding, is functionally interchangeable between AGO1 and AGO10, supporting a complementary function.

The reduced *S.indica* colonisation observed at early stages in the *ago1ago2* mutant suggests that AGO2 is essential for the initial establishment of *S.indica* colonisation (Figure 1). This observation is in line with recent results from Ruf, Thieron, Nasfi et al. (2024), suggesting that these AGOs often operate in a more redundant manner and are subject to cross-regulation rather than functioning as isolated components of the RNAi machinery. This mechanism may contribute to the precise regulation of *S. indica* colonisation in Arabidopsis roots.

Expression analysis further supports this functional redundancy. Loss of AGO1, or combined loss of AGO1 and AGO10, resulted in increased AGO2 expression (Figure 2b). Similarly, AGO10 expression was upregulated in the absence of AGO2 (Figure 2c). These compensatory expression patterns suggest that AGOs may substitute for one another to maintain RNAi activity, potentially including the capacity to bind *Si*sRNAs. Such a regulation highlights the specificity of the mutualistic exchange between *At* and *S.indica,* in which the fungus uses the plant RNAi machinery without hijacking, as commonly observed in plant -pathogen interaction (Wang et al., 2017; Weiberg et al., 2013). Instead, both organisms engage in a more harmonious and balanced interaction that supports mutual benefit.

In this study, we also confirmed that cross-kingdom communication occurs during Arabidopsis -*S.indica* interaction. *S.indica* sRNAs were detected to be loaded in both AGO1 and AGO2, indicating their transfer from the fungus to the plant RNAi machinery. In this interaction, the sorting rules for Arabidopsis AGOs were as described and developed by the literature for the plant ´s endogenous sRNAs, with AGO1 mainly binding 21 nt *At*sRNAs with a 5'-U and AGO2 binding *At*sRNAs with 5'-A in the IP fractions (Figures 4c and 5c) (Mi et al., 2008; Takeda et al., 2008). However, when analysing *S. indica* sRNAs, a slight shift toward the canonical sorting 5'-nt was observed, yet a heterogeneous population of *Si*sRNAs was clearly loaded in both AGO1 and AGO2 (Figures 6b and 7b).

These findings indicate that the strict AGO sorting rules described for plant sRNAs, and in some pathogens-derived sRNAs, do not fully apply to mutualistic endophytes. This further supports the idea that mutualistic interactions prioritise the functional outcome of the interaction, such as nutritional exchange, growth and nutrition-related gene regulation in the plant, promoting colonisation, and modification of plant root morphology (Nasfi et al., 2024), rather than complete suppression of the host defence system. Such flexibility in AGO loading may facilitate mutualism and stable *S. indica* colonisation.

Although cross-kingdom RNA transfer between *At* and *S. indica* has been confirmed, the functional activity of *Si*sRNAs on Arabidopsis transcripts and their role in post-transcriptional gene silencing require further investigation. Four *Si*sRNAs identified in both AGO1- and AGO2-IP were selected and their targets predicted using psRNATarget. Targets were selected based on their established role in mutualism. *PATL5* (*AT1G09160*) showed downregulation of its mRNA transcript in Arabidopsis protoplasts following targeting by *Si*sRNA-IP-11. Pattelins belong to the SEC14-like phosphatidylinositol transfer protein family and participate in membrane lipid binding, vesicle trafficking, and auxin-mediated root growth regulation (Montag et al., 2023.; Zhou et al., 2019). They are also involved in plasma membrane-associated signalling pathways, such as the Ca2+ pathway, which is important in Arabidopsis roots inoculated with *S.indica* (Pérez-Alonso et al., 2022). Given the significant role of patellins, their downregulation may affect membrane remodelling and signalling events required for regulating *S. indica* colonisation. The cell wall and plasma membrane constitute central regulatory layers during Arabidopsis root colonisation by S. *indica*. Studies have shown that *S.indica* colonisation induces callose deposition and suppresses cell wall-associated immune responses to promote symbiosis (Jacobs et al., 2011). Nasfi et al. (2024) demonstrated that Pectin acetyl esterase (*PAE2, AT1G57590*), a cell wall-modifying enzyme, was significantly downregulated in Arabidopsis roots inoculated with *S.indica* at 3 and 7 dpi. At the plasma membrane, auxin transporter proteins such as PIN2 are transcriptionally downregulated under *S.indica* colonisation (González Ortega-Villaizán et al., 2024). This evidence of the involvement of the cell wall and cell membrane in Arabidopsis *S. indica* interaction further emphasises the potential role of PATL5 in this interaction. All four

predicted Arabidopsis genes are highly expressed in leaves and roots (Rich-Griffin et al., 2020), however, no downregulation was observed for *CPK1* (*AT1G18890*), *ORG1* (*AT5G53450*) and *SFGH* (*AT2G41530*) suggesting limited cleavage efficiency under the tested conditions. Factors such as mRNA secondary structure or RNA-binding proteins can make the binding site inaccessible. While AGO1 is highly expressed in both leaves and roots (Bohmert et al., 1998), AGO2 is typically low and induced by biotic stress (Zhang et al., 2011). Tissue-specific differences must be considered, as differences in abundance, isoforms, and associated cofactors can strongly influence RISC complex efficiency. Protoplasts may not accurately reflect the AGO environment present in colonised roots. Although the recently developed pipeline by Nasfi et al. (2024) provides an efficient framework, tissue specificity remains a major challenge when using the Arabidopsis protoplast system to test *Si*sRNAs in PTGS-mediated regulation.

Transcriptome profiling during *At-S.indica* interaction is mandatory to identify key genes affected by fungal colonisation and to specifically confirm the downregulation of *PATL5* in colonised roots. Differential expression analysis will generate candidate target gene lists that should be paired to the detected *Si*sRNAs repertoire in AGO1- and AGO2-IP. In parallel, combining target gene prediction with transcriptomic data and customised *Si*sRNA-mRNA pairing criteria will facilitate the selection of the most relevant *Si*sRNA-target gene pairs while minimising false positives.

Mapping *Si*sRNA cleavage sites is a critical subsequent step. This can be achieved by co-expressing *Si*sRNA candidates with their predicted target transcripts, followed by NIL-TDS, a sensitive method for detecting and quantifying sRNA site-specific slicing activities (Werner and Nasfi et al., 2025). This approach offers a second layer of validation beyond transcriptomic and whole degradome analyses, especially for functional validation, where only a few targets can be studied in depth.

Finally, to establish biological relevance, candidate *Si*sRNAs should be tested in whole plants. Arabidopsis transgenic lines expressing *Si*sRNAs should be generated, and the impact on predicted target transcripts levels should be examined to confirm PTGS *in planta*. Phenotypic changes and fungal colonisation patterns should be analysed in lines showing stable *Si*sRNA expression. In parallel, T-DNA insertion mutants of selected target genes inoculated with *S. indica* will determine whether the loss of these genes promotes

S. indica colonisation. Such findings would not only validate *Si*sRNAs function in mutualism but also provide a foundation for future agricultural applications.

Conclusion

This study demonstrates that Arabidopsis AGO1, AGO2, and AGO10 proteins are involved in the mutualistic interaction between Arabidopsis and *S. indica*. Notably, *S. indica* sRNAs are transferred into plant cells and loaded into AGO1 and AGO2, demonstrating a clear cross-kingdom sRNA trafficking during beneficial interactions. While standard AGO sorting and loading rules apply to Arabidopsis sRNAs, these rules do not strictly apply to *S.indica* sRNAs. The regulatory activity of immunoprecipitation-detected *Si*sRNAs and transcriptomic analysis of *S.indica* colonised Arabidopsis roots should be further investigated.

<u>Supplementary material</u>

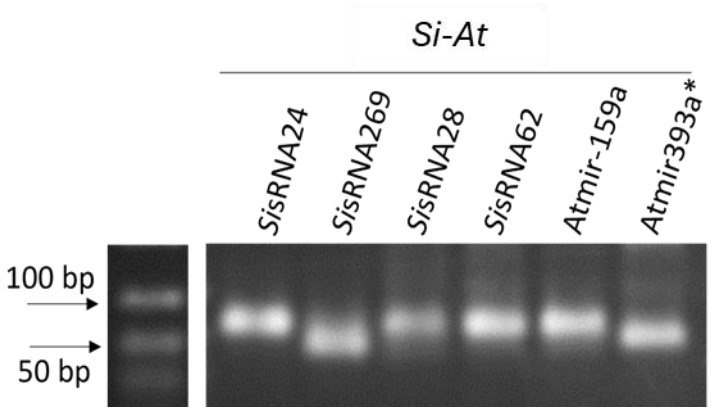

Supplementary Figure 1. *Si*sRNAs co-immunopurified with AGO2 from Si-colonised Arabidopsis roots IP fraction. Multiplexed stem-loop PCR showing the detection of *S. indica*–derived sRNAs (*Si*sRNA24, *Si*sRNA269, *Si*sRNA28, and *Si*sRNA62) together with *Arabidopsis* miRNAs (*At*miR159a and *At*miR393a*) in colonized roots.

*Sis*RNA-IP-11 21 UCCUGGAACUUUGGUUUUCCA 1
: :::.:::.:..::.:::::
AT1G09160 376 AUGACUUUGGAGUCAGAAGGU 396

*Sis*RNA-IP-148 21 CGGUAAUACGGUCACAGGAUU 1
:::: : :::::::::.::::
AT1G18890 1752 GCCAG-ACGCCAGUGUUCUAA 1771

*Sis*RNA-IP-1603 21 CGGUACGCUAAGCUCUUCAAU 1
.::.:::: :::::::::
AT5G53450 2033 GGAGUGUGAUUGGAGAAGUUA 2053

*Sis*RNA-IP-1342 21 UUGCUGGGUAAGAUGGUGACU 1
::::::: .:::::::: ::::
AT2G41530 984 AACGACCAGUUCUACC-CUGA 1003

Supplementary Figure 2. Visualisation of the predicted *Si*sRNA-target mRNA alignment, as presented by the psRNATarget web tool. The upper line presents the 21-nucleotide *Si*sRNA, and the lower line the mRNA target region. Perfect matches are represented by (:), and (.) and ( ) indicates a bulge or a mismatch.

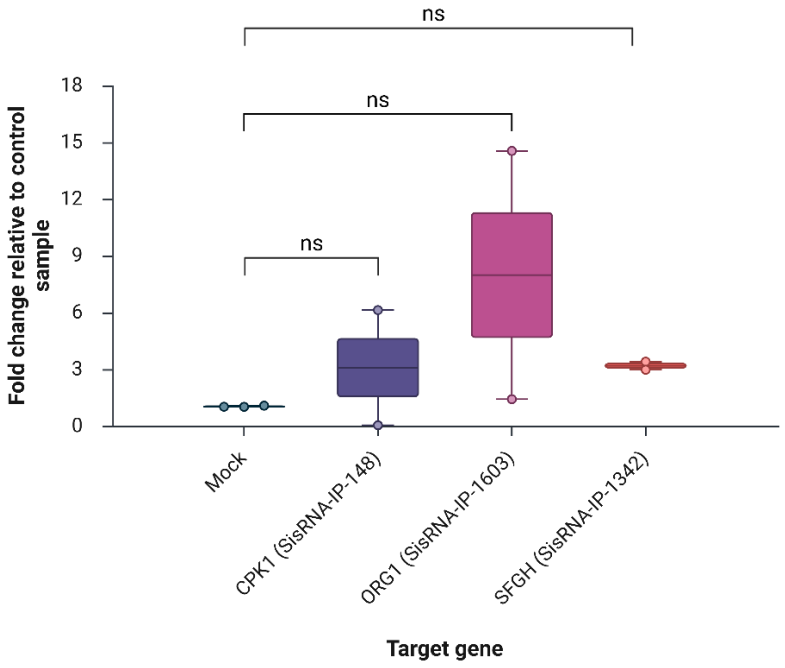

Supplementary Figure 3. qPCR analysis of target gene silencing in Arabidopsis protoplasts 24hptr with *Si*sRNA-IP-148, *Si*sRNA-IP-1603 and *Si*sRNA-IP-1342 identified

from AGO1- and AGO2-IP sequencing versus control protoplasts without *Si*sRNAs (mock). mRNA transcript level of target genes *CPK1* (*AT1G18890*), *ORG1* (*AT5G53450*) and *SFGH* (*AT2G41530*) was normalised to the endogenous housekeeping genes, Ubiquitin (*UBQ5, AT3G62250*) and Elongation Factor-1 alpha (*ef1α, AT5G60390*), and Ct values of target genes were normalised to the RFP Ct values. mRNA transcript levels are displayed as fold change relative to mock (without *Si*sRNA construct). Data are the average of 2 biological replicates ± SD. The Mann-Whitney U test was used for statistical analysis. ns=non-significant. The graph was created with Biorender.

Supplementary Table 1: Primer List (Fwd= forward, Rev=reverse, hp=hairpin)

Primer name	Primer sequence
ITS-Fwd	CAACACATGTGCACGTCGAT
ITS-Rev	CCAATGTGCATTCAGAACGA
UBQ5-Fwd	AAGAAGACTTACACCAAGCCGAAG
UBQ5-Rev	ACAGCGAGCTTAACCTTCTTATGC
UBC21-Fwd	GCTTGGAGTCCTGCTTGGACG
UBC21-Rev	CGCAGTTAAGAGGACTGTCCGGC
ef1α-Fwd	CTGTTGTAACAAGATGGATGCC
ef1α-Rev	CCCTCGAATCCAGAGATTGG
AGO1-Fwd	CTAGCAGCTTTTAGGGCTCG
AGO1-Rev	TCTACCAGCCATTCCACCTC
AGO2-Fwd	TGCAGAAGCTCATCTTCGAG
AGO2-Rev	GCGGCTGCTTAAAGTTCTTC
AGO10-Fwd	GTCTCTATAGTTCCTCCAGCG
AGO10-Rev	TCCTTCAAGGCTGGTAAAGG
PATL5-Fwd	TAGAGGAGTCAAATCATACGGCG
PATL5-Rev	CCTCTAGCTTCGCAGTCTCTG
CPK1-Fwd	CTACGGGAAGCTTTAGCGGA
CPK1-Rev	CGTCCGTCCTTGTCAGTGT
ORG1-Fwd	CCGTCGAGTCTTCCTGTAGC

ORG1-Rev	CCAATCACACTCCCAGGTGAA
SFGH-Fwd	GCTGCTTGGGAGGAATACGA
SFGH-Rev	TGCACGCCTCCTCAAACTT
*Si*sRNA24-hp	GTCGTATCCAGTGCAGGGTCCGAGGTATTCGCACTGGATAC GACg agaac
*Si*sRNA24-Fwd	TCGCTttgaccaatttttct
*Si*sRNA28-hp	GTCGTATCCAGTGCAGGGTCCGAGGTATTCGCACTGGATAC GACagatcc
*Si*sRNA28-Fwd	TCGCTacaactttcaacaac
*Si*sRNA62-hp	GTCGTATCCAGTGCAGGGTCCGAGGTATTCGCACTGGATAC GACcagagt
*Si*sRNA62-Fwd	TCGCTatccacggccatagg
*Si*sRNA269-hp	GTCGTATCCAGTGCAGGGTCCGAGGTATTCGCACTGGATAC GACggccat
*Si*sRNA269-Fwd	TCGCTaacttctcgaatcgc
*At*miR159a-hp	GTCGTATCCAGTGCAGGGTCCGAGGTATTCGCACTGGAT ACGACtagagc
*At*miR159-Fwd	TCGCTtttggattgaaggga
*At*miR393a*-hp	GTCGTATCCAGTGCAGGGTCCGAGGTATTCGCACTGGATAC GACaatcca
*At*miR393b*-Fwd	TCGCTatcatgcgatctctt
Universal-stem loop-Rev	GTATCCAGTGCAGGGTCCGAGGT

Supplementary table 2: 75 mer oligonucleotides used for cloning *Si*sRNAs into the pUC18-*At*MIR390a-B/c-RFP vector.

Oligonucleotide name	**75 mer sequence**
*Si*sRNA-IP-11-75-Fwd	TGTAACCTTTTGGTTTCAAGGTCCTATGATGATCACATTCGTTATCTATTT TTTAGGACCTTGACACCAAAAGGT

*Si*sRNA-IP-11-75-Rev	AATGACCTTTTGGTGTCAAGGTCCTAAAAAATAGATAACGAATGTGATC AT CATAGGACCTTGAAACCAAAAGGT
*Si*sRNA-IP-148-75-Fwd	TGTATTAGGACACTGGCATAATGGCATGATGATCACATTCGTTATCTATT TTTTGCCATTATGCAAGTGTCCTAA
*Si*sRNA-IP-148-75-Rev	AATGTTAGGACACTTGCATAATGGCAAAAAATAGATAACGAATGTGATC ATCATGCCATTATGCCAGTGTCCTAA
*Si*sRNA-IP-1603-75-Fwd	TGTATAACTTCTCGAATCGCATGGCATGATGATCACATTCGTTATCTATT TTTTGCCATGCGATGCGAGAAGTTA
*Si*sRNA-IP-1603-75-Rev	AATGTAACTTCTCGCATCGCATGGCAAAAAATAGATAACGAATGTGAT CATCATGCCATGCGATTCGAGAAGTTA
*Si*sRNA-IP-1342-75-Fwd	TGTATCAGTGGTAGAATGGGTCGTTATGATGATCACATTCGTTATCTATTT TTTAACGACCCATGCTACCACTGA
*Si*sRNA-IP-1342-75-Rev	AATGTCAGTGGTAGCATGGGTCGTTAAAAAATAGATAACGAATGTGATC ATCATAACGACCCATTCTACCACTGA

Supplementary Table 3: List of *Si*sRNAs, sequences, 5´terminal nucleotide and raw reads normalised to *Si-Bd* colonised from our previous study (Šečić *et al.,* 2021) used in this study.

sRNA name	**sRNA sequence**	**5´ terminal nucleotides**	**Raw reads normalised to *Si-Bd* colonized**
*Si*sRNA24	TTGACCAATTTTTCTGTTCTC	T	165,27
*Si*sRNA28	ACAACTTTCAACAACGGATCT	A	44,43
*Si*sRNA62	ATCCACGGCCATAGGACTCTG	A	2033,18
*Si*sRNA269	AACTTCTCGAATCGCATGGCC	A	2,33

Supplementary Table 4: List of top 20 miRNAs identified from *At*sRNA sequencing from *Si*-colonised Arabidopsis roots in Total, AGO1- and AGO2- IP samples

miRNA in Total fraction	**miRNAs in AGO1-IP**	**miRNAs in AGO2-IP**
miR156	miR156	miR156
miR157	Not detected	miR157
miR158	miR158	miR158
miR159	miR159	Not detected
miR160	miR160	miR160
miR161	miR161	miR161
miR162	miR162	Not detected
miR164	miR164	not detected
miR165	miR165	miR165
miR166	Not detected	miR166
miR167	miR167	Not detected
miR168	miR168	Not detected
miR169	Not detected	Not detected
miR170	miR170	Not detected
miR171	miR171	Not detected
miR172	miR172	Not detected
miR319	miR319	Not
miR390	miR390	Not detected
miR393	miR393	miR393*
miR396	miR396	miR396

Supplementary Table 5: List of *Si*sRNAs and their sequences identified from AGO1- and AGO2-IP sequencing, their predicted targets and their function studied for post-transcriptional gene silencing in protoplasts.

***Si*sRNA name**	***Si*sRNA sequence**	**Raw read in AGO1-IP**	**Raw read in AGO2-IP**	**Predicted Target**	**Predicted target function**	**Expectation value**	**Mode of regulation**
*Si*sRNA-IP-11	ACCTTTTGGTTTCAAGGTCCT	6 (rep1) 5 (rep 2)	2 (rep 1) 4 (rep2)	AT4G09160	Member of the Patellin family. Participates in membrane lipid binding, vesicle trafficking and membrane signalling	2.5	Cleavage
*Si*sRNA-IP-148	TTAGGACACTGGCATAATGGC	15 (rep 1) 9 (rep 2)	1 (rep 1) 4 (rep 2)	AT1G18890	Encodes a calcium-dependent protein kinase (CPK1), involved in regulation of stress and immune responses.	4.5	Cleavage
*Si*sRNA-IP-1603	TAACTTCTCGAATCGCATGGC	21 (rep 1) 7 (rep2)	14 (rep 1) 11 (rep 2)	AT5G53450	FBN11 or ORG1 a member of the fibrillin	3.5	Cleavage

					protein family associated with oxidative stress.		
*Si*sRNA-IP-1342	TCAGTGGTAGAATGGGTCGTT	9 (rep1) 1 (rep 2)	3 (rep 1) 4 (rep 2)	AT2G41530	Encodes S-formylglutathione hydrolase (SFGH) involved in cellular redox homeostasis and regulating ROS balance.	4.5	Cleavage

CHAPTER 6-

Isolation and characterization of *Serendipita indica* extracellular vesicles as potential carriers of small RNAs

(Contribution as first author)

Authors

Sabrine Nasfi[1], Nathan Nikodemus Neurohr[1], Ruth Eichmann[1], Karl-Heinz Kogel[1,2], Patrick Schäfer[1,*]

Affiliations

[1] Institute of Phytopathology, Research Centre for BioSystems, Land Use and Nutrition, Justus Liebig University, 35392, Giessen, Germany

[2] Institut de Biologie Moléculaire des Plantes, CNRS, Université de Strasbourg, 12 rue du Général Zimmer, 67084, Strasbourg, France

Abstract

Extracellular vesicles (EVs) are known as mediators of cross-kingdom communication. However, their presence and function in mutualistic fungi remain unexplored. In this study, we investigated whether *Serendipita indica* (*Si*) produces EV-like particles and examined their potential to transport small RNAs (sRNAs) to *Arabidopsis thaliana*. *Si* particles were isolated from liquid cultures by differential ultracentrifugation and characterised by transmission electron microscopy (TEM) and nanoparticle tracking analysis (NTA). Typical cup-shaped EVs were observed; however, their final identity remains uncertain. We also detected *Serendipita indica* small RNAs previously associated with *Serendipita indica-Arabidopsis thaliana* interaction in the isolated EVs-like particles, suggesting a possible role in cross-kingdom communication. Our findings provide initial insights and a methodological basis for future studies on beneficial fungal

EVs and their potential involvement in small RNA trafficking in plant-mutualistic interactions.

Introduction

Extracellular vesicles (EVs) are heterogeneous structures surrounded by a lipid bilayer membrane and secreted by both prokaryotic and eukaryotic cells. First identified and described in blood in the 1960s, they were initially considered to be cellular waste products (Johnstone et al., 1987; Wolf, 1967). However, over the years, it has become clear that EVs are active mediators of intracellular communication, capable of carrying a wide range of bioactive molecules rather than simple byproducts.

The cargo of EVs is remarkably diverse, including DNA, RNA, lipids, and proteins. These molecules can be found within the vesicle lumen or on the surface (Colombo et al., 2014; J. Zhang et al., 2024b). Among nucleic acids, RNA molecules are particularly predominant and of interest for their role in cross-kingdom (ck) communication. While most EV-associated RNAs are small RNAs, longer transcripts have also been detected (Rutter & Innes, 2018). High-throughput sequencing of RNA extracted from isolated EVs from many organisms has identified a broad repertoire, including mRNAs, microRNA (miRNA), small nucleolar RNA (snoRNA), small nuclear RNA (snRNA), transfer RNA (tRNA), Piwi-interacting RNA (piRNA), ribosomal RNA (rRNA), and circular RNA (circRNA) (Cai et al., 2018; Kwon et al., 2021; Zand Karimi et al., 2022).

Fungal EVs were first reported in *Cryptococcus neoformans* in the 1970s (Takeo et al., 1973), but their structure and functions were only characterised decades later (Rodrigues et al., 2007). Since then, research has expanded dramatically, establishing EVs as mediators of plant-microbe interactions. Pathogenic fungi, such as *Botrytis cinerea*, were shown to utilise EVs to transfer sRNA into Arabidopsis, mainly via clathrin-mediated endocytosis (CME) (He et al., 2023b). On the other hand, it was shown that Arabidopsis cells secrete exosome-like EVs containing sRNAs into *B. cinerea,* indicating a bidirectional exchange that supports ck RNA interference (Cai et al., 2018). Nevertheless, a controversial study showed that *Arabidopsis* EVs are responsive to environmental and biotic stimuli and contribute to plant immunity by inhibiting fungal growth (*C. Higginsianum*, powdery mildew *Golovinomyces cichoracearum*, and *Botrytis*

cinerea). However, these EVs do not appear to carry sRNAs into pathogens, suggesting that EVs do not mediate ck RNA interference, at least in the case of *Arabidopsis* (Koch et al., 2025).

However, the agricultural potential of EVs is gaining increased interest. RNA-based strategies, such as spray-induced gene silencing (SIGS), already demonstrate the potential of RNA molecules for crop protection. Yet the efficient delivery of RNA into plant tissues remains a major bottleneck. EVs, with their natural capacity to transport sRNAs and other regulatory molecules, may provide a safe and effective carrier system for targeted gene regulation in both hosts and pathogens (Nasfi & Kogel, 2022).

Despite these advances, EV research continues to face technical and conceptual challenges. Isolation methods, such as differential ultracentrifugation, can yield large quantities of vesicles, but they are often low-specificity and species-dependent protocols. Other current approaches rely on complementary strategies, including analysis of physical properties (size, concentration, charge), morphology (electron microscopy), and molecular profiling (proteomics, RNA-sequencing, lipidomics) (Thieron et al., 2024). As methods and workflows continue to improve, it will be possible to define functional EV subtypes with greater precision and to elucidate their diverse roles across biological systems.

In this chapter, we investigated whether *Serendipita indica* secretes EVs under axenic culture conditions. We established a protocol for EVs isolation from *S.indica* and characterised them using Transmission Electron Microscopy (TEM) and Nanoparticle Tracking Analysis (NTA). Furthermore, we explored whether these vesicles carry sRNAs that could contribute to the molecular dialogue with *Arabidopsis thaliana*. These preliminary results are expected to broaden our understanding of *S. indica* biology and could lay the groundwork for future research projects.

Material and Methods

The following parts of the material and method section of this chapter were performed as previously described in Nasfi et al., 2024 (Chapter 3 of this PhD thesis)

- Plant, fungi, and plant inoculation

- Total RNA extraction

- Stem-loop PCR

- pGEM-T cloning, colony PCR and sanger sequencing

Additional material and methods

Double staining of *Arabidopsis* roots during interaction with *S. Indica*

Arabidopsis roots inoculated with *S.indica* were harvested at 7 dpi and fixed in a solution of ethanol/chloroform (4:1) containing 0.15% trichloroacetic acid (TCA). The roots were then washed with water and phosphate-buffered saline (PBS) (pH 7.4) and incubated with wheat germ agglutinin (WGA) conjugated to Alexa Fluor 488 (10 µg/ml; Thermo Fisher Scientific), with two rounds of vacuum infiltration. After incubation on ice in the dark, samples were washed with PBS and stored at 4 °C. Prior to microscopy, WGA-stained roots were immersed in 10 µM SynaptoRed (SFM 4-64, SynaptoRed™ C2; Fisher Scientific) and examined using a confocal microscope (TCS SP8; Leica Microsystems).

Cultivation of *Serendipita indica* in liquid medium

For EVs isolation, *S. indica* was cultivated in 500 ml Erlenmeyer flasks containing 300 ml of liquid complete medium (CM) without sugar (-) and a mycelium plug from a 6-week-old plate of *S.indica*. The axenic culture was grown for 7 days on a shaker at 180 rpm under sterile semi-dark conditions.

EVs isolation

For EVs isolation from *S. indica* liquid cultures, the grown mycelium was first removed using double-layered Miracloth, and the filtrate was centrifuged at 4,000 × g for 20 min at room temperature to remove any remaining mycelium debris. The supernatant was then sequentially filtered using 0.45 µm and 0.22 µm Rapid-Flow Bottle Top Filters (500 ml, SFCA membrane, 75 mm diameter; Thermo Scientific™ Nalgene). The filtered supernatant was then concentrated fivefold using a tangential flow filtration concentrator (TFF-Easy, HansaBioMed Life Sciences, Austria). The Concentrate was transferred to six centrifuge tubes (13.2 ml; Herolab Centrifuge Labware PA) and ultracentrifuged at 100,000 × g for 1 h at 4 °C (Sorvall® Discovery 90 with SW 41 Ti Swinging-Bucket Rotor,

Beckman Coulter Life Sciences). The Pellets were resuspended in 200 µl of 1× PBS and stored at −80 °C until further analysis. An overview of the *Si*-EVs isolation workflow is shown in Supplementary Figure S1.

Nanoparticle tracking analysis (NTA)

For EVs characterisation, samples were diluted 1:100 to a final concentration of 1×10^{6} and 1×10^{10} particles/ml. Particle size and concentration were determined using nanoparticle tracking analysis with (ZetaView, Particle Metrix, Germany). NTA measurements were performed at the Biozentrum, Faculty of Biology, Ludwig-Maximilian-University (LMU), Munich.

Transmission electron microscopy (TEM)

For TEM analysis, imaging was performed using carbon-coated 400-mesh copper grids. 5 µl of the potential EVs sample was incubated for 3 min at room temperature and negatively stained with 2% uranyl acetate. Microscopy was performed at 120 kV using a ZEISS EM912a/b transmission electron microscope. Imaging was performed in collaboration with the Department of Imaging at the Biomedical Research Centre Seltersberg, Gießen.

Results and discussion

Dual fluorescence staining suggests vesicle concentration at *Arabidopsis–S. indica* contact zones

Double fluorescence staining with WGA and SynaptoRed revealed that *S. indica* hyphae (green) colonise *Arabidopsis thaliana* root cells (red), with fungal structures extending intracellularly and maintaining close contact with host tissues (Figure 1). Discrete red fluorescent spots were detected at multiple interaction sites, either alongside or surrounding hyphae (indicated by white arrows). These spots appeared as localised aggregates, distinguishable from the diffuse background signal of the host tissue and were consistently concentrated at the hyphal–host interaction point. The close proximity of these structures to intracellular hyphae suggests that colonisation triggers localised host responses, possibly involving vesicle trafficking.

Such interaction zones could represent an accumulation of Arabidopsis vesicles moving toward the *Si* hyphae. This result is in line with previously reported observations of cellular reorganisation and activation of membrane trafficking pathways during *Si* root colonisation (Jacobs et al., 2011; Šečić et al., 2021). Moreover, these same interaction points suggest *Si* secretory activity, with *Si* vesicles being potentially released into the surrounding Arabidopsis tissue. Although our staining cannot strictly identify the exact origin of EVs, the strong association between these interaction points and colonisation sites suggests that vesicle activity may contribute to symbiosis and possibly support material exchange between partners.

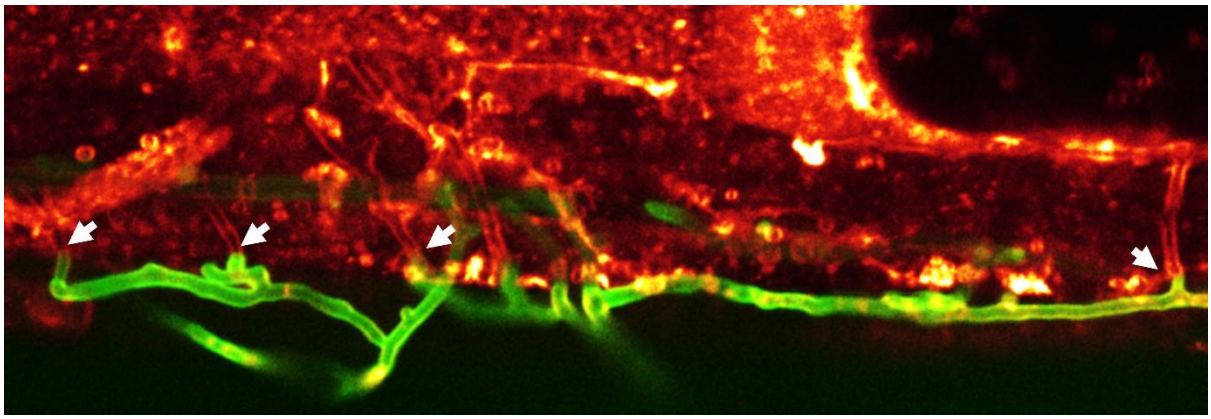

Figure 1: Localised fluorescence signals in Arabidopsis roots colonised by *S.indica*. Confocal microscopy of *Arabidopsis thaliana* root tissue colonised by *Serendipita indica* using double fluorescence staining. Hyphae were visualised with wheat germ agglutinin (WGA) conjugated to Alexa Fluor 488 (green; excitation 488 nm, emission 500–550 nm), and host membranes with SynaptoRed (red; excitation 561 nm, emission 570–650 nm). Hyphae extend along the root surface and penetrate host cells. Discrete red spots are detected in close proximity to hyphae, marking localised interaction zones at the host–fungus interface (indicated with white arrows).

Recovery and characterisation of extracellular vesicles from *S. Indica*

Crude EVs–like pellet was recovered from CM– culture of *S. indica* after ultracentrifugation. NTA analysis showed that most particles were between 120 and 250 nm in size (Figure 2a), which corresponds to the expected sizes range for fungal EVs (Palatinus et al., 2025). Particle concentration was 3.17×10^9 particles/ml, indicating the presence of a large number of nanoparticles. The zeta potential of these particles ranged

from –20 to –45 mV (Figure 2b), which is a negative surface charge typical for vesicles, indicating their stability in the solution.

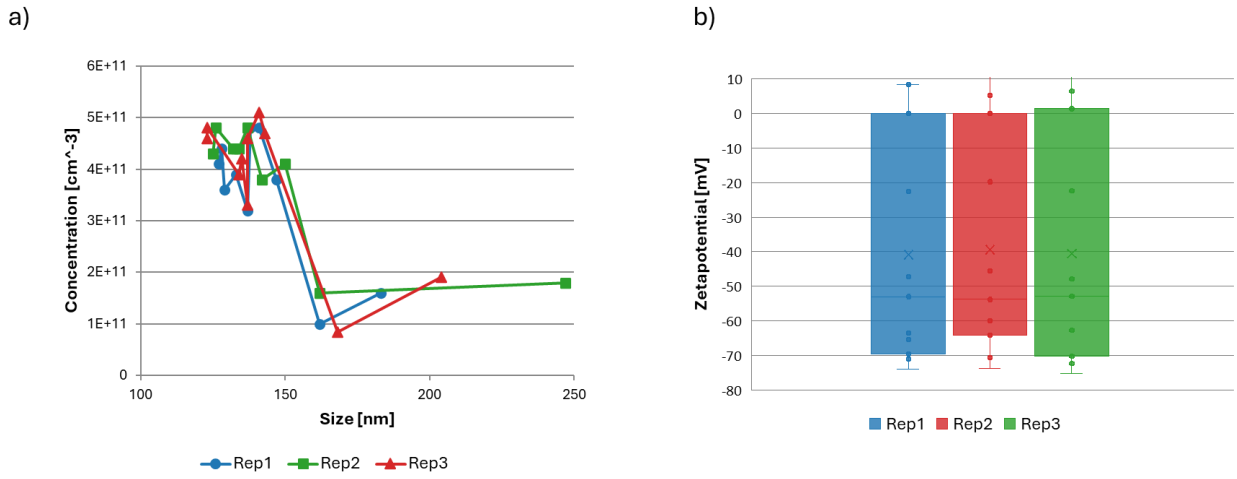

Figure 2. Biophysical characterisation of S. *indica*-EVs. Nanoparticle tracking analysis (NTA) of *Si*-EVs preparations showing **(a)** typical size distribution of ca. 120-250 nm sized particles and corresponding concentration for three independent replicates, and **(b)** Zeta potential measurements of the same *Si*-EVs preparations presented as boxplots with individual data points. Negative ζ-values indicate the negative surface charge of the vesicles, consistent across replicates.

Next, we examined the morphology of the crude EVs sample using TEM. Although we detected structures in the correct size range and with a vesicle-like appearance similar to cup-shaped morphology, the presence of EVs could not be confirmed. However, the majority of detected particles were protein aggregates and debris (Figure S2). This outcome highlights both the technical challenges of fungal EV visualization and the limitations of working with crude pellets.

A critical factor contributing to the inconclusive TEM results is the absence of a further purification step in our workflow. Unlike density gradient centrifugation or EVs purification columns, which separate vesicles from contaminants and improve membrane preservation, simple ultracentrifugation produces heterogeneous pellets containing both vesicles and non-vesicular particles (Jia et al., 2022.; Linares et al.,

2015). Consequently, true EVs may be masked or structurally altered during preparation. Moreover, negative staining in TEM presents an additional challenge for EVs analysis, as this procedure can lead to membrane collapse and reduced structural clarity. Variations in staining conditions may also affect contrast, making it difficult to reliably distinguish EVs from artefacts (Cizmar & Yuana, 2017). Nevertheless, the inability to discern clear vesicle morphology in TEM does not rule out EV secretion by *S. indica* but rather emphasises the importance of additional purification steps for reliable structural characterisation.

S. indica sRNAs were recovered from ultracentrifuged pellets

To determine whether the pelleted *S. indica* EV-like fraction from ultracentrifugation contains any biological material, we analysed its RNA content. We previously identified *S. indica* sRNAs during *Si-At* interaction with a potential role in cross-kingdom RNAi (Nasfi et al., 2024). Therefore, we investigated whether *Si*sRNA24 and *Si*sRNA28, along with two other *Si*sRNAs previously detected in *Si* axenic culture, in *At Si*-colonised roots (Nasfi et al., 2024) and from AGO1- and AGO2-IP sequencing (Chapter 5), could be detected in the EV-like pellet. All four *Si*sRNAs (*Si*sRNA24, *Si*sRNA28, *Si*sRNA62 and *Si*sRNA148), as well as the Arabidopsis *At*miR159a, used as a negative control, showed a band after stem-loop PCR and gel electrophoresis analysis (Figure 3). However, only the sequences of *Si*sRNA24 and *Si*sRNA28 were detected by Sanger sequencing and confirmed to be identical to those detected in the axenic culture, *At-Si* interaction, and *At*AGO-IPs (Supplemental Table 2).

Sanger sequencing of *Si*sRNA62 and *Si*sRNA148 yielded sequences different from those previously detected in axenic culture and in *At-Si* interaction, suggesting the presence of alternative *Si*sRNA variants, a result previously observed in Nasfi et al. (2024). For *At*miR159a, we observed unspecific amplification, likely due to multiplexing of hairpin primers in Stem-loop PCR or to partial complementarity of the hairpin primer to a non-target sequence. Our results highlight the technical challenges of working with crude EV-like fractions and the need for a purified vesicle population for higher throughput analysis

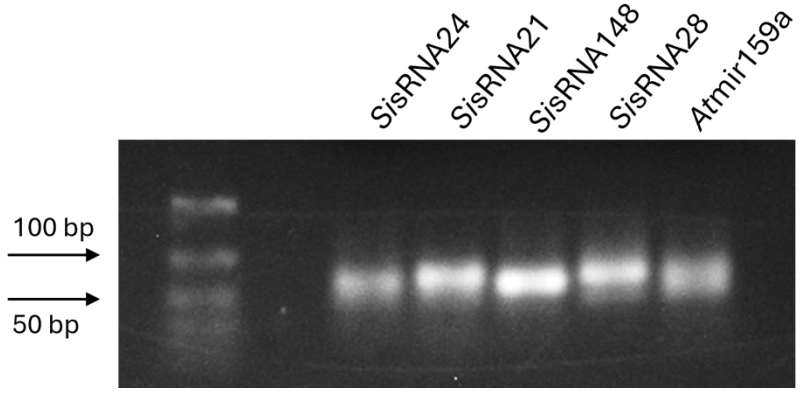

Figure 3: Stem–loop PCR detection of *Si*sRNAs in *Serendipita indica* extracellular vesicles. Gel electrophoresis of multiplexed stem–loop PCR products from EV pellets isolated from 3 days growing *S.indica* in CM medium without sucrose confirmed the presence of *Si*sRNAs. A PCR product of the expected size of 62 bp (sum of the 21 bp of the sRNA sequence, loop region, plus the forward primer and the reverse primer length) is visualised in a 2% agarose gel. The plant *At*miR159a of 21 nt in length served as a negative control. A non-specific amplification was detected for the *At*miR159a due to the multiplexing of hairpin primers or a partial complementarity of the hairpin primer to a non-target sequence.

*Si*sRNA24 is an snRNA involved in spliceosomal assembly, and *Si*sRNA28 is an rRNA component of the ribosome. Even though the total RNA yield from the EVs-like pellet was low, the detection of these *Si*sRNAs shows that RNA molecules are present in the isolated material.

Finding sRNAs after several isolation steps is important for our study. Free, unprotected RNAs would neither pellet efficiently during ultracentrifugation nor remain intact without protection. Naked RNAs are highly unstable and are susceptible to rapid degradation, making it unlikely that they would survive the isolation process. sRNA presence in the EVs pellet, suggests that they are protected within vesicles or bound to RNA-binding proteins or lipoprotein complexes that co-precipitate with EVs.

Taken together, the detection of *Si*sRNA24 and *Si*sRNA28 suggests that *S. indica* releases vesicle-like particles that can carry RNA cargo. Purifying EVs using density gradient media

such as OptiPrep and performing size-exclusion chromatography to separate various EVs, are essential steps to exclude contaminants and confirm that these particles are vesicles (Palatinus et al., 2025). Still, these findings provide a first indication that *S. indica* EVs may carry sRNAs, potentially facilitating communication with host plants

This study is the first investigation of whether *S. indica* releases extracellular vesicles in axenic culture. Results from NTA, zeta potential measurements, and RNA analysis indicate that vesicle-like particles are present and potentially carrying *S. indica* RNAs, including sRNAs potentially involved in cross-kingdom interactions. However, the absence of a clear cup-shaped morphology in TEM and the observation of aggregates highlight the limitations of ultracentrifugation alone as an EVs isolation method and the need for additional purification and imaging approaches.

Subsequent experiments should include enzymatic treatments and disruption assays to confirm vesicle integrity and cargo protection. Proteinase K digestion, micrococcal nuclease (MNase) treatment, and detergent disruption with Triton X-100 can indicate whether *Si*sRNAs are bound to the surface of the EVs or encapsulated within them. Furthermore, protein profiling using Coomassie staining in combination with proteomic analysis, such as liquid chromatography mass spectrometry, will facilitate the identification of vesicle-associated proteins and thereby identify *S. indica* EVs biomarkers (Thieron et al., 2024).

Conclusion

The recovery of *S. indica* sRNAs from isolate EVs-like particles supports the notion that mutualists are highly probable to release vesicle-like particles that may serve as vehicles for RNA stabilisation and delivery. Although the current dataset does not definitively confirm vesicle secretion, our work provides a methodological framework with an open window for improvement. Methods such as density gradient centrifugation, an optimised double-staining protocol, and complementary labelling of EV-associated proteins will be essential for further understanding.

In conclusion, these findings lay a foundation for future studies on mutualistic fungal EVs and suggest their potential role in cross-kingdom RNA communication.

Supplementary material

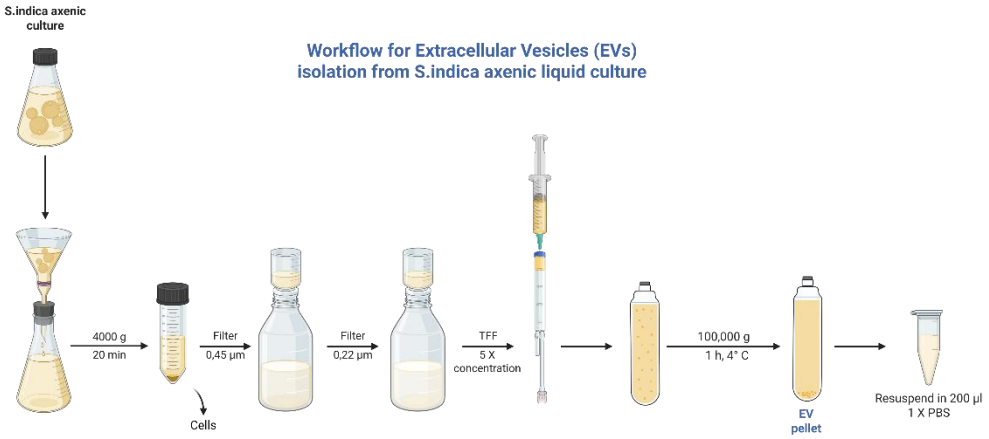

Supplementary Figure S1. Workflow for isolation of extracellular vesicles from *Serendipita indica* axenic liquid culture. Schematic representation of the workflow used to isolate extracellular vesicles (EVs) from *S. indica* grown in axenic liquid culture. After removal of fungal biomass by filtration and centrifugation at 4000 × g for 20 min, the culture supernatant was sequentially filtered through 0.45 µm and 0.22 µm filters. The filtrate was 5× concentrated using tangential flow filtration (TFF) and subjected to ultracentrifugation at 100,000 × g for 1 h at 4 °C to pellet EVs. The EVs pellet was subsequently resuspended in 200 µl of 1× PBS for downstream analyses.

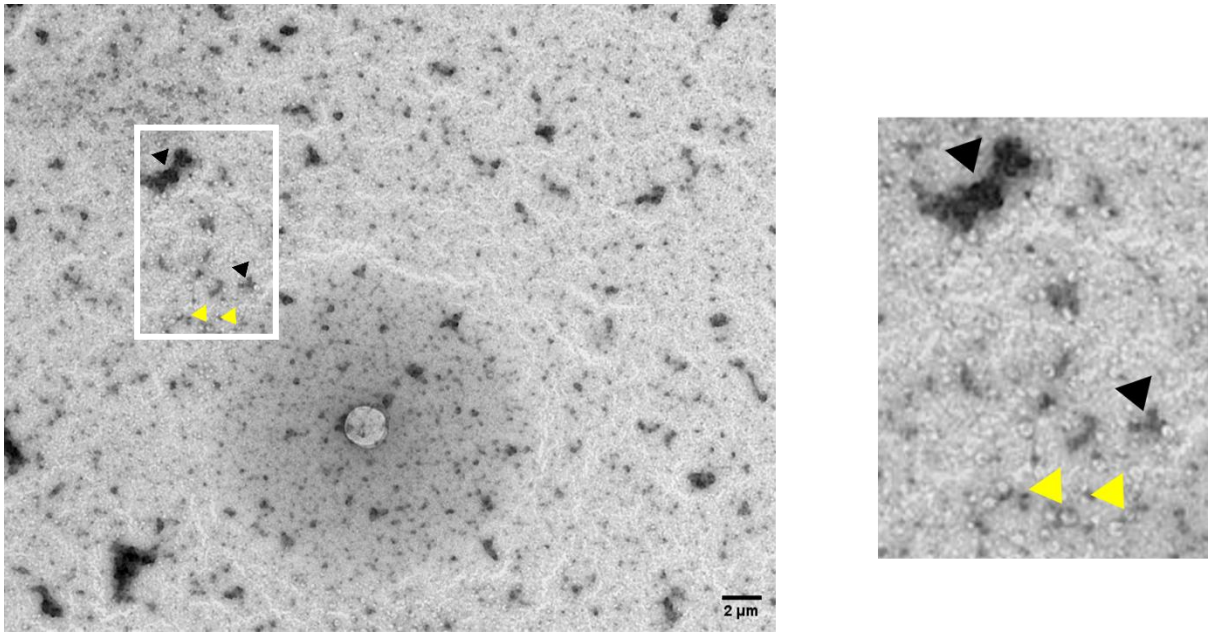

Supplementary Figure S2. Transmission Electron Microscopy with negative staining of *Serendipita indica* EVs-like particles resuspended in 1x PBS. The left panel provides an overview of vesicle sample, and the right panel shows a magnified area marked with a white box. Yellow arrowheads point at potential EV-like structures, and black arrowheads at protein or debris aggregates.

Supplementary Table 1: Primer list used in stem-loop PCR (hp=hairpin, Fwd= forward)

Primer name	Primer sequence
*Si*sRNA21-hp	GTCGTATCCAGTGCAGGGTCCGAGGTATTCGCACTGGATACG ACaggacc
*Si*sRNA21-Fwd	TCGCTacctttggtttcaa
*Si*sRNA24-hp	GTCGTATCCAGTGCAGGGTCCGAGGTATTCGCACTGGATACG ACgagaac
*Si*sRNA24-Fwd	TCGCTttgaccaatttttct
*Si*sRNA28-hp	GTCGTATCCAGTGCAGGGTCCGAGGTATTCGCACTGGATACG ACagatcc
*Si*sRNA28-Fwd	TCGCTacaactttcaacaac
*Si*sRNA148-hp	GTCGTATCCAGTGCAGGGTCCGAGGTATTCGCACTGGAT ACGACgccatt
*Si*sRNA148-Fwd	TCGCTttaggacactggcat

Universal Reverse Primer	GTATCCAGTGCAGGGTCCGAGGT

Supplementary Table 2: Sequences of *Si*sRNA detected in *Si* axenic, *Si-At* interaction, and *At*AGO-IP compared to the respective stem-loop PCR amplicons detected from pelleted *Si* EVs-like particles.

*Si*sRNA name	*Si*sRNA sequence in axenic culture, *At-Si* interaction or *At*AGO1-IP	*Si*sRNA identified by Sanger sequencing
*Si*sRNA24	TTGACCAATTTTTCTGTTCTC	TTGACCAATTTTTCTGTTCTC
*Si*sRNA21	ACCTTTTGGTTTCAAGGTCCT	ACCTTTTGGTTTCAATGGCGT
*Si*sRNA28	ACAACTTTCAACAACGGATCT	ACAACTTTCAACAACGGATCT
*Si*sRNA148	TTAGGACACTGGCATAATGGC	TTAGGACACTGGCATCGTATC
*At*mir159a	TTTGGATTGAAGGGA GCTCTA	TTTGGATTGAAGGGAGCTCTA

Red letters indicate different nucleotides of *Si*sRNAs detected in EVs-like pellet.

CHAPTER 7 –

High Precision Quantification of small RNA Slicing Activity- Native Index Ligation-based Targeted Degradome Sequencing (NIL-TDS)

(Equal Contribution as first Author)

Summary:

This chapter contains the publication "**High Precision Quantification of small RNA Slicing Activity- Native Index Ligation-based Targeted Degradome Sequencing (NIL-TDS)"**, under revision in RNA journal and preprint available on bioRxiv (DOI:10.1101/2025.09.30.679503)

The use of small RNAs to target host mRNAs in a cross-kingdom interference concept offers a promising strategy for controlling plant diseases and developing new plant protection strategies. However, designing and identifying effective small RNAs requires precise assessment of their slicing activities. Although existing degradome profiling methods, such as PARE and RLM-RACE, have contributed to this field, they are often labour-intensive, have low sensitivity, and lack quantitative precision.

To overcome these limitations, we developed Native Index Ligation-based Targeted Degradome Sequencing (NIL-TDS), a novel and cost-effective method based on Oxford Nanopore sequencing (ONT). NIL-TDS enables direct, high-resolution detection and quantification of sRNA-mediated slicing events.

High Precision Quantification of small RNA Slicing Activity - Native Index Ligation-based Targeted Degradome Sequencing (NIL-TDS)

AUTHORS

Bernhard T. Werner[1,†,*], Sabrine Nasfi[1,†], M. Lienhard Schmitz[2], Manar Makhoul[3], Jens Steinbrenner[1,4], Patrick Schäfer[1,*]

[1] Institute of Phytopathology, Research Centre for BioSystems, Land Use and Nutrition, Justus Liebig University Giessen, Heinrich-Buff-Ring 26, 35392 Giessen, Germany.

[2] Institute of Biochemistry, Medical Faculty, Friedrichstrasse 24, Justus Liebig University Giessen, 35392 Giessen, Germany

[3] Department of Plant Breeding, Research Centre for Biosystems, Land Use and Nutrition, Justus Liebig University Giessen, Heinrich-Buff-Ring 26, 35392 Giessen, Germany

[4] Andermatt Biocontrol Suisse AG, Research & Development, Stahlermatten 6, 6146 Grossdietwil, Switzerland

* To whom correspondence should be addressed. Tel: +49 641/99-37490; Fax: +49 641/99-37499; Email: Patrick.Schaefer@agrar.uni-giessen.de

Correspondence may also be addressed to. Tel: +49 641/99-37498; Email: Bernhard.T.Werner@agrar.uni-giessen.de

† Joint Authors

SHORTENED VERSION OF THE TITLE: Precise Quantification of sRNA Slicing Activity

KEYWORDS

Small RNA cleavage, RLM-RACE, Nanopore sequencing, Arabidopsis thaliana, human lung carcinoma

GRAPHICAL ABSTRACT

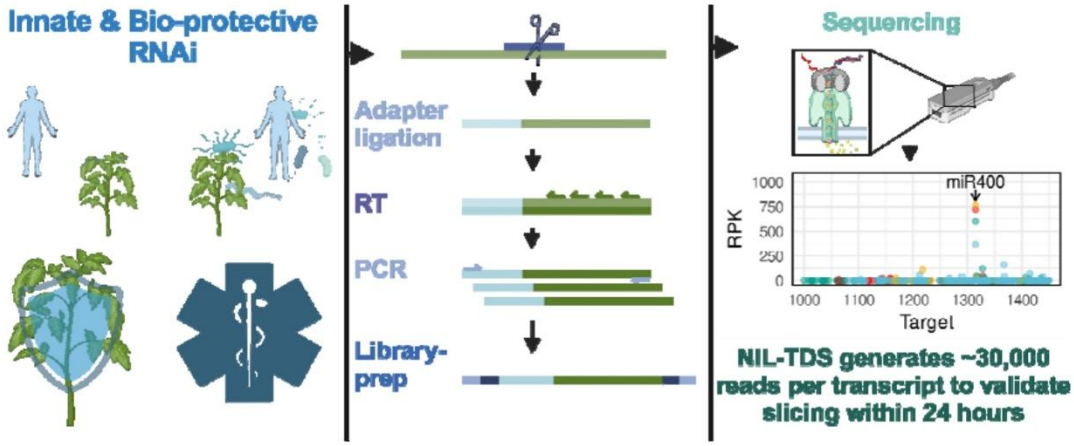

ABSTRACT

RNA interference (RNAi) is an effective and precise regulatory mechanism in eukaryotes in which small RNAs mediate endonucleolytic slicing of complementary target mRNAs. Despite the potential of RNAi for human therapeutics and crop bio-protection, analytical platforms to quantitatively validate the slicing activities of small RNAs remain limited. Here, we present NIL-TDS, a cost-effective method that combines RNA ligase-mediated PCR with Nanopore Sequencing for direct, rapid, and high-resolution detection and quantification of sRNA-mediated slicing events. Using NIL-TDS, we quantitatively detected minute changes in *Ath*-mir400 mediated slicing of *PPR1* in heat and salt stressed Arabidopsis plants. We further demonstrate the broader applicability of NIL-TDS by detecting rare slicing events in a mammalian system. Of relevance for malignancy of certain cancers, and tumor progression and metastasis, NIL-TDS further confirmed *miR-196-HOXB8* interactions in lung cancer cells and discovered a novel miR-7162-HOXA10-AS slicing site. These findings demonstrate the sensitivity of NIL-TDS for uncovering small RNA mediated regulatory mechanisms of gene expression and disease progression in eukaryotes.

41

42 **INTRODUCTION**

43 RNA interference (RNAi) is a conserved mechanism in eukaryotes in which small regulatory
44 RNAs (sRNA) guide the RNA-induced silencing complex (RISC) to slice and thus degrade
45 complementary mRNAs (Shabalina and Koonin 2008). sRNAs are short (~18-30 nt), double-
46 stranded RNAs that regulate mRNA stability based on sequence complementarity to control
47 fundamental biological processes in eukaryotes. These functions range from growth,
48 development, stress adaptation, and immunity, to cellular processes such as genome stability
49 (Ketting 2011). Variations in this sequence-specific functionality that affect sRNA-mRNA
50 complementarity or accessibility can lead to diseases and developmental defects in animals
51 and plants. For example, a target site mutation in the B-cell activating factor gene, essential
52 for the survival and function of B lymphocytes (a type of white blood cells), abolishes RNAi-
53 mediated suppression, which correlates with an increased risk of autoimmune diseases (Steri
54 et al. 2017). Similarly, a synonymous polymorphism in the target site of microRNA-196 (miR-
55 196) in the immunity-related GTPase M is associated with Crohn's disease (Brest et al. 2011).
56 In plants, miR164 suppresses the initiation of axillary shoot buds, and mutations in this miR
57 lead to significant morphological changes (Raman et al. 2008).

58

59

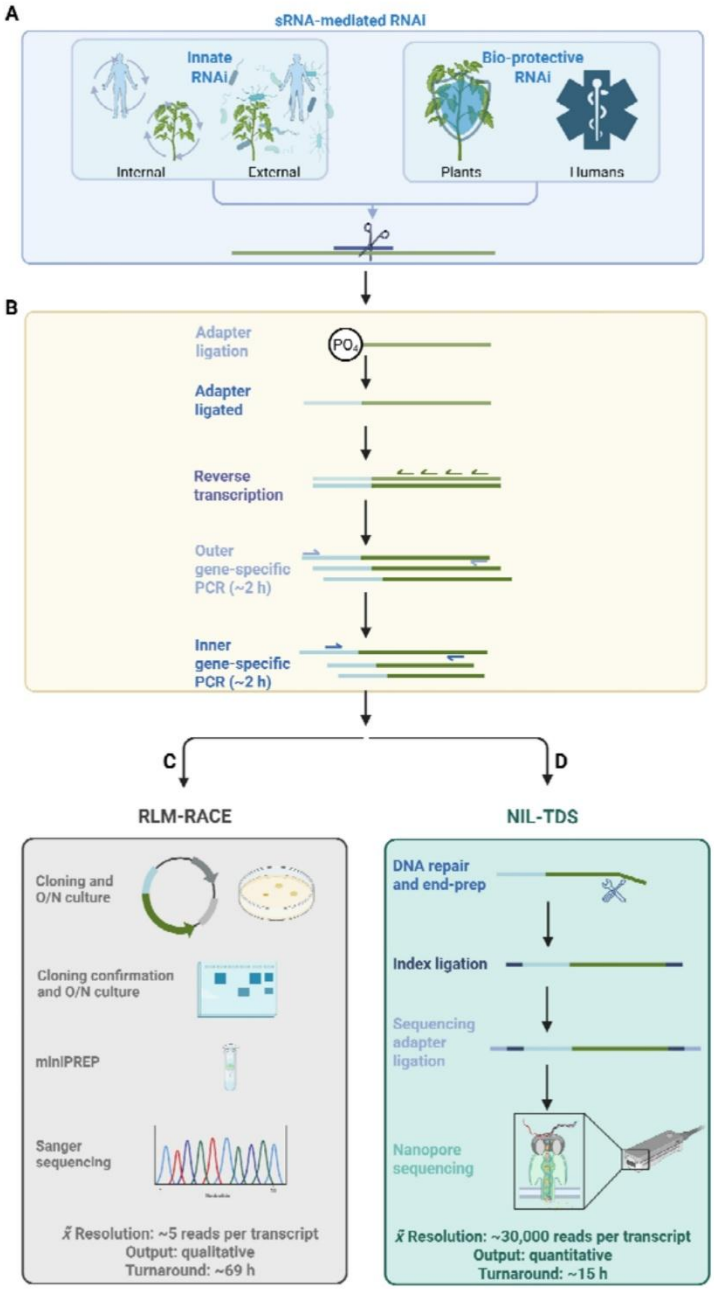

Figure 1: Workflow of quantitative NIL-TDS in comparison to qualitative RLM-RACE.

sRNAs trigger RNAi in eukaryotes and can protect plant and human health (A). RNAi generates characteristic 5′-monophosphate RNA ends at RNAi-mediated slice sites that allow specific adapter ligation and detection by RLM-RACE (B-C) or by NIL-TDS (B-D)) resolution and indicated turnaround times for each method are based on our experience and

79 published data (Wang and Fang 2015). Only NIL-TDS generates quantitative outputs. Created
80 with BioRender.com

81 Designing and engineering sRNAs for RNAi application allows to specifically regulate gene
82 levels with the unique potential to develop customised bio-protective and therapeutic
83 agents for plant and human health (Cai et al. 2018) (Fig. 1A). However, this potential must
84 account for the complexity of sRNA-mRNA target interactions. Depending on the degree of
85 sRNA complementarity, the mRNA target is degraded or translationally inhibited by a
86 process that is still not fully understood (Kern et al. 2019). In addition to mRNA target
87 complementarity, abundance, as well as sRNA subcellular localisation, and interactions with
88 other RNAs or RNA binding proteins (e.g. sponging effect) shape sRNA-mRNA interactions
89 (Diener et al. 2023). Considering this complexity and the continuous progress in next
90 generation sequencing-based discovery of sRNA candidates (Benesova et al. 2021), the
91 development of rapid and highly sensitive methods for the quantification of sRNA-mediated
92 slicing activities is urgently needed. Currently RNA ligase-mediated rapid amplification of
93 cDNA ends (RLM-RACE) (Fig. 1B-C) is the standard procedure for the detection and
94 validation of slicing-based RNAi activity of candidate sRNAs. It has, however, some
95 significant shortcomings. In RLM-RACE, an RNA adapter is ligated to the 5'-monophosphate
96 of the sliced RNA, and this adapter is used for reverse transcription Liave et al. (2002),
97 German et al. 2008). Subsequently, gene-specific primers amplify cDNA ends in a nested PCR
98 reaction. The resulting products are then cloned into a vector, followed by DNA sequencing
99 (Liave et al. 2002). Each clone represents only one RNA-end read, and because of the costly
100 and laborious nature of the procedure, only a few reads are commonly generated for a given
101 gene. As a results, RLM-RACE is a low-throughput approach for validating known candidates
102 that is prone to PCR amplification biases, and does not provide quantitative, statistically

103 confirmable insights into cleavage efficiencies. High-throughput sequencing approaches,
104 such as parallel analysis of RNA ends (PARE) (Zhai et al. 2013) are also used for detection and
105 validation of sRNA slicing activity, where a type II restriction enzyme produces 20-nucleotide
106 long tags, which are further ligated to another 3′-adapter for a second PCR prior to
107 sequencing. Although PARE can potentially provide data on the entire degradome, the
108 detection of slicing events correlates with transcript copy numbers, resulting in insufficient
109 coverage for most, especially low abundant, transcripts (German et al. 2008. Currently, a
110 standard Illumina sequencer can produce billions of reads in the span of a single day, making
111 it compatible for PARE (Wetterstrand 2024; Kumar et al. 2024). However, this technique is not
112 cost-effective for validating single target genes, which are often required for the
113 development of RNAi-based therapeutics. The lack of read depth either in RLM-RACE or in
114 PARE generally results in qualitative data and prevents statistical validation of sRNA slicing
115 events making both methods limited in detecting rare cleavage products and potentially
116 leading to an underestimation of sRNA-mediated slicing events. Fortunately, advancements
117 in sequencing technologies supports the development of alternative approaches (Kumar et al.
118 2024). The ONT Flongle sequencing platform is an affordable hardware for direct DNA
119 sequencing, which significantly reduces library preparation time. Moreover, throughput and
120 run time are scalable, and single runs to analyse slicing of selected candidates can be
121 operated at competitive costs (De Cesare et al. 2024).

122 In this study, we utilized the latest sequencing features to develop an innovative workflow for
123 high resolution slice site detection in eukaryotes. We combined the ONT Flongle native
124 ligation-based barcoding platform with RNA adapter ligation-mediated PCR approaches to
125 establish Native Index Ligation-based Targeted Degradome Sequencing (NIL-TDS) for the
126 direct quantification of slicing activities of sRNA candidates (Fig. 1B-D). NIL-TDS offers higher

sequencing depth as compared to RLM-RACE and PARE, which is most critical to detect slicing events in lowly expressed mRNAs. In addition, NIL-TDS is scalable, more specific, cost-effective, and offers a short turnaround time, while also being independent of tedious and bias-prone cloning. The high-read coverage and long-read capability of ONT enable precise detection of both high and low abundance slicing events. As a proof of concept, NIL-TDS was validated by analysing miRNA-induced slicing in plant seedlings and human cell lines. It revealed a previously unknown miRNA-mRNA cleavage-based interaction from a lowly expressed, highly relevant transcripts. The generated unprecedentedly detailed degradome profiles, quantified changes in sRNA slicing activity that improved our understanding of miRNA-mediated gene regulation.

RESULTS

NIL-TDS procedure outline

As a first step, an RNA adapter was ligated to the 5′-monophosphate ends of a sliced RNA, ensuring selective amplification of sRNA-effected cleavage products. This ligated RNA was converted to cDNA by reverse transcription, followed by PCR amplification using adapter-specific and target mRNA-specific primers to enrich for sliced mRNA amplicons. These amplicons were subjected to ONT Flongle sequencing using the native ligation-based barcoding platform, enabling multiplexing and parallel analysis on the same chip of samples or replicates, yielding more than 0.5 million reads per run. Sequencing reads were aligned to the reference transcriptome, and a bioinformatics pipeline was used to identify and quantify sRNA slicing sites. We developed an R script (see Supplementary Methods) for rapid data analysis. The script trims and aligns the base called and demultiplexed reads to the respective RNA to create high-resolution t-plots.

Quantitative validation of the miR-196-*HOXB8* slice site

Human microRNAs (mir) are involved in almost every cellular process and their dysregulations have been shown to contribute to different human diseases including neurodegenerative diseases and cancer. Mir-196 is a conserved miRNA-family encoded within the HOX gene clusters and known to fine tune the expression of its target gene *HOMEOBOX B8* (HOX8B) and its aberrant expression is associated with tumerogenesis and development of lung metastases (Chen et al. 2011). To benchmark NIL-TDS sensitivity, we reanalysed the interaction of miR-196 with the *HOXB8* gene as the first discovered cleavage-mediated RNAi guide-target pair in mammals (Yekta et al. 2004). In their seminal study, Yekta et al. (2004) showed *HOXB8* cleavage activity with 8 RLM-RACE reads from total mouse RNA. Using NIL-TDS, we confirmed the expected mRNA cleavage at position 4918 as dominant signal (Fig. 2A), with $^{211}/_{3,368}$ total reads in human lung carcinoma A549 cells which robustly expressed *HOXB8* (Jiang et al. 2024). Interestingly, additional and previously undescribed slicing signals were detected in both repetitions at positions 5,097, 5,123 and 5,144.

Identification of a formerly unknown miR-7162-*HOXA10-AS* slice site with relevance in carcinogenesis

To test NIL-TDS capabilities to elucidate rare and potentially unknown slicing events, we investigated the complex and convoluted regulation of the HOX-gene cluster and its important regulator miR-196. One interesting precursor transcript of miR-196 is *HOXA10-AS* (antisense). HOXA10-AS is emerging as an key player in cancer biology, frequently overexpressed in several tumor types including glioma, breast, gastric and colorectal cancer. Its role in promoting cancer progression suggests its potential as a diagnostic and

prognostic biomarker, making it a promosing target for therapeutic interventions (Hu et al. 2025). We were particularly interested in a potential miR-196 target site in this transcript, which would constitute a negative feedback loop to regulate miR-196 expression. Additionally, we wanted to investigate a potential regulatory mechanism that could decouple *HOX* gene expression from the suppressing influence of miR-196 which is co-transcribed from the same gene cluster (Hu et al. 2025). Therefore, we generated three replicates of NIL-TDS with a total of 64,350 reads from the *HOXA10-AS* transcript (Fig. 2B) in A549 cells. Surprisingly, we identified one highly consistent degradation signal at position 623, with 647, 638 and 636 reads per 1000 reads (RPK). This position corresponded to the predicted slice site of miR-7162, a yet undescribed interaction, indicating suitability of NIL-TDS for discovering previously unknown miRNA activities (Fig. 2B). In the course of our studies, we anticipated that NIL-TDS might introduce PCR duplication events in sRNA targets resulting in an overestimation of slicing. To quantify the extent of PCR duplication, HOXA10-AS was reanalysed with the incorporation of unique molecular identifiers (UMIs). In a first step, random RNA heptameres were ligated to RNAs, to serve as UMIs, followed by 5′ phosphorylation and RNA adapter ligation. We observed that this UMI approach incorporated unspecific 5′ phosphorylation, leading to the amplification of all RNAs and reducing the fraction of reads mapping to HOXA10-AS to 13 % (2472 / 18,460). However, the obtained 2,472 reads represented 371 unique barcodes with a saturating sequencing depth

192 and a dominant and statistically approvable slicing signal at position 623 (Fig. S1).

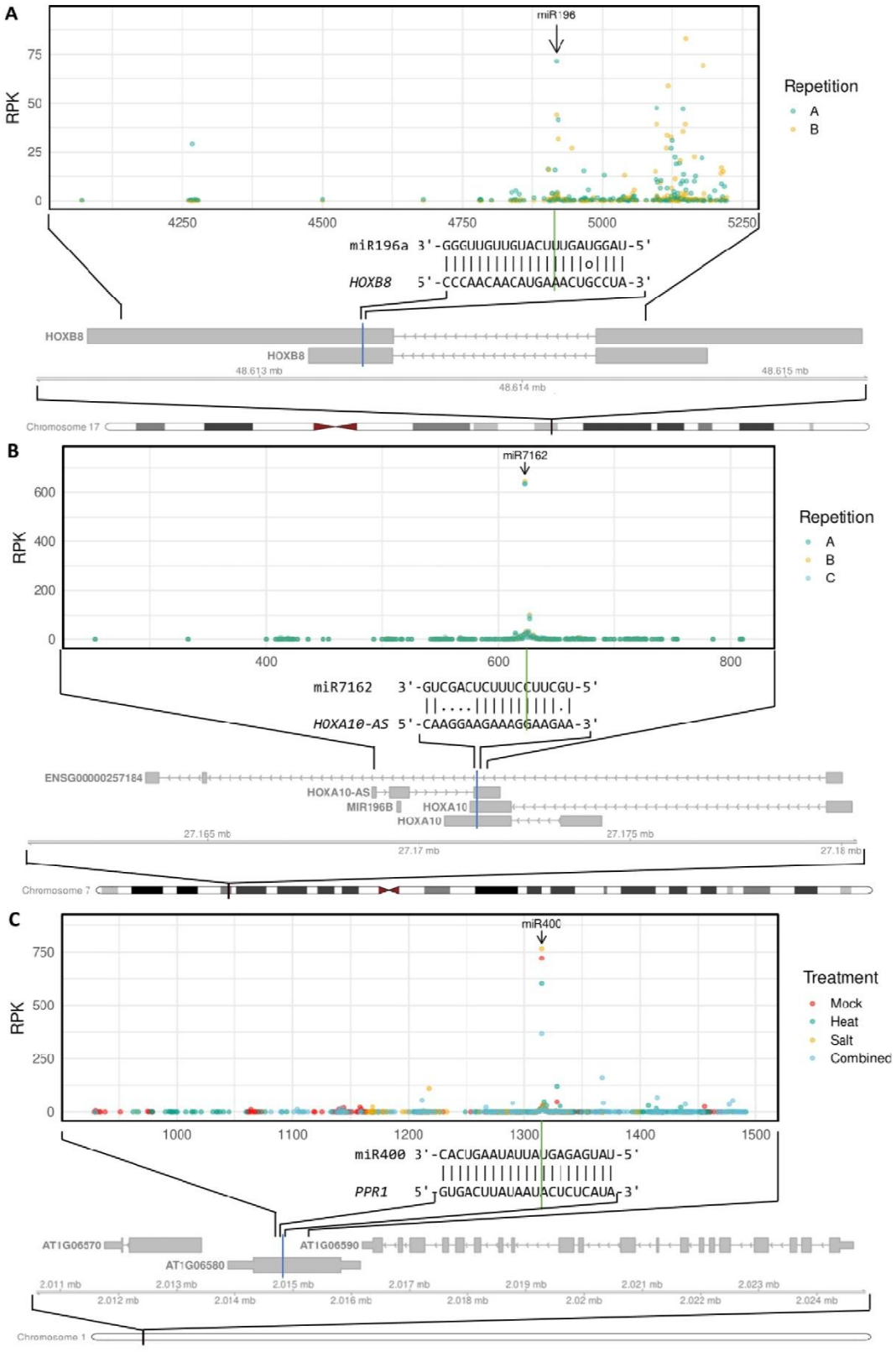

193

Figure 2: Quantitative NIL-TDS output in human and plant cells. NIL-TDS-based detection of HOXB8 slicing by miR-196 in human cells (A), HOXA10-AS slicing by miR-7162 in human cells (B), and PPR1 slicing by miR400 in Arabidopsis thaliana seedlings (C). Plotted positions are indicated on the genomic tracks, and blue lines mark respective miRNA target sites. Each point shows the number of reads per 1000 total reads, that aligned with their 5'-end to the respective mRNA base position indicating mRNA fragment ends. Arrows indicate the respective slice sites in the plots. Legends show colour-coded stress treatments or repetitions. The alignment between miRNA and target RNA is shown with a green line indicating slice-sites.

Detection of climate stress-induced minute changes in miR400-mediated slicing of PPR1

To validate the applicability and sensitivity of NIL-TDS across eukaryotes, we analysed the slicing site of *Arabidopsis thaliana* miR400 (*Ath*-miR400) and its target *PENTATRICOPEPTIDE REPEAT 1* (*PPR1*; *AT1G06580*). *Ath*-miR400 is downregulated (Barciszewska-Pacak et al. 2015) while *PPR1* is upregulated during various stresses, such as salt and heat stress (Kilian et al. 2007). However, the hypothesised reduction in slicing activity has never been experimentally validated. Therefore, we treated *Ath* seedlings with 250 mM NaCl (salt stress), without NaCl (mock), exposed them to 37°C (heat stress), or subjected them to a combination of salt and heat stress (combined stress). In total, we generated 214,087 reads, of which 154,786 fulfilled the quality criteria to carry the ligated slicing-adapter and to align end-to-end with at least 100 nt to the target transcript (Tab. S1). NIL-TDS provided an unprecedented resolution of the *Ath*-miR400 target site degradation profile on *PPR1* (Fig. 2C). Confirming NIL-TDS

quantitative sensitivity. We observed a slight reduction of slicing activity upon heat stress, which was significantly attenuated upon combined stress treatments (Fig. 2C, Fig. S2).

NIL-TDS is precise and reproducible, but amplifies rare exosomal degradation events in the absence of targeted slicing

To further evaluate the precision and reproducibility of NIL-TDS, we conducted two control experiments. First, we measured NIL-TDS accuracy by amplifying a 590 bp long amplicon (from outer amplicon of 691 bp) of *PPR1* cDNA from each *Ath* sample. Over 80% of all reads mapped to the respective inner primer binding site or 1 nt downstream, while 4% mapped to the outer amplicon (Fig. 3). This demonstrated the precision (Fig. 3A) and the reproducibility between replicates (Fig. 3B) across PCR, sequencing and bioinformatics.

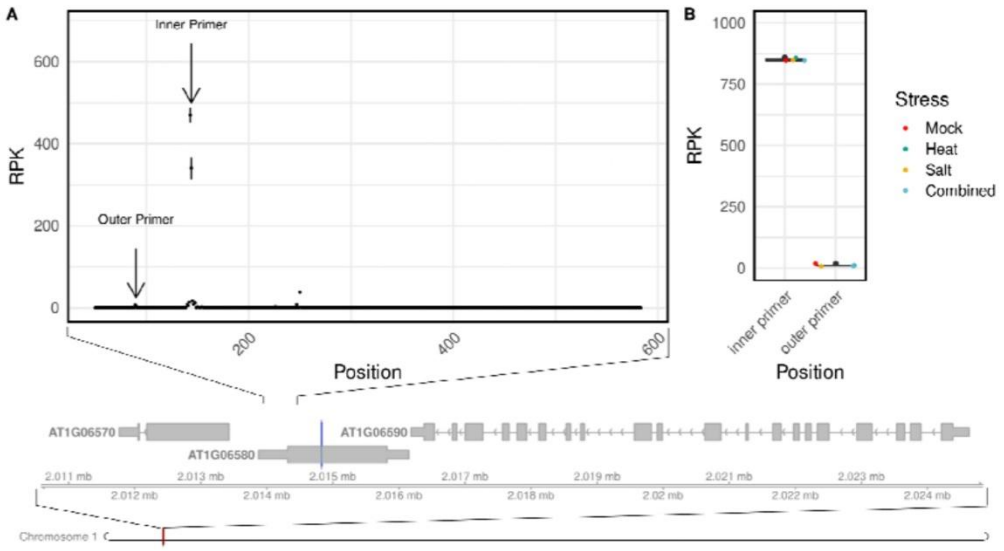

Figure 3: Precision of NIL-TDS on a cDNA amplicon. A nested PCR was conducted using *A. thaliana* Col-0 cDNA for the amplification of *PPR1* amplicon from four different stress treatments. Amplicons were sequenced on a nanopore Flongle cell. Start sites of alignments (A). Fraction of reads within the primer start site +/-2 bp (B). Each point shows the number of

reads per 1000 total reads, that aligned with their 5′-end to the respective mRNA base position indicating mRNA fragment ends. Bars show the standard deviation between the treatments. Plotted positions are indicated on the genomic tracks, and a blue line marks the miRNA target site.

226

227 Secondly, we applied NIL-TDS to a region of *PPR1* with no known slicing sites (Fig. 4). Some
228 positions showed a slicing signal independent of the different stress treatments, which we
229 interpreted as unspecific exonucleolytic degradation. In fact, these sites were clearly
230 distinguishable from true slicing events by analysing replicates of nested PCR reactions.
231 Accurate and specific slicing events typically exhibited consistent read patterns
232 corresponding to the known miRNA target sites, while unspecific degradation showed a
233 random distribution of read points, which were not detected in replicates.

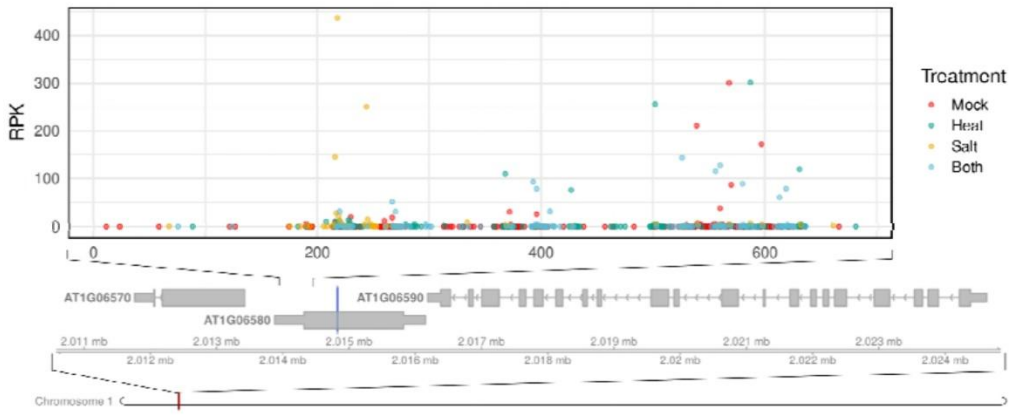

Figure 4: Comparative NIL-TDS readout of a non-target site of *PPR1* under abiotic stress. NIL-TDS readout of an untargeted site of *PPR1*. Each point shows the number of reads per 1000 total reads, that aligned with their 5′-end to the respective mRNA base position indicating mRNA fragment ends. Stress treatments are indicated by colour (mock

(red), heat (green), salt (yellow), and combined (blue)). Plotted positions are indicated on the genomic tracks, and blue lines mark respective miRNA target sites. Positions indicate the first base after the slice-site, which is also the first base after the 5′ RLM-adapter.

Consistent with this, in all experiments, the mean predicted sequencing error rate was below 0.001 (≥ Q30) as indicated by the base calling algorithm, and the median relative alignment edit distance was below 3%.

DISCUSSION

Revisiting miR-196 slicing activity reveals high sensitivity of NIL-TDS

Our study indicated NIL-TDS as a highly sensitive and accurate tool for mapping sRNA slicing sites and quantifying their activity. Integrating nanopore sequencing, NIL-TDS generated up to 100,000 times more reads than current standard methods (RLM-RACE, PARE), facilitating the detection and statistical validation of abundant to rare slicing events. Compared to RLM-RACE, it offers higher scalability and precision while providing a streamlined, ready-to-use workflow with broad applicability in basic and applied life sciences. As a validation for the methodology, we quantified the degree of slicing in the first ever discovered RNA-guided slicing event in mammalian systems. The detection of miR-196-mediated slicing of *HOXB8* had been a challenging task in past studies. Bracken et al. (2011) could not detect slicing of *HOXB8*, despite using mouse embryonic tissue, as used by Yekta et al. (2004) in their seminal study, via PARE. While Shin et al. (2010) were able to show *HOXB8* slicing with a PARE approach in HeLa cells, their approach produced only two reads of *HOXB8* and only one read was located at the expected slice site. This highlights the difficulty of detecting slicing events

for genes with low expression, like *HOXB8* in HeLa cells (Sjöstedt et al. 2020), with current methods.

We selected A549 cell lines, known for their more robust expression of *HOXB8*. Due to the inverse correlation of gene expression and slicing activity, the selection of a cell line with robust *HOXB8* expression for our experiments carried the risk of undetectable slicing activities. In contrast, the selection of HeLa cell lines, by Shin et al. (2010), with a diminished *HOXB8* expression generated barely sufficient reads. Therefore, we expected a lower fraction of sliced *HOXB8* transcripts in A549 as compared to HeLa cells. The low percentage of only 6% (in contrast to 50% in HeLa cells detected by Shin et al. (2010) of all reads at the slice site of miR-196 confirmed this expectation. Due to the higher sensitivity of NIL-TDS, we were still able to robustly detect the very rare slicing event.

Significance of a new slice site in a miR-196-precursor

HOX genes have pro-oncogenic functions in many types of cancers (Bhatlekar et al. 2014; Morgan et al. 2022). Surprisingly, miR-196, which can downregulate a fourth of all *HOX* genes, also has pro-oncogenic effects and is regarded as a potential cancer biomarker (Khalilian et al. 2024). This motivated us to analyse the biogenesis of miR-196b, which originates from the *HOXA10-AS* transcript, and we found that it involves miR-7162. The expression of miR-7162 is undetectable in all cell lines in miRmine (a database of human miRNA expression profiles) (Panwar et al. 2017), and therefore, miR-7162 activity remained elusive. The previously unknown slicing activity of miR-7162-5p detected in our study might explain reduced miR-196 expression in the A549 cell and other cell lines or tissues. Importantly, our findings represent a promising starting point for future functional analyses of miR-196 and miR-7162. The sensitivity and accuracy of NIL-TDS can be particularly

276 valuable in such studies. Recent studies suggested that miR-7162-3p, delivered via exosomes
277 from human umbilical cord mesenchymal stem cells, plays an important role in repairing
278 endometrial stromal cell injuries by targeting and restricting *Apolipoprotein L6* (*APOL6*), a
279 protein associated with tumour aggressiveness, thereby reducing cell death and
280 inflammation (Shi et al. 2021). Furthermore, Chakraborty and Nath (2022) reported miR-
281 7162-5p to potentially target *COL5A1*, a gene encoding the alpha-1 chain of type V collagen,
282 which is associated with malignancy of certain cancers, including lung cancer, promoting
283 tumour progression and metastasis. The latter study suggested that the absence of miR-
284 7162-5p may contribute to oncogenic processes by regulating *COL5A1* expression, thereby
285 potentially enhancing cancer cell proliferation and metastasis. NIL-TDS could validate this
286 role of miR-7162-5p in healthy tissues. Therefore, further analyses of miR-7162 mimics
287 (synthetic miRNAs behaving similarly to endogenous miRNAs) and NIL-TDS based analyses
288 may elucidate the role of miR-196 in cancer development and potentially open new avenues
289 for miRNA-based drugs and therapeutics.

290 **Stress-induced changes of *Ath*-miR400 slicing activity explain *PPR1* induction**

291 Different studies have analysed the expression of *Ath*-miR400 and its target gene *PPR1* upon
292 abiotic stress in *A.* thaliana (Barciszewska-Pacak et al. 2015; Kilian et al. 2007). Overexpression
293 of *Ath*-miR400 results in an increased susceptibility of *A. thaliana* plants to bacterial and
294 fungal pathogens (Park et al. 2014). Commonly, these studies rely on multi-omics
295 approaches, correlating sRNA and mRNA expression patterns and determining target
296 cleavage via RLM-RACE. To validate the causative relation between sRNA and mRNA
297 expression, sRNA overexpression lines along with mRNA knockout mutants are often
298 analysed by RLM-RACE. To demonstrate that this tedious endeavour can be circumvented

299 with NIL-TDS on stressed plants, we analysed the slice site of *Ath*-miR400 under various
300 stress conditions. Our analysis generated, for the first time, quantitative data that confirmed
301 previous qualitative results. Importantly, this quantitative NIL-TDS read-out of *Ath*-miR400
302 activity might elucidate the significance of target transcript abundances and turnover in plant
303 adaptative signalling to climate stress. It suggests a regularity model in which RNAi-based
304 slicing finetunes transcript levels at high spatio-temporal tissue resolution and compensate
305 for the regulatory less dynamic mRNA biogenesis machinery.

306 **Potential of NIL-TDS for quantitative slicing measurements**

307 Several poorly understood parameters can influence the effectiveness of sRNAs (Diener et al.
308 2023), while off-target effects pose significant challenges in mode-of-action studies of
309 therapeutics and plant protectants. At the same time, computational target prediction
310 algorithms can identify a plethora of potential off-targets (Kern et al.2019), and bioinformatic
311 dsRNA design tools can minimize but not completely avoid off-target activities (Ahmed et al.
312 2020). Off-target alleviation is often attempted by using sRNA pools, either through the
313 usage of long dsRNA, which can produce an array of siRNAs, or by the design of up to 30
314 different sRNAs as an effort to "dilute" off-target effects (Ahmed et al. 2020; Neumeier and
315 Meister 2021). The so called "too many targets for miRNA effect" (TMTME) highlights the
316 prevalence of these issues (Zhang et al. 2021). NIL-TDS can address underlying challenges by
317 detecting even rare off-target events. The generated data sets can be used to further
318 improve target prediction algorithms. In terms of application, NIL-TDS can assist in the
319 development of RNA-based therapeutics and plant protection products by assessing the
320 efficiency of multiple formulations and different degrees of sRNA-target complementarity.

321 **Excessive PCR cycles overamplify exonuclease degradation**

The application of NIL-TDS to an untargeted region of *PPR1* revealed seemingly random peaks in the degradomes of different samples, despite the demonstrated precision of the technique. Such incidences are, to our opinion, the result of the amplification of undirected exonuclease degradation products, which also carry monophosphate-ends. In our efforts to distinguish between true and false signals we successfully developed several strategies. For the de-novo discovery of miR-7162-mediated slicing, we conducted multiple independent replicates, which showed a consistent slicing signal, confirming targeted slicing activity. Additionally, in the case of miR400 and miR-7162, target genes showed a dominant slice site, indicating targeted exonucleolytic cleavage. In the cases of miR-196- and miR400-mediated slicing we could found our conclusions, additionally to the independent replications, on prior knowledge. The most reliable strategy to distinguish true slicing events from random exonuclease products is to perform biological replicates, ensuring that reproducible cleavage sites reflect directed endonuclease activity. Repeating nested PCR reactions across independent samples helps confirm the consistency of true slice sites. While the directed endonuclease slice sites are reproducible, undirected exonuclease products are not. For instance, German et al. (2008) alleviated a similar challenge by knocking-out the responsible nuclease *XRN1* in *A. thaliana* (Benesova et al. 2021).

Flongle provides optimal throughput and read lengths for targeted degradome sequencing

Dynamic development of sequencing technologies provided platforms varying in cost efficiency and throughput. For NIL-TDS, we considered different approaches on different sequencing platforms. We aimed at 50,000 reads per sample to obtain sufficient read-depth saturation for individual targets. Compared to the ONT Flongle, other platforms have critical

drawbacks. While Illumina sequencing by synthesis technology reads are cost competitive on the highest throughput devices (Tab. S2), it faces limitations with long templates. In addition, obtaining short read depths of 50K reads per sample at competitive costs using high throughput NextSeq2000 flow cells would involve the almost infeasible multiplexing of 36K samples (Tab. S2). Additionally, NIL-TDS on Flongle is twice as fast as the iSeq100, and the low cost of the sequencer device makes in-house sequencing affordable and convenient. Together with a simpler and faster library preparation the NIL-TDS workflow is currently the most time and cost-effective solution for targeted slice site analyses in specific transcripts (Fig. 1).

To conclude, NIL-TDS represents notable progress in quantifying sRNA slicing activity and offers an unprecedented increase in read depth compared to traditional methods like RLM-RACE. This increased sensitivity enables the identification of rare slicing events, as demonstrated in the identification of miR-7162-*HOXA10-AS* slice-site, and confirming miR-196-*HOXB8* interactions in human lung carcinoma cells. The accuracy and sensitivity of the method in different eukaryotes was also confirmed by validating minute changes in stress-induced miRNA-mRNA interactions in *Arabidopsis thaliana* quantifying *Ath*-mir400 slicing of PPR1. By utilising the ONT flongle flow cell, NIL-TDS offers a fast, accurate and cost-effective solution for in-house transcript-specific degradation analyses, making it a scalable and competitive alternative to conventional methods.

MATERIAL AND METHODS

Plant material and stress treatment

Arabidopsis thaliana Columbia-0 (Col-0) seeds were grown on vertical square Petri dishes on ½ MS (Murashige and Skoog) media for 14 days in a 22°C day/18°C night cycle (8 h of light) preceded by 2 days stratification at 4°C. Complete seedlings were harvested and placed in a flask with ½ MS liquid media. Heat-treated plants were subject to 37°C temperature for two hours. For salt stress treatment, NaCl concentration was adjusted to 250 mM. Seedlings exposed to a combination of heat and salt stress contained 250 mM NaCl and were subject to 2 h heat at 37°C. Mock seedlings were incubated for 2 h in ½ MS liquid culture and put back in the growth chamber.

Human cell line

A549 (ECACC86012804) cells were grown in DMEM containing Glucose, GlutaMAX and pyruvate supplemented with 100 U/ml penicillin, 100 µg/ml streptomycin and 10% (v/v) fetal bovine serum (all from Thermo Fisher Scientific, USA). The cells were cultured at 37°C and 5% CO_2 in a humidified atmosphere.

RNA extraction from plant material

Whole Arabidopsis seedlings were harvested from ½ MS liquid medium, briefly dried on a soft tissue, shock-frozen in liquid nitrogen, and processed to powder using a tissue lyser (Qiagen Retsch TissueLyser II). Total RNA was extracted using Direct-zol RNA Miniprep (Zymo Research, R2051) according to the manufacturer's instructions with on-column DNase I treatment. RNA concentration was determined using NanoDrop ND-1000 spectrophotometer (Thermo Fisher Scientific, USA), and purity was determined by measuring A260/280 and A260/230 ratios. RNAs were stored at -80°C until further use.

RNA extraction from human cells

For cell lysis, 5 ml of Trizol was added to the human cell line (A549) pellet (50x10^6 cells), and 1 ml was taken for forward RNA extraction. The lysed cells were incubated at room temperature for 5 minutes and then centrifuged at 16,000x g for 1 minute to remove cell debris. The supernatant was transferred to a new tube. 200 µl of chloroform was added, and the cells were vortexed vigorously for 15 seconds, incubated at room temperature for 3 minutes, then centrifuged at 12,000x g for 15 minutes at 4°C. The upper aqueous phase containing RNA was transferred to a new tube. 2x volume of cold 100% ethanol was added, and the sample was incubated overnight at -20°C and then centrifuged at 12,000x g for 10 minutes at 4°C. The supernatant was removed, and RNA pellet was washed with 1 ml of 75% ethanol. The sample was mixed by vortexing and centrifuged at 7500x g for 5 min at 4°C. The washing step was repeated, and all ethanol residues were removed. The pellet was air-dried, and the RNA was dissolved in 50 µl DEPC water.

RNA adapter ligation

Two µg of RNA isolated from both *Ath* plants and A549 human cells were used as a template for ligation with 2 µl 5´RLM-RACE adapter (5'-GCUGAUGGCGAUGAAUGAACACUGCGUUUGCUGGCUUUGAUGAAA-3') [0.3µg/µl] (Eurofins Genomics, Germany). The ligation was performed using T4 RNA Ligase [10 U/µL] and its accompanying reagents (Thermo Fisher Scientific, USA). The reaction mixture contained 1 µl of 10X Reaction buffer, 1 µl BSA [1 mg/ml], 1 µl of T4 RNA ligase, and DEPC water, adjusted to a final volume of 10 µl. The reaction mixture was incubated for 60 min at 37°C in a thermocycler, following Wang et al. (2015). All components were added individually and not in a master mix, with the RNA and the RLM adapter being added last.

Reverse transcription

The total ligated RNA (10 µl) was used directly to generate the first cDNA strand using the RevertAid Reverse Transcriptase (Thermo Fisher Scientific, USA). A master mix was prepared for cDNA generation containing 1 µl of random hexamers [100 pmol/µl], 4 µl of 5X Reaction buffer, 0.5 µl of Ribolock RNase inhibitor, 2 µl of dNTP mix [10 mM], and 1 µl of RevertAid reverse transcriptase (Thermo Fisher Scientific, USA). The volume was adjusted to 20 µl with water. The reaction was run at 25°C for 10 min, 42°C for 60 min, and 70°C for 10 min.

UMI-RLM adapter ligation and reverse transcription

2 µg RNA from A549 human cells were first ligated to a Unique Molecular Identifiers (UMI) adapter (Random RNA Heptamer: 5´-NNNNNNN-3´) [0.3 µg/µl] (Integrated DNA Technologies, USA) in a 10 µl reaction using T4 RNA ligase following the protocol previously described for the RLM adapter ligation. The total UMI ligated RNA product was phosphorylated using 1 µl [10 U/µl] T4 Polynucleotide Kinase Ligation (T4 PNK, New England Biolabs, M0201S), 4 µl PKN Buffer and 5 µl dATPs [10 mM] in a total volume of 10 µl. The mixture was incubated at 37°C for 30 min, followed by an inactivation step at 65°C for 20 min. The phosphorylated UMI-ligated RNA was purified using the RNA clean and concentration kit (Zymo Research, R1017) and eluted in 10 µl nuclease-free water. The entire eluate was then used for RLM-adapter ligation using T4 RNA ligase as previously described in a 15 µl reaction. The resulting UMI-RNA-RLM adapter product was subsequently used to generate the first cDNA strand. Reverse transcription was carried out in a total volume of 25 µl, replacing random hexamers with Oligo dT (16x, 18x, 20x) primer [100 pmol/µl] and in a total volume of 25µl.

Nested PCR

Two rounds of nested hot-start touch-down PCR were performed using outer (first) and inner (second) 5´-RLM-RACE universal primers in combination consecutively with gene outer specific (e.g., PPR1_Target_Outer) and gene inner specific (e.g. PPR1_Target_Inner) primers. GoTaq® G2 Hot Start Master Mix (Promega, M7432) was used for the nested PCR. A master-mix was prepared for both outer and inner PCRs, containing 25 µl of 2X GoTaq® G2 Hot Start Master Mix, 1.5 µl of RLM-Universal Outer/Inner Primer [10 pmol/µl], 1.5 µl of RLM-Outer/Inner-Specific Primer [10 pmol/µl], and 2.5 µl of cDNA or prior PCR product, with the total volume adjusted to 50 µl with water. As a control, PPR1_Non-Target_Outer and PPR1_Non-Target_Inner primers were used for amplification of a non-target site of *PPR1*, replacing PPR1_Target_Outer and PPR1_Target_Inner primers in the reaction. The thermocycler was preheated at 95° C and samples were denatured at 95°C for 5 minutes followed by 18 touch-down cycles of denaturation at 95°C for 30 sec, annealing at 68°C (incrementally decreased by 0.5°C per cycle) for 30 sec, and extension at 72°C for 30 sec. After the first 18 cycles, 20 additional cycles of 30 sec denaturation at 95°C for 30 seconds is performed, followed by annealing at 62°C for 30 seconds and extension at 72°C for 30 seconds. The final extension step is 72°C for 5 minutes, and the reaction is then held at 4°C.

For the human cell line (A549), 3.5 µl cDNA or PCR product from the prior outer PCR reaction was used as a template for the nested PCR. For the human cell line (A549) initial annealing temperature for the touchdown PCR was optimised for 66°C. Inner and outer PCR products were evaluated in a 1% agarose gel and bands from 100 to 1000 bp were excised. Products were cleaned with the Wizard® SV Gel and PCR Clean-Up System (Promega). DNA

457 concentration was measured using Qubit™ dsDNA HS Assay Kit (ThermoFisher Scientific,
458 USA; Invitrogen, USA) and purified PCR products were stored at -20°C until further use. All
459 used oligonucleotides are listed in Table 1.

460 **Table 1: Primer list**

Primer name	Primer sequence
Hoxb8_Inner	GCGCAGACAACAGAACAAAGT
Hoxb8_Outer	AACTCTTCCGCCCTTTTCAGG
HoxA10_Inner	TGGAGTGCTGTGCTGTGTTTA
HoxA10_Outer	AAATGGCCCCTGTCTTCGG
PPR1_Target_Inner	TAGAAGACCGTGAATGCAAAGC
PPR1_Target_Outer	ATTGTAAGTGAATGTGTCACCATCC
PPR1_Non-Target_Inner	CAGAGCAAGAGAGAGTCGAGC
PPR1_Non-Target_Outer	ACTATGCTGGGCTCAAAACCA
PPR1-DNA-Inner-Fwd	CAGAGCAAGAGAGAGTCGAGC
PPR1-DNA-Outer-Fwd	ACTATGCTGGGCTCAAAACCA
PPR1-DNA-Inner-Rev	ACCCATTTGCCAAAAACGTCG
PPR1-DNA-Outer-Rev	GAGCATGTGAAACAACAGACAAAGA
RLM-Universal_Outer	GCTGATGGCGATGAATGAACACTG

RLM-UniversaI_Inner	GAACACTGCGTTTGCTGGCTTTGATG

461

462 **PCR amplification for cDNA control**

463 Two µg of the RNA extracted from *Ath* plants (mock and stress treated) were used for
464 reverse transcription (as previously described) without an adapter ligation step. As a control,
465 two rounds of hot-start touch-down PCR were performed using PPR1_DNA-outer-Fwd and
466 Rev primers (first round) and PPR1_DNA-Inner-Fwd and Rev primers (second round) for the
467 amplification of a *PPR1* amplicon. The GoTaq® G2 Hot Start Master Mix (Promega, M7432)
468 was used for the nested PCR. A master mix was prepared for both outer and inner PCRs. The
469 assembled reaction and the thermocycler program are as described in the nested-PCR
470 section using the mentioned primers (Tab. 1).

471 **Sequencing**

472 Libraries were prepared for 12 - 16 PCR products according to the Ligation sequencing
473 amplicons - Native Barcoding Kit 24 V14 protocol (SQK-NBD114.24)
474 (https://community.nanoporetech.com/docs/prepare/library_prep_protocols/ligation-
475 sequencing-amplicons-native-barcoding-v14-sqk-nbd114-24/) of Oxford Nanopore
476 Technologies (ONT). Libraries were run on an ONT MinION Mk1B device with a flongle
477 adapter on a Flongle Flow Cell (R10.4.1). Libraries were loaded according to Russel (2023).
478 Sequencing data was recorded for 24h with a length cut-off of 20bp as pod5 data.

479 **Bioinformatics**

Sequencing, trimming & alignment. Sequencing raw data was basecalled via the ONT dorado (v0.5.2+7969fab) with a minimal q-score of 12, the kit option SQK-NBD114-24 and the Super Accuracy ("sup") basecalling algorithm. Reads were not trimmed, and a fastq-file was emitted which was subsequently demultiplexed. Quality control was conducted via FastQC v0.12.1 (Andrews 2010). To remove adapters and orient the reads, the RLM-adapter sequence from inner primer binding site to adapter-3'-end (TTTCATCAAAGCCAGCAAACGCA) was used to trim reads with cutadapt v4.2 (Martin 2011) with Python 3.11.6 (Van Rossum and Drake 2018). Correct orientation of reads was ensured by options "--rc" and "--trimmed-only". Trimmed reads were aligned with bowtie2 v2.5.0 (Langmead and Salzberg 2012) in end-to-end mode and score-min set to "L,0,-0.6". Unique molecular identifiers (UMIs) were extracted before alignment and alignments were deduplicated with umi_tools v1.1.6 (Smith et al. 2017).

Analysis & plotting. To analyse the alignments, the bowtie pseudo sam-files were read into R (Team 2014) v4.3.1 via read.delim. Alignments were filtered by flag 16 and afterwards, the alignment start position indicates the slice site. Results were plotted with ggplot2 (Wickham 2024) v3.4.3, ggpubr (Kassambara 2024) v0.6.0 using the palettes of wesanderson (Ram et al. 2024) v0.3.6. An example script is provided as R-Script S1. Genomic tracks were created with Gviz (Hahne and Ivanek 2016) v1.46.1. Track information was either downloaded from UCSC genome browser (Lee et al. 2019) for the human chromosomes (hg38, GCF_000001405.40) via the UcscTrack function or from NCBI RefSeq (O'Leary et al. 2015) for the *A. thaliana* chromosome (GCF_000001735.4) via the makeTxDbFromGFF function from GenomicFeatures (Lawrence et al. 2013) v.1.54.4.

ABBREVIATIONS

NIL-TDS: Native index ligation-based targete degradome sequencing

RLM-RACE: RNA ligase-mediated rapid amplification of cDNA ends

PARE: parallel analysis of RNA ends

HOX: *HOMEOBOX*

ONT: Oxford Nanopore Technology

A549: Human lung carcinoma cells

DECLARATIONS

Availability of data and materials

The data underlying this article are available in the EMBL-EBI European Nucleotide Archive (ENA) at https://www.ebi.ac.uk/ena/, and can be accessed with PRJEB85122. Direct access to sequencing data is provided via: https://ftp.sra.ebi.ac.uk/vol1/run/ERR141/ and the accessions in Table S1.

Competing interests

The authors declare no competing interests.

Funding

This work was funded by the Federal Ministry of Education and Research (grant BMBF FKZ_031B1226A to P.S.), the Deutsche Forschungsgemeinschaft (grant BI316/20-1 to P.S.), and by the Dr. Ernst-Leopold Klipstein Foundation grant to S.N.

Authors´ contributions

Bernhard T. Werner: Conceptualization, Data curation, Formal analysis, Investigation, Methodology, Project administration, Software, Resources, Supervision, Validation, Visualization, Writing – original draft, Writing – review & editing. Sabrine Nasfi: Conceptualization, Funding acquisition, Investigation, Methodology, Resources, Validation, Writing – original draft, Writing – review & editing. Jens Steinbrenner: Conceptualization, Methodology, Writing – review & editing. M. Lienhard Schmitz: Investigation, Resources, Writing – review & editing. Manar Makhoul: Investigation, Methodology, Resources, Writing – review & editing. Patrick Schäfer: Conceptualization, Funding acquisition, Project administration, Resources, Supervision, Writing – original draft, Writing – review & editing

Acknowledgements

We want to thank Markus Schwinn for providing materials and Marek Bartkuhn for scientific discussions.

SUPPLEMENTARY DATA

Supplementary Data will be available on RNA journal online upon publication.

REFERENCES

Ahmed F, Senthil-Kumar M, Dai X, Ramu VS, Lee S, Mysore KS, Zhao PX. pssRNAit: A Web Server for Designing Effective and Specific Plant siRNAs with Genome-Wide Off-Target Assessment. Plant Physiol. 2020;184:65–81.

Andrews S. FastQC: a quality control tool for high throughput sequence data. 2010;1-1.

Barciszewska-Pacak M, Milanowska K, Knop K, Bielewicz D, Nuc P, Plewka P, Pacak AM, Vazquez F, Karlowski W, Jarmolowski A, et al. Arabidopsis microRNA expression regulation in a wide range of abiotic stress responses. Front Plant Sci. 2015;6.

Benesova S, Kubista M, Valihrach L. Small RNA-Sequencing: Approaches and considerations for miRNA analysis. Diagnostics. 2021;11:964.

Bhatlekar S, Fields JZ, Boman BM. HOX genes and their role in the development of human cancers. J Mol Med. 2014;92:811–23.

Bracken CP, Szubert JM, Mercer TR, Dinger ME, Thomson DW, Mattick JS, Michael MZ, Goodall GJ. Global analysis of the mammalian RNA degradome reveals widespread miRNA-dependent and miRNA-independent endonucleolytic cleavage. Nucleic Acids Res. 2011;39:5658–68.

Brest P, Lapaquette P, Souidi M, Lebrigand K, Cesaro A, Vouret-Craviari V, Mari B, Barbry P, Mosnier J-F, Hébuterne X, et al. A synonymous variant in IRGM alters a binding site for miR-196 and causes deregulation of IRGM-dependent xenophagy in Crohn's disease. Nat Genet. 2011;43:242–5.

Cai Q, He B, Kogel KH, Jin H. Cross-kingdom RNA trafficking and Environmental RNAI—Nature's blueprint for modern crop protection strategies. Curr Opin Microbiol. 2018;46.

Chakraborty S, Nath D. A Study on microRNAs Targeting the Genes Overexpressed in Lung Cancer and their Codon Usage Patterns. Mol Biotechnol. 2022;64:1095–1119.

Chen C, Zhang Y, Zhang L, Weakley SM, Yao Q. MicroRNA-196: critical roles and clinical applications in development and cancer. J Cell Mol Med. 2011;15:14–23.

561 De Cesare M, Mwenda M, Jeffreys AE, Chirwa J, Drakeley C, Schneider K, Mambwe B, Glanz K,
562 Ntalla C, Carrasquilla M, et al. Flexible and cost-effective genomic surveillance of P.
563 falciparum malaria with targeted nanopore sequencing. Nat Commun. 2024;15.

564 Diener C, Keller A, Meese E. The miRNA–target interactions: An underestimated intricacy.
565 Nucleic Acids Res. 2023;52:1544–57.

566 German MA, Pillay M, Jeong D-H, Hetawal A, Luo S, Janardhanan P, Kannan V, Rymarquis LA,
567 Nobuta K, German R, et al. Global identification of microRNA–target RNA pairs by parallel
568 analysis of RNA ends. Nat Biotechnol. 2008;26:941–6.

569 Hahne F, Ivanek R. Visualizing genomic data using GVIZ and Bioconductor. In: Methods in
570 Molecular Biology. 2016;10.1007/978-1-4939-3578-9_16.

571 Hu X, Wang Y, Zhang S, Gu X, Zhang X, Li L. LncRNA HOXA10-AS as a novel biomarker and
572 therapeutic target in human cancers. Front Mol Biosci. 2025;11.

573 Jiang S, Wang T, Han Y, Hida T, Afzal MZ, Zhou C, Zhu J, Wang H. Downregulation of
574 homeobox B8 in attenuating non-small cell lung cancer cell migration and invasion though
575 the epithelial-mesenchymal transition pathway. Transl Cancer Res. 2024;13:413–22.

576 Kassambara A. ggpubr: "ggplot2" based publication ready plots.
577 2024;10.32614/cran.package.ggpubr.

578 Kern F, Backes C, Hirsch P, Fehlmann T, Hart M, Meese E, Keller A. What's the target:
579 understanding two decades of in silico microRNA-target prediction. Brief Bioinform.
580 2019;21:1999–2010.

581 Ketting RF. The many faces of RNAI. Dev Cell. 2011;20:148–61.

582 Khalilian S, Imani SZH, Abedinlou H, Omrani M-A, Ghafouri-Fard S. miR-196a in the
583 carcinogenesis and other disorders with an especial focus on its biomarker capacity. Pathol
584 Res Pract. 2024;260:155433.

585 Kilian J, Whitehead D, Horak J, Wanke D, Weinl S, Batistic O, D'Angelo C, Bornberg-Bauer E,
586 Kudla J, Harter K. The AtGenExpress global stress expression data set: protocols, evaluation
587 and model data analysis of UV-B light, drought and cold stress responses. Plant J.
588 2007;50:347–63.

589 Kumar K, Cowley M, Davis R. Next-generation sequencing and emerging technologies. Semin
590 Thromb Hemost. 2024;Thieme Medical Publishers.

591 Langmead B, Salzberg SL. Fast gapped-read alignment with Bowtie 2. Nat Methods.
592 2012;9:357–9.

593 Lawrence M, Huber W, Pagès H, Aboyoun P, Carlson M, Gentleman R, Morgan MT, Carey VJ.
594 Software for computing and annotating genomic ranges. PLoS Comput Biol.
595 2013;9:e1003118.

596 Lee CM, Barber GP, Casper J, Clawson H, Diekhans M, Gonzalez JN, Hinrichs AS, Lee BT,
597 Nassar LR, Powell CC, et al. UCSC Genome Browser enters 20th year. Nucleic Acids Res.
598 2019;10.1093/nar/gkz1012.

599 Llave C, Xie Z, Kasschau KD, Carrington JC. Cleavage of Scarecrow-like mRNA targets
600 directed by a class of arabidopsis mIRNA. Science. 2002;297:2053–6.

601 Martin M. Cutadapt removes adapter sequences from high-throughput sequencing reads.
602 EMBnet J. 2011;17:10.

603 Morgan R, Hunter K, Pandha HS. Downstream of the HOX genes: Explaining conflicting
604 tumour suppressor and oncogenic functions in cancer. Int J Cancer. 2022;150:1919–32.

605 Neumeier J, Meister G. SiRNA specificity: RNAI Mechanisms and Strategies to Reduce Off-
606 Target Effects. Front Plant Sci. 2021;11.

607 O'Leary NA, Wright MW, Brister JR, Ciufo S, Haddad D, McVeigh R, Rajput B, Robbertse B,
608 Smith-White B, Ako-Adjei D, et al. Reference sequence (RefSeq) database at NCBI: current
609 status, taxonomic expansion, and functional annotation. Nucleic Acids Res. 2015;44:D733–
610 D745.

611 Panwar B, Omenn GS, Guan Y. miRmine: a database of human miRNA expression profiles.
612 Bioinformatics. 2017;33:1554–60.

613 Park YJ, Lee HJ, Kwak KJ, Lee K, Hong SW, Kang H. MicroRNA400-Guided Cleavage of
614 Pentatricopeptide Repeat Protein mRNAs Renders Arabidopsis thaliana More Susceptible to
615 Pathogenic Bacteria and Fungi. Plant Cell Physiol. 2014;55:1660–8.

616 Ram K, Wickham H. wesanderson: A Wes Anderson palette generator.
617 2024;10.32614/cran.package.wesanderson.

618 Raman S, Greb T, Peaucelle A, Blein T, Laufs P, Theres K. Interplay of miR164, CUP□SHAPED
619 COTYLEDON genes and LATERAL SUPPRESSOR controls axillary meristem formation in
620 Arabidopsis thaliana. Plant J. 2008;55:65–76.

621 Russell SD. ONT Flongle Flowcell Loading with Q20+ (V14) Chemistry v2. Protocols.io.
622 2023;10.17504/protocols.io.ewov1nm5pgr2/v4.

623 Shabalina S, Koonin E. Origins and evolution of eukaryotic RNA interference. Trends Ecol Evol.
624 2008;23:578–87.

625 Shi Q, Wang D, Ding X, Yang X, Zhang Y. Exosome-shuttled miR-7162-3p from human
626 umbilical cord derived mesenchymal stem cells repair endometrial stromal cell injury by
627 restricting APOL6. Arch Biochem Biophys. 2021;707:108887.

628 Shin C, Nam J-W, Farh KK-H, Chiang HR, Shkumatava A, Bartel DP. Expanding the MicroRNA
629 Targeting Code: Functional Sites with Centered Pairing. Mol Cell. 2010;38:789–802.

630 Sjöstedt E, Zhong W, Fagerberg L, Karlsson M, Mitsios N, Adori C, Oksvold P, Edfors F,
631 Limiszewska A, Hikmet F, et al. An atlas of the protein-coding genes in the human, pig, and
632 mouse brain. Science. 2020;367.

633 Smith T, Heger A, Sudbery I. UMI-tools: modeling sequencing errors in Unique Molecular
634 Identifiers to improve quantification accuracy. Genome Res. 2017;27:491–9.

635 Steri M, Orrù V, Idda ML, Pitzalis M, Pala M, Zara I, Sidore C, Faà V, Floris M, Deiana M, et al.
636 Overexpression of the cytokine BAFF and autoimmunity risk. N Engl J Med. 2017;376:1615–26.

637 Team RC. R: A language and environment for statistical computing. MSOR Connect. 2014;1.

638 Van Rossum G, Drake F. The Python language reference: Release 3.6.4. 2018.

639 Wang C, Fang J. RLM-RACE, PPM-RACE, and QRT-PCR: an integrated strategy to accurately
640 validate miRNA target genes. Methods Mol Biol. 2015;10.1007/978-1-4939-2547-6_16.

641 Wetterstrand KA. DNA Sequencing Costs: Data from the NHGRI Genome Sequencing
642 Program (GSP) Available at: www.genome.gov/sequencingcostsdata. Accessed 07.04.2024.

643 Wickham H. ggplot2: Elegant graphics for data analysis. 2024.

644 Yekta S, Shih I-H, Bartel DP. MicroRNA-Directed cleavage of HOXB8 mRNA. Science.
645 2004;304:594–6.

646 Zhai J, Arikit S, Simon SA, Kingham BF, Meyers BC. Rapid construction of parallel analysis of
647 RNA end (PARE) libraries for Illumina sequencing. Methods. 2013;67:84–90.

648 Zhang S, Cheng Z, Wang Y, Han T. The Risks of miRNA therapeutics: In a drug target
649 perspective. Drug Des Devel Ther. 2021;15:721–33.

650

651 **TABLE AND FIGURES LEGENDS**

652 **Table 1. Primer list.**

653 **Figure 1: Workflow of quantitative NIL-TDS in comparison to qualitative RLM-RACE.**
654 sRNAs trigger RNAi in eukaryotes and can protect plant and human health (A). RNAi
655 generates characteristic 5′-monophosphate RNA ends at RNAi-mediated slice sites that allow
656 specific adapter ligation and detection by RLM-RACE (B-C) and NIL-TDS (B-D). Median ($\tilde{x}$)
657 resolution and indicated turnaround times for each method are based on our experience and
658 published data (Wang and Fang 2015). Only NIL-TDS generates quantitative outputs. Created
659 with BioRender.com

660 **Figure 2. Quantitative NIL-TDS output in human and plant cells.** NIL-TDS-based
661 detection of *HOXB8* slicing by miR-196 in human cells (A), *HOXA10-AS* slicing by miR-7162
662 in human cells (B), and *PPR1* slicing by miR400 in *Arabidopsis thaliana* seedlings (C). Plotted
663 positions are indicated on the genomic tracks, and blue lines mark respective miRNA target

664 sites. Each point shows the number of reads per 1000 total reads, that aligned with their 5′-
665 end to the respective mRNA base position indicating mRNA fragment ends. Arrows indicate
666 the respective slice sites in the plots. Legends show colour-coded stress treatments or
667 repetitions. The alignment between miRNA and target RNA is shown with a green line
668 indicating slice-sites.

669 **Figure 3. Precision of NIL-TDS on a cDNA amplicon.** A nested PCR was conducted using *A.*
670 *thaliana* Col-0 cDNA for the amplification of *PPR1* amplicon from four different stress
671 treatments. Amplicons were sequenced on a nanopore Flongle cell. Start sites of alignments
672 (A). Fraction of reads within the primer start site +/-2 bp (B). Each points shows the number
673 of reads per 1000 total reads, that aligned with their 5′-end to the respective mRNA base
674 position indicating mRNA fragment ends. Bars show the standard deviation between the
675 treatments. Plotted positions are indicated on the genomic tracks, and a blue line marks the
676 miRNA target site.

677 **Figure 4. Comparative NIL-TDS readout of a non-target site of *PPR1* under abiotic**
678 **stress.** NIL-TDS readout of an untargeted site of *PPR1*. Each point shows the number of
679 reads per 1000 total reads, that aligned with their 5′-end to the respective mRNA base
680 position indicating mRNA fragment ends. Stress treatments are indicated by colour (mock
681 (red), heat (green), salt (yellow), and combined (blue)). Plotted positions are indicated on the
682 genomic tracks, and blue lines mark respective miRNA target sites. Positions indicate the first
683 base after the slice-site, which is also the first base after the 5′ RLM-adapter.

684 Figure S1. Effect of deduplication via UMIs. To assess the effect of PCR duplicates on NIL-TDS
685 UMIs were incorporated in the workflow and reads were deduplicated with UMI_tools. Due
686 to PNK1 phosphorylation during library prep, 2,147 reads of the 18,460 generated reads

687 aligned to HOXA10-AS. After deduplication 241 reads remained, confirming prior results.
688 Each point shows the number of reads per 1000 total reads, that aligned with their 5′-end to
689 the respective mRNA base position indicating mRNA fragment ends. The arrow indicates the
690 respective slice site of miR-7162. Colour indicates results before (yellow) and after (blue)
691 deduplication.

692 Figure S2. NIL-TDS-based detection of slicing by miR400 in *PPR1* (Repetition). Plotted
693 positions are indicated on the genomic tracks and a blue line marks the miRNA target site.
694 The number of reads per 1000 total reads (RPK) of total reads corresponding to the
695 respective position of the target RNA are shown. The respective slice sites are indicated by
696 arrows and text. Stress treatments are indicated by colour. The alignment between miRNA
697 and target RNA is shown and a blue line indicates the slice-site.

698 Table S1: Sequencing statistics related to the samples, their quality, read lengths, sequencing
699 depth and the ENA accessions. The table gives information for each library. Total reads are
700 reads for the respective library after demultiplexing. Mean Q is the mean of means of -
701 $\log_{10}$(error rate). SD stands for standard deviation and L for read length. Filtered reads shows
702 the number of reads with a proper RNA adapter.

703 Table S2: Cost and throughput of different sequencing platforms. The here presented costs
704 are the list prices from the manufacturers homepages (January 2025).

705 RScript S1. A script to easily evaluate NIL-TDS data and to produce t-plots.

Conclusion:

This study establishes NIL-TDS as a precise and reliable tool for investigating RNAi-mediated regulation. In stressed Arabidopsis plants, NIL-TDS confirmed and quantified the reduction in slicing activity of PPR1 by *Ath*-miR400, demonstrating its accuracy in detecting sRNA activity. NIL-TDS improves degradome analyses, facilitating the discovery of silencing events and supporting the development of RNA-based crop protection strategies. Beyond plant systems, its applicability extends to human medicine, as demonstrated by the detection of a previously non-quantifiable slicing event such as miR-196-HOXB8 in lung cancer, as well as the identification of a rare undiscovered miR-7162-HOX10A-AS interaction, highlighting the method's potential for studying gene regulation and disease control.

CHAPTER 8 –

Packaged or unpackaged: appearance and transport of extracellular noncoding RNAs in the plant apoplast

(Contribution as first author)

Summary:

This chapter contains the publication "**Packaged or unpackaged: appearance and transport of extracellular noncoding RNAs in the plant apoplast"**, a peer-reviewed comment article on the publication of Zand Karimi H, Baldrich P, Rutter BD, *et al*. 2022 "Arabidopsis apoplastic fluid contains sRNA- and circular RNA-protein complexes that are located outside extracellular vesicles" (Plant Cell 2022;34:1863-81). The publication was accepted by ExRNA journal on May 19, 2022, and published online on May 31, 2022 (DOI:10.21037/exrna-22-11).

Extracellular vesicles continue to attract increasing interest not only in medicine as delivery carriers for drug and RNA-based therapeutics in cancer treatments but also in agriculture, particularly for RNA delivery approaches such as Spray-induced-Gene-Silencing to enhance plant protection. Here, we critically assess the ongoing debate regarding the localisation, transport, molecular interactions, and functional roles of extracellular RNAs, with a focus on how different RNA biotypes are delivered, both inside and/or outside of Extracellular vesicles (EVs).

Editorial Commentary

Packaged or unpackaged: appearance and transport of extracellular noncoding RNAs in the plant apoplast

Sabrine Nasfi, Karl-Heinz Kogel

Institute of Phytopathology, Research Centre for BioSystems, Land Use and Nutrition, Justus Liebig University, Giessen, Germany

Correspondence to: Karl-Heinz Kogel. Institute of Phytopathology, iFZ Gießen, Heinrich-Buff-Ring 26, D-35392 Giessen, Germany. Email: karl-heinz.kogel@agrar.uni-giessen.de.

Comment on: Zand Karimi H, Baldrich P, Rutter BD, *et al.* Arabidopsis apoplastic fluid contains sRNA- and circular RNA-protein complexes that are located outside extracellular vesicles. Plant Cell 2022;34:1863-81.

Received: 30 April 2022; Accepted: 19 May 2022; Published: 31 May 2022.

doi: 10.21037/exrna-22-11

View this article at: https://dx.doi.org/10.21037/exrna-22-11

Here, we discuss the current status of the controversial debate on the localization, transport, molecular interactions, and activities of different types of extracellular noncoding RNAs as highlighted by a new publication (1) of the group of Roges Innes, Indiana University, on RNAs in the apoplastic intercellular washing fluid (IWF) of *Arabidopsis thaliana*.

Since the astonishingly successful development of new vaccines based on ribonucleic acid—better known as RNA—the compound has attracted a lot of attention. In the field of medicine, RNA vaccines are seen as promising drugs for treating serious diseases, such as certain types of cancer and neurodegenerative diseases, and thus receive special public attention. Only a minority is aware of the potentially effective use of RNA technology in agriculture and pest control, even though the alternative has been hotly debated among experts long before the Corona pandemic. Even without the current political disaster, it was clear that global crop yields would have to roughly double in the next 40 years to meet the increasing food and energy demands of the growing population—and this global goal must be achieved in the face of a changing climate and associated extreme weather (2).

Therefore, it is very clear that humanity also will face immense challenges in the area of agricultural production in the coming years. One of the few possible answers from research lies in the knowledge-based development of improved active ingredients that must be highly effective, selective and yet uncompromisingly environmentally compatible and biodiversity-friendly. Biologicals, i.e., natural substances and beneficial microorganisms that meet this requirement for modern agents, are increasingly found in nature today—RNA is one of them. As a highly effective yet very selective Biological, RNA could actually play an important role in crop protection and production (3-6). A fundamental discovery in 2016 was that cotton plants are naturally capable of producing small RNAs (sRNAs), in this case micro RNAs (miRNAs), that inhibit the growth of *Verticillium dahliae*, a fungal pathogen that infects plants and causes Verticillium wilt diseases on many crops (7). Two miRNAs, miR166 and miR159, were exported to the fungal hyphae to target two *Verticillium dahliae* genes encoding a Ca^{2+}-dependent cysteine protease (*Clp-1*) and an isotrichodermin C-15 hydroxylase (*HiC-15*), respectively, both essential for fungal virulence. An earlier discovery had already shown that fungal pathogens also produce sRNA that interact with target genes in the plants and thus weaken the plants' immune system (8). This bidirectional exchange of sRNA was termed cross-kingdom RNAi and requires key enzymes of the RNA interference (RNAi) pathway.

The agronomic relevance of dsRNA was demonstrated in 2006 when Huang *et al.* (9) reported reduced nematode infectivity when root-knot nematodes (RKN) fed on *Arabidopsis thaliana* expressing a 16D10 dsRNA targeting the *16D10* gene that encodes a conserved secretory root growth-stimulating RKN peptide involved in parasitism. That sRNA can indeed travel from a plant to an attacking pathogen was demonstrated in 2010 by Patrick Schweizer's group, and these authors coined the term host-induced gene silencing (HIGS) (10). Transient accumulation of dsRNA and antisense RNA with sequence similarity to

fungal mRNA in plant cells reduced the development of the biotrophic fungus *Blumeria graminis* on barley and wheat leaves. For instance, silencing the fungal effector *Avr10* resulted in reduced fungal development in the absence but not in presence of the corresponding resistance gene *MLa10*.

Since then, the expression of dsRNAs with complementary sequences to genes of pathogens and pests has been used to build resistance in plants to various species of viruses, bacteria, oomycetes, fungi, nematodes and insects (11). However, it is not clear how the sRNAs are transferred between plant and pathogen cells. Considering the literature on RNA transport in mammalian tissues, it is plausible to assume that these extracellular RNAs (exRNAs) must either be tightly associated with RNA-binding proteins or encapsulated in EVs to avoid degradation (12,13). However, whether EVs and/or RNA-binding proteins are required for RNA secretion or movement within the plant apoplast is still controversial (14,15). How plant RNA is taken up by microbial pathogens and pests and whether the uptake process can be improved is an unresolved question that is also critical for agricultural practice. The rapid uptake of topical RNA, resulting in a mechanism called spray-induced silencing (SIGS) (16,17), is a prerequisite for successful use of RNA in crop protection. Nematodes possess the protein SID-1 (Systemic RNA Interference Defective), which enables RNA transmembrane transport and the binding of double-stranded RNA (18). Moreover, some but by no means all insect groups have SID-like transporters, and it is added that dsRNA-degrading nucleases are widespread in insect groups, so that control of insets by topical RNA is concentrated in a few amenable groups (6,19). Fungi most likely do not have such channels. However, treatment of barley leaves with topical RNA resulted in its uptake by the leaf-colonizing *Fusarium graminearum* fungus (16); and leaves and fruits treated with topical RNA also showed reduced symptoms of the grey mould *B. cinerea* (17), suggesting that at least some fungi can take up RNA from the environment. Consistent with this, the uptake mechanism in *Sclerotinia sclerotiorum* occurs through clathrin-mediated endocytosis (CME). RNAi-mediated knockdown of several CME transcripts confirmed the involvement of this cellular uptake process in facilitating RNAi in *S. sclerotiorum* (20).

But what is the uptake mechanism for RNAs produced naturally in plants as cross-kingdom sRNAs or as products of a transgene (HIGS sRNAs)? A summary of the current state of knowledge is shown in *Figure 1*. In a landmark publication, it was reported that cells of *Arabidopsis thaliana* secrete exosome-like extracellular vesicles containing sRNA cargo that can subsequently be detected in the leaf-colonizing grey mold pathogen *Botrytis cinerea* (22). These sRNA-containing vesicles accumulate at infection sites and are taken up by fungal cells. A clear indication of sRNA uptake in this experiment was evidence of their RNAi activity, as they induced silencing of fungal target genes critical for pathogenicity. This EV-mediated RNA transport and delivery, although it seems plausible given the wealth of literature on mammalian EV cargo, is partially challenged by a recent publication by Roger Innes' group (1). In their work they found less evidence of EV-mediated transport claiming that the majority of apoplastic RNAs are not bound to EVs but rather protected by RNA-binding proteins. The starting point of their work was previous findings that the intercellular wash fluid (IWF) of healthy (non-infected) *Arabidopsis thaliana* leaves contains different types of sRNAs, including miRNAs (21–22 nucleotides, nt), small interfering RNAs (siRNAs; 21–24 nt), and less defined tiny RNAs (tyRNAs; 10–17 nt) with unknown functions (23,24). Only the apoplastic tyRNAs copurified with EVs when using a density gradient, while siRNAs and miRNAs were largely missing from density gradient-purified EVs, although they were present in total IWF. The authors interpreted this then to mean that EVs may not be the primary carrier of apoplastic siRNAs and miRNAs (23). They further argued that in light of previous publications, it cannot be ruled out that large RNA-protein complexes copurify with EVs or that RNAs adhere to the surface of EVs, questioning that all RNAs are cargo of EVs. To eliminate extravesicular RNA-protein complexes and RNA adhering to the surface of EVs, most previous work used micrococcal nuclease treatment but refrained from treating purified EVs first with proteases to remove any RNA-binding proteins and then with nuclease to degrade unprotected RNAs. To distinguish EV-bound cargo RNA fractions from non-EV cargo RNA fractions, Zand Karimi *et al.* (1) now isolated IWF of Arabidopsis leaves by centrifugation (P40 fraction), and subsequently treated the pellet first with the protease trypsin and then RNase A, resulting in a strong shift of the portion of these RNAs *vs.* RNA isolated without treatment. Importantly, combined treatment reduced the amount of sRNA dramatically with only a few sRNA species resisting the treatment. A deeper differential expression analysis identified seven miRNAs inside EVs after trypsin and RNase treatment. Interestingly, six of the seven identified miRNAs corresponded to

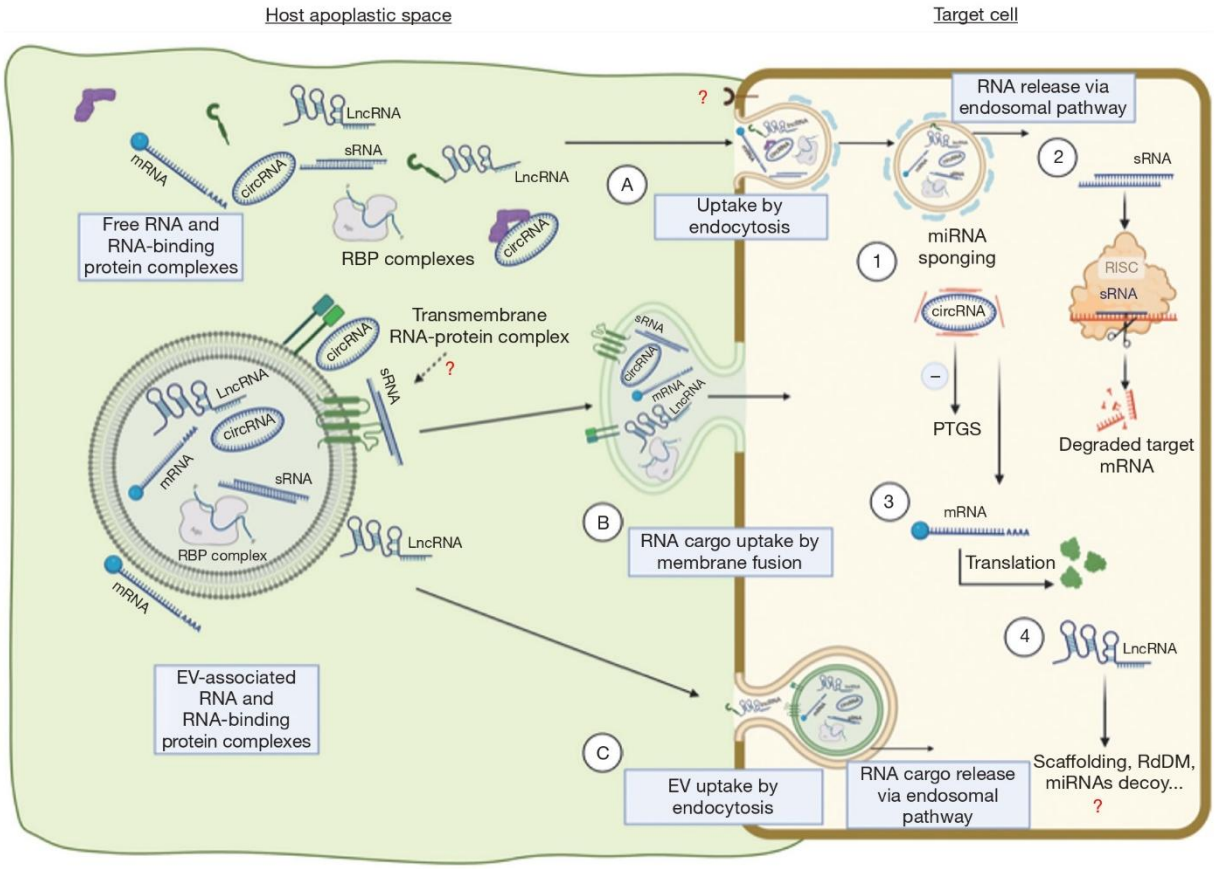

Figure 1 Presumed location, transportation, molecular interactions, and activities of different RNA types in the apoplastic intercellular washing fluid (IWF) of a plant and their uptake into a fungal target cell in cross kingdom communication. Different types of RNAs, including circular RNA (circRNA), long noncoding RNA (lncRNA), mRNA, and small 21- to 24-nt RNA (sRNA) virtually appear (I) as a free molecule or bound to RNA-binding proteins (RBPs) that form RNA-protein complexes; (II) as cargo of extracellular vesicles (EVs) in association with RBPs, or (III) attached to EVs surface through nonspecific interactions or as yet unknown putative RNA-binding molecules, including transmembrane RNA-binding proteins. Uptake of differentially localized RNAs occurs via (A) membrane invagination and clathrin-mediated endocytosis (CME), although a specific receptor for RNA that induces localization of clathrin and its adaptor to the membrane is still unknown in fungi. Acidification of vesicles by vacuolar H+ ATPase in the late endosome induces the release of RNA into the cytoplasm (12), (B) Fusion of EVs with the plasma membrane of the target cell and direct release of RNA into the cytoplasm (13), (C) uptake of EVs, which then follow the endosomal pathway where the cargo is released into the cytoplasm (21). After release into the cytoplasm of the target cell, the different RNA types unfold different mechanisms of action: ① While the complete picture of circRNA function in plants is not known, possible functions include micro RNA (miRNA) sponging, protein expression, and possibly all types of antisense activities. ② sRNAs enter the pathways for post-transcriptional gene silencing (PTGS) or transcriptional gene silencing (TGS). ③ mRNA is translated, and potentially interfering with fungal pathogenesis, and ④ lncRNA is involved in protein scaffolds, RdDM, and possibly miRNA decoys. Note that most of these activities are not well studied in fungi (This figure was created based on the Biorender® licence MG23UYBPCM).

passenger strands of active miRNAs, raising the question if those miRNAs have a role in silencing. The same analysis was applied by focusing on apoplastic trans-acting (tasi) RNAs, including Tas1c_16_461 and Tas2_0_56, that are believed to be involved in cross-kingdom RNAi (22). Consistent with their reasoning, Zand Karimi *et al.* (1) were also unable to detect these tasiRNA after treatment of the apoplastic sample with trypsin and nuclease, so none of

them appeared to be protected and enriched in the EVs. Although the above findings seem comprehensible, it must be pointed out that in the Zamt Karimi reference uninfected Arabidopsis plants were used as biological material; at least it cannot be completely excluded that RNA-loaded vesicles are secreted especially in response to biological stress. Moreover, despite the abundance of current literature, plant research on EVs and exRNA carriers is still very challenged and limited, especially by (I) the heterogeneity of EVs and their RNA cargo (differences between cell types and organs); (II) the sample-to-sample heterogeneity of EVs and other RNA carriers; (III) the differences in the methods used to isolate EVs and other RNA carriers; (IV the differences in sensitivity, specificity, reproducibility, and bias of different RNA profiling methods; and last but not least, the bias in the knowledge of plant EVs due to the predominantly mammalian-focused literature on EVs and their RNA carriers (12).

Of note, further analysis of apoplastic RNA detected both sRNAs and long noncoding RNAs (lncRNAs), including circular RNAs (circRNAs), and these RNAs were highly enriched in the posttranscriptional modification N6-methyladenine (m6A) (1). Consistent with this, the putative m6A-binding protein GLYCINE-RICH RNA-BINDING PROTEIN 7 (GRP7) as well as the sRNA-binding protein AGO2 was found in the IWF. These two proteins coimmunoprecipitated with lncRNAs, including circRNAs. Mutation of GRP7 or AGO2 caused changes in both the sRNA and lncRNA content of IWF, suggesting that these proteins contribute to the secretion and/or stabilization of apoplastic RNA. Previous work already identified already several RNA-binding proteins in the apoplast of Arabidopsis leaves, including AGO1, ANNEXIN1 and 2, and RNA HELICASE11 and 37 (15). However, the exact localization of these proteins, like that of RNA, is unclear, as definitive proof of their localization in EVs would require at least protease protection assays showing that these proteins remain undigested in the presence of trypsin and thus are located within EVs.

The circRNA, now also discovered in IWF from Arabidopsis leaves, is increasingly becoming the focus of research in plant pathology. In mammals, circRNAs were initially associated with their function as miRNA sponges that influence mRNA turnover (25). More recent findings show their function in regulating transcription and translation, sequestering and translocating proteins, facilitating interactions between proteins, and translating to proteins (26). Of note, the RNA base modification m6A, now found in IWF, is known to efficiently initiate translation of circRNAs (27). Cytoplasmic circRNAs can arise from exons (exonic circRNA) (28) and are thus the candidates for secretion into the apoplast. circRNA has also been detected in plants such as rice (*Oryza sativa*) and *Arabidopsis thaliana* (29) and they seem to accumulate in response to biotic stress (30) and abiotic stress, such as phosphate-sufficient and -starvation conditions. Due to the structural stability of the circular form and its potentially multifunctional roles they may play in plant pathogens and pests, circRNAs are promising candidates for agronomical application.

Problems to be solved: future application in crop protection

The use of RNA in agriculture has become a realistic scenario in recent years. Not surprisingly for scientists in this field, GMO approaches such as HIGS have proven to be particularly effective. What does the Zand Karimi paper (1) tell us about the future application of RNA in crop production? While the uptake of RNAi-inducing dsRNA by microbial pathogens and pests from the environment is uncontroversial, questions remain, such as how exactly RNA is transferred from the plant host to a colonizing microbe and what type of (apoplastic) RNAs play a key role in influencing the growth of a pathogenic microbe on its host.

What are the pitfalls that have to be avoided in order to introduce the RNA approach to the market? First of all, the products would need to be taken up more efficiently into the plants and pathogens/pests, even under adverse weather conditions, and the RNA must be protected – as it is under natural conditions by RNA-binding proteins and/or vesicles –over a certain period of time in order to enter the plants without being inactivated. What seems optimal for the environmental effect of RNA, namely its very rapid degradation in arable soil, especially by ubiquitous microorganisms and their RNA-degrading enzymes, the nucleases, is initially a disadvantage for the efficacy of applied RNA in crop protection. Therefore, the greatest challenge in RNA research is to package the RNA to improve its uptake by pathogens and pests. So, as with RNA vaccines, the biggest problem in crop protection is getting the very "sensitive" molecule to its site of action. Analogous to RNA vaccines, packaging the RNA in lipid droplets, for example, could also provide a solution. Moreover, the size and structure of the RNA molecule is critical for uptake by

a pathogen and its RNAi activity (31). In some insects, it has been found that only RNA molecules with more than 60 nt are effective (6). In fungi, the optimal length of RNA molecules to be administered is not well understood. An emerging possibility is the use of circRNA, as this type of RNA is ubiquitous and seems to be more stable and possibly more efficient than dsRNA.

Acknowledgments

Funding: We thank the German Research Foundation (DFG) for supporting our research on RNA in plant-pathogen interactions by granting the DFG research unit RU5116 on exRNA. SN is supported by the Dr. Ernst-Leopold Klipstein-Stiftung, Paderborn, Giessen.

Footnote

Provenance and Peer Review: This article was commissioned by the editorial office, *ExRNA*. The article has undergone external peer review.

Conflicts of Interest: Both authors have completed the ICMJE uniform disclosure form (available at https://exrna.amegroups.com/article/view/10.21037/exrna-22-11/coif). The research has been funded by the Dr. Ernst-Leopold Klipstein Foundation and a publication license was grant to Sabrine Nasfi for use in journal publications. The authors have no other conflict of interest to declare.

Ethical Statement: The authors are accountable for all aspects of the work in ensuring that questions related to the accuracy or integrity of any part of the work are appropriately investigated and resolved.

References

1. Zand Karimi H, Baldrich P, Rutter BD, et al. Arabidopsis apoplastic fluid contains sRNA- and circular RNA-protein complexes that are located outside extracellular vesicles. Plant Cell 2022;34:1863-81.
2. Brooks J, Deconinck K, Giner C. Three Key Challenges Facing Agriculture and How Start Solving Them. 2019. Accessed November 18, 2021. Available online: https://www.oecd.org/agriculture/key-challenges-agriculture-how-solve
3. Cai Q, He B, Kogel KH, Jin H. Cross-kingdom RNA trafficking and environmental RNAi-nature's blueprint for modern crop protection strategies. Curr Opin Microbiol 2018;46:58-64.
4. Taning CN, Arpaia S, Christiaens O, et al. RNA-based biocontrol compounds: current status and perspectives to reach the market. Pest Manag Sci 2020;76:841-5.
5. Fletcher SJ, Reeves PT, Hoang BT, et al. A Perspective on RNAi-Based Biopesticides. Front Plant Sci 2020;11:51.
6. Liu S, Jaouannet M, Dempsey DA, et al. RNA-based technologies for insect control in plant production. Biotechnol Adv 2020;39:107463.
7. Zhang T, Zhao YL, Zhao JH, et al. Cotton plants export microRNAs to inhibit virulence gene expression in a fungal pathogen. Nat Plants 2016;2:16153.
8. Weiberg A, Wang M, Lin FM, et al. Fungal small RNAs suppress plant immunity by hijacking host RNA interference pathways. Science 2013;342:118-23.
9. Huang G, Allen R, Davis EL, et al. Engineering broad root-knot resistance in transgenic plants by RNAi silencing of a conserved and essential root-knot nematode parasitism gene. Proc Natl Acad Sci U S A 2006;103:14302-6.
10. Nowara D, Gay A, Lacomme C, et al. HIGS: host-induced gene silencing in the obligate biotrophic fungal pathogen Blumeria graminis. Plant Cell 2010;22:3130-41.
11. Koch A, Wassenegger M. Host-induced gene silencing - mechanisms and applications. New Phytol 2021;231:54-9.
12. Zhang Y, Liu Y, Liu H, et al. Exosomes: biogenesis, biologic function and clinical potential. Cell Biosci 2019;9:19.
13. O'Brien K, Breyne K, Ughetto S, et al. RNA delivery by extracellular vesicles in mammalian cells and its applications. Nat Rev Mol Cell Biol 2020;21:585-606.
14. Rutter BD, Innes RW. Extracellular Vesicles Isolated from the Leaf Apoplast Carry Stress-Response Proteins. Plant Physiol 2017;173:728-41.
15. He B, Cai Q, Qiao L, et al. RNA-binding proteins contribute to small RNA loading in plant extracellular vesicles. Nat Plants 2021;7:342-52.
16. Koch A, Biedenkopf D, Furch A, et al. An RNAi-Based

Control of Fusarium graminearum Infections Through Spraying of Long dsRNAs Involves a Plant Passage and Is Controlled by the Fungal Silencing Machinery. PLoS Pathog 2016;12:e1005901.
17. Wang M, Weiberg A, Lin FM, et al. Bidirectional cross-kingdom RNAi and fungal uptake of external RNAs confer plant protection. Nat Plants 2016;2:16151.
18. Winston WM, Molodowitch C, Hunter CP. Systemic RNAi in C. elegans requires the putative transmembrane protein SID-1. Science 2002;295:2456-9.
19. Cooper AM, Silver K, Zhang J, et al. Molecular mechanisms influencing efficiency of RNA interference in insects. Pest Manag Sci 2019;75:18-28.
20. Wytinck N, Sullivan DS, Biggar KT, et al. Clathrin mediated endocytosis is involved in the uptake of exogenous double-stranded RNA in the white mold phytopathogen Sclerotinia sclerotiorum. Sci Rep 2020;10:12773.
21. Joshi BS, de Beer MA, Giepmans BNG, et al. Endocytosis of Extracellular Vesicles and Release of Their Cargo from Endosomes. ACS Nano 2020;14:4444-55.
22. Cai Q, Qiao L, Wang M, et al. Plants send small RNAs in extracellular vesicles to fungal pathogen to silence virulence genes. Science 2018;360:1126-9.
23. Baldrich P, Rutter BD, Karimi HZ, et al. Plant Extracellular Vesicles Contain Diverse Small RNA Species and Are Enriched in 10- to 17-Nucleotide "Tiny" RNAs. Plant Cell 2019;31:315-24.
24. Budak H, Kaya SB, Cagirici HB. Long Non-coding RNA in Plants in the Era of Reference Sequences. Front Plant Sci 2020;11:276.
25. Hansen TB, Jensen TI, Clausen BH, et al. Natural RNA circles function as efficient microRNA sponges. Nature 2013;495:384-8.
26. He AT, Liu J, Li F, et al. Targeting circular RNAs as a therapeutic approach: current strategies and challenges. Signal Transduct Target Ther 2021;6:185.
27. Yang Y, Fan X, Mao M, et al. Extensive translation of circular RNAs driven by N6-methyladenosine. Cell Res 2017;27:626-41.
28. Jeck WR, Sharpless NE. Detecting and characterizing circular RNAs. Nat Biotechnol 2014;32:453-61.
29. Zhang P, Li S, Chen M. Characterization and Function of Circular RNAs in Plants. Front Mol Biosci 2020;7:91.
30. Fan J, Quan W, Li GB, et al. circRNAs Are Involved in the Rice-Magnaporthe oryzae Interaction. Plant Physiol 2020;182:272-86.
31. Šečić E, Kogel KH. Requirements for fungal uptake of dsRNA and gene silencing in RNAi-based crop protection strategies. Curr Opin Biotechnol 2021;70:136-42.

doi: 10.21037/exrna-22-11
Cite this article as: Nasfi S, Kogel KH. Packaged or unpackaged: appearance and transport of extracellular noncoding RNAs in the plant apoplast. ExRNA 2022;4:13.

Conclusion:

In this commentary, we discuss the challenges associated with the use of exRNAs in plant protection, focusing on their instability under environmental stress. Rapid RNA degradation in soil, mainly by microbial nucleases and environmental factors (UV, rain, heat...), poses a major barrier. Recent findings reveal that many apoplastic RNAs, including sRNAs and circRNAs, exist outside vesicles but are bound to proteins, suggesting further investigation of alternative stabilisation strategies. Packaging and formulation approaches such as lipid encapsulation, along with the use of circRNAs and optimised RNA structures, could improve the stability, delivery, and efficacy of RNA-based applications in agriculture.

CHAPTER 9 –

Practical advice for extracellular vesicle isolation in plant–microbe interactions: Concerns, considerations, and conclusions

(Contribution as Co-author)

Summary:

This chapter contains the publication **"Practical advice for extracellular vesicle isolation in plant–microbe interactions: Concerns, considerations, and conclusions"** accepted by the journal of Extracellular Vesicles on November 24, 2024, and published online on December 12, 2024 (DOI:10.1002/jev2.70022).

As research interest in plant–microbe EVs grows, researchers often rely on mammalian-developed guidelines (e.g. MISEV), that only partially address plant-specific challenges. Based on current studies and the expertise of the exRNA consortium (RU5116), this guideline provides step-by-step recommendations including experimental design, optimization, quality control, improving yield and purity, and reproducibility of EV isolation from plants and associated microbes.

Received: 12 June 2024 | Accepted: 24 November 2024

DOI: 10.1002/jev2.70022

PERSPECTIVE

Practical advice for extracellular vesicle isolation in plant–microbe interactions: Concerns, considerations, and conclusions

Hannah Thieron[1] | **Laura Krassini**[2] | **Seomun Kwon**[3] | **Sebastian Fricke**[4] | **Sabrine Nasfi**[5] | **Lorenz Oberkofler**[2] | **Alessa Ruf**[2] | **Julia Kehr**[4] | **Karl-Heinz Kogel**[5] | **Arne Weiberg**[2] | **Michael Feldbrügge**[3] | **Silke Robatzek**[2] | **Ralph Panstruga**[1]

[1]Unit for Plant Molecular Cell Biology, Institute for Biology I, RWTH Aachen University, Aachen, Germany

[2]LMU Munich Biocenter, Ludwig-Maximilian-University of Munich, Munich, Germany

[3]Institute for Microbiology, Cluster of Excellence on Plant Sciences, Heinrich-Heine University Düsseldorf, Düsseldorf, Germany

[4]Institute of Plant Science and Microbiology, Department of Biology, Universität Hamburg, Hamburg, Germany

[5]Institute of Phytopathology, Research Centre for BioSystems, Land Use and Nutrition, Justus-Liebig-University Giessen, Giessen, Germany

Correspondence
Ralph Panstruga, Unit for Plant Molecular Cell Biology, Institute for Biology I, RWTH Aachen University, Aachen, Germany.
Email: panstruga@bio1.rwth-aachen.de

Funding information
European Research Council, Grant/Award Number: 884235; Deutsche Forschungsgemeinschaft, Grant/Award Numbers: 433194101, SFB924/3TP15

Abstract

In recent years, extracellular vesicles (EVs) have emerged as novel key players in plant–microbe interactions. While it is immensely useful to draw on the established "minimal information for studies of extracellular vesicles" (MISEV) guidelines and precedents in mammalian systems, working with plants and their associated microbes poses specific challenges. To navigate researchers through these obstacles, we offer detailed step-by-step suggestions for those embarking on EV research in the context of plant–microbe interactions. The advice is based on recent publications and our collective experience from the diverse plant and microbe systems studied in a dedicated research consortium. We provide considerations for experimental design, optimization, quality control, and recommendations on how to increase yield, purity, and reproducibility of EV isolation. With this perspective article, we aim not only to assist researchers in our field but also to promote discussions on plant and microbe EVs in the broader EV community.

KEYWORDS

plant-microbe interactions, EV isolation, EV size profile, EV marker, EV quality control, biological fluid, axenic culture, apoplastic wash fluid

1 | BACKGROUND

Extracellular vesicles (EVs) are central mediators in inter-cellular and inter-organismal communication across diverse biological systems. These membranous structures can be generated and released via different cellular pathways and cell types to the extracellular space (Box 1; Colombo et al., 2014). In the interaction of plants with both pathogenic and beneficial microbes, EVs have garnered significant interest owing to their potential to modulate the relationship between both partners (Cai, Qiao, et al., 2018; Chalupowicz et al., 2023; Wang et al., 2016).

Hannah Thieron, Laura Krassini, and Seomun Kwon contributed equally to the study.

Particle types defined by the minimal information for studies of extracellular vesicles (MISEV) guideline and examples thereof from the field of plant–microbe interactions

Extracellular vesicles (EVs): "Particles that are released from cells, are delimited by a lipid bilayer, and cannot replicate on their own" (Welsh et al., 2024). Example: In samples derived from colonized plants, these can be of plant or microbe origin.
Non-vesicular extracellular particles (NVEPs): "Multimolecular assemblies that are released from cells and do not have a lipid bilayer (non-vesicular extracellular particle fraction" (Welsh et al., 2024). Example: If working with plant samples one might look out for RuBisCo complexes or lipoproteins. For samples originating from liquid cultures, particles from the medium might be contaminants.
Extracellular particles (EPs): "Umbrella term for all particles outside the cell, including EVs and NVEPs" (Welsh et al., 2024). Example: See above as for EVs and NVEPs.
EV mimetic: "EV-like particles that are produced through direct artificial manipulation" (Welsh et al., 2024). Example: Unintentionally generated vesicles derived from cell lysis, for example, by infiltration or centrifugation during apoplastic wash fluid (AWF) isolation.
Artificial cell-derived vesicles (ACDVs): "EV mimetics that are produced in the laboratory under conditions of induced cell disruption, such as extrusion" (Welsh et al., 2024). Example: In the plant field, vesicles sourced from juices or disrupted tissue have also been termed "plant-derived nanovesicles" (PDNVs; Pinedo et al., 2021).

Examples of known and suggested EV markers for plants and plant-colonizing microbes

Plants
- *Arabidopsis thaliana*: PENETRATION1 (PEN1) and PATELLIN1 (PATL1) (Rutter & Innes, 2017), TETRASPANIN8 (TET8) (Cai, Qiao, et al., 2018), EXOCYST COMPONENT OF 70 kDa PROTEIN E2 (EXO70E2) (Wang et al., 2010)
- *Sorghum bicolor*: *A. thaliana* PENETRATION (PEN1) orthologs (Chaya et al., 2024)

Phytopathogenic fungi
- *Botrytis cinerea*: PUNCHLESS1 (PLS1) (He et al., 2023)
- *Colletotrichum higginsianum*: Brain modulosignalin homolog1 (Bmh1) (Rutter et al., 2022)
- *Fusarium graminearum*: Suppressor of Rvs167 mutation (Sur7) (Garcia-Ceron et al., 2021)
- *Fusarium oxysporum* f.sp. *vasinfectum*: Heat shock protein of 70 kDa (Hsp70) (Bleackley et al., 2020)
- *Zymoseptoria tritici*: Suppressor of Rvs167 mutation (Sur7) (Hill & Solomon, 2020)

Phytopathogenic oomycetes
- *Phytophthora sojae*: TETRASPANIN1 (TET1), TETRASPANIN3 (TET3) (Zhu et al., 2023)

Phytopathogenic bacteria
- *Pseudomonas syringae* pv. *tomato* DC3000: Outer membrane protein F (OprF), Ampicillin C (AmpC) (Janda et al., 2023)
- *Xanthomonas oryzae*: ELONGATION FACTOR-Thermo unstable (EF-Tu) (Bahar et al., 2016)
- *Xylella fastidiosa*: Lipase/esterase A (LesA), Motility protein B (MopB) (Nascimento et al., 2016)

Research efforts discerning the composition of EV cargos of plants and associated microbes, at present, typically focus on proteins and various RNA classes, including small RNAs, messenger RNAs, long non-coding RNAs, circular RNAs, and fragments of transfer as well as ribosomal RNAs (Kusch et al., 2023; Kwon et al., 2021; Ruf et al., 2022; Wang et al., 2023). In particular, the bidirectional RNA exchange between plants and microbes has been suggested to tune the interaction in several systems (Cai, Qiao, et al., 2018; Cheng et al., 2023; Dunker et al., 2020; Wang et al., 2016; Weiberg et al., 2013; Wong-Bajracharya et al., 2022) and is serving as a blueprint for the development of novel types of pesticides (Cai, He, et al., 2018). Accordingly, there is an increasing interest in studying EVs and their cargos in the context of plant–microbe interactions, which necessitates suitable EV isolation protocols.

However, EV isolation procedures in plant, microbial, and mammalian systems vary due to differences in physiology (e.g., the presence/absence of a cell wall; Brown et al., 2015) and cultivation. The current lack of recommendations for experimental procedures and documentation standards regarding plant(-microbe) systems in the MISEV (minimal information for studies of extracellular vesicles) guideline hinders reproducibility and comparability across such studies (Welsh et al., 2024). Consequently,

the importance of well-documented and reproducible workflows cannot be overstated, serving as the foundation for robust scientific conclusions. Previous reviews have sought to address these issues for EV isolations from (healthy) plants (Pinedo et al., 2021; Rutter & Innes, 2020). Nonetheless, further refinements and tailored protocols specific to this field are urgently needed, especially for scientists studying plant–microbe interactions.

In this perspective article, we attempt to provide comprehensive support for the establishment and optimization of EV isolation procedures in the context of plant–microbe interactions. Drawing upon recent advancements and novel insights from first-hand experience gained in the context of a dedicated research consortium (Research Unit FOR5116 "exRNA" funded by the Deutsche Forschungsgemeinschaft [DFG]; https://www.biologie.uni-hamburg.de/en/forschung/forschungsverbuende/dfg-ru5116.html), we wish to supply researchers new to this burgeoning field with practical advice to master the complexities of EV isolation. These include hints regarding the cultivation of organisms and the retrieval of biological fluids for EV isolation, the actual EV isolation procedure, and measures for EV quality control. By this, we aim to empower scientists to elucidate the nuanced mechanisms governing potential cross-kingdom plant–microbe communication mediated by EVs or to discover novel potential colonization strategies enabled by EVs.

2 | CULTIVATION AND RETRIEVAL OF BIOLOGICAL FLUIDS FOR EV ISOLATION

Living cells can release EVs into their environment. Depending on the cell type and organism of interest, this environment can be very diverse in the plant–microbe field. Appropriate cultivation of the source organisms significantly influences the experimental EV isolation success. Isolation of EVs typically requires some kind of biological fluid as starting material, which is ideally fully devoid of cells and cellular debris. The latter is usually achieved through filtration (0.22 or 0.45 μm pore size) and low-speed centrifugation of EV-containing samples (reviewed in Pinedo et al., 2021; Rutter & Innes, 2020). Plant samples are typically centrifuged at 10,000 × *g* (Cai, He, et al. 2018; Cai, Qiao, et al., 2018; Regente et al., 2009; Rutter & Innes, 2017), fungal samples between 4000 × *g* and 15,000 × *g* (in some instances by two consecutive cleaning steps; Bleackley et al., 2020; Hill & Solomon, 2020; Kwon et al., 2021; Rutter et al., 2022), and bacterial samples between 4500 × *g* and 10,000 × *g* (Bahar et al., 2016; Janda et al., 2023; McMillan & Kuehn, 2023; Nascimento et al., 2016). In cases involving microbial or liquid plant cultures (e.g., plant cell suspension cultures, plant tissue cultures, or hydroponic systems), EVs can be directly isolated from culture supernatants (De Palma et al., 2020; Janda et al., 2023; Kocholata et al., 2022; Kwon et al., 2021). For whole plants grown in soil or other solid substrates (e.g., mineral composites such as vermiculite or solid media for in vitro cultivation), growth conditions need to be optimized to isolate apoplastic wash fluid (AWF)—a frequently used source for EV isolation from plants approximating the full repertoire of naturally secreted EVs. AWF is a liquid commonly obtained by infiltrating buffer into the intercellular space (apoplast) and subsequent centrifugation of the infiltrated plant specimens to collect the buffer along with (nano-)particles and molecules present in the apoplast (O'Leary et al., 2014).

2.1 | Plants

For plants grown on solid substrates, AWF can be isolated from entire seedlings or adult plants, isolated leaves, and potentially roots, as accomplished in many different plant species (Chen et al., 2022; Kusch et al., 2023; Regente et al., 2017; Rutter & Innes, 2017). Preceding growth conditions notably affect buffer infiltration. For instance, high humidity supports infiltration efficiency, because stomata are wide open (Chincinska, 2021; Rumyantseva et al., 2023). We, therefore, recommend increasing the humidity at least several hours before buffer infiltration by covering plants with a lid. However, it is crucial to note that adjusting humidity levels may alter plant gene expression and hence affect the interaction with any microbes under study (Yao et al., 2023).

Apart from AWF, EVs have also been isolated from the liquid medium of plant cell or tissue cultures (Boccia et al., 2022; Kocholata et al., 2022). On the one hand, this approach reduces potential contaminations due to cell damage through infiltration-centrifugation steps during AWF isolation, and a direct comparison could be used to identify these in AWF samples. On the other hand, plant liquid culture experiments neglect the systemic context and are restricted to systems for which the microbe of study can be co-cultivated. Hydroponic plant systems also offer the possibility to retrieve EVs from the medium but are not necessarily suitable for all types of plant–microbe interactions (De Palma et al., 2020).

Disruptive methods such as tissue blending are unsuitable for EV isolation due to associated contamination from cellular debris. This can lead to the generation of artificial cell-derived vesicles, EV mimetics, which in the plant field, have been termed "plant-derived nanovesicles" (Box 1; Pinedo et al., 2021). In general, the generation of such plant-derived nanovesicles is undesirable in the context of EV isolation. However, comparing their characteristics with those of EVs can support the existence of unique EV profiles. Depending on the plant species, obtaining sufficient AWF volume for EV isolation can be challenging. To enhance AWF yield, we suggest employing young(er) plants with soft(er) tissue and optimising buffer infiltration with an efficient vacuum pump (employed vacuum typically between 25 and 45 kPa; Figueir et al., 2018; Regente et al., 2008). Vacuum infiltration is followed by a very low-speed centrifugation step. Applied centrifugation forces range between 400 and 900 × *g* depending on

the plant species (Cai, Qiao, et al., 2018; Regente et al., 2008; Rutter & Innes, 2017). We do not recommend exceeding 900 × *g* unless a higher force is necessary to obtain the fluid (Lohaus et al., 2001). Further, customized growth conditions are proposed to find the best balance between plant age and leaf size—larger and younger leaves will yield more AWF than smaller or older leaves (Chen et al., 2022). Significant scale-up may be necessary for sufficient AWF (and thus EV) yield, especially when microbial EVs should be co-enriched. In cases where infiltration is aggravated due to high lignin content or cuticular waxes, one might consider using low amounts of a non-ionic detergent (e.g., Tween 20) in the infiltration buffer to break surface tension (Nouchi et al., 2012). If the EVs are stable, this treatment is unlikely to affect their integrity and might aid their stability during storage (van de Wakker et al., 2022). However, attention should be paid when performing measurements of the zeta potential (an indicator of particle surface charge) as it might be altered (Midekessa et al., 2020).

We further advise assessing cell viability of infiltrated plant tissue post-AWF isolation, for example, using trypan blue staining to visualize potential damage (e.g., dead cells; Mulaosmanovic et al., 2020) and/or inspect the retrieved AWF by microscopy for organelle debris potentially released because of cell injury during its isolation. At the molecular level, immunoblotting of AWF samples with antibodies targeting abundant intracellular proteins (e.g., of endomembrane or cytoplasmic origin, e.g., chloroplast components) should complement these efforts to validate proper AWF isolation. In principle, such cellular content could also result from organelle secretion, which has been described recently for animal cells (Suh & Lee, 2024). However, although we cannot exclude the possibility that certain plant species or cell types may secrete organelles, this has not been reported to the best of our knowledge. Hence, we consider any organelle debris detected in AWF samples rather a putative byproduct of the unavoidably harsh conditions of the isolation process. Recurring cytoplasmic contamination is often indicated by green (chlorophyll-based) coloration in the case of leaf-derived AWF. In such instances, we recommend streamlining the AWF isolation to minimize the damage to the plant material. This may include selecting an infiltration buffer that does not compromise cell integrity, as do high detergent or non-isotonic salt concentrations; opting for the lowest effective infiltration time; centrifuging as slowly and shortly as possible; and handling the plant samples with great care (avoid agitation and tissue damage). Special attention is warranted when working with plants infected by necrotrophic or hemibiotrophic pathogens, which cause cell damage and tissue lesions during pathogenesis. In these instances, AWF should be preferably collected at the early infection stage before necrotic lesions occur. The above-outlined methods can be used to confirm that pathogen growth has not yet compromised plant cell integrity.

2.2 | Culturable microorganisms

Several plant-associated microbes can be cultivated in vitro. While EVs from microbial axenic cultures (i.e., cultures in the absence of the plant) are most likely not equivalent to those produced during interaction with their plant hosts, the relative ease of handling and scalability are advantageous for an initial survey of EV characteristics and EV-associated molecules.

As outlined above for plants, the first step is choosing appropriate growth conditions since these can impact EV production and EV cargo (Jonca et al., 2021; McMillan & Kuehn, 2023; Welsh et al., 2024). It is further important to consider the microbial growth or developmental stage at the time point of EV isolation and any potential factor that may impinge on the physiology and cellular activities. EV biogenesis and the permeability of cellular barriers, such as the microbial cell wall, can vary greatly depending on the cellular morphology influenced by the growth conditions. Furthermore, the biological functions of EVs can differ depending on the microbial growth stage (Saad et al., 2024) and lifestyle (Johnston et al., 2023). The latter can be influenced by growing the microbes in liquid media or on agar plates for biofilm formation, and EVs can be isolated from both conditions (Janda et al., 2023). Multicellular growth forms such as bacterial biofilms or mycelia of fungi and oomycetes may increase the heterogeneity of EVs. For mycelia, EV diffusion into the medium can be hindered, for example, by the cell wall (Rutter et al., 2022). Because of the aforementioned variability, experimental details such as nutrient composition and pH of the culture medium, aeration/rotation, cultivation time, growth phase, and temperature should be well documented and reported to increase reproducibility (Welsh et al., 2024).

Opting for liquid culture over colonized plant materials is usually a compromise between relevance to the biological question and EV yield. In some systems, culture conditions can be adjusted to allow the microbial cells to simulate developmentally and transcriptionally certain stages of plant colonization, for example, by the addition of plant extracts or dedicated salts (Kwon et al., 2021; Li et al., 2022). Moreover, there are media known that resemble specific plant locations, such as the apoplast (Rico & Preston, 2008) or xylem (Hiery et al., 2013; Neumann & Dobinson, 2003), or that trigger virulence in phytobacteria (Wengelnik et al., 1996) or mimic symbiotic conditions (Li et al., 2022). It is helpful to understand, for example, based on existing transcriptomics or proteomics data, to what extent a given culture condition simulates the situation *in planta*. If -omics resources are limited for testing different conditions, one could use expression levels of hallmark genes for colonization that are specifically upregulated during certain infection stages as an indicator of whether the growth conditions mimic the *in planta* situation. We propose using defined media composition for microbial cultures instead of complex media with ill-defined components of natural origin, such as yeast extract, which may contain EV-like nanoparticles. Contamination from such components can be reduced by filtration or ultracentrifugation, similar to how blood sera are particle-depleted before their addition to mammalian cell cultures (Lehrich et al., 2021). The potential effect of this procedure on the growth of the microorganisms should be, however, assessed carefully.

If unavoidable, the unconditioned complex medium should be included in all experiments as an important negative control for comparison (Welsh et al., 2024).

Any optimization to increase the viability and the intactness of the EV-secreting microbes during culture and harvesting of conditioned media would reduce the contamination by EV mimetics (Box 1). In general, high cell viability (commonly ≥95%, certified by vital staining) at the time point of EV isolation is advised (Shekari et al., 2023). However, a compromise may be necessary to increase the EV yield. For example, starvation (Debbi et al., 2022) or cell wall stress (Olicón-Hernández et al., 2015) may increase the release of EV-like particles (Box 1). In some fungi, such as *Colletotrichum higginsianum*, it may be necessary to use cell wall-degrading enzymes to break apart the mycelium partially and to release EVs from the paramural space (Rutter et al., 2022). We recommend taking such steps with caution, because several studies have demonstrated that the vesicle cargo of some bacterial and fungal species is influenced by nutrient availability (Bahar et al., 2016; Dauros Hill & Solomon, 2020; Hong et al., 2019; McMillan & Kuehn, 2023; Singorenko et al., 2017). It must also be noted that many commercially available protoplasting enzyme preparations tend to be crude mixtures with additional proteinase and RNase activities and are often derived from fungi, which may confound any -omics analyses of fungal EVs. While such organism-specific treatments may be necessary to yield sufficient EV quantities, it is important to address the potential consequences on the cellular status, the occurrence of putative contaminants, and the biological relevance of the EVs obtained.

Prior to EV isolation, microbial cells must be removed from the culture medium. This can be achieved by centrifugation and/or filtration. Centrifugation time and force, as well as filtration pressure, should be reduced as much as possible to prevent cell lysis and minimize changes in cell physiology. At this point, defined aliquots of the cells should be snap-frozen for later comparison with the isolated EVs. This can be done by an immunoblot or gene expression analysis via quantitative reverse transcriptase-polymerase chain reaction (qRT-PCR), for example. To address any putative contamination of the EV preparations with living cells, it is suggested to introduce streak controls of the samples on a solid medium. These should take place instantly after the removal of microbial cells from the liquid culture and after obtaining the crude EV suspension. A quick quality control via microscopy and, optionally, organelle staining, would be beneficial to address contamination from dead or lysed cells before proceeding with EV isolation. It should be noted, though, that certain organisms may secrete organelles, similar to various animal cell types that recently have been reported to secrete mitochondria (Suh & Lee, 2024), which would render such organelles unsuitable as markers for cell lysis. If cellular, non-EV marker proteins are already known, an aliquot from each step in preparing the biological fluid and EV isolation can be tested for cellular contamination by immunoblotting.

3 | EV ISOLATION

Once the biological source fluid (e.g., AWF or culture medium) has been obtained and cleared of cellular material, EV isolation can proceed. The methods published for the isolation of EVs from plants, plant-colonizing microbes, and colonized plants include a combination of differential ultracentrifugation, ultrafiltration, size exclusion chromatography, and density gradient centrifugation (Bleackley et al., 2020; Cai, Qiao, et al., 2018; Janda et al., 2023; Kwon et al., 2021; Regente et al., 2017; Rutter & Innes, 2017). We encourage researchers to explore diverse methods used in the plant–microbe field, especially if generating sufficient quantities of biological source fluid is critical (Rutter et al., 2022). In these instances, scientists might consider a low specificity/high recovery approach such as a precipitation (polymer)-based method to obtain more EVs in the crude pellet (Welsh et al., 2024). For detailed considerations on designing a suitable differential ultracentrifugation protocol, we refer to the review by Rutter & Innes (2020). It should be noted that the appropriate procedure depends on the size and density of EVs of the targeted organism(s), which may differ between biological fluids obtained from uncolonized and colonized plants. Thus, centrifugation force and rotors should be selected with great care as this might influence the accumulation of different EV subclasses or even contaminants (Box 1), making it necessary to establish the ideal rotor type for the given system. Fixed angle rotors have a higher pelleting efficiency (lower k-factor) compared to swing-out rotors that hold equivalent sample tube volumes and, therefore, may be more suitable for obtaining the crude EV pellets from a larger volume of starting biological fluid, while swing-out rotors are essential for density gradients. For a detailed overview of the effect of rotor types on EV isolation, we refer the readers to a previous study (Cvjetkovic et al., 2014). Common centrifugation forces are between 40,000 and 100,000 × *g* in the case of plants and fungi (Bleackley et al., 2020; Cai, Qiao, et al., 2018; Hill & Solomon, 2020; Kwon et al., 2021; Regente et al., 2009; Rutter & Innes, 2017; Rutter et al., 2022), and between 31,000 and 150,000 × *g* in case of bacteria (Bahar et al., 2016; Janda et al., 2023; McMillan & Kuehn, 2023; Nascimento et al., 2016). In general, centrifugation time should be minimized as prolonged centrifugation time can lead to the accumulation of impurities (Box 1), cause artifacts, and might affect EV integrity (Cvjetkovic et al., 2014). Typical centrifugation times for an EV pelleting step (in some instances several runs are performed) are usually 60 min for plant AWF (Cai, Qiao, et al., 2018; Regente et al., 2009; Rutter & Innes, 2017), between 60 and 90 min for fungal cultures (Bleackley et al., 2020; Hill & Solomon, 2020; Kwon et al., 2021; Rutter et al., 2022), and between 90 and 180 min for bacterial cultures (Bahar et al., 2016; Janda et al., 2023; McMillan & Kuehn, 2023; Nascimento et al., 2016). Purification of crude EV pellets obtained by any of the abovementioned methods is recommended, particularly for explorative downstream analyses such as any -omics approaches and should exploit different physical and biochemical properties than the initial EV isolation procedure (Welsh et al., 2024).

A specific challenge when isolating EVs in the context of plant–microbe interactions is distinguishing between the EVs originating from the different organisms or even separating them physically. In the case of bacterial OMVs, researchers might benefit from recent advancements. For example, a fluorescent probe sensitive to outer membrane vesicles (OMVs) with aggregation-induced emission (AIE) characteristics that could aid in distinguishing between plant and bacterial EVs has been reported lately (Wang et al., 2023). Alternatively, the separation of OMVs from plant EVs in a mixture could, at some point, be facilitated by targeting bacterial lipopolysaccharides exploiting a secreted effector protein of the bacterial species *Cupriavidus necator* (Hofer, 2021). If technically possible, the separate characterization of plant- and microbe-derived EVs enables the assessment of changes that occur during plant colonization. This can be, for example, achieved by measuring the zeta potential, which in addition to EV size, can reveal differences in EV surface charge (see below; Janda et al., 2023). It is important to note that isolating EVs from the natural interaction site rather than from (co-)cultivated plants and microbes may allow for conclusions with higher biological relevance. Allocation of EV-associated molecules is possible if reference datasets are available for each organism, even when no specific EV markers (see below) have been identified yet. If desired, plant- and microbe-derived EVs may be separated by immunoaffinity capture or fluorescence-activated cell sorting (He et al., 2021; Kondratov et al., 2020). However, for these procedures, reliable EV biomarkers and suitable antibodies are required, which remain an exception for many species (as discussed below). Particularly for obligate biotrophic microbes, which cannot be cultivated without their host plant, the establishment of EV biomarkers would be highly desired to capture microbe-derived EVs from the colonized plant tissue.

4 | EV QUALITY CONTROL PARAMETERS

To characterize isolated particles and to verify if these are genuine EVs (see Box 1 for alternative particle categories), we recommend three types of analysis: (1) an estimation of EV particle size and concentration measurements, (2) visual inspection by electron microscopy, and (3) molecular analysis for the presence of EV biomarker proteins. In agreement with the MISEV guideline, we advise to use at least two of these independent yet complementing methods (Théry et al., 2018; Welsh et al., 2024).

4.1 | EV size profiles and concentration

Common single particle-based methods to analyse the size and concentration of nanoparticles in plant EV samples are nanoparticle tracking analysis (NTA) and dynamic light scattering (Welsh et al., 2024). To measure the sample concentration, NTA is a popular method since besides the concentration, it determines the size profile and, depending on the manufacturer, the zeta potential, which represents the overall electric charge of the EV's surface (Varga et al., 2020; Welsh et al., 2024). Both, changes in the zeta potential and the size profile in EV samples derived from infected plants as compared to uncolonized plants and microbial EVs can be a hint for the co-presence of plant and microbial EVs (Janda et al., 2023). Nonetheless, NTA does not distinguish between EVs and other spherical particles (Box 1) such as bigger protein complexes. Further, the concentration of smaller particles such as EVs in polydisperse samples might be underrepresented due to the intense light scattering of larger particles, preventing smaller particles from being tracked (Filipe et al., 2010). Newer NTA generations include lasers to detect EV particles via a fluorescence light detector. If available, measuring EVs with fluorescently labelled biomarkers (see below) or staining of EVs with lipophilic dyes or probes prior to the measurement can enable a more precise estimation of the EV size profile and concentration, as fewer non-EV or non-lipid contaminants, respectively, will be measured. However, it is crucial to include appropriate controls, such as buffer only, to demonstrate that unbound dye has been removed from the sample. Of note, the binding of antibodies or the intercalation of membrane dyes could lead to a distortion of the actual particle size (Varga et al., 2020). One also has to consider that NTA and dynamic light scattering measure, in fact, the hydrodynamic diameter and provide an overestimation of the actual EV diameter, which has to be taken into account when comparing it with size estimates from electron micrographs (Varga et al., 2020). We, therefore, encourage researchers to explore also advanced single-particle analysers (e.g. nanoflow cytometry or microfluidic resistive pulse sensing) that at present are not commonly used in the field.

The EV quantity can also be derived based on the total lipid, protein, or nucleic acid content (Bahar et al., 2016; McMillan & Kuehn, 2023; McMillan et al., 2021). For protein concentration measurements, commonly used methods are the Bradford assay or staining with bicinchoninic acid (BCA). However, the respective substances also react with reducing sugars and phospholipids and do not discriminate contaminants from EVs (Théry et al., 2018). The total lipid content is typically quantified by staining EVs with lipid dyes such as FM4-64, DiOC6, and DiR, followed by fluorescence intensity measurements (Rutter & Innes, 2017). Some dyes stain nucleic acids, such as RiboGreen, or the RNA dye SYTOTM RNASelectTM (Fortunato et al., 2021). While the single-particle-based techniques can give further information on different EV (sub-)populations by measuring size, such differences cannot be revealed by quantifying total lipid, nucleic acid, or protein concentrations (Welsh et al., 2024).

4.2 | Morphology

Electron microscopic techniques are the method of choice to characterize the morphological features of EVs. In addition, electron microscopy can provide information about the purity of EV samples and the potential occurrence of different EV (sub-)populations (Bahar et al., 2016; Janda et al., 2023; McMillan et al., 2021; Rutter & Innes, 2017). Currently, the most precise albeit tedious approach is cryo-electron microscopy (Chernyshev et al., 2015; Skliar et al., 2018). Other frequently used electron microscopic techniques like transmission or scanning electron microscopy will underestimate the diameter of EVs as these will desiccate in the process of sample preparation (Bachurski et al., 2019; Chuo et al., 2018). In transmission electron micrographs, EVs typically appear as cup-shaped structures (Panagopoulou et al., 2020; Rutter et al., 2020), whereas in scanning electron micrographs, EVs are usually spherical blebs (Chernyshev et al., 2015; Janda et al., 2023). Attention should be given when the electron micrographs reveal impurities such as flagellar structures when working with bacterial EVs (Janda et al., 2023) or organellar structures when working with plant or fungal samples as they are indicators of impurities. These contaminants can have severe effects on any downstream experiments and it might be necessary to optimize the purification process before proceeding with further analyses.

4.3 | EV biomarkers and molecular cargo

There are ongoing efforts to establish suitable EV markers in the plant(-microbe) field. EV biomarkers are molecules (in particular proteins) that are characteristic of EVs or EV sub-types of a given organism (Welsh et al., 2024). They can significantly improve the EV quality and quantity assessment, might allow for EV purification via immunoaffinity capture, and increase the portfolio for experimental downstream analyses (He et al., 2021). We encourage following the MISEV guidelines regarding the recommendation to establish at least two different positive EV biomarkers. Ideally, one of these should be an integral membrane or glycosylphosphatidylinositol (GPI)-anchored protein (or outer membrane for Gram-negative bacteria) and the other a cytosolic (or periplasmic for Gram-negative bacteria) protein with lipid- or membrane protein-binding ability. It is advised to establish additionally one negative marker, which could be a common co-isolated contaminant, for example, a constituent of non-vesicular extracellular particles (Théry et al., 2018; Box 1). Moreover, a proper EV biomarker should be abundant in the EV fractions for easy and reliable detection.

For finding organism-specific EV markers, there is a benefit in using organisms that can be grown in liquid culture, as EVs are obtained from a single species and it is easier to avoid contaminations from lysed cells due to handling. For obligate parasites or symbionts, the mixture of EVs obtained and the potential homology of proteins and nucleic acids in mixed samples may complicate the analyses. A first step to establish a new EV biomarker might be a proteomic survey, which can provide a list of candidate proteins. Such data can be used to select candidates that show potential relevance for plant–microbe interactions (e.g., association of a protein with a nucleic acid of interest; Cai, Qiao, et al., 2018), or that have homology to established marker proteins in other biological systems. Currently, there are only a handful of commonly tested EV markers in the field, including a homolog of human tetraspanin CD63 in the dicotyledonous reference plant *Arabidopsis thaliana* (TET8; Cai, He, et al., 2018; Cai, Qiao, et al., 2018; Box 2). Orthologs of well-established mammalian EV markers such as tetraspanins are absent in certain fungi and bacteria, but other biomarker proteins have been suggested for these organisms (Box 2). Larger collections of EV proteomics data such as Vesiclepedia or EVpedia (Chitti et al., 2024; Kim et al., 2015), which also include established EV biomarkers, can help deciding which candidate protein(s) to select.

If specific antibodies are available or epitope-tagged protein variants can be expressed, the candidate list can be further narrowed down based on protease protection or immunoaffinity capture assays to gain information on which proteins are rather inside the EV lumen than only loosely associated with the EV surface (forming the so-called EV corona; Heidarzadeh et al., 2023). Particularly useful would be an EV-associated integral membrane protein with both an "extracellular" and "cytosolic" terminus. These termini could be labelled by genetic engineering with a reporter tag on the luminal side (e.g., for EV quantification) and with an epitope tag on the extra-vesicular side (e.g. for immunoaffinity capture). However, such an approach requires the genetic manipulation of the organism(s) of interest to express labelled EV markers, which is not always possible.

Protease protection assays are commonly used to determine the localization of EV-associated proteins. They are based on the proteolytic digestion of EV-associated proteins in the presence or the absence of an EV-disrupting detergent (Cvjetkovic et al., 2016). A typical protease protection assay would include EVs treated with buffer-only, protease-only, detergent-only, and protease with detergent. Harsh protease treatments may compromise the integrity of EVs and could lead to false results where even intraluminal proteins are degraded (Foers et al., 2018). Therefore, we highly recommend including the detergent-only control. If, for example, luminescence originating from EVs with luciferase-tagged intraluminal proteins increases with the detergent-only control but disappears upon protease treatment, the protease concentration should be reduced (Bonsergent et al., 2021). If there is already evidence suggesting that the protein of interest is a cargo, a less invasive alternative to determine the localization might

be immunoaffinity capture or immunogold labelling. However, EVs will only be able to bind to the solid phase or be markable if the epitope for the antibody is present on the outside of the EV.

A similar approach could be used for EV-associated nucleic acids (nuclease protection assay). Many EV-associated nucleic acids are protected by proteins (He et al., 2021). Hence, addition of a protease might be necessary in addition to the nuclease to access the nucleic acid for digestion (Zand Karimi et al., 2022). This setup increases the complexity of required controls further. Protease and nuclease treatments should be carried out on fresh EVs and may require a washing step to remove the respective hydrolytic enzyme sufficiently. Therefore, these would be performed immediately after obtaining a crude EV preparation, before further purification. As some proteins can be associated with the EV corona but still be relevant for the plant–microbe interaction, it may be important to optimize protease treatment to suit the biological question at hand. If it is not possible to generate transgenic organisms that express tagged EV markers, surface labelling with membrane-impermeant biotinylation reagents may help distinguishing internal and external cargo (Cvjetkovic et al., 2016).

4.4 | Controls

Stepwise quality checks are necessary during optimization and troubleshooting of an EV isolation protocol. The effect of altering each step in the protocol should be assessed by the above-mentioned approaches. While this may be a tedious process, it is necessary for maximising the EV yield (as opposed to other EV-like particles, Box 1), assessing suitable storage conditions, or decreasing intracellular and other contaminants. During initial method establishment and troubleshooting for sources of contamination, it is useful to include the liquid medium (if any), buffers, or even filtered distilled water as negative controls to determine the extent of nanoparticle contamination derived from the materials, equipment, and handling. It is further important to assess for contaminants following the removal of cells from the medium or AWF, and also after subsequent centrifugation or filtration steps. If ultracentrifugation is used to pellet EVs, then it may be informative to examine the supernatant for EVs, especially if the EV pellet is loose or difficult to see. It is not uncommon to deal with EV pellets that are not visible to the naked eye. If ultrafiltration is used to concentrate the samples, it is worth testing for EVs bound to the membrane or eluting with the filtrate. The same ideas apply to immunoaffinity capture, where one would compare the input crude EVs, the supernatant after each wash step, the eluate, and the beads after elution.

In the mammalian field, EVs are typically stored for longer periods at −80°C; however, preserving EV integrity during storage remains a matter of debate (Görgens et al., 2022). Similarly, experience within the Research Unit FOR5116 has revealed that the suitability for EV storage greatly depends on the source organism and is generally improved when so-called low-bind tubes are used (Evtushenko et al., 2020). We recommend initially comparing stored EVs that have undergone freeze-thawing and fresh EVs for their intactness (e.g., by transmission electron microscopy or NTA), content (e.g., by Bioanalyzer-based nucleic acid profiling), and biological activity (e.g., by enzymatic or other functional assays). EV storage conditions are dependent on the purpose and the biological question at hand. Generally, measurements of morphology, biophysical size and concentration, for example, by NTA or electron microscopy, should be performed with fresh EVs, which we propose to store short-term (e.g., overnight) at 4°C with gentle rotation, if necessary. However, it may be possible to snap-freeze freshly prepared EV samples for subsequent protein and nucleic acid analyses, for example, in case it is challenging to extract EV content on the same day that the EVs are obtained. Ideally, freshly prepared EVs are directly used for protein or nucleic acid extraction up to a point where the samples are safe for storage.

5 | CONCLUDING REMARKS

Here we present a practical proposal for establishing EV work in the field of plant–microbe interactions (see Figure 1 for a proposed workflow and Table 1 for a synopsis of questions and recommendations). While the existing MISEV guidelines and resources from the mammalian field are highly informative, the diversity and complexity of our systems, comprising two interacting organisms, present specific challenges. There are no one-size-fits-all solutions for striking a balance between sufficient EV yield and purity and identifying specific molecular markers. We encourage scientists to be creative to bypass these obstacles. At the same time, adapting protocols to the EV research in the context of plant–microbe interactions, the thorough use of controls, and precise documentation are essential for creating new field-specific standards. An open exchange of challenges and solutions can help the plant–microbe EV field to grow in the future.

AUTHOR CONTRIBUTIONS

Hannah Thieron: Conceptualization (equal); visualization (lead); writing—original draft (equal); writing—review and editing (equal). **Laura Krassini**: Conceptualization (equal); writing—original draft (equal); writing—review and editing (equal). **Seomun Kwon**: Conceptualization (equal); writing—original draft (equal); writing—review and editing (equal). **Sebastian Fricke**: Conceptualization (supporting); writing—review and editing (supporting). **Sabrine Nasfi**: Conceptualization (supporting);

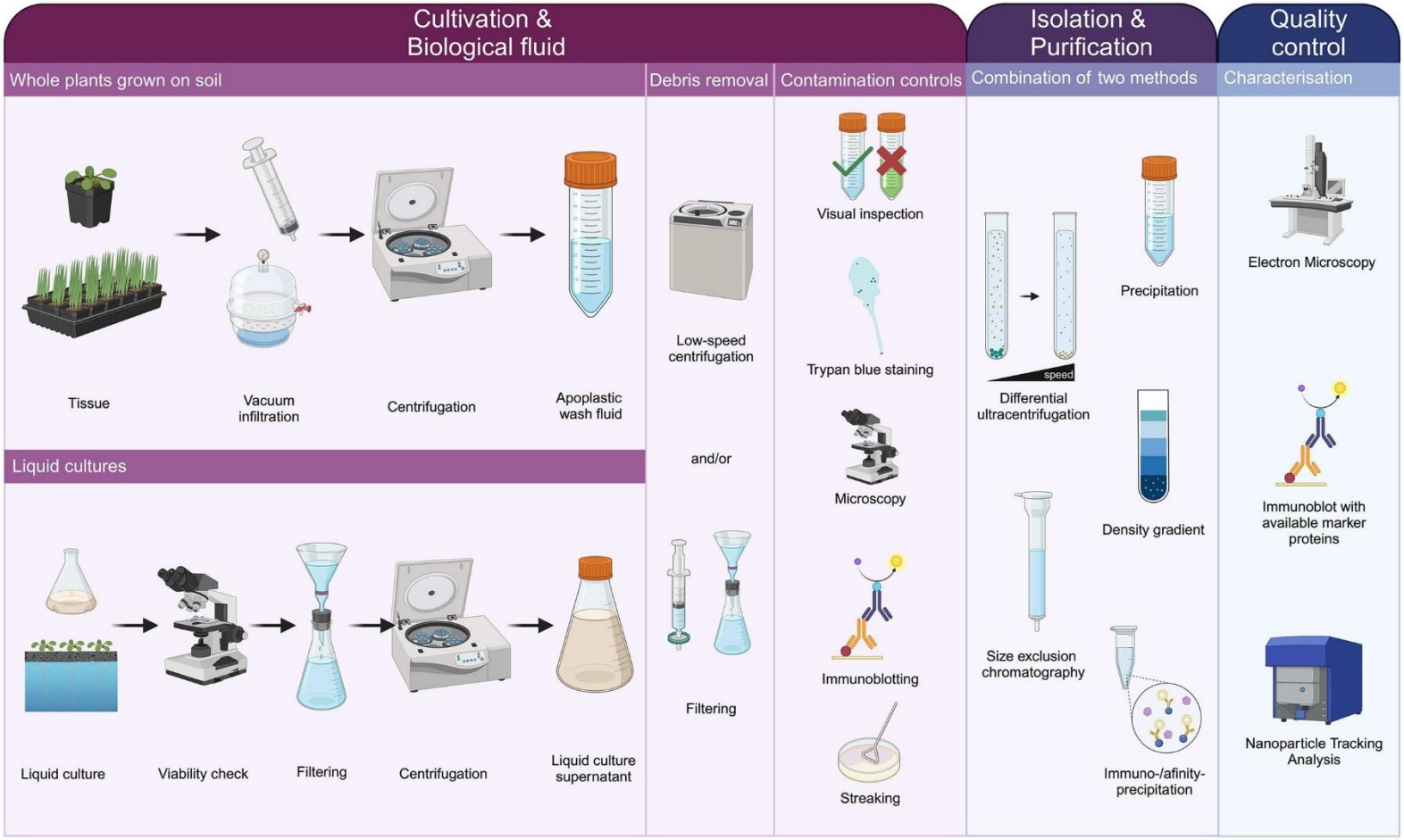

FIGURE 1 A workflow for designing EV isolation procedures from different sources in plant–microbe systems. The growth conditions of the source organism and the research question determine the downstream workflow for EV isolation. Cultivation and biological fluid: For plants grown on soil, the biological fluid, AWF, is commonly obtained by vacuum infiltration followed by very low-speed centrifugation. Removal of cellular debris involves low-speed centrifugation and filtering. Contamination controls for the tissue include visual inspection of the AWF colour (if applicable), viability stains (e.g., trypan blue), microscopy for organelle debris, and immunoblotting targeting intracellular proteins. When organisms are grown in liquid culture (e.g., microbes, plant cell cultures, hydroponic systems), the culture supernatant or medium serves as the biological fluid. For cell cultures, viability checks of source cells before harvesting the supernatant are advised. Removal of intact cells and larger debris involves filtering and centrifugation, followed by another step of low-speed centrifugation and/or filtering for cell debris. Controls for contamination with live cells or cell debris are microscopy, immunoblotting with known non-EV markers, and streaking of the cell-free culture supernatant, where applicable. Isolation and purification of EVs can be achieved by precipitation via polymers, differential ultracentrifugation, density gradient centrifugation, size exclusion chromatography, or immuno-/affinity-purification. Details may vary based on research questions and the manageability of obtaining biological fluid. We refer to the MISEV 2023 guidelines for a detailed register of pros and cons for the different approaches (Welsh et al., 2024). Working with crude EV samples is acceptable for pilot studies, but purification with a second method exploiting different physical and biological properties should be performed for thorough examination. Quality control and initial characterization of isolated (and purified) EVs largely overlap. Two independent methods are recommended for EV characterization, with regular quality control suggested. Electron microscopy confirms the presence of typical structures, and nanoparticle tracking validates consistent particle size isolation, both independent of knowledge about biomarkers. If available, EVs can be tested for the presence of suitable marker proteins by immunoblotting. When EVs are isolated from unicellular organisms, streaking of the EV pellet aids in corroborating that no replicating entities are present. Created with BioRender.com. AWF, apoplastic wash fluid; EV, extracellular vesicles; MISEV, minimal information for studies of extracellular vesicles.

TABLE 1 Synopsis of questions and recommendations for EV isolation in plant–microbe interactions.

Question	Recommendation	Sample type	Reference
1) Cultivation			
a) How to obtain microbial EVs from axenic cultures that are biologically relevant for plant–microbe interactions?	- Try different media mimicking *in planta* conditions. *e.g., apoplast or xylem* - Compare the transcriptome and proteome of cultured cells to those from colonised plant material to determine how representative the cultures are. *e.g., are the so-called "plant-specific" genes, or those important for plant colonization up-regulated? Are the developmental stage, morphology, and physiology of the cultured cells matching the colonization stage of interest?*	Liquid culture	(Hiery et al., 2013; Jonca et al., 2021; Kwon et al., 2021; Li et al., 2022; McMillan & Kuehn, 2023; Rico & Preston, 2008; Wengelnik et al., 1996)
b) How to cultivate my organism for good EV yield?	- Scale up *It may be too laborious to harvest the biological fluid, isolate the EVs, and perform quality controls and extractions on the same day. To determine a stopping point, test for stability of the biological material from suitable steps in the procedure, when stored*, e.g., *biological fluid, EV pellet, or suspension*	All	–
	- Adjust conditions to open stomata to improve infiltration *e.g., humidity or light conditions* - Use younger plants	Plants grown on soil	(Chincinska, 2021; Nouchi et al., 2012; Rumyantseva et al., 2023)
	- Optimise conditions for cultivation *e.g., rich vs. minimal medium, pH etc.* - Increase surface area exposed to medium e.g., smaller mycelial clumps for fungi - Degrade the cell wall to release paramural vesicles *Stress conditions may increase vesiculation but can compromise the biological relevance of the EV cargos*	Liquid culture	(McMillan & Kuehn, 2023; Rutter et al., 2022)
c) How to choose the right cultivation time?	- Perform vesicle isolation in a time series to check for EV yield and relevant EV cargos if known - Check for cell viability by staining (ideally ≥95%; see below)	Liquid culture	(Janda et al., 2023; Shekari et al., 2023)
2) Obtaining biological fluid and EV isolation			
a) How to increase apoplastic fluid yield?	- Optimise vacuum pressure for infiltration - Optimise centrifugation time and force *The goal is to find a balance between infiltration/extraction efficiency and cell integrity (see 2b)* - Use surfactants to decrease the leaf hydrophobicity *Should only be considered in extreme cases when no AWF can be obtained otherwise* - Use more plants	Plants grown on soil	RU5116 (own experience) (Nouchi et al., 2012)
b) How and when to check for contamination with cells/cell debris?	- Immunoblotting with antibodies directed against endomembrane/cytoplasmic contaminants - Perform (light) microscopy (check for organelle contamination) *Consider the possibility of bona fide secretion of organelles, especially for organisms other than plants*	All	(Delaunois et al., 2013)
	After infiltration/centrifugation: - Green AWF and pellets indicate cell lysis - Trypan blue staining	Plants grown on soil	(Mulaosmanovic et al., 2020) RU5116 (own experience)
	- Viability staining (e.g., propidium iodide) staining of cultures just prior to EV isolation (ideally ≥95% viable) - Check via microscopy: - Cell morphology and signs of lysis before and after removing them from culture supernatant - Cell-free culture supernatant for carried over cells and debris - Streak cell-free culture supernatant and EV suspension on agar plate to check for contamination with living cells *It is possible to work as sterile as possible under the clean bench, with sterile filtered solutions and sterilised ultracentrifuge tubes*	Liquid culture	RU5116 (own experience) (Janda et al., 2023; Shekari et al., 2023)

(Continues)

TABLE 1 (Continued)

2) Obtaining biological fluid and EV isolation			
c) How to reduce contamination from cell lysis?	- Settle with the lowest possible time for infiltration; find a balance between yield and purity (see above) - Handle the leaves with great care when blotting dry and otherwise - Choose infiltration buffer that does not compromise cell integrity	Plants grown on soil	(O'Leary et al., 2014)
	- Minimise centrifugation force and time - Apply gentle vacuum when filtering	All	RU5116 (own experience)
d) How to determine which EV subpopulations are relevant for my biological question?	- Further purify and fractionate crude EV preparation according to their biophysical properties or known markers, e.g., size exclusion chromatography, density gradients, immunoaffinity capture, fluorescence-activated cell sorting, or advanced single-particle analysers - Check resulting fractions for molecules of interest	All	(Bleackley et al., 2020; Cai, Qiao, et al., 2018; Garcia-Ceron et al., 2021; Rutter & Innes, 2017)
e) What is the best ultracentrifugation force/duration for isolating my vesicles?	- Dependent on the size and density of the EVs, of the organism(s), and of the density of the used media/buffer - Different pellets have to be compared if not much is known about the organism - Centrifuge as short as possible	All	(Rutter & Innes, 2020)
f) How to distinguish between plant vesicles and microbe vesicles?	- Take advantage of specific plant and microbial vesicle markers if available - Comparison of properties from EVs isolated from microbe, plant, and colonised plant	All	(Janda et al., 2023)
3) Quality check			
a) How to determine if a protein or nucleic acid of interest is EV cargo?	- Carry out immunoaffinity capture assay - Carry out nuclease or protease protection assays: - Check if luminal cargo is removed after treatment with detergent (Triton X-100 etc.) and hydrolytic enzyme (e.g., protease or nuclease) *One might check for sufficient EV disruption under the electron microscope*	All	(Bonsergent et al., 2021; Huang et al., 2021; Kwon et al., 2021; Zand Karimi et al., 2022)
b) How to identify the correct storage conditions?	- Check EVs in NTA/transmission electron microscopy for aggregate formation - Perform immunoblot analysis with antibodies directed against intraluminal cargo *Protein integrity is used as a proxy for EV integrity* - Perform immunoaffinity capture *Signal intensity in subsequent immunoblot analysis should decrease if EVs were disrupted and membrane fragments fused in random orientation* - Use low-bind tubes - Some EVs cannot be frozen *In some cases, freezing can have a negative effect on the properties of the EVs. In these cases, short-term storage of the EVs at 4° C with slight rotation can be considered.*	All	FOR5116 (own experience) (Evtushenko et al., 2020; Görgens et al., 2022)
c) How to differentiate EVs from other particles?	- Perform NTA (size profile and zeta potential) - Stain with a lipophilic dye (e.g., FM4-64, DiOC6, DiR) - Transmission electron microscopy (TEM) - Comparison of the results obtained using the above methods with literature - Use of advanced single-particle analysers such as nanoflow cytometry or microfluidic resistive pulse sensing *Try to compare recorded EV properties with the ones of closely related species or universal EV properties where applicable, e.g., NTA size profiles and zeta potentials or cup-shaped structures in TEM micrographs, respectively. Consider testing differing experimental conditions until the ideal cultivation/isolation procedure is found.*	All	(Welsh et al., 2024)

Abbreviation: EV, extracellular vesicles.

writing—review and editing (supporting). **Lorenz Oberkofler**: Conceptualization (supporting); writing—review and editing (supporting). **Alessa Ruf**: Conceptualization (supporting); writing—review and editing (supporting). **Julia Kehr**: Funding acquisition (equal); supervision (equal); writing—review and editing (supporting). **Karl-Heinz Kogel**: Funding acquisition (equal); supervision (equal); writing—review and editing (supporting). **Arne Weiberg**: Funding acquisition (equal); supervision (equal); writing—review and editing (equal). **Michael Feldbrügge**: Funding acquisition (equal); supervision (equal); writing—review and editing (supporting). **Silke Robatzek**: Funding acquisition (equal); supervision (equal); writing—review and editing (support-

ing). **Ralph Panstruga**: Conceptualization (supporting); funding acquisition (equal); project administration (lead); supervision (lead); writing—review and editing (lead).

ACKNOWLEDGEMENTS

We appreciate the usage of BioRender (https://www.biorender.com/) to create Figure 1. This work was enabled by grants within the research unit FOR5116 "exRNA" funded by the Deutsche Forschungsgemeinschaft (DFG; project number 433194101). Individual grants of this research unit comprise FE 448/15-1 to M.F., KE 856/8-1 to J.K., KO 1208/30-1 to K.-H.K., PA 861/22-1 to R.P., RO 3550/16-1 to S.R., and WE 5707/2-1 to A.W.). Work in the lab of S.R. in the context of this article was further funded by a project within the DFG-funded Collaborative Research Centre SFB924 "Yield" (SFB924/3TP15) and the Advanced Grant "MultiX" (grant number 884235) of the European Research Council (ERC). S.N. was supported by a Dr. Ernst-Leopold Klipstein Foundation scholarship.

Open access funding enabled and organized by Projekt DEAL.

CONFLICT OF INTEREST STATEMENT

The authors declare no conflicts of interests.

DATA AVAILABILITY STATEMENT

Data sharing not applicable to this article as no datasets were generated or analysed during the current study.

ORCID

Hannah Thieron https://orcid.org/0000-0002-0670-7328
Laura Krassini https://orcid.org/0009-0005-7613-910X
Seomun Kwon https://orcid.org/0000-0002-0514-1465
Sebastian Fricke https://orcid.org/0009-0004-0859-4437
Sabrine Nasfi https://orcid.org/0000-0001-5916-0824
Lorenz Oberkofler https://orcid.org/0000-0002-9506-2751
Alessa Ruf https://orcid.org/0000-0003-0919-9717
Julia Kehr https://orcid.org/0000-0003-3617-9981
Karl-Heinz Kogel https://orcid.org/0000-0003-1226-003X
Arne Weiberg https://orcid.org/0000-0003-4300-4864
Michael Feldbrügge https://orcid.org/0000-0003-0046-983X
Silke Robatzek https://orcid.org/0000-0002-9788-322X
Ralph Panstruga https://orcid.org/0000-0002-3756-8957

REFERENCES

Bachurski, D., Schuldner, M., Nguyen, P.-H., Malz, A., Reiners, K. S., Grenzi, P. C., Babatz, F., Schauss, A. C., Hansen, H. P., Hallek, M., & Pogge von Strandmann, E. (2019). Extracellular vesicle measurements with nanoparticle tracking analysis—An accuracy and repeatability comparison between NanoSight NS300 and ZetaView. *Journal of Extracellular Vesicles*, *8*, 1596016. https://doi.org/10.1080/20013078.2019.1596016

Bahar, O., Mordukhovich, G., Luu, D. D., Schwessinger, B., Daudi, A., Jehle, A. K., Felix, G., & Ronald, P. C. (2016). Bacterial outer membrane vesicles induce plant immune responses. *Molecular Plant-Microbe Interactions*, *29*(5), 374–384. https://doi.org/10.1094/MPMI-12-15-0270-R

Bitto, N. J., Petrovski, S., Hill, A. F., & Kaparakis-Liaskos, M. (2023). Planktonic and biofilm-derived *Pseudomonas aeruginosa* outer membrane vesicles facilitate horizontal gene transfer of plasmid DNA. *Microbiology Spectrum*, *11*, e05179–e05122. https://doi.org/10.1128/spectrum.05179-22

Bleackley, M. R., Samuel, M., Garcia-Ceron, D., McKenna, J. A., Lowe, R. G. T., Pathan, M., Zhao, K., Ang, C. S., Mathivanan, S., & Anderson, M. A. (2020). Extracellular vesicles from the cotton pathogen *Fusarium oxysporum* f. sp. *vasinfectum* induce a phytotoxic response in plants. *Frontiers in Plant Science*, *10*, 1610. https://doi.org/10.3389/fpls.2019.01610

Boccia, E., Alfieri, M., Belvedere, R., Santoro, V., Colella, M., Del Gaudio, P., Moros, M., Dal Piaz, F., Petrella, A., Leone, A., & Ambrosone, A. (2022). Plant hairy roots for the production of extracellular vesicles with antitumor bioactivity. *Communications Biology*, *5*(1), 848. https://doi.org/10.1038/s42003-022-03781-3

Bonsergent, E., Grisard, E., Buchrieser, J., Schwartz, O., Théry, C., & Lavieu, G. (2021). Quantitative characterization of extracellular vesicle uptake and content delivery within mammalian cells. *Nature Communications*, *12*, 1864. https://doi.org/10.1038/s41467-021-22126-y

Brown, L., Wolf, J. M., Prados-Rosales, R., & Casadevall, A. (2015). Through the wall: Extracellular vesicles in Gram-positive bacteria, mycobacteria and fungi. *Nature Reviews Microbiology*, *13*(10), 620–630. https://doi.org/10.1038/nrmicro3480

Cai, Q., He, B., Kogel, K. H., & Jin, H. (2018a). Cross-kingdom RNA trafficking and environmental RNAi — nature's blueprint for modern crop protection strategies. *Current Opinion in Microbiology*, *46*, 58–64. https://doi.org/10.1016/j.mib.2018.02.003

Cai, Q., Qiao, L., Wang, M., He, B., Lin, F., Palmquist, J., & Jin, H. (2018b). Plants send small RNAs in extracellular vesicles to fungal pathogen to silence virulence genes. *Science*, *360*(6393), 1126–1129. https://doi.org/10.1126/science.aar4142

Chalupowicz, L., Mordukhovich, G., Assoline, N., Katsir, L., Sela, N., & Bahar, O. (2023). Bacterial outer membrane vesicles induce a transcriptional shift in arabidopsis towards immune system activation leading to suppression of pathogen growth in planta. *Journal of Extracellular Vesicles*, *12*(1), 12285. https://doi.org/10.1002/jev2.12285

Chaya, T., Banerjee, A., Rutter, B. D., Adekanye, D., Ross, J., Hu, G., Innes, R. W., & Caplan, J. L. (2024). The extracellular vesicle proteomes of *Sorghum bicolor* and *Arabidopsis thaliana* are partially conserved. *Plant Physiology*, *194*(3), 1481–1497. https://doi.org/10.1093/plphys/kiad644

Chen, A., He, B., & Jin, H. (2022). Isolation of extracellular vesicles from arabidopsis. *Current Protocols*, *2*(1), e352. https://doi.org/10.1002/cpz1.352

Cheng, A. P., Lederer, B., Oberkofler, L., Huang, L., Johnson, N. R., Platten, F., Dunker, F., Tisserant, C., & Weiberg, A. (2023). A fungal RNA-dependent RNA polymerase is a novel player in plant infection and cross-kingdom RNA interference. *PLoS Pathogens*, *19*(12), e1011885. https://doi.org/10.1371/journal.ppat.1011885

Chernyshev, V. S., Rachamadugu, R., Tseng, Y. H., Belnap, D. M., Jia, Y., Branch, K. J., Butterfield, A. E., Pease, L. F., Bernard, P. S., & Skliar, M. (2015). Size and shape characterization of hydrated and desiccated exosomes. *Analytical and Bioanalytical Chemistry*, *407*(12), 3285–3301. https://doi.org/10.1007/s00216-015-8535-3

Chincinska, I. A. (2021). Leaf infiltration in plant science: Old method, new possibilities. *Plant Methods*, *17*(1), 83. https://doi.org/10.1186/s13007-021-00782-x</./bib>

Chitti, S. V., Gummadi, S., Kang, T., Shahi, S., Marzan, A. L., Neveda, C., Sanwlani, R., Bramich, K., Stewart, S., Petrovska, M., Sen, B., Ozkan, A., Akinfenwa, M., Foneska, P., & Mathivanan, S. (2024). Vesiclepedia 2024: An extracellular vesicles and extracellular particles repository. *Nucleic Acids Research*, *52*(D1), D1694–1D698. https://doi.org/10.1093/nar/gkad1007

Chuo, S. T. Y., Chien, J. C. Y., & Lai, C. P. K. (2018). Imaging extracellular vesicles: Current and emerging methods. *Journal of Biomedical Science*, *25*, 91. https://doi.org/10.1186/s12929-018-0494-5

Colombo, M., Raposo, G., & Théry, C. (2014). Biogenesis, secretion, and intercellular interactions of exosomes and other extracellular vesicles. *Annual Review of Cell and Developmental Biology*, *30*, 255–289. https://doi.org/10.1146/annurev-cellbio-101512-122326

Cvjetkovic, A., Jang, S. C., Konečná, B., Höög, J. L., Sihlbom, C., Lässer, C., & Lötvall, J. (2016). Detailed analysis of protein topology of extracellular vesicles-evidence of unconventional membrane protein orientation. *Scientific Reports*, *6*, 36338. https://doi.org/10.1038/srep36338

Cvjetkovic, A., Lötvall, J., & Lässer, C. (2014). The influence of rotor type and centrifugation time on the yield and purity of extracellular vesicles. *Journal of Extracellular Vesicles*, *3*(1), 23111. https://doi.org/10.3402/jev.v3.23111

Dauros Singorenko, P., Chang, V., Whitcombe, A., Simonov, D., Hong, J., Phillips, A., Swift, S., & Blenkiron, C. (2017). Isolation of membrane vesicles from prokaryotes: A technical and biological comparison reveals heterogeneity. *Journal of Extracellular Vesicles*, *6*(1), 1324731. https://doi.org/10.1080/20013078.2017.1324731

Debbi, L., Guo, S., Safina, D., & Levenberg, S. (2022). Boosting extracellular vesicle secretion. *Biotechnology Advances 2*, *59*, 107983. https://doi.org/10.1016/j.biotechadv.2022.107983

Delaunois, B., Colby, T., Belloy, N., Conreux, A., Harzen, A., Baillieul, F., Clément, C., Schmidt, J., Jeandet, P., & Cordelier, S. (2013). Large-scale proteomic analysis of the grapevine leaf apoplastic fluid reveals mainly stress-related proteins and cell wall modifying enzymes. *BMC Plant Biology*, *13*, 24. https://doi.org/10.1186/1471-2229-13-24

De Palma, M., Ambrosone, A., Leone, A., Del Gaudio, P., Ruocco, M., Turi, L., Bokka, R., Fiume, I., Tucci, M., & Pocsfalvi, G. (2020). Plant roots release small extracellular vesicles with antifungal activity. *Plants*, *9*(12), 1777. https://doi.org/10.3390/plants9121777

Dunker, F., Trutzenberg, A., Rothenpieler, J. S., Kuhn, S., Pröls, R., Schreiber, T., Tissier, A., Kemen, A., Kemen, E., Hückelhoven, R., & Weiberg, A. (2020). Oomycete small RNAs bind to the plant RNA-induced silencing complex for virulence. *Elife*, *9*, e56096. https://doi.org/10.7554/eLife.56096

Evtushenko, E. G., Bagrov, D. V., Lazarev, V. N., Livshits, M. A., & Khomyakova, E. (2020). Adsorption of extracellular vesicles onto the tube walls during storage in solution. *PLoS ONE*, *15*(12), e0243738. https://doi.org/10.1371/journal.pone.0243738

Figueiredo, J., Sousa Silva, M., & Figueiredo, A. (2018). Subtilisin-like proteases in plant defence: The past, the present and beyond. *Molecular Plant Pathology*, *19*(4), 1017–1028. https://doi.org/10.1111/mpp.12567

Filipe, V., Hawe, A., & Jiskoot, W. (2010). Critical evaluation of nanoparticle tracking analysis (NTA) by NanoSight for the measurement of nanoparticles and protein aggregates. *Pharmaceutical Research*, *27*(5), 796–810. https://doi.org/10.1007/s11095-010-0073-2

Foers, A. D., Chatfield, S., Dagley, L. F., Scicluna, B. J., Webb, A. I., Cheng, L., Hill, A. F., Wicks, I. P., & Pang, K. C. (2018). Enrichment of extracellular vesicles from human synovial fluid using size exclusion chromatography. *Journal of Extracellular Vesicles*, *7*(1), 1490145. https://doi.org/10.1080/20013078.2018.1490145

Fortunato, D., Mladenović, D., Criscuoli, M., Loria, F., Veiman, K. L., Zocco, D., Koort, K., & Zarovni, N. (2021). Opportunities and pitfalls of fluorescent labeling methodologies for extracellular vesicle profiling on high-resolution single-particle platforms. *International Journal of Molecular Sciences*, *22*(19), 10510. https://doi.org/10.3390/ijms221910510

Garcia-Ceron, D., Lowe, R. G. T., McKenna, J. A., Brain, L. M., Dawson, C. S., Clark, B., Berkowitz, O., Faou, P., Whelan, J., Bleackley, M. R., & Anderson, M. A. (2021). Extracellular vesicles from *Fusarium graminearum* contain protein effectors expressed during infection of corn. *Journal of Fungi*, *7*(11), 977. https://doi.org/10.3390/jof7110977

Görgens, A., Corso, G., Hagey, D. W., Jawad Wiklander, R., Gustafsson, M. O., Felldin, U., Lee, Y., Bostancioglu, R. B., Sork, H., Liang, X., Zheng, W., Mohammad, D. K., van de Wakker, S. I., Vader, P., Zickler, A. M., Mamand, D. R., Ma, L., Holme, M. N., Stevens, M. M., … El Andaloussi, S. (2022). Identification of storage conditions stabilizing extracellular vesicles preparations. *Journal of Extracellular Vesicles*, *11*(6), 12238. https://doi.org/10.1002/jev2.12238

He, B., Cai, Q., Qiao, L., Huang, C. Y., Wang, S., Miao, W., Ha, T., Wang, Y., & Jin, H. (2021). RNA-binding proteins contribute to small RNA loading in plant extracellular vesicles. *Nature Plants*, *7*(3), 342–352. https://doi.org/10.1038/s41477-021-00863-8

He, B., Wang, H., Liu, G., Chen, A., Calvo, A., Cai, Q., & Jin, H. (2023). Fungal small RNAs ride in extracellular vesicles to enter plant cells through clathrin-mediated endocytosis. *Nature Communications*, *14*(1), 1–15. https://doi.org/10.1038/s41467-023-40093-4

Heidarzadeh, M., Zarebkohan, A., Rahbarghazi, R., & Sokullu, E. (2023). Protein corona and exosomes: New challenges and prospects. *Cell Communication and Signaling*, *21*, 64. https://doi.org/10.1186/s12964-023-01089-1

Hiery, E., Adam, S., Reid, S., Hofmann, J., Sonnewald, S., & Burkovski, A. (2013). Genome-wide transcriptome analysis of *Clavibacter michiganensis* subsp. *michiganensis* grown in xylem mimicking medium. *Journal of Biotechnology*, *168*(4), 348–354. https://doi.org/10.1016/j.jbiotec.2013.09.006

Hill, E. H., & Solomon, P. S. (2020). Extracellular vesicles from the apoplastic fungal wheat pathogen *Zymoseptoria tritici*. *Fungal Biology and Biotechnology*, *7*, 13. https://doi.org/10.1186/s40694-020-00103-2

Hofer, U. (2021). Lassoing OMVs with an LPS receptor. *Nature Reviews Microbiology*, *19*(11), 682. https://doi.org/10.1038/s41579-021-00633-5

Hong, J., Dauros-Singorenko, P., Whitcombe, A., Payne, L., Blenkiron, C., Phillips, A., & Swift, S. (2019). Analysis of the *Escherichia coli* extracellular vesicle proteome identifies markers of purity and culture conditions. *Journal of Extracellular Vesicles*, *8*(1), 1632099. https://doi.org/10.1080/20013078.2019.1632099

Huang, Y., Wang, S., Cai, Q., & Jin, H. (2021). Effective methods for isolation and purification of extracellular vesicles from plants. *Journal of Integrative Plant Biology*, *63*(12), 2020–2030. https://doi.org/10.1111/jipb.13181

Janda, M., Rybak, K., Krassini, L., Meng, C., Feitosa-junior, O., Stigliano, E., Szulc, B., Menke, F. L. H., Malone, J. G., Brachmann, A., Klingl, A., Ludwig, C., & Robatzek, S. (2023). Biophysical and proteomic analyses of *Pseudomonas syringae* pv. tomato DC3000 extracellular vesicles suggest adaptive functions during plant infection. *MBio*, *14*, e03589–e03522. https://doi.org/10.1128/mbio.03589-22

Jonca, J., Waleron, M., Czaplewska, P., Bogucka, A., Steć, A., Dziomba, S., Jasiecki, J., Rychłowski, M., & Waleron, K. (2021). Membrane vesicles of pectobacterium as an effective protein secretion system. *International Journal of Molecular Sciences*, *22*(22), 12574. https://doi.org/10.3390/ijms222212574

Kim, D. K., Lee, J., Kim, S. R., Choi, D. S., Yoon, Y. J., Kim, J. H., Go, G., Nhung, D., Hong, K., Jang, S. C., Kim, S. H., Park, K. S., Kim, O. Y., Park, H. T., Seo, J. H., Aikawa, E., Baj-Krzyworzeka, M., van Balkom, B. W., Belting, M., … Gho, Y. S. (2015). EVpedia: A community web portal for extracellular vesicles research. *Bioinformatics*, *31*(6), 933–939. https://doi.org/10.1093/bioinformatics/btu741

Kocholata, M., Prusova, M., Auer Malinska, H., Maly, J., & Janouskova, O. (2022). Comparison of two isolation methods of tobacco-derived extracellular vesicles, their characterization and uptake by plant and rat cells. *Scientific Reports*, *12*, 19896. https://doi.org/10.1038/s41598-022-23961-9

Kondratov, K., Nikitin, Y., Fedorov, A., Kostareva, A., Mikhailovskii, V., Isakov, D., Ivanov, A., & Golovkin, A. (2020). Heterogeneity of the nucleic acid repertoire of plasma extracellular vesicles demonstrated using high-sensitivity fluorescence-activated sorting. *Journal of Extracellular Vesicles*, *9*(1), 1743139. https://doi.org/10.1080/20013078.2020.1743139

Kusch, S., Singh, M., Thieron, H., Spanu, P. D., & Panstruga, R. (2023). Site-specific analysis reveals candidate cross-kingdom small RNAs, tRNA and rRNA fragments, and signs of fungal RNA 2 phasing in the barley-powdery mildew interaction. *Molecular Plant Pathology*, *24*(6), 570–587. https://doi.org/10.1111/mpp.13324

Kwon, S., Rupp, O., Brachmann, A., Blum, C. F., Kraege, A., Goesmann, A., & Feldbrügge, M. (2021). mRNA inventory of extracellular vesicles from *Ustilago maydis*. *Journal of Fungi*, *7*(7), 562. https://doi.org/10.3390/jof7070562

Lehrich, B. M., Liang, Y., & Fiandaca, M. S. (2021). Foetal bovine serum influence on in vitro extracellular vesicle analyses. *Journal of Extracellular Vesicles*, *10*(3), e12061. https://doi.org/10.1002/jev2.12061

Li, D., Li, Z., Wu, J., Tang, Z., Xie, F., Chen, D., Lin, H., & Li, Y. (2022). Analysis of outer membrane vesicles indicates that glycerophospholipid metabolism contributes to early symbiosis between *Sinorhizobium fredii* HH103 and soybean. *Molecular Plant-Microbe Interactions*, *35*(4), 311–322. https://doi.org/10.1094/MPMI-11-21-0288-R

Lohaus, G., Pennewiss, K., Sattelmacher, B., Hussmann, M., & Hermann Muehling, K. (2001). Is the infiltration-centrifugation technique appropriate for the isolation of apoplastic fluid? A critical evaluation with different plant species. *Physiologia Plantarum*, *111*(4), 457–465. https://doi.org/10.1034/j.1399-3054.2001.1110405.x

McMillan, H. M., & Kuehn, M. J. (2023). Proteomic profiling reveals distinct bacterial extracellular vesicle subpopulations with possibly unique functionality. *Applied and Environmental Microbiology*, *89*(1), e01686–e01622. https://doi.org/10.1128/aem.01686-22

McMillan, H. M., Rogers, N., Wadle, A., Hsu-Kim, H., Wiesner, M. R., Kuehn, M. J., & Hendren, C. O. (2021). Microbial vesicle-mediated communication: Convergence to understand interactions within and between domains of life. *Environmental Science: Processes and Impacts*, *23*(5), 664–677. https://doi.org/10.1039/d1em00022e

Midekessa, G., Godakumara, K., Ord, J., Viil, J., Lättekivi, F., Dissanayake, K., Kopanchuk, S., Rinken, A., Andronowska, A., Bhattacharjee, S., Rinken, T., & Fazeli, A. (2020). Zeta potential of extracellular vesicles: Toward understanding the attributes that determine colloidal stability. *ACS Omega*, *5*(27), 16701–16710. https://doi.org/10.1021/acsomega.0c01582

Mulaosmanovic, E., Lindblom, T. U. T., Bengtsson, M., Windstam, S. T., Mogren, L., Marttila, S., Stützel, H., & Alsanius, B. W. (2020). High-throughput method for detection and quantification of lesions on leaf scale based on trypan blue staining and digital image analysis. *Plant Methods*, *16*, 62. https://doi.org/10.1186/s13007-020-00605-5

Nascimento, R., Gouran, H., Chakraborty, S., Gillespie, H. W., Almeida-Souza, H. O., Tu, A., Rao, B. J., Feldstein, P. A., Bruening, G., Goulart, L. R., & Dandekar, A. M. (2016). The type II secreted lipase/esterase LesA is a key virulence factor required for *Xylella fastidiosa* pathogenesis in grapevines. *Scientific Reports*, *6*, 18598. https://doi.org/10.1038/srep18598

Neumann, M. J., & Dobinson, K. F. (2003). Sequence tag analysis of gene expression during pathogenic growth and microsclerotia development in the vascular wilt pathogen *Verticillium dahliae*. *Fungal Genetics and Biology*, *38*(1), 54–62. https://doi.org/10.1016/S1087-1845(02)00507-8

Nouchi, I., Hayashi, K., Hiradate, S., Ishikawa, S., Fukuoka, M., Chen, C. P., & Kobayashi, K. (2012). Overcoming the difficulties in collecting apoplastic fluid from rice leaves by the infiltration-centrifugation method. *Plant and Cell Physiology*, *53*(9), 1659–1668. https://doi.org/10.1093/pcp/pcs102

O'Leary, B. M., Rico, A., McCraw, S., Fones, H. N., & Preston, G. M. (2014). The infiltration-centrifugation technique for extraction of apoplastic fluid from plant leaves using *Phaseolus vulgaris* as an example. *Journal of Visualized Experiments: JoVE*, *19*(94), e52113. https://doi.org/10.3791/52113

Olicón-Hernández, D. R., Hernández-Lauzardo, A. N., Pardo, J. P., Peña, A., Velázquez-del Valle, M. G., & Guerra-Sánchez, G. (2015). Influence of chitosan and its derivatives on cell development and physiology of *Ustilago maydis*. *International Journal of Biological Macromolecules*, *79*, 654–660. https://doi.org/10.1016/j.ijbiomac.2015.05.057

Panagopoulou, M. S., Wark, A. W., Birch, D. J. S., & Gregory, C. D. (2020). Phenotypic analysis of extracellular vesicles: A review on the applications of fluorescence. *Journal of Extracellular Vesicles*, *9*(1), 1710020. https://doi.org/10.1080/20013078.2019.1710020

Pinedo, M., Canal, L., & Marcos Lousa, C. (2021). A call for Rigor and standardization in plant extracellular vesicle research. *Journal of Extracellular Vesicles*, *10*(6), e12048. https://doi.org/10.1002/jev2.12048

Regente, M., Corti Monzón, G., & De La Canal, L. (2008). Phospholipids are present in extracellular fluids of imbibing sunflower seeds and are modulated by hormonal treatments. *Journal of Experimental Botany*, *59*(3), 553–562. https://doi.org/10.1093/jxb/erm329

Regente, M., Corti-Monzón, G., Maldonado, A. M., Pinedo, M., Jorrín, J., & de la Canal, L. (2009). Vesicular fractions of sunflower apoplastic fluids are associated with potential exosome marker proteins. *FEBS Letters*, *583*(20), 3363–3366. https://doi.org/10.1016/j.febslet.2009.09.041

Regente, M., Pinedo, M., Clemente, H. S., Balliau, T., Jamet, E., & De La Canal, L. (2017). Plant extracellular vesicles are incorporated by a fungal pathogen and inhibit its growth. *Journal of Experimental Botany*, *68*(20), 5485–5495. https://doi.org/10.1093/jxb/erx355

Rico, A., & Preston, G. M. (2008). *Pseudomonas syringae* pv. tomato DC3000 uses constitutive and apoplast-induced nutrient assimilation pathways to catabolize nutrients that are abundant in the tomato apoplast. *Molecular Plant-Microbe Interactions*, *21*(2), 269–282. https://doi.org/10.1094/MPMI-21-2-0269

Ruf, A., Oberkofler, L., Robatzek, S., & Weiberg, A. (2022). Spotlight on plant RNA-containing extracellular vesicles. *Current Opinion in Plant Biology*, *69*, 102272. https://doi.org/10.1016/j.pbi.2022.102272

Rumyantseva, N. I., Valieva, A. I., Kostyukova, Y. A., & Ageeva, M. V. (2023). The effect of leaf plasticity on the isolation of apoplastic fluid from leaves of tartary buckwheat plants grown in vivo and in vitro. *Plants*, *12*(23), 4048. https://doi.org/10.3390/plants12234048

Rutter, B. D., Chu, T. T. H., Dallery, J. F., Zajt, K. K., O'Connell, R. J., & Innes, R. W. (2022). The development of extracellular vesicle markers for the fungal phytopathogen *Colletotrichum higginsianum*. *Journal of Extracellular Vesicles*, *11*(5), e12216. https://doi.org/10.1002/jev2.12216

Rutter, B. D., & Innes, R. W. (2017). Extracellular vesicles isolated from the leaf apoplast carry stress-response proteins. *Plant Physiology*, *173*(1), 728–741. https://doi.org/10.1104/pp.16.01253

Rutter, B. D., & Innes, R. W. (2020). Growing pains: Addressing the pitfalls of plant extracellular vesicle research. *New Phytologist*, *228*(5), 1505–1510. https://doi.org/10.1111/nph.16725

Saad, M. G., Beyenal, H., & Dong, W. J. (2024). Dual roles of the conditional extracellular vesicles derived from *Pseudomonas aeruginosa* biofilms: Promoting and inhibiting bacterial biofilm growth. *Biofilm*, *7*, 100183. https://doi.org/10.1016/j.bioflm.2024.100183

Shekari, F., Alibhai, F. J., Baharvand, H., Börger, V., Bruno, S., Davies, O., Giebel, B., Gimona, M., Salekdeh, G. H., Martin-Jaular, L., Mathivanan, S., Nelissen, I., Nolte-'t Hoen, E., O'Driscoll, L., Perut, F., Pluchino, S., Pocsfalvi, G., Salomon, C., Soekmadji, C., … Nieuwland , R. (2023). Cell culture-derived extracellular vesicles: Considerations for reporting cell culturing parameters. *Journal of Extracellular Biology*, *2*(10), e115. https://doi.org/10.1002/jex2.115

Skliar, M., Chernyshev, V. S., Belnap, D. M., Sergey, G. V., Al-Hakami, S. M., Bernard, P. S., Stijleman, I. J., & Rachamadugu, R. (2018). Membrane proteins significantly restrict exosome mobility. *Biochemical and Biophysical Research Communications*, *501*(4), 1055–1059. https://doi.org/10.1016/j.bbrc.2018.05.107

Suh, J., & Lee, Y. S. (2024). Mitochondria as secretory organelles and therapeutic cargos. *Experimental and Molecular Medicine*, *56*, 66–85. https://doi.org/10.1038/s12276-023-01141-7

Théry, C., Witwer, K. W., Aikawa, E., Alcaraz, M. J., Anderson, J. D., Andriantsitohaina, R., Antoniou, A., Arab, T., Archer, F., Atkin-Smith, G. K., Ayre, D. C., Bach, J. M., Bachurski, D., Baharvand, H., Balaj, L., Baldacchino, S., Bauer, N. N., Baxter, A. A., Bebawy, M., … Zuba-Surma, E. K. (2018). Minimal information for studies of extracellular vesicles 2018 (MISEV2018): A position statement of the International Society for Extracellular Vesicles and update of the MISEV2014 guidelines. *Journal of Extracellular Vesicles*, *7*(1), 1535750. https://doi.org/10.1080/20013078.2018.1535750

van de Wakker, S. I., van Oudheusden, J., Mol, E. A., Roefs, M. T., Zheng, W., Görgens, A., El Andaloussi, S., Sluijter, J. P. G., & Vader, P. (2022). Influence of short term storage conditions, concentration methods and excipients on extracellular vesicle recovery and function. *European Journal of Pharmaceutics and Biopharmaceutics*, *170*, 59–69. https://doi.org/10.1016/j.ejpb.2021.11.012

Varga, Z., Fehér, B., Kitka, D., Wacha, A., Bóta, A., Berényi, S., Pipich, V., & Fraikin, J. L. (2020). Size measurement of extracellular vesicles and synthetic liposomes: The impact of the hydration shell and the protein corona. *Colloids and Surfaces B: Biointerfaces*, *192*, 111053. https://doi.org/10.1016/j.colsurfb.2020.111053

Wang, F., Ho, P. Y., Kam, C., Yang, Q., Liu, J., Wang, W., Zhao, E., & Chen, S. (2023). An AIE-active probe for efficient detection and high-throughput identification of outer membrane vesicles. *Aggregate*, *4*(4), e312. https://doi.org/10.1002/agt2.312

Wang, J., Ding, Y., Wang, J., Hillmer, S., Miao, Y., Lo, S. W., Wang, X., Robinson, D. G., & Jiang, L. (2010). EXPO, an exocyst-positive organelle distinct from multivesicular endosomes and autophagosomes, mediates cytosol to cell wall exocytosis in Arabidopsis and tobacco cells. *Plant Cell*, *22*(12), 4009–4030. https://doi.org/10.1105/tpc.110.080697

Wang, M., Weiberg, A., Lin, F.-M., Thomma, B. P. H. J., Huang, H.-D., & Jin, H. (2016). Bidirectional cross-kingdom RNAi and fungal uptake of external RNAs confer plant protection. *Nature Plants*, *2*, 16151. https://doi.org/10.1038/nplants.2016.151

Wang, S., He, B., Wu, H., Cai, Q., Ramírez-Sánchez, O., Abreu-Goodger, C., Birch, P. R. J., & Jin, H. (2023). Plant mRNAs move into a fungal pathogen via extracellular vesicles to reduce infection. *Cell Host & Microbe*, *32*(1), 93–105. https://doi.org/10.1016/j.chom.2023.11.020

Weiberg, A., Wang, M., Lin, F.-M., Zhao, H., Zhang, Z., Kaloshian, I., Huang, H.-D., & Jin, H. (2013). Fungal small RNAs suppress plant immunity by hijacking host RNA interference pathways. *Science*, *342*(6154), 118–123. https://doi.org/10.1126/science.1239705

Welsh, J. A., Goberdhan, D. C. I., O'Driscoll, L., Buzas, E. I., Blenkiron, C., Bussolati, B., Cai, H., Di Vizio, D., Driedonks, T. A. P., Erdbrügger, U., Falcon-Perez, J. M., Fu, Q. L., Hill, A. F., Lenassi, M., Lim, S. K., Mahoney, M. G., Mohanty, S., Möller, A., Nieuwland, R., … Witwer, K. W. (2024). Minimal information for studies of extracellular vesicles (MISEV2023): From basic to advanced approaches. *Journal of Extracellular Vesicles*, *13*(2), e12404. https://doi.org/10.1002/jev2.12404

Wengelnik, K., Marie, C., Russel, M., & Bonas, U. (1996). Expression and localization of HrpA1, a protein of *Xanthomonas campestris* pv. *vesicatoria* essential for pathogenicity and induction of the hypersensitive reaction. *Journal of Bacteriology*, *178*(4), 1061–1069. https://doi.org/10.1128/jb.178.4.1061-1069.1996

Wong-Bajracharya, J., Singan, V. R., Monti, R., Plett, K. L., Ng, V., Grigoriev, I. V., Martin, F. M., Anderson, I. C., & Plett, J. M. (2022). The ectomycorrhizal fungus *Pisolithus microcarpus* encodes a microRNA involved in cross-kingdom gene silencing during symbiosis. *Proceedings of the National Academy of Sciences of the United States of America*, *119*(3), e2103527119. https://doi.org/10.1073/pnas.2103527119

Yao, L., Jiang, Z., Wang, Y., Hu, Y., Hao, G., Zhong, W., Wan, S., & Xin, X. (2023). High air humidity dampens salicylic acid pathway and NPR1 function to promote plant disease. *EMBO Journal*, *42*(21), e113499. https://doi.org/10.15252/embj.2023113499

Zand Karimi, H., Baldrich, P., Rutter, B. D., Borniego, L., Zajt, K. K., Meyers, B. C., & Innes, R. W. (2022). Arabidopsis apoplastic fluid contains SRNA- and circular RNA-protein complexes that are located outside extracellular vesicles. *Plant Cell*, *34*(5), 1863–1881. https://doi.org/10.1093/plcell/koac043

Zhu, J., Qiao, Q., Sun, Y., Xu, Y., Shu, H., Zhang, Z., Liu, F., Wang, H., Ye, W., Dong, S., Wang, Y., Ma, Z., & Wang, Y. (2023). Divergent sequences of tetraspanins enable plants to specifically recognize microbe-derived extracellular vesicles. *Nature Communications*, *14*, 4877. https://doi.org/10.1038/s41467-023-40623-0

How to cite this article: Thieron, H., Krassini, L., Kwon, S., Fricke, S., Nasfi, S., Oberkofler, L., Ruf, A., Kehr, J., Kogel, K.-H., Weiberg, A., Feldbrügge, M., Robatzek, S., & Panstruga, R. (2024). Practical advice for extracellular vesicle isolation in plant–microbe interactions: Concerns, considerations, and conclusions. *Journal of Extracellular Vesicles*, *13*, e70022. https://doi.org/10.1002/jev2.70022

Conclusion:

This guideline addresses a key methodological gap by adapting EV isolation protocols to the plant–microbe context, where contamination, low yield, and heterogeneity present significant challenges. We build on established MISEV standards but adapt the recommendations to plant-microbe systems, including detailed quality controls (e.g. marker panels, size profiling), optimised centrifugation steps, and validation methods. Our motivation came from studying EVs' isolation from *Serendipita indica* during our research on cross-kingdom communication between *Si* and *At*, as described in chapter 6.

CHAPTER 10 – General discussion

10.1 Cross-kingdom RNAi: Exploring a new layer of gene regulation

Ck RNAi, originally discovered in plant-pathogen interactions (Wang et al., 2016; Weiberg et al., 2013), is nowadays a widely explored and recognised RNA-based regulatory mechanism. sRNAs, major players in this mechanism, were attributed multiple gene-modulation functions within and between both interacting organisms.

This thesis investigates whether mutualistic interactions, one of the earliest and oldest plant associations on earth, also employ the ck RNAi mechanism.

Early evidence of ck-RNAi in mutualism was observed during the interaction between the monocot model plant *Brachypodium distachyon* and the endophyte fungus *Serendipita indica*. The study showed that early colonisation of Brachypodium roots by *S. indica* induces changes in gene expression and transcriptional reprogramming in both organisms (Figure 3, Table 1 and Table 2, Chapter 2, Šečić et al., 2021). These molecular changes support the previous observations that the host immune system is modulated during mutualism (Deshmukh et al., 2006; Jacobs et al., 2011), with similar patterns observed in arbuscular mycorrhizal symbiosis (Plett et al., 2024; Plett & Martin, 2018; Qiao et al., 2023). Profiling and sequencing of sRNAs during the interaction of Brachypodium with *S. indica* confirmed the involvement of sRNAs in symbiotic interactions (Figure 5, Chapter 2, Šečić et al., 2021).

To further investigate the functional role of *S. indica* sRNAs (*Si*sRNA) in manipulating host genes, a pipeline was developed in Nasfi et al., 2024 (Chapter 3) to identify and validate *Si*sRNAs function during their interaction with the dicot model plant *Arabidopsis thaliana*.

A set of *Si*sRNAs from *S. indica* sRNA sequencing (available in the Array Express database under accession number E-MTAB-10650, Chapter 2, Šečić et al., 2021) were first confirmed to be expressed in *S. indica* axenic culture and in *S. indica* inoculated Arabidopsis roots, indicating their potential transfer from the endophyte to the host plant (Figures 2 and 3, Chapter 3). Using a transient expression system, the accumulation of *Si*sRNAs overexpressed in Arabidopsis protoplasts was confirmed, as was the

downregulation of their corresponding predicted host target transcripts. Downregulated transcripts were involved in cell wall organisation, hormonal signalling, immunity, and gene regulation (Figure 8, Chapter 3, Nasfi et al., 2024). Interestingly, the downregulation of some of the predicted target transcripts in *S. indica* colonised Arabidopsis roots was also confirmed (Figure 9, Chapter 3, Nasfi et al., 2024). To further answer whether *Si*sRNAs exploit the host RNAi machinery, we confirmed their binding to the canonical AGO1 protein (Figures 10 and 11, Chapter 3, Nasfi et al., 2024). Together with the functional assay, this provides evidence of ck-RNAi between Arabidopsis and *S. indica*.

10.2 Argonaute-mediated regulation of *S. indica* colonisation

Argonautes are core to the plant RNAi machinery and primary executors of RNA-guided gene silencing (Carbonell, 2017; Fang & Qi, 2016). Transcriptional analysis of AGO and DCL gene expression in Col-0 Arabidopsis roots inoculated with *S. indica* showed a downregulation of AGO4 expression, while the expression levels of other AGOs and DCLs remained unchanged (Figure 5a, Chapter 4, Ruf, Thieron, Nasfi et al., 2024). Further analysis of Arabidopsis *ago* and *dcl* mutant roots inoculated with *S. indica* showed reduced root colonisation in single *ago2* and *ago10* mutants, whereas *ago1*, *ago4*, and the triple mutant *dcl2/3/4* exhibited wild-type colonisation levels (Figure 5b, Chapter 4, Ruf, Thieron, Nasfi et al., 2024). These findings suggest that AGO2 and AGO10 positively regulate the symbiotic interaction between Arabidopsis and *S. indica* (Chapter 4, Ruf, Thieron, Nasfi et al., 2024).

Analysis of higher-order mutants further refined this model and clarified functional interactions among AGO proteins. The *ago1ago10* double mutant showed an increased *S.indica* colonisation at both early and later stages; in contrast, *S. indica* colonisation was reduced in *the ago1ago2* double mutant (Figure 1, Chapter 5). These results support the previous observation that AGO2 and AGO10 promote *S. indica* mutualism (Figure 5b, Chapter 4, Ruf, Thieron, Nasfi et al., 2024). Single- and double-*ago* mutant data further suggest a potential functional interaction between AGO1, AGO2, and AGO10. In the absence of AGO1 alone, *S. indica* exhibited a wild-type colonisation pattern. However, simultaneous loss of AGO1 and AGO10 resulted in increased colonisation. This observation suggests a possible compensatory mechanism, likely between AGO1 and AGO2, as the absence of AGO10 alone showed a reduced colonisation. Moreover, AGO

expression analysis in single and double mutants showed that Arabidopsis regulates AGO expression during *S. indica* colonisation. AGO2 was highly expressed in *ago1* and in *ago1ago10* mutant roots (Figure 2b, Chapter 5). In turn, AGO10 was upregulated in *ago2* mutant but not in the *ago1ago2* mutant (Figure 2c, Chapter 5). These findings further highlight the compensatory role of AGO1 and AGO2 during Arabidopsis *S. indica* interaction and suggest a more complex regulation among clade I AGOs, particularly AGO1 and AGO10. Overall, these results support a model in which AGO1, AGO2, and AGO10 are functionally interconnected and act together during *S. indica* colonisation of Arabidopsis roots. This model suggests that AGO2 and AGO10 promote *S. indica* colonisation, whereas AGO1 counteracts this effect, depending on the genetic background.

In pathosystems, AGO1 and AGO2 are known for their role in the plant defence responses (Carbonell & Carrington, 2015; Harvey et al., 2011; Mallory et al., 2009) whereas AGO10 is primarily associated with plant development and regulation of meristem activity through sequestration of miR165/166, thereby indirectly influencing AGO1 activity (Ji et al., 2011; Zhu et al., 2011). While AGO protein activities are mainly related to responses against pathogen attack and triggering a robust immune response, their function in mutualistic interactions appears to involve an adaptable regulatory network that promotes symbiosis and molecular exchange. This finding is supported by mechanistic evidence. AGO1 and AGO2 immunoprecipitation of Arabidopsis roots colonised by *S. indica*, followed by sRNA sequencing, demonstrated that *S. indica* sRNAs are bound to AGO1 and AGO2, confirming their loading into the Arabidopsis RNAi complex (Figures 6 and 7, Chapter 5). Comparable argonaute binding has been observed for pathogenic sRNAs, proving their gene silencing activity and the existence of ck-RNAi (Dunker et al., 2020, 2021; Weiberg et al., 2013).

These mechanistic and functional studies confirm the existence of cross-kingdom communication during the interaction between *Arabidopsis thaliana* and *Serendipita indica,* and potentially in mutualistic interactions more broadly. Furthermore, these results indicate that Arabidopsis RNAi machinery does not function strictly as a defence barrier during mutualism but rather fine-tunes its machinery to accommodate the specific outcome of the interaction and the identity of the microorganism interacting with

it, enabling it as a host to distinguish friends from foes at the molecular level. Figure 1 of this discussion chapter is a suggested model of *S.indica* Arabidopsis interaction based on the results and the outcome of this thesis.

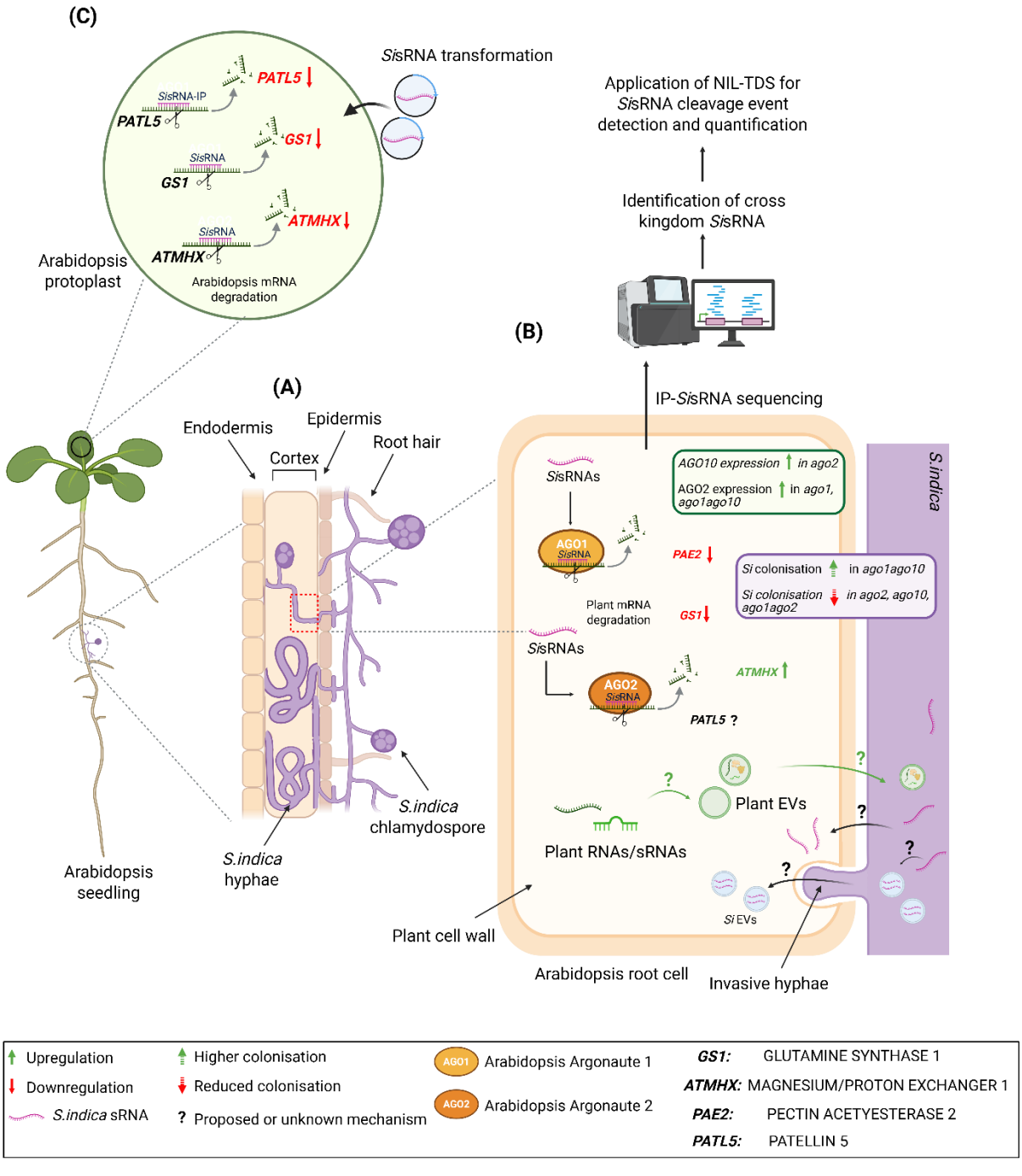

Figure 1. Graphical summary of a proposed model describing the outcome of the interaction between *Serendipita indica* and *Arabidopsis thaliana*. **(A)** The endophytic fungus *S.indica* colonises Arabidopsis roots, specifically the root hairs, epidermis and

cortex, where it forms intercellular hyphae and coils. **(B)** Variation in colonisation is observed in Arabidopsis argonaute (*ago*) mutant backgrounds with higher *S.indica* colonisation in *ago1ago10* mutant and reduced colonisation in *ago2*, *ago10* and *ago1ago2* mutants. AGO's expression analysis revealed upregulation of AGO10 in ago2 and of AGO2 in *ago1* and *ago1ago10* mutants. AGO1- and AGO2- immunoprecipitation identified *Si*sRNAs with a potential cross-kingdom communication function. *Si*sRNAs are transferred into Arabidopsis root cells, where they are bound and loaded into AGO1 and AGO2, resulting in PTGS and downregulation of Arabidopsis target genes such as GLUTAMINE SYNTHASE1 (GS1) and PECTIN ACETYLESTERASE 2 (PAD2). NIL-TDS, a novel method, is required to detect and quantify precise and real *Si*sRNA cleavage events. The mechanism by which *Si*sRNAs are transferred into Arabidopsis roots, e.g. extracellular vesicles, and whether Arabidopsis also send RNA molecules to *S.indica* via vesicles remains hypothetical. **(C)** Functional validation of *Si*sRNAs was performed using the Arabidopsis protoplast transformation assay, where they induced PTGS in predicted Arabidopsis target genes.

10.3 Biogenesis, sorting and loading of sRNAs in Argonaute: known principles and new insights

The biogenesis of sRNAs is the first step that determines their regulatory role in plants. miRNAs are transcribed by RNA polymerase II, capped and polyadenylated, then folded into hairpin structures. Subsequently, they are processed in the nucleus by DCL1, with Hyopnastic leaves 1 (HYL1) and Serrate (SE), into 21nt miRNA/miRNA* duplexes (Bologna & Voinnet, 2014; Vaucheret, 2008; Vaucheret et al., 2004). In contrast, siRNAs are generated from double-stranded RNA precursors produced by RNA-dependent RNA Polymerase (RdRP), processed by different DCLs into sRNA of distinct sizes, methylated by Hua Enhancer 1 (HEN1), and exported to the cytoplasm (Axtell et al., 2006; Carthew & Sontheimer, 2009b). The length, structure, and duplex configuration of sRNAs are critical criteria for their sorting and loading onto AGOs.

Early research in Arabidopsis identified 5'-nt of the sRNA is the primary determinant of sRNA sorting and loading into AGOs. sRNAs with 5'- U are preferentially bound and

loaded into AGO1, while 5'-A sRNAs are more commonly associated with AGO2 and AGO4 (Mi et al., 2008; Takeda et al., 2008). However, further studies from AGOs' immunoprecipitation and high-throughput sequencing showed that AGOs can bind and load sRNA with different 5'-nt, confirming that the 5'-nt sorting criterion is highly dependent on experimental conditions, and the nature of the plant-microbe interactions, including stress and environmental factors (Czech & Hannon, 2011; Morgado et al., 2017). Besides the 5'-nt, studies showed that the stability, the thermodynamic, the sequence and the secondary structure of the sRNA duplex influence the selection of the guide strand for AGO loading, although these aspects require further investigation (Czech & Hannon, 2011; Eamens et al., 2009). Zang et al. (2014) concluded that the structure of miRNA duplexes, the presence of a mismatch at position 15, and the QF-V motif within the conserved PIWI domain of Arabidopsis AGO1 and AGO2 are essential for AGO function and are involved in base pairing at position 15. These criteria play a fundamental role in sRNA sorting and the RNA silencing pathway (Zhang et al., 2014).

Computational studies using machine learning on AGO-IP datasets suggested that sRNA k-mer (a sequence of k consecutive nucleotides) composition and both 5' and 3' ends influence AGO association (Morgado et al., 2017). Moreover, sRNA sorting is significantly affected by biological context. Factors such as AGO expression patterns, feedback regulation, and cell specificity reshape the standard sRNA sorting rules. AGO availability and competition among miRNAs, siRNAs, and potentially other sRNA species further impact sRNA-AGO interactions. Interactions among different AGO-sRNA complexes during plant-microbe interactions can also influence gene silencing activity, suggesting that RNAi machinery cross-talk may reshape plant regulatory mechanisms (Liang et al., 2023).

Altogether, the interaction between sRNA and AGOs is not based on a single strict criterion. From sRNA biogenesis establishing the sRNA duplex pool and their structures to the sorting guided by 5'-nt, size, mismatches and thermodynamic, to the loading that focuses on AGOs regulation, expression and biological context explain the immense permissivity of AGOs and give a hint why AGOs can bind both endogenous and foreign sRNAs allowing them to enter the plant RNAi machinery either to fine -tune its defence mechanism and regulation of to take it over.

10.4 sRNA slicing activity from target prediction to cleavage detection

In eucaryotic RNAi, RNA slicing or cleavage is a catalytic process in which an sRNA binds to an AGO protein, guided to a target mRNA, which is subsequently cleaved by the PIWI domain of the catalytic AGO (Baulcombe, 2004; Iwakawa & Tomari, 2022). For cleavage to occur, the 5' end of the sRNA must be anchored in the AGO MID domain, and nucleotides 2 to 8 of the sRNA initiate binding. An almost perfect match between the sRNA and the mRNA at positions 9 to 12 is required for cleavage. Then, mRNA cleavage occurs between the nucleotides paired to sRNA positions 10 and 11 (Mallory & Vaucheret, 2010).

In humans, there are 4 Argonaute proteins, with AGO2 being the main and only slicer (Meister, 2013). Meanwhile, all 10 Argonaute proteins in Arabidopsis have a conserved catalytic motif, with AGO1 functioning as the main slicer in plants (Carbonell, 2017).

In silico prediction of sRNA targets across multiple organisms or microorganisms is typically based on standardised algorithms relying on the previously mentioned rules of complementarity and positioning. However, experimental and computational studies indicate that RNA silencing mechanisms are kingdom dependent. In plants, tools like TargetFinder and psRNATarget apply strict complementarity rules (Dai et al., 2018; Schwab et al., 2006), whereas tools like TargetScan and miRanda allow for more mismatches in animals (Agarwal et al., 2015; John et al., 2005). In the fungal system, these predictive rules do not fully align with those in mammals or plants due to the distinct phylogenetic differences, highlighting that accurate kingdom specific target prediction is essential to understand gene regulation across kingdoms. Although most prediction tools are based on common principles such as complementarity and interaction-site accessibility, their predictions often show limited overlap. This limitation can lead to missed true targets, increased off-target detection, and failure to identify non-canonical target sites or targets of sRNA types other than miRNAs or siRNAs that also associate with AGO proteins. These challenges underscore the need for whole transcriptome sequencing, integration of expression data, experimental validation, and the development of kingdom specific prediction and tailored prediction tools for effective study of RNAi and cross-kingdom communication (Grešová et al., 2022; Neumeier & Meister, 2021; Riolo et al., 2020).

Besides sRNA-target prediction, RNAi silencing investigation requires reliable detection and validation methods that can i) identify cleavage sites at single nucleotide resolution, ii) distinguish a real functional cleavage signal from random and or aberrant degradation, and iii) quantify these events within a biological context. A classical approach for mapping cleavage sites is RNA-ligase mediated 5'-RACE (RLM-RACE) in which an adapter is ligated to the cleaved RNA 5'-monophosphate, followed by fragment amplification and sequencing. While this method is able to detect a true functional slicing event and is cost-effective, it is low-throughput, cloning-biased, and often yields a very low number of sequencing reads (Liave et al., 2002). Another cleavage detection method is degradome sequencing (Addo-Quaye et al., 2008), also known as PARE (Parallel Analysis of RNA Ends) (German et al., 2008), and its low RNA input version NanoPARE (Schon et al., 2018). In this method, an adapter is also ligated to the 5'-monophosphate, followed by reverse transcription and high-throughput sequencing. Even though PARE provides genome-wide coverage and generates a substantial number of reads, it remains costly, requires advanced bioinformatics and statistical analysis, and is affected by strong background noise, leading to missing cleavage signal in highly degraded transcripts. To improve quantification and cleavage site detection precision, Werner and Nasfi et al. (2025) developed NIL-TDS, a method that integrates the principles of 5' RLM-RACE and nanopore sequencing. This method achieved high read depth at predicted sites and, with greater sensitivity compared to existing methods, quantified cleavage abundance, including low-abundant events, and effectively distinguished dominant biological signals from random degradation noise (Werner and Nasfi et al., 2025). Accurate prediction and detection of sRNA targets in RNA-based regulatory systems will deepen our understanding of sRNAomics field and facilitate the translation of fundamental knowledge into applied strategies for both human health and crop improvement.

10.5 RNA application between medicine and plant biology

Although RNAomics research is gaining interest, it has not yet achieved the breadth or impact of proteomics or genomics. A PubMed search using the terms "proteomic" vs. "small RNA" revealed that studies and publications on proteomics greatly outnumber those on small RNAs, both globally and in Arabidopsis thaliana-focused studies. This disparity confirms that sRNAomics, the study of sRNAs, remains a less developed

discipline. A similar imbalance is evident when comparing sRNA publications in human and mammalian research to those in plant and crop science, reflecting a predominant biomedical focus, particularly in cancer and disease studies. In contrast, studies of plant and crop sRNAs remain limited in number and often focus on model species or a few major crops. Various RNA-based technologies, including sRNAs, miRNAs, dsRNAs, mRNA, and the emerging circular RNAs (circRNAs), are increasingly used for targeted gene silencing in both medicine and crop protection. Patisiran, sold under the name Onpattro, is the first siRNA-based therapeutic approved by the US Food and Drug Administration (FDA). It is used for the treatment of hereditary Tranthyretin-Mediated Amyloidosis (hATTR), a rare and severe disease in which a mutated protein transthyretin (TTR) causes nerve damage and heart failure. The administrated siRNA, encapsulated in a lipid nanoparticle, binds to the TTR mRNA and uses the endogenous RNAi mechanism to degrade the transcript, thereby reducing production of the mutated protein (Adams et al., 2018; Research, 2024). Another famous RNA-based clinical success is the use of mRNA technology in COVID-19 vaccines, which were also delivered using lipid nanoparticles (Polack et al., 2020). Similar technologies are under development for cancer vaccines, with several treatments advancing to phase II and III clinical trials, demonstrating the growing success of RNA therapeutics in human medicine (Ho et al., 2022; Rupaimoole & Slack, 2017). On the other hand, only two RNAi-based products are currently commercialised in agriculture. Genetically modified maize MON 87411 expresses dsRNA targeting the Snf7 gene in corn rootworm essential for intracellular trafficking and membrane recycling together with three insecticidal proteins from *Bacillus thuringiensis* (Cry3Bb1 and Cry34Ab1/Cry35Ab1). Insects feeding on this maize ingest the dsRNA, which is processed into siRNAs that hijack the insect RNAi machinery, leading to gene silencing and mortality (Darlington et al., 2022). This product has been approved and considered safe in multiple countries, including the European Union, but excludes cultivation in the EU (EFSA GMO Panel, 2018). Another example is Calantha, the first and only dsRNA-based foliar bio-insecticide for crop protection. Calantha is effective against Colorado potato beetles, and its efficacy has been proven in laboratory, greenhouse, and field trials. When beetles feed on sprayed plants, they ingest dsRNA targeting PSMB5 (Proteasome subunit beta 5) gene. Impairing this protein is lethal. Calantha acts at the mRNA level, leading to transcript degradation, disruption of protein

synthesis, accumulation of defective proteins, cellular dysfunction, the beetle stops eating and dies within days (T. B. Rodrigues et al.,2021).

Although the potential of RNA products and RNA-based technologies, such as host-induced gene silencing (HIGS) and spray-induced gene silencing (SIGS), has been demonstrated through multiple proof-of-concept studies, significant challenges related to delivery, stability, cost, and biological variability remain to be addressed. Naked RNA degrades rapidly under environmental conditions, reducing its effectiveness in field applications. As a result, the development of effective formulations is ongoing. Efficiency also varies across microorganisms and species, mainly due to differences in uptake, systemic distribution, and RNAi machinery. Moreover, large-scale production of RNA products for field application is costly and requires continuous optimisation, particularly when produced in microbial or viral systems. Public acceptance presents an additional challenge. Regulatory issues and public confusion surrounding SIGS and genetically modified organisms (GMOs) further impede the transition from research to practical application of RNAi-based crop protection strategies (Hernández-Soto & Chacón-Cerdas, 2021; Zhao et al., 2024).

10.6 Application of *S. indica* in agriculture

The increasing demand for biological crop protection strategies and sustainable agriculture has highlighted the advantage of using beneficial microbes as eco-friendly and robust solution. *Serendipita indica* has a wide host range and is known for its numerous beneficial effects, including promoting plant growth, enhancing nutrient uptake, and increasing tolerance to biotic and abiotic stresses. Since its discovery, *S. indica* has been studied as a promising microorganism for agriculture. Lately, *S. indica* has been formulated as a “Rootonic” by combining fungal inoculum with nanoparticles such as copper (Rajak et al., 2017), zinc oxide, and carbon nanotubes (Varma et al., 2017), and applied to plant roots demonstrating its potential as a nanofertilizer. However, the use of chemical nanoparticles for agriculture is not widely accepted and may pose a risk to human health. In a recent study, dip-inoculated winter wheat roots in *S. indica* conidia suspension investigated the priming effect of *S.indica* against *Blumeria graminis* f. sp. *tritici*. In this study, fifteen, eight, and two quantitative trait loci (QTLs) were associated with resistance to Blumeria, shoot growth response, and root fresh growth

response, respectively. Additionally, thirty genes were identified as potentially involved in *S. indica*-induced priming, providing a basis for further investigation into the underlying mechanisms and the utility of *S.indica* in agriculture (Thielmann et al., 2026).

1.7 Conclusion and outlook

This project demonstrated that *S.indica* produces sRNA during interactions with Brachypodium and Arabidopsis. A pipeline was developed to study and validate the role of *Si*sRNAs in PTGS of Arabidopsis predicted target genes. Our results indicated that *Si*sRNAs are loaded into Arabidopsis AGO1 and AGO2, leading to mRNA degradation of Arabidopsis target genes. Moreover, a large pool of *Si*sRNAs is likely to be directly involved in cross-kingdom communication. We also showed that the Arabidopsis RNAi machinery is regulated upon *S.indica* colonisation and certain AGOs are required for promoting colonisation in a genotype-dependent manner with a potential functional redundancy between AGO1, AGO2 and AGO10.

This work, along with future functional analyses of *Si*sRNAs, will expand our understanding of plant-mutualistic interactions and the roles of sRNAs and potentially other RNA molecules in establishing mutualism. Given that *S. indica* colonises a wide range of crops and plants, comparative analysis across different *S.indica* crop species will answer whether these ck *Si*sRNAs are conserved or species-specific.

From an applied perspective, identifying functionally conserved *Si*sRNAs could facilitate the development and formulation of *Si*sRNAs-based products to enhance crop yield, either by priming crop protection against pathogens or by promoting growth and yield. More broadly, sRNAs are promising tools for innovative crop protection methods and technologies.

References

Adams, D., Gonzalez-Duarte, A., O'Riordan, W. D., Yang, C.-C., Ueda, M., Kristen, A. V., Tournev, I., Schmidt, H. H., Coelho, T., Berk, J. L., Lin, K.-P., Vita, G., Attarian, S., Planté-Bordeneuve, V., Mezei, M. M., Campistol, J. M., Buades, J., Brannagan, T. H., Kim, B. J., … Suhr, O. B. (2018). Patisiran, an RNAi Therapeutic, for Hereditary Transthyretin Amyloidosis. *New England Journal of Medicine*, *379*(1), 11–21. https://doi.org/10.1056/NEJMoa1716153

Addo-Quaye, C., Eshoo, T. W., Bartel, D. P., & Axtell, M. J. (2008). Endogenous siRNA and miRNA Targets Identified by Sequencing of the *Arabidopsis* Degradome. *Current Biology*, *18*(10), 758–762. https://doi.org/10.1016/j.cub.2008.04.042

Adhikari, S., Turner, M., & Subramanian, S. (2013). Hairpin Priming Is Better Suited than In Vitro Polyadenylation to Generate cDNA for Plant miRNA qPCR. *Molecular Plant*, *6*(1), 229–231. https://doi.org/10.1093/mp/sss106

Agarwal, V., Bell, G. W., Nam, J.-W., & Bartel, D. P. (2015). Predicting effective microRNA target sites in mammalian mRNAs. *eLife*, *4*, e05005. https://doi.org/10.7554/eLife.05005

Akum, F. N., Steinbrenner, J., Biedenkopf, D., Imani, J., & Kogel, K.-H. (2015). The Piriformospora indica effector PIIN_08944 promotes the mutualistic Sebacinalean symbiosis. *Frontiers in Plant Science*, *6*. https://doi.org/10.3389/fpls.2015.00906

Atia, M. A. M., Abdeldaym, E. A., Abdelsattar, M., Ibrahim, D. S. S., Saleh, I., Elwahab, M. A., Osman, G. H., Arif, I. A., & Abdelaziz, M. E. (2020). Piriformospora indica promotes cucumber tolerance against Root-knot nematode by modulating photosynthesis and innate responsive genes. *Saudi Journal of Biological Sciences*, *27*(1), 279–287. https://doi.org/10.1016/j.sjbs.2019.09.007

Aukerman, M. J., & Sakai, H. (2003). Regulation of Flowering Time and Floral Organ Identity by a MicroRNA and Its APETALA2-Like Target Genes. *The Plant Cell*, *15*(11), 2730–2741. https://doi.org/10.1105/tpc.016238

Axtell, M. J. (2013). ShortStack: Comprehensive annotation and quantification of small RNA genes. *RNA*, *19*(6), 740–751. https://doi.org/10.1261/rna.035279.112

Ayaz, M., Ali, Q., Zhao, W., Chi, Y.-K., Ali, F., Rashid, K. A., Cao, S., He, Y., Bukero, A. A., Huang, W.-K., & Qi, R.-D. (2024). Exploring plant growth promoting traits and biocontrol potential of new isolated Bacillus subtilis BS-2301 strain in suppressing Sclerotinia sclerotiorum through various mechanisms. *Frontiers in Plant Science*, *15*. https://doi.org/10.3389/fpls.2024.1444328

Bajaj, R., Huang, Y., Gebrechristos, S., Mikolajczyk, B., Brown, H., Prasad, R., Varma, A., & Bushley, K. E. (2018). Transcriptional responses of soybean roots to colonization with the root endophytic fungus Piriformospora indica reveals altered phenylpropanoid and secondary metabolism. *Scientific Reports*, *8*, 10227. https://doi.org/10.1038/s41598-018-26809-3

Bartel, D. P. (2009). MicroRNA Target Recognition and Regulatory Functions. *Cell*, *136*(2), 215–233. https://doi.org/10.1016/j.cell.2009.01.002

Baulcombe, D. (2004). RNA silencing in plants. *Nature*, *431*(7006), Article 7006. https://doi.org/10.1038/nature02874

Bleackley, M. R., Samuel, M., Garcia-Ceron, D., McKenna, J. A., Lowe, R. G. T., Pathan, M., Zhao, K., Ang, C.-S., Mathivanan, S., & Anderson, M. A. (2020). Extracellular Vesicles From the Cotton Pathogen Fusarium oxysporum f. Sp. Vasinfectum Induce a Phytotoxic Response in Plants. *Frontiers in Plant Science*, *10*. https://doi.org/10.3389/fpls.2019.01610

Bohmert, K., Camus, I., Bellini, C., Bouchez, D., Caboche, M., & Benning, C. (1998). AGO1 defines a novel locus of Arabidopsis controlling leaf development. *The EMBO Journal*, *17*(1), 170–180. https://doi.org/10.1093/emboj/17.1.170

Bologna, N. G., & Voinnet, O. (2014). The diversity, biogenesis, and activities of endogenous silencing small RNAs in Arabidopsis. *Annual Review of Plant Biology*, *65*, 473–503. https://doi.org/10.1146/annurev-arplant-050213-035728

Boorboori, M. R., & Zhang, H.-Y. (2022). The Role of Serendipita indica (Piriformospora indica) in Improving Plant Resistance to Drought and Salinity Stresses. *Biology*, *11*(7), Article 7. https://doi.org/10.3390/biology11070952

Boualem, A., Laporte, P., Jovanovic, M., Laffont, C., Plet, J., Combier, J.-P., Niebel, A., Crespi, M., & Frugier, F. (2008). MicroRNA166 controls root and nodule development in Medicago truncatula. *The Plant Journal*, *54*(5), 876–887. https://doi.org/10.1111/j.1365-313X.2008.03448.x

Bramlett, M., Plaetinck, G., & Maienfisch, P. (2020). RNA-Based Biocontrols—A New Paradigm in Crop Protection. *Engineering*, *6*(5), 522–527. https://doi.org/10.1016/j.eng.2019.09.008

Branscheid, A., Sieh, D., Pant, B. D., May, P., Devers, E. A., Elkrog, A., Schauser, L., Scheible, W.-R., & Krajinski, F. (2010). Expression Pattern Suggests a Role of MiR399 in the Regulation of the Cellular Response to Local Pi Increase During Arbuscular Mycorrhizal Symbiosis. *Molecular Plant-Microbe Interactions®*, *23*(7), 915–926. https://doi.org/10.1094/MPMI-23-7-0915

Brodersen, P., Sakvarelidze-Achard, L., Bruun-Rasmussen, M., Dunoyer, P., Yamamoto, Y. Y., Sieburth, L., & Voinnet, O. (2008). Widespread Translational Inhibition by Plant miRNAs and siRNAs. *Science*, *320*(5880), 1185–1190. https://doi.org/10.1126/science.1159151

Brosseau, C., El Oirdi, M., Adurogbangba, A., Ma, X., & Moffett, P. (2016). Antiviral Defense Involves AGO4 in an Arabidopsis–Potexvirus Interaction. *Molecular Plant-Microbe Interactions®*, *29*(11), 878–888. https://doi.org/10.1094/MPMI-09-16-0188-R

Brosseau, C., & Moffett, P. (2015). Functional and Genetic Analysis Identify a Role for Arabidopsis ARGONAUTE5 in Antiviral RNA Silencing. *The Plant Cell*, *27*(6), 1742–1754. https://doi.org/10.1105/tpc.15.00264

Bucher, G., Scholten, J., & Klingler, M. (2002). Parental RNAi in *Tribolium* (Coleoptera). *Current Biology*, *12*(3), R85–R86. https://doi.org/10.1016/S0960-9822(02)00666-8

C, L., Z, X., Kd, K., & Jc, C. (2002). Cleavage of Scarecrow-like mRNA targets directed by a class of Arabidopsis miRNA. *PubMed*. https://pubmed.ncbi.nlm.nih.gov/12242443/

Cai, Q., Qiao, L., Wang, M., He, B., Lin, F.-M., Palmquist, J., Huang, S.-D., & Jin, H. (2018). Plants send small RNAs in extracellular vesicles to fungal pathogen to silence virulence genes. *Science*, *360*(6393), 1126–1129. https://doi.org/10.1126/science.aar4142

Carbonell, A. (2017). Plant ARGONAUTEs: Features, Functions, and Unknowns. In A. Carbonell (Ed.), *Plant Argonaute Proteins: Methods and Protocols* (pp. 1–21). Springer. https://doi.org/10.1007/978-1-4939-7165-7_1

Carbonell, A., & Carrington, J. C. (2015). Antiviral roles of plant ARGONAUTES. *Current Opinion in Plant Biology, Cell Signalling and Gene Regulation*, *27*, 111–117. https://doi.org/10.1016/j.pbi.2015.06.013

Carthew, R. W., & Sontheimer, E. J. (2009). Origins and Mechanisms of miRNAs and siRNAs. *Cell*, *136*(4), 642–655. https://doi.org/10.1016/j.cell.2009.01.035

Chen, X. (2009). Small RNAs and Their Roles in Plant Development. *Annual Review of Cell and Developmental Biology*, *25*, 21–44. https://doi.org/10.1146/annurev.cellbio.042308.113417

Cizmar, P., & Yuana, Y. (2017). *Detection and Characterization of Extracellular Vesicles by Transmission and Cryo-Transmission Electron Microscopy*. https://doi.org/10.1007/978-1-4939-7253-1_18

Colombo, M., Raposo, G., & Théry, C. (2014). Biogenesis, secretion, and intercellular interactions of exosomes and other extracellular vesicles. *Annual Review of Cell and Developmental Biology*, *30*, 255–289. https://doi.org/10.1146/annurev-cellbio-101512-122326

Combier, J.-P., Frugier, F., de Billy, F., Boualem, A., El-Yahyaoui, F., Moreau, S., Vernié, T., Ott, T., Gamas, P., Crespi, M., & Niebel, A. (2006). MtHAP2-1 is a key transcriptional regulator of symbiotic nodule development regulated by microRNA169 in Medicago truncatula. *Genes & Development*, *20*(22), 3084–3088. https://doi.org/10.1101/gad.402806

Compant, S., Cassan, F., Kostić, T., Johnson, L., Brader, G., Trognitz, F., & Sessitsch, A. (2025). Harnessing the plant microbiome for sustainable crop production. *Nature Reviews Microbiology*, *23*(1), 9–23. https://doi.org/10.1038/s41579-024-01079-1

Czech, B., & Hannon, G. J. (2011). Small RNA sorting: Matchmaking for Argonautes. *Nature Reviews. Genetics*, *12*(1), 19–31. https://doi.org/10.1038/nrg2916

Dai, X., Zhuang, Z., & Zhao, P. X. (2018). psRNATarget: A plant small RNA target analysis server (2017 release). *Nucleic Acids Research*, *46*(Web Server issue), W49–W54. https://doi.org/10.1093/nar/gky316

Dalakouras, A., Katsaouni, A., Avramidou, M., Dadami, E., Tsiouri, O., Vasileiadis, S., Makris, A., Georgopoulou, M. E., & Papadopoulou, K. K. (2023). A beneficial fungal root endophyte triggers systemic RNA silencing and DNA methylation of a host reporter gene. *RNA Biology*, *20*(1), 20–30. https://doi.org/10.1080/15476286.2022.2159158

Dalio, R. J. D., Paschoal, D., Arena, G. D., Magalhães, D. M., Oliveira, T. S., Merfa, M. V., Maximo, H. J., & Machado, M. A. (2021). Hypersensitive response: From NLR pathogen recognition to cell death response. *Annals of Applied Biology*, *178*(2), 268–280. https://doi.org/10.1111/aab.12657

Darlington, M., Reinders, J. D., Sethi, A., Lu, A. L., Ramaseshadri, P., Fischer, J. R., Boeckman, C. J., Petrick, J. S., Roper, J. M., Narva, K. E., & Vélez, A. M. (2022). RNAi for Western Corn Rootworm Management: Lessons Learned, Challenges, and Future Directions. *Insects*, *13*(1), 57. https://doi.org/10.3390/insects13010057

De Rocchis, V., Jammer, A., Camehl, I., Franken, P., & Roitsch, T. (2022). Tomato growth promotion by the fungal endophytes *Serendipita indica* and *Serendipita herbamans* is associated with sucrose *de-novo* synthesis in roots and differential local and systemic effects on carbohydrate metabolisms and gene expression. *Journal of Plant Physiology*, *276*, 153755. https://doi.org/10.1016/j.jplph.2022.153755

Deleris, A., Gallego-Bartolome, J., Bao, J., Kasschau, K. D., Carrington, J. C., & Voinnet, O. (2006). Hierarchical Action and Inhibition of Plant Dicer-Like Proteins in Antiviral Defense. *Science*, *313*(5783), 68–71. https://doi.org/10.1126/science.1128214

Deshmukh, S., Hückelhoven, R., Schäfer, P., Imani, J., Sharma, M., Weiss, M., Waller, F., & Kogel, K.-H. (2006). The root endophytic fungus Piriformospora indica requires host cell death for proliferation during mutualistic symbiosis with barley. *Proceedings of the National Academy of Sciences*, *103*(49), 18450–18457. https://doi.org/10.1073/pnas.0605697103

Dodds, P. N., & Rathjen, J. P. (2010). Plant immunity: Towards an integrated view of plant–pathogen interactions. *Nature Reviews Genetics*, *11*(8), 539–548. https://doi.org/10.1038/nrg2812

Duan, C.-G., Zhang, H., Tang, K., Zhu, X., Qian, W., Hou, Y.-J., Wang, B., Lang, Z., Zhao, Y., Wang, X., Wang, P., Zhou, J., Liang, G., Liu, N., Wang, C., & Zhu, J.-K. (2015). Specific but interdependent functions for Arabidopsis AGO4 and AGO6 in RNA-directed DNA methylation. *The EMBO Journal*, *34*(5), 581–592. https://doi.org/10.15252/embj.201489453

Dunker, F., Lederer, B., & Weiberg, A. (2021). Plant ARGONAUTE Protein Immunopurification for Pathogen Cross Kingdom Small RNA Analysis. *Bio-Protocol*, *11*(3), e3911. https://doi.org/10.21769/BioProtoc.3911

Dunker, F., Trutzenberg, A., Rothenpieler, J. S., Kuhn, S., Pröls, R., Schreiber, T., Tissier, A., Kemen, A., Kemen, E., Hückelhoven, R., & Weiberg, A. (2020). Oomycete small RNAs bind to the plant RNA-induced silencing complex for virulence. *eLife*, *9*, e56096. https://doi.org/10.7554/eLife.56096

Eamens, A. L., Smith, N. A., Curtin, S. J., Wang, M.-B., & Waterhouse, P. M. (2009). *The Arabidopsis thaliana double-stranded RNA binding protein DRB1 directs guide strand selection from microRNA duplexes*. https://doi.org/10.1261/rna.1646909

Fang, X., & Qi, Y. (2016). RNAi in Plants: An Argonaute-Centered View. *The Plant Cell*, *28*(2), 272–285. https://doi.org/10.1105/tpc.15.00920

Feng, F., Sun, J., Radhakrishnan, G. V., Lee, T., Bozsóki, Z., Fort, S., Gavrin, A., Gysel, K., Thygesen, M. B., Andersen, K. R., Radutoiu, S., Stougaard, J., & Oldroyd, G. E. D. (2019). A combination of chitooligosaccharide and lipochitooligosaccharide recognition promotes arbuscular mycorrhizal associations in Medicago truncatula. *Nature Communications*, *10*(1), 5047. https://doi.org/10.1038/s41467-019-12999-5

Fire, A., Xu, S., Montgomery, M. K., Kostas, S. A., Driver, S. E., & Mello, C. C. (1998). Potent and specific genetic interference by double-stranded RNA in Caenorhabditis elegans. *Nature*, *391*(6669), 806–811. https://doi.org/10.1038/35888

Fu, W.-L., Wu, W.-J., Xiao, Z.-Y., Wang, F.-L., Cheng, J.-Y., Zou, Y.-N., Hashem, A., Abd_Allah, E. F., & Wu, Q.-S. (2024). Serendipita indica: A Promising Biostimulant for Improving Growth, Nutrient Uptake, and Sugar Accumulation in Camellia oleifera. *Horticulturae*, *10*(9), Article 9. https://doi.org/10.3390/horticulturae10090936

Galli, M., Feldmann, F., Vogler, U. K., & Kogel, K.-H. (2024). Can biocontrol be the game-changer in integrated pest management? A review of definitions, methods and strategies. *Journal of Plant Diseases and Protection*, *131*(2), 265–291. https://doi.org/10.1007/s41348-024-00878-1

Gao, Z., Liu, H.-L., Daxinger, L., Pontes, O., He, X., Qian, W., Lin, H., Xie, M., Lorkovic, Z. J., Zhang, S., Miki, D., Zhan, X., Pontier, D., Lagrange, T., Jin, H., Matzke, A. J. M., Matzke, M., Pikaard, C. S., & Zhu, J.-K. (2010). An RNA polymerase II- and AGO4-associated protein acts in RNA-directed DNA methylation. *Nature*, *465*(7294), 106–109. https://doi.org/10.1038/nature09025

Gasciolli, V., Mallory, A. C., Bartel, D. P., & Vaucheret, H. (2005). Partially Redundant Functions of Arabidopsis DICER-like Enzymes and a Role for DCL4 in Producing trans-Acting siRNAs. *Current Biology*, *15*(16), 1494–1500. https://doi.org/10.1016/j.cub.2005.07.024

Gautam, V., Singh, A., Verma, S., Kumar, A., Kumar, P., Mahima, Singh, S., Mishra, V., & Sarkar, A. K. (2017). Role of miRNAs in root development of model plant Arabidopsis thaliana. *Indian Journal of Plant Physiology*, *22*(4), 382–392. https://doi.org/10.1007/s40502-017-0334-8

German, M. A., Pillay, M., Jeong, D.-H., Hetawal, A., Luo, S., Janardhanan, P., Kannan, V., Rymarquis, L. A., Nobuta, K., German, R., De Paoli, E., Lu, C., Schroth, G., Meyers, B. C., & Green, P. J. (2008). Global identification of microRNA–target RNA pairs by parallel analysis of RNA ends. *Nature Biotechnology*, *26*(8), 941–946. https://doi.org/10.1038/nbt1417

Germing, K., Navarrete, C. A. D., Schiermeyer, A., Hommen, U., Zühl, L., Eilebrecht, S., & Eilebrecht, E. (2025). Crop protection by RNA interference: A review of recent approaches, current state of developments and use as of 2013. *Environmental Sciences Europe*, *37*(1), 15. https://doi.org/10.1186/s12302-025-01052-6

Glaeser, S. P., Imani, J., Alabid, I., Guo, H., Kumar, N., Kämpfer, P., Hardt, M., Blom, J., Goesmann, A., Rothballer, M., Hartmann, A., & Kogel, K.-H. (2016). Non-pathogenic Rhizobium radiobacter F4 deploys plant beneficial activity independent of its host Piriformospora indica. *The ISME Journal*, *10*(4), 871–884. https://doi.org/10.1038/ismej.2015.163

Gong, X.-Y., Wang, Z.-H., Bashir, M., Tang, T., Gan, X., & Yang, W.-C. (2025). Recent Application of CRISPR/Cas in Plant Disease Detection. *TrAC Trends in Analytical Chemistry*, 118251. https://doi.org/10.1016/j.trac.2025.118251

González Ortega-Villaizán, A., King, E., Patel, M. K., Pérez-Alonso, M.-M., Scholz, S. S., Sakakibara, H., Kiba, T., Kojima, M., Takebayashi, Y., Ramos, P., Morales-Quintana, L., Breitenbach, S., Smolko, A., Salopek-Sondi, B., Bauer, N., Ludwig-Müller, J., Krapp, A., Oelmüller, R., Vicente-Carbajosa, J., & Pollmann, S. (2024). The endophytic fungus Serendipita indica affects auxin distribution in Arabidopsis thaliana roots through alteration of auxin transport and conjugation to promote plant growth. *Plant, Cell & Environment*, *47*(10), 3899–3919. https://doi.org/10.1111/pce.14989

Grešová, K., Alexiou, P., & Giassa, I.-C. (2022). Small RNA Targets: Advances in Prediction Tools and High-Throughput Profiling. *Biology*, *11*(12), 1798. https://doi.org/10.3390/biology11121798

Harvey, J. J. W., Lewsey, M. G., Patel, K., Westwood, J., Heimstädt, S., Carr, J. P., & Baulcombe, D. C. (2011). An Antiviral Defense Role of AGO2 in Plants. *PLOS ONE*, *6*(1), e14639. https://doi.org/10.1371/journal.pone.0014639

He, B., Cai, Q., Qiao, L., Huang, C.-Y., Wang, S., Miao, W., Ha, T., Wang, Y., & Jin, H. (2021). RNA-binding proteins contribute to small RNA loading in plant extracellular vesicles. *Nature Plants*, *7*(3), 342–352. https://doi.org/10.1038/s41477-021-00863-8

He, B., Wang, H., Liu, G., Chen, A., Calvo, A., Cai, Q., & Jin, H. (2023a). Fungal small RNAs ride in extracellular vesicles to enter plant cells through clathrin-mediated endocytosis. *Nature Communications*, *14*(1), 4383. https://doi.org/10.1038/s41467-023-40093-4

Henderson, I. R., Zhang, X., Lu, C., Johnson, L., Meyers, B. C., Green, P. J., & Jacobsen, S. E. (2006). Dissecting Arabidopsis thaliana DICER function in small RNA processing, gene silencing and DNA methylation patterning. *Nature Genetics*, *38*(6), 721–725. https://doi.org/10.1038/ng1804

Hernández-Soto, A., & Chacón-Cerdas, R. (2021). RNAi Crop Protection Advances. *International Journal of Molecular Sciences*, *22*(22), 12148. https://doi.org/10.3390/ijms222212148

Hill, E. H., & Solomon, P. S. (2020). Extracellular vesicles from the apoplastic fungal wheat pathogen Zymoseptoria tritici. *Fungal Biology and Biotechnology*, *7*(1), 13. https://doi.org/10.1186/s40694-020-00103-2

Ho, P. T. B., Clark, I. M., Le, L. T. T., Ho, P. T. B., Clark, I. M., & Le, L. T. T. (2022). MicroRNA-Based Diagnosis and Therapy. *International Journal of Molecular Sciences*, *23*(13). https://www.mdpi.com/1422-0067/23/13/7167

Holland, S., & Roth, R. (2023). Extracellular Vesicles in the Arbuscular Mycorrhizal Symbiosis: Current Understanding and Future Perspectives. *Molecular Plant-Microbe Interactions®*, *36*(4), 235–244. https://doi.org/10.1094/MPMI-09-22-0189-FI

Hosseini, F., Mosaddeghi, M. R., & Dexter, A. R. (2017). Effect of the fungus *Piriformospora indica* on physiological characteristics and root morphology of wheat under combined drought and mechanical stresses. *Plant Physiology and Biochemistry*, *118*, 107–120. https://doi.org/10.1016/j.plaphy.2017.06.005

Iwakawa, H., & Tomari, Y. (2022). Life of RISC: Formation, action, and degradation of RNA-induced silencing complex. *Molecular Cell*, *82*(1), 30–43. https://doi.org/10.1016/j.molcel.2021.11.026

Jacobs, S., Zechmann, B., Molitor, A., Trujillo, M., Petutschnig, E., Lipka, V., Kogel, K.-H., & Schäfer, P. (2011). Broad-Spectrum Suppression of Innate Immunity Is Required for Colonization of Arabidopsis Roots by the Fungus Piriformospora indica. *Plant Physiology*, *156*(2), 726–740. https://doi.org/10.1104/pp.111.176446

Jaubert, M., Bhattacharjee, S., Mello, A. F. S., Perry, K. L., & Moffett, P. (2011). ARGONAUTE2 Mediates RNA-Silencing Antiviral Defenses against Potato virus X in Arabidopsis. *Plant Physiology*, *156*(3), 1556–1564. https://doi.org/10.1104/pp.111.178012

Ji, L., Liu, X., Yan, J., Wang, W., Yumul, R. E., Kim, Y. J., Dinh, T. T., Liu, J., Cui, X., Zheng, B., Agarwal, M., Liu, C., Cao, X., Tang, G., & Chen, X. (2011). ARGONAUTE10 and ARGONAUTE1 Regulate the Termination of Floral Stem Cells through Two MicroRNAs in Arabidopsis. *PLoS Genetics*, *7*(3), e1001358. https://doi.org/10.1371/journal.pgen.1001358

Jia, Y., Niu, H., Zhao, P., Li, X., Yan, F., Wang, C., & Qiu, Z. (2023). Synergistic biocontrol of Bacillus subtilis and Pseudomonas fluorescens against early blight disease in tomato. *Applied Microbiology and Biotechnology*, *107*(19), 6071–6083. https://doi.org/10.1007/s00253-023-12642-w

Jia, Y., Yu, L., Ma, T., Xu, W., Qian, H., Sun, Y., & Shi, H. (n.d.). *Small extracellular vesicles isolation and separation: Current techniques, pending questions and clinical applications*. Retrieved 25 January 2026, from https://www.thno.org/v12p6548.htm

John, B., Enright, A. J., Aravin, A., Tuschl, T., Sander, C., & Marks, D. S. (n.d.). *Correction: Human MicroRNA Targets*. https://doi.org/10.1371/journal.pbio.0030264

Johnstone, R. M., Adam, M., Hammond, J. R., Orr, L., & Turbide, C. (1987). Vesicle formation during reticulocyte maturation. Association of plasma membrane

activities with released vesicles (exosomes). *Journal of Biological Chemistry*, *262*(19), 9412–9420. https://doi.org/10.1016/S0021-9258(18)48095-7

Jones, J. D. G., & Dangl, J. L. (2006). The plant immune system. *Nature*, *444*(7117), 323–329. https://doi.org/10.1038/nature05286

Jones-Rhoades, M. W., Bartel, D. P., & Bartel, B. (2006). MicroRNAS and their regulatory roles in plants. *Annual Review of Plant Biology*, *57*, 19–53. https://doi.org/10.1146/annurev.arplant.57.032905.105218

Kellari, L. M., Dalakouras, A., Tsiouri, O., Vletsos, P., Katsaouni, A., Uslu, V. V., & Papadopoulou, K. K. (2025). Cross-kingdom RNAi induced by a beneficial endophytic fungus to its host requires transitivity and amplification of silencing signals. *Plant Biology (Stuttgart, Germany)*, *27*(4), 504–514. https://doi.org/10.1111/plb.70026

Kidner, C. A., & Martienssen, R. A. (2005). The role of ARGONAUTE1 (AGO1) in meristem formation and identity. *Developmental Biology*, *280*(2), 504–517. https://doi.org/10.1016/j.ydbio.2005.01.031

Kim, J.-H., Dubey, S. K., Ryu, T. H., Lee, S. S., & Chung, B. Y. (2025). Argonaute 2 regulates nuclear DNA damage, repair, and phenotypes in *Arabidopsis* under genotoxic stress. *Plant Physiology and Biochemistry*, *220*, 109528. https://doi.org/10.1016/j.plaphy.2025.109528

Kloppholz, S., Kuhn, H., & Requena, N. (2011). A Secreted Fungal Effector of *Glomus intraradices* Promotes Symbiotic Biotrophy. *Current Biology*, *21*(14), 1204–1209. https://doi.org/10.1016/j.cub.2011.06.044

Koch, B. L., Rutter, B. D., Borniego, M. L., Singla-Rastogi, M., Gardner, D. M., & Innes, R. W. (2025). Arabidopsis Produces Distinct Subpopulations of Extracellular Vesicles That Respond Differentially to Biotic Stress, Altering Growth and Infectivity of a Fungal Pathogen. *Journal of Extracellular Vesicles*, *14*(5), e70090. https://doi.org/10.1002/jev2.70090

Kong, X., Yang, M., Le, B. H., He, W., & Hou, Y. (2022). The master role of siRNAs in plant immunity. *Molecular Plant Pathology*, *23*(10), 1565–1574. https://doi.org/10.1111/mpp.13250

Kurihara, Y., & Watanabe, Y. (2004). Arabidopsis micro-RNA biogenesis through Dicer-like 1 protein functions. *Proceedings of the National Academy of Sciences*, *101*(34), 12753–12758. https://doi.org/10.1073/pnas.0403115101

Kusch, S., Frantzeskakis, L., Thieron, H., & Panstruga, R. (2018). Small RNAs from cereal powdery mildew pathogens may target host plant genes. *Fungal Biology*, *122*(11), 1050–1063. https://doi.org/10.1016/j.funbio.2018.08.008

Kwon, S., Rupp, O., Brachmann, A., Blum, C. F., Kraege, A., Goesmann, A., & Feldbrügge, M. (2021). mRNA Inventory of Extracellular Vesicles from Ustilago maydis. *Journal of Fungi*, *7*(7), Article 7. https://doi.org/10.3390/jof7070562

Lee, Y.-C., Johnson, J. M., Chien, C.-T., Sun, C., Cai, D., Lou, B., Oelmüller, R., & Yeh, K.-W. (2011). Growth promotion of Chinese cabbage and Arabidopsis by

Piriformospora indica is not stimulated by mycelium-synthesized auxin. *Molecular Plant-Microbe Interactions: MPMI*, *24*(4), 421–431. https://doi.org/10.1094/MPMI-05-10-0110

Li, L., Feng, Y., Qi, F., & Hao, R. (2023). Research Progress of Piriformospora indica in Improving Plant Growth and Stress Resistance to Plant. *Journal of Fungi*, *9*(10), 965. https://doi.org/10.3390/jof9100965

Li, Q.-S., Xie, Y.-C., Rahman, M. M., Hashem, A., Abd_Allah, E. F., & Wu, Q.-S. (2022). Arbuscular Mycorrhizal Fungi and Endophytic Fungi Activate Leaf Antioxidant Defense System of Lane Late Navel Orange. *Journal of Fungi*, *8*(3), 282. https://doi.org/10.3390/jof8030282

Li, X., Wajjiha, B., Zhang, P., Dang, Y., Prasad, R., Wei, Y., & Zhang, S.-H. (2023). Serendipita indica chitinase protects rice from the blast and bakanae diseases. *Journal of Basic Microbiology*, *63*(7), 734–745. https://doi.org/10.1002/jobm.202200349

Liang, C., Wang, X., He, H., Xu, C., Cui, J., Liang, C., Wang, X., He, H., Xu, C., & Cui, J. (2023). Beyond Loading: Functions of Plant ARGONAUTE Proteins. *International Journal of Molecular Sciences*, *24*(22). https://www.mdpi.com/1422-0067/24/22/16054

Linares, R., Tan, S., Gounou, C., Arraud, N., & Brisson, A. R. (2015). High-speed centrifugation induces aggregation of extracellular vesicles. *Journal of Extracellular Vesicles*, *4*(1), 29509. https://doi.org/10.3402/jev.v4.29509

Lincoln, C., Britton, J. H., & Estelle, M. (1990). Growth and development of the axr1 mutants of Arabidopsis. *The Plant Cell*, *2*(11), 1071–1080.

Liu, B., Jing, D., Liu, F., Ma, H., Liu, X., & Peng, L. (2021). Serendipita indica alleviates drought stress responses in walnut (Juglans regia L.) seedlings by stimulating osmotic adjustment and antioxidant defense system. *Applied Microbiology and Biotechnology*, *105*(23), 8951–8968. https://doi.org/10.1007/s00253-021-11653-9

Liu, C., Xin, Y., Xu, L., Cai, Z., Xue, Y., Liu, Y., Xie, D., Liu, Y., & Qi, Y. (2018). *Arabidopsis* ARGONAUTE 1 Binds Chromatin to Promote Gene Transcription in Response to Hormones and Stresses. *Developmental Cell*, *44*(3), 348-361.e7. https://doi.org/10.1016/j.devcel.2017.12.002

Livak, K. J., & Schmittgen, T. D. (2001). Analysis of relative gene expression data using real-time quantitative PCR and the 2(-Delta Delta C(T)) Method. *Methods (San Diego, Calif.)*, *25*(4), 402–408. https://doi.org/10.1006/meth.2001.1262

Loreti, E., Betti, F., Ladera-Carmona, M. J., Fontana, F., Novi, G., Valeri, M. C., & Perata, P. (2020). ARGONAUTE1 and ARGONAUTE4 Regulate Gene Expression and Hypoxia Tolerance1 [OPEN]. *Plant Physiology*, *182*(1), 287–300. https://doi.org/10.1104/pp.19.00741

Ma, X., Nicole, M.-C., Meteignier, L.-V., Hong, N., Wang, G., & Moffett, P. (2015). Different roles for RNA silencing and RNA processing components in virus recovery and virus-

induced gene silencing in plants. *Journal of Experimental Botany*, *66*(3), 919–932. https://doi.org/10.1093/jxb/eru447

Mallory, A. C., Hinze, A., Tucker, M. R., Bouché, N., Gasciolli, V., Elmayan, T., Lauressergues, D., Jauvion, V., Vaucheret, H., & Laux, T. (2009). Redundant and Specific Roles of the ARGONAUTE Proteins AGO1 and ZLL in Development and Small RNA-Directed Gene Silencing. *PLOS Genetics*, *5*(9), e1000646. https://doi.org/10.1371/journal.pgen.1000646

Mallory, A., & Vaucheret, H. (2010). Form, Function, and Regulation of ARGONAUTE Proteins. *The Plant Cell*, *22*(12), 3879–3889. https://doi.org/10.1105/tpc.110.080671

Margis, R., Fusaro, A. F., Smith, N. A., Curtin, S. J., Watson, J. M., Finnegan, E. J., & Waterhouse, P. M. (2006). The evolution and diversification of Dicers in plants. *FEBS Letters*, *580*(10), 2442–2450. https://doi.org/10.1016/j.febslet.2006.03.072

Marrassini, V., Ercoli, L., Paredes, A. V. A., & Pellegrino, E. (2025). Positive response to inoculation with indigenous arbuscular mycorrhizal fungi as modulated by barley genotype. *Agronomy for Sustainable Development*, *45*(2), 21. https://doi.org/10.1007/s13593-025-01016-3

Meister, G. (2013). Argonaute proteins: Functional insights and emerging roles. *Nature Reviews Genetics*, *14*(7), 447–459. https://doi.org/10.1038/nrg3462

Mewalal, R., Yin, H., Hu, R., Jawdy, S., Vion, P., Tuskan, G. A., Le Tacon, F., Labbé, J. L., & Yang, X. (2019). Identification of Populus Small RNAs Responsive to Mutualistic Interactions With Mycorrhizal Fungi, Laccaria bicolor and Rhizophagus irregularis. *Frontiers in Microbiology*, *10*. https://doi.org/10.3389/fmicb.2019.00515

Mi, S., Cai, T., Hu, Y., Chen, Y., Hodges, E., Ni, F., Wu, L., Li, S., Zhou, H., Long, C., Chen, S., Hannon, G. J., & Qi, Y. (2008). Sorting of Small RNAs into Arabidopsis Argonaute Complexes Is Directed by the 5' Terminal Nucleotide. *Cell*, *133*(1), 116–127. https://doi.org/10.1016/j.cell.2008.02.034

Molitor, A., Zajic, D., Voll, L. M., Pons-Kühnemann, J., Samans, B., Kogel, K.-H., & Waller, F. (2011). Barley Leaf Transcriptome and Metabolite Analysis Reveals New Aspects of Compatibility and Piriformospora indica–Mediated Systemic Induced Resistance to Powdery Mildew. *Molecular Plant-Microbe Interactions®*, *24*(12), 1427–1439. https://doi.org/10.1094/MPMI-06-11-0177

Montag, K., Ivanov, R., & Bauer, P. (n.d.). *Frontiers | Role of SEC14-like phosphatidylinositol transfer proteins in membrane identity and dynamics*. https://doi.org/10.3389/fpls.2023.1181031

Montgomery, T. A., Howell, M. D., Cuperus, J. T., Li, D., Hansen, J. E., Alexander, A. L., Chapman, E. J., Fahlgren, N., Allen, E., & Carrington, J. C. (2008). Specificity of ARGONAUTE7-miR390 Interaction and Dual Functionality in *TAS3 Trans*-Acting siRNA Formation. *Cell*, *133*(1), 128–141. https://doi.org/10.1016/j.cell.2008.02.033

Morgado, L., Jansen, R. C., & Johannes, F. (2017). *Learning sequence patterns of AGO-sRNA affinity from high-throughput sequencing libraries to improve* in silico

functional small RNA detection and classification in plants. https://doi.org/10.1101/173575

Napoli, C., Lemieux, C., & Jorgensen, R. (1990). Introduction of a Chimeric Chalcone Synthase Gene into Petunia Results in Reversible Co-Suppression of Homologous Genes in trans. *The Plant Cell*, *2*(4), 279–289.

Nasfi, S., & Kogel, K.-H. (2022). Packaged or unpackaged: Appearance and transport of extracellular noncoding RNAs in the plant apoplast. *ExRNA; Vol 4 (May 31, 2022): ExRNA*. https://exrna.amegroups.com/article/view/64855

Nasfi, S., Shahbazi, S., Bitterlich, K., Šečić, E., Kogel, K.-H., & Steinbrenner, J. (2024). A pipeline for validation of Serendipita indica effector-like sRNA suggests cross-kingdom communication in the symbiosis with Arabidopsis. *Journal of Experimental Botany*, erae515. https://doi.org/10.1093/jxb/erae515

Neumeier, J., & Meister, G. (2021). *Frontiers | siRNA Specificity: RNAi Mechanisms and Strategies to Reduce Off-Target Effects*. https://doi.org/10.3389/fpls.2020.526455

Nguyen, Q.-M., Iswanto, A. B. B., Son, G. H., & Kim, S. H. (2021). Recent Advances in Effector-Triggered Immunity in Plants: New Pieces in the Puzzle Create a Different Paradigm. *International Journal of Molecular Sciences*, *22*(9), 4709. https://doi.org/10.3390/ijms22094709

Ngwene, B., Boukail, S., Söllner, L., Franken, P., & Andrade-Linares, D. R. (2016). Phosphate utilization by the fungal root endophyte Piriformospora indica. *Plant and Soil*, *405*(1), 231–241. https://doi.org/10.1007/s11104-015-2779-8

Nizam, S., Qiang, X., Wawra, S., Nostadt, R., Getzke, F., Schwanke, F., Dreyer, I., Langen, G., & Zuccaro, A. (2019). Serendipita indica E5'NT modulates extracellular nucleotide levels in the plant apoplast and affects fungal colonization. *EMBO Reports*, *20*(2), e47430. https://doi.org/10.15252/embr.201847430

Oerke, E.-C. (2006). Crop losses to pests. *The Journal of Agricultural Science*, *144*(1), 31–43. https://doi.org/10.1017/S0021859605005708

Oldroyd, G. E. D. (2013). Speak, friend, and enter: Signalling systems that promote beneficial symbiotic associations in plants. *Nature Reviews Microbiology*, *11*(4), 252–263. https://doi.org/10.1038/nrmicro2990

Organisms (GMO), E. P. on G. M., Naegeli, H., Birch, A. N., Casacuberta, J., De Schrijver, A., Gralak, M. A., Guerche, P., Jones, H., Manachini, B., Messéan, A., Nielsen, E. E., Nogué, F., Robaglia, C., Rostoks, N., Sweet, J., Tebbe, C., Visioli, F., Wal, J.-M., Ardizzone, M., … Ramon, M. (2018). Assessment of genetically modified maize MON 87411 for food and feed uses, import and processing, under Regulation (EC) No 1829/2003 (application EFSA-GMO-NL-2015-124). *EFSA Journal*, *16*(6), e05310. https://doi.org/10.2903/j.efsa.2018.5310

Osborne, R., Rehneke, L., Lehmann, S., Roberts, J., Altmann, M., Altmann, S., Zhang, Y., Köpff, E., Dominguez-Ferreras, A., Okechukwu, E., Sergaki, C., Rich-Griffin, C., Ntoukakis, V., Eichmann, R., Shan, W., Falter-Braun, P., & Schäfer, P. (2023). Symbiont-host interactome mapping reveals effector-targeted modulation of

hormone networks and activation of growth promotion. *Nature Communications*, *14*(1), 4065. https://doi.org/10.1038/s41467-023-39885-5

Palatinus, L. R., Schlemmer, T., & Koch, A. (2025). Technical advances in extracellular vesicle isolation from fungi and oomycetes: Insights from plant-pathogenic species. *Fungal Biology Reviews*, *53*, 100444. https://doi.org/10.1016/j.fbr.2025.100444

Palli, S. R. (2014). RNA interference in Colorado potato beetle: Steps toward development of dsRNA as a commercial insecticide. *Current Opinion in Insect Science*, *6*, 1–8. https://doi.org/10.1016/j.cois.2014.09.011

Pandey, C., Prabha, D., Negi, Y. K., Maheshwari, D. K., Dheeman, S., & Gupta, M. (2023). Macrolactin A mediated biocontrol of Fusarium oxysporum and Rhizoctonia solani infestation on Amaranthus hypochondriacus by Bacillus subtilis BS-58. *Frontiers in Microbiology*, *14*. https://doi.org/10.3389/fmicb.2023.1105849

Pellegrino, E., Nuti, M., & Ercoli, L. (2022). Multiple Arbuscular Mycorrhizal Fungal Consortia Enhance Yield and Fatty Acids of Medicago sativa: A Two-Year Field Study on Agronomic Traits and Tracing of Fungal Persistence. *Frontiers in Plant Science*, *13*. https://doi.org/10.3389/fpls.2022.814401

Pérez-Alonso, M., Guerrero-Galán, C., González Ortega-Villaizán, A., Ortiz-García, P., Scholz, S. S., Ramos, P., Sakakibara, H., Kiba, T., Ludwig-Müller, J., Krapp, A., Oelmüller, R., Vicente-Carbajosa, J., & Pollmann, S. (2022). The calcium sensor CBL7 is required for Serendipita indica-induced growth stimulation in Arabidopsis thaliana, controlling defense against the endophyte and K+ homoeostasis in the symbiosis. *Plant, Cell & Environment*, *45*(11), 3367–3382. https://doi.org/10.1111/pce.14420

Pieterse, C. M. J., Does, D. V. der, Zamioudis, C., Leon-Reyes, A., & Wees, S. C. M. V. (2012). Hormonal Modulation of Plant Immunity. *Annual Review of Cell and Developmental Biology*, *28*(Volume 28, 2012), 489–521. https://doi.org/10.1146/annurev-cellbio-092910-154055

Pieterse, C. M. J., Zamioudis, C., Berendsen, R. L., Weller, D. M., Van Wees, S. C. M., & Bakker, P. A. H. M. (2014). Induced systemic resistance by beneficial microbes. *Annual Review of Phytopathology*, *52*, 347–375. https://doi.org/10.1146/annurev-phyto-082712-102340

Plett, J. M., Kohler, A., & Martin, F. (2024). Masters of Manipulation: How Our Molecular Understanding of Model Symbiotic Fungi and Their Hosts Is Changing the Face of "Mutualism". In Y.-P. Hsueh & M. Blackwell (Eds), *Fungal Associations* (pp. 249–272). Springer International Publishing. https://doi.org/10.1007/978-3-031-41648-4_10

Plett, J. M., & Martin, F. M. (2018). Know your enemy, embrace your friend: Using omics to understand how plants respond differently to pathogenic and mutualistic microorganisms. *The Plant Journal*, *93*(4), 729–746. https://doi.org/10.1111/tpj.13802

Polack, F. P., Thomas, S. J., Kitchin, N., Absalon, J., Gurtman, A., Lockhart, S., Perez, J. L., Marc, G. P., Moreira, E. D., Zerbini, C., Bailey, R., Swanson, K. A., Roychoudhury, S., Koury, K., Li, P., Kalina, W. V., Cooper, D., Frenck, R. W., Hammitt, L. L., … Gruber, W. C. (2020). Safety and Efficacy of the BNT162b2 mRNA Covid-19 Vaccine. *New England Journal of Medicine*, *383*(27), 2603–2615. https://doi.org/10.1056/NEJMoa2034577

Pontecorvo, G., Roper, J. A., Chemmons, L. M., Macdonald, K. D., & Bufton, A. W. J. (1953). The Genetics of *Aspergillus nidulans*. In M. Demerec (Ed.), *Advances in Genetics* (Vol. 5, pp. 141–238). Academic Press. https://doi.org/10.1016/S0065-2660(08)60408-3

Pradhan, M., Baldwin, I. T., & Pandey, S. P. (2023). Argonaute7 (AGO7) optimizes arbuscular mycorrhizal fungal associations and enhances competitive growth in Nicotiana attenuata. *New Phytologist*, *240*(1), 382–398. https://doi.org/10.1111/nph.19155

Qiang, X., Weiss, M., Kogel, K.-H., & Schäfer, P. (2012). Piriformospora indica—A mutualistic basidiomycete with an exceptionally large plant host range. *Molecular Plant Pathology*, *13*(5), 508–518. https://doi.org/10.1111/j.1364-3703.2011.00764.x

Qiang, X., Zechmann, B., Reitz, M. U., Kogel, K.-H., & Schäfer, P. (2012). The Mutualistic Fungus Piriformospora indica Colonizes Arabidopsis Roots by Inducing an Endoplasmic Reticulum Stress–Triggered Caspase-Dependent Cell Death. *The Plant Cell*, *24*(2), 794–809. https://doi.org/10.1105/tpc.111.093260

Qiao, S. A., Gao, Z., & Roth, R. (2023). A perspective on cross-kingdom RNA interference in mutualistic symbioses. *New Phytologist*, *240*(1), 68–79. https://doi.org/10.1111/nph.19122

Rajak, J., Bawaskar, M., Rathod, D., Agarkar, G., Nagaonkar, D., Gade, A., & Rai, M. (2017). Interaction of copper nanoparticles and an endophytic growth promoter Piriformospora indica with Cajanus cajan. *Journal of the Science of Food and Agriculture*, *97*(13), 4562–4570. https://doi.org/10.1002/jsfa.8324

Rebolledo-Prudencio, O. G., Estrada-Rivera, M., Dautt-Castro, M., Arteaga-Vazquez, M. A., Arenas-Huertero, C., Rosendo-Vargas, M. M., Jin, H., & Casas-Flores, S. (2022). The small RNA-mediated gene silencing machinery is required in Arabidopsis for stimulation of growth, systemic disease resistance, and suppression of the nitrile-specifier gene NSP4 by Trichoderma atroviride. *The Plant Journal*, *109*(4), 873–890. https://doi.org/10.1111/tpj.15599

Regente, M., Pinedo, M., San Clemente, H., Balliau, T., Jamet, E., & de la Canal, L. (2017). Plant extracellular vesicles are incorporated by a fungal pathogen and inhibit its growth. *Journal of Experimental Botany*, *68*(20), 5485–5495. https://doi.org/10.1093/jxb/erx355

Reinhart, B. J., Weinstein, E. G., Rhoades, M. W., Bartel, B., & Bartel, D. P. (2002). MicroRNAs in plants. *Genes & Development*, *16*(13), 1616–1626. https://doi.org/10.1101/gad.1004402

Ren, B., Wang, X., Duan, J., & Ma, J. (2019). Rhizobial tRNA-derived small RNAs are signal molecules regulating plant nodulation. *Science (New York, N.Y.)*, *365*(6456), 919–922. https://doi.org/10.1126/science.aav8907

Research, C. for D. E. and. (2024). New Class of Drugs Fulfills Promise of RNA-based Medicine. *FDA*. https://www.fda.gov/drugs/spotlight-cder-science/new-class-drugs-fulfills-promise-rna-based-medicine?utm_source=chatgpt.com

Rich-Griffin, C., Eichmann, R., Reitz, M. U., Hermann, S., Woolley-Allen, K., Brown, P. E., Wiwatdirekkul, K., Esteban, E., Pasha, A., Kogel, K.-H., Provart, N. J., Ott, S., & Schäfer, P. (2020). Regulation of Cell Type-Specific Immunity Networks in Arabidopsis Roots. *The Plant Cell*, *32*(9), 2742–2762. https://doi.org/10.1105/tpc.20.00154

Riolo, G., Cantara, S., Marzocchi, C., Ricci, C., Riolo, G., Cantara, S., Marzocchi, C., & Ricci, C. (2020). miRNA Targets: From Prediction Tools to Experimental Validation. *Methods and Protocols*, *4*(1). https://www.mdpi.com/2409-9279/4/1/1

Rodrigues, M. L., Nimrichter, L., Oliveira, D. L., Frases, S., Miranda, K., Zaragoza, O., Alvarez, M., Nakouzi, A., Feldmesser, M., & Casadevall, A. (2007). Vesicular Polysaccharide Export in Cryptococcus neoformans Is a Eukaryotic Solution to the Problem of Fungal Trans-Cell Wall Transport. *Eukaryotic Cell*, *6*(1), 48–59. https://doi.org/10.1128/EC.00318-06

Rodrigues, T. B., Mishra, S. K., Sridharan, K., Barnes, E. R., Alyokhin, A., Tuttle, R., Kokulapalan, W., Garby, D., Skizim, N. J., Tang, Y., Manley, B., Aulisa, L., Flannagan, R. D., Cobb, C., & Narva, K. E. (n.d.). *Frontiers | First Sprayable Double-Stranded RNA-Based Biopesticide Product Targets Proteasome Subunit Beta Type-5 in Colorado Potato Beetle (Leptinotarsa decemlineata)*. https://doi.org/10.3389/fpls.2021.728652

Rodríguez-Leal, D., Castillo-Cobián, A., Rodríguez-Arévalo, I., & Vielle-Calzada, J.-P. (2016). A Primary Sequence Analysis of the ARGONAUTE Protein Family in Plants. *Frontiers in Plant Science*, *7*. https://doi.org/10.3389/fpls.2016.01347

Romano, N., & Macino, G. (1992). Quelling: Transient inactivation of gene expression in Neurospora crassa by transformation with homologous sequences. *Molecular Microbiology*, *6*(22), 3343–3353. https://doi.org/10.1111/j.1365-2958.1992.tb02202.x

Roussin-Léveillée, C., Silva-Martins, G., & Moffett, P. (2020). ARGONAUTE5 Represses Age-Dependent Induction of Flowering through Physical and Functional Interaction with miR156 in Arabidopsis. *Plant and Cell Physiology*, *61*(5), 957–966. https://doi.org/10.1093/pcp/pcaa022

Roylawar, P., Khandagale, K., Randive, P., Shinde, B., Murumkar, C., Ade, A., Singh, M., Gawande, S., & Morelli, M. (2021a). Piriformospora indica Primes Onion Response against Stemphylium Leaf Blight Disease. *Pathogens*, *10*(9), Article 9. https://doi.org/10.3390/pathogens10091085

Ruf, A., Thieron, H., Nasfi, S., Lederer, B., Fricke, S., Adeshara, T., Postma, J., Blumenkamp, P., Kwon, S., Brinkrolf, K., Feldbrügge, M., Goesmann, A., Kehr, J.,

Steinbrenner, J., Šečić, E., Göhre, V., Weiberg, A., Kogel, K.-H., Panstruga, R., … Consortium, the exRNA. (2024). Broad-scale phenotyping in Arabidopsis reveals varied involvement of RNA interference across diverse plant-microbe interactions. *Plant Direct*, *8*(11), e70017. https://doi.org/10.1002/pld3.70017

Rupaimoole, R., & Slack, F. J. (2017). MicroRNA therapeutics: Towards a new era for the management of cancer and other diseases. *Nature Reviews Drug Discovery*, *16*(3), 203–222. https://doi.org/10.1038/nrd.2016.246

Rutter, B. D., & Innes, R. W. (2018). Extracellular vesicles as key mediators of plant–microbe interactions. *Current Opinion in Plant Biology*, *44*, 16–22. https://doi.org/10.1016/j.pbi.2018.01.008

Saleem, S., Sekara, A., & Pokluda, R. (2022). Serendipita indica—A Review from Agricultural Point of View. *Plants*, *11*(24), Article 24. https://doi.org/10.3390/plants11243417

Sánchez-Correa, M. del S., Isidra-Arellano, M. C., Pozas-Rodríguez, E. A., Reyero-Saavedra, M. del R., Morales-Salazar, A., del Castillo, S. M. L.-C., Sanchez-Flores, A., Jiménez-Jacinto, V., Reyes, J. L., Formey, D., & Valdés-López, O. (2022). Argonaute5 and its associated small RNAs modulate the transcriptional response during the rhizobia-Phaseolus vulgaris symbiosis. *Frontiers in Plant Science*, *13*. https://doi.org/10.3389/fpls.2022.1034419

Schäfer, P., Khatabi, B., & Kogel, K.-H. (2007). Root cell death and systemic effects of Piriformospora indica: A study on mutualism. *FEMS Microbiology Letters*, *275*(1), 1–7. https://doi.org/10.1111/j.1574-6968.2007.00848.x

Schauer, S. E., Jacobsen, S. E., Meinke, D. W., & Ray, A. (2002). *DICER-LIKE1*: Blind men and elephants in *Arabidopsis* development. *Trends in Plant Science*, *7*(11), 487–491. https://doi.org/10.1016/S1360-1385(02)02355-5

Scholz, S. S., Barth, E., Clément, G., Marmagne, A., Ludwig-Müller, J., Sakakibara, H., Kiba, T., Vicente-Carbajosa, J., Pollmann, S., Krapp, A., & Oelmüller, R. (2023). The Root-Colonizing Endophyte Piriformospora indica Supports Nitrogen-Starved Arabidopsis thaliana Seedlings with Nitrogen Metabolites. *International Journal of Molecular Sciences*, *24*(20), 15372. https://doi.org/10.3390/ijms242015372

Schon, M. A., Kellner, M. J., Plotnikova, A., Hofmann, F., & Nodine, M. D. (2018). NanoPARE: Parallel analysis of RNA 5' ends from low-input RNA. *Genome Research*, *28*(12), 1931–1942. https://doi.org/10.1101/gr.239202.118

Schwab, R., Ossowski, S., Riester, M., Warthmann, N., & Weigel, D. (2006). Highly specific gene silencing by artificial microRNAs in Arabidopsis. *The Plant Cell*, *18*(5), 1121–1133. https://doi.org/10.1105/tpc.105.039834

Šečić, E., Zanini, S., Wibberg, D., Jelonek, L., Busche, T., Kalinowski, J., Nasfi, S., Thielmann, J., Imani, J., Steinbrenner, J., & Kogel, K.-H. (2021). A novel plant-fungal association reveals fundamental sRNA and gene expression reprogramming at the onset of symbiosis. *BMC Biology*, *19*, 171. https://doi.org/10.1186/s12915-021-01104-2

Sepehri, M., Ghaffari, M. r., Khayam Nekoui, M., Sarhadi, E., Moghadam, A., Khatabi, B., & Hosseini Salekdeh, G. (2021). Root endophytic fungus Serendipita indica modulates barley leaf blade proteome by increasing the abundance of photosynthetic proteins in response to salinity. *Journal of Applied Microbiology*, *131*(4), 1870–1889. https://doi.org/10.1111/jam.15063

Serfling, A., Wirsel, S. G. R., Lind, V., & Deising, H. B. (2007). Performance of the Biocontrol Fungus Piriformospora indica on Wheat Under Greenhouse and Field Conditions. *Phytopathology®*, *97*(4), 523–531. https://doi.org/10.1094/PHYTO-97-4-0523

Sharma, N., & Varma, A. (2021). Role of Endophytic Fungus Piriformospora indica in Nutrient Acquisition and Plant Health. In N. Shrivastava, S. Mahajan, & A. Varma (Eds), *Symbiotic Soil Microorganisms: Biology and Applications* (pp. 161–169). Springer International Publishing. https://doi.org/10.1007/978-3-030-51916-2_10

Sharma, P., Patel, A. N., Saini, M. K., & Deep, S. (2012). Field Demonstration of Trichoderma harzianum as a Plant Growth Promoter in Wheat (Triticum aestivum L). *Journal of Agricultural Science*, *4*(8), Article 8. https://doi.org/10.5539/jas.v4n8p65

Silvestri, A., Fiorilli, V., Miozzi, L., Accotto, G. P., Turina, M., & Lanfranco, L. (2019). In silico analysis of fungal small RNA accumulation reveals putative plant mRNA targets in the symbiosis between an arbuscular mycorrhizal fungus and its host plant. *BMC Genomics*, *20*, 169. https://doi.org/10.1186/s12864-019-5561-0

Silvestri, A., Ledford, W. C., Fiorilli, V., Votta, C., Scerna, A., Tucconi, J., Mocchetti, A., Grasso, G., Balestrini, R., Jin, H., Rubio-Somoza, I., & Lanfranco, L. (2025). A fungal sRNA silences a host plant transcription factor to promote arbuscular mycorrhizal symbiosis. *New Phytologist*, *246*(3), 924–935. https://doi.org/10.1111/nph.20273

Song, L., Fang, Y., Chen, L., Wang, J., & Chen, X. (2021). Role of non-coding RNAs in plant immunity. *Plant Communications*, *2*(3), 100180. https://doi.org/10.1016/j.xplc.2021.100180

Stein, E., Molitor, A., Kogel, K.-H., & Waller, F. (2008). Systemic Resistance in Arabidopsis Conferred by the Mycorrhizal Fungus Piriformospora indica Requires Jasmonic Acid Signaling and the Cytoplasmic Function of NPR1. *Plant and Cell Physiology*, *49*(11), 1747–1751. https://doi.org/10.1093/pcp/pcn147

Subramanian, S., Fu, Y., Sunkar, R., Barbazuk, W. B., Zhu, J.-K., & Yu, O. (2008). Novel and nodulation-regulated microRNAs in soybean roots. *BMC Genomics*, *9*, 160. https://doi.org/10.1186/1471-2164-9-160

Takeda, A., Iwasaki, S., Watanabe, T., Utsumi, M., & Watanabe, Y. (2008). The Mechanism Selecting the Guide Strand from Small RNA Duplexes is Different Among Argonaute Proteins. *Plant and Cell Physiology*, *49*(4), 493–500. https://doi.org/10.1093/pcp/pcn043

Takeo, K., Uesaka, I., Uehira, K., & Nishiura, M. (1973). Fine Structure of Cryptococcus neoformans Grown In Vitro as Observed by Freeze-Etching. *Journal of Bacteriology*, *113*(3), 1442–1448. https://doi.org/10.1128/jb.113.3.1442-1448.1973

Taochy, C., Gursanscky, N. R., Cao, J., Fletcher, S. J., Dressel, U., Mitter, N., Tucker, M. R., Koltunow, A. M. G., Bowman, J. L., Vaucheret, H., & Carroll, B. J. (2017). A Genetic Screen for Impaired Systemic RNAi Highlights the Crucial Role of DICER-LIKE 2. *Plant Physiology*, *175*(3), 1424–1437. https://doi.org/10.1104/pp.17.01181

Thielmann, J., Soleimani, B., Matros, A., Schikora, A., Schäfer, P., Kogel, K.-H., & Wehner, G. (2026). Genomic loci for priming-induced powdery mildew resistance and plant biomass in wheat. *Current Plant Biology*, *45*, 100568. https://doi.org/10.1016/j.cpb.2025.100568

Thieron, H., Krassini, L., Kwon, S., Fricke, S., Nasfi, S., Oberkofler, L., Ruf, A., Kehr, J., Kogel, K., Weiberg, A., Feldbrügge, M., Robatzek, S., & Panstruga, R. (2024). Practical advice for extracellular vesicle isolation in plant–microbe interactions: Concerns, considerations, and conclusions. *Journal of Extracellular Vesicles*, *13*(12), e70022. https://doi.org/10.1002/jev2.70022

Tucker, M. R., Okada, T., Hu, Y., Scholefield, A., Taylor, J. M., & Koltunow, A. M. G. (2012). Somatic small RNA pathways promote the mitotic events of megagametogenesis during female reproductive development in Arabidopsis. *Development*, *139*(8), 1399–1404. https://doi.org/10.1242/dev.075390

Vadassery, J., Ritter, C., Venus, Y., Camehl, I., Varma, A., Shahollari, B., Novák, O., Strnad, M., Ludwig-Müller, J., & Oelmüller, R. (2008). The Role of Auxins and Cytokinins in the Mutualistic Interaction Between Arabidopsis and Piriformospora indica. *Molecular Plant-Microbe Interactions®*, *21*(10), 1371–1383. https://doi.org/10.1094/MPMI-21-10-1371

Varkonyi-Gasic, E., & Hellens, R. P. (2011). Quantitative stem-loop RT-PCR for detection of microRNAs. *Methods in Molecular Biology (Clifton, N.J.)*, *744*, 145–157. https://doi.org/10.1007/978-1-61779-123-9_10

Varma, A., Bakshi, M., Lou, B., Hartmann, A., & Oelmueller, R. (2012). Piriformospora indica: A Novel Plant Growth-Promoting Mycorrhizal Fungus. *Agricultural Research*, *1*(2), 117–131. https://doi.org/10.1007/s40003-012-0019-5

Varma, A., Uma, & Khanuja, M. (2017). *Role of Nanoparticles on Plant Growth with Special Emphasis on Piriformospora indica: A Review*. https://doi.org/10.1007/978-3-319-46835-8_14

Vaucheret, H. (2008). Plant ARGONAUTES. *Trends in Plant Science*, *13*(7), 350–358. https://doi.org/10.1016/j.tplants.2008.04.007

Vaucheret, H., Vazquez, F., Crété, P., & Bartel, D. P. (2004). The action of ARGONAUTE1 in the miRNA pathway and its regulation by the miRNA pathway are crucial for plant development. *Genes & Development*, *18*(10), 1187–1197. https://doi.org/10.1101/gad.1201404

Vazquez, F., Vaucheret, H., Rajagopalan, R., Lepers, C., Gasciolli, V., Mallory, A. C., Hilbert, J.-L., Bartel, D. P., & Crété, P. (2004). Endogenous trans-acting siRNAs regulate the accumulation of Arabidopsis mRNAs. *Molecular Cell*, *16*(1), 69–79. https://doi.org/10.1016/j.molcel.2004.09.028

Verma, S., Varma, A., Rexer, K.-H., Hassel, A., Kost, G., Sarbhoy, A., Bisen, P., Bütehorn, B., & Franken, P. (1998). Piriformospora indica, gen. Et sp. Nov., a new root-colonizing fungus. *Mycologia*, *90*(5), 896–903. https://doi.org/10.1080/00275514.1998.12026983

Voß, S., Betz, R., Heidt, S., Corradi, N., & Requena, N. (2018). RiCRN1, a Crinkler Effector From the Arbuscular Mycorrhizal Fungus Rhizophagus irregularis, Functions in Arbuscule Development. *Frontiers in Microbiology*, *9*. https://doi.org/10.3389/fmicb.2018.02068

Waller, F., Achatz, B., Baltruschat, H., Fodor, J., Becker, K., Fischer, M., Heier, T., Hückelhoven, R., Neumann, C., von Wettstein, D., Franken, P., & Kogel, K.-H. (2005). The endophytic fungus Piriformospora indica reprograms barley to salt-stress tolerance, disease resistance, and higher yield. *Proceedings of the National Academy of Sciences of the United States of America*, *102*(38), 13386–13391. https://doi.org/10.1073/pnas.0504423102

Wang, M., Weiberg, A., Lin, F.-M., Thomma, B. P. H. J., Huang, H.-D., & Jin, H. (2016). Bidirectional cross-kingdom RNAi and fungal uptake of external RNAs confer plant protection. *Nature Plants*, *2*(10), Article 10. https://doi.org/10.1038/nplants.2016.151

Wang, M., Weiberg ,Arne, Dellota Jr.,Exequiel, Yamane ,Daniel, & and Jin, H. (2017). Botrytis small RNA Bc-siR37 suppresses plant defense genes by cross-kingdom RNAi. *RNA Biology*, *14*(4), 421–428. https://doi.org/10.1080/15476286.2017.1291112

Wang, S., He, B., Wu, H., Cai, Q., Ramírez-Sánchez, O., Abreu-Goodger, C., Birch, P. R. J., & Jin, H. (2024). Plant mRNAs move into a fungal pathogen via extracellular vesicles to reduce infection. *Cell Host & Microbe*, *32*(1), 93-105.e6. https://doi.org/10.1016/j.chom.2023.11.020

Weiberg, A., Wang, M., Lin, F.-M., Zhao, H., Zhang, Z., Kaloshian, I., Huang, H.-D., & Jin, H. (2013). Fungal small RNAs suppress plant immunity by hijacking host RNA interference pathways. *Science (New York, N.Y.)*, *342*(6154), 118–123. https://doi.org/10.1126/science.1239705

Werner, B. T., Koch, A., Šečić, E., Engelhardt, J., Jelonek, L., Steinbrenner, J., & Kogel, K.-H. (2021). Fusarium graminearum DICER-like-dependent sRNAs are required for the suppression of host immune genes and full virulence. *PLOS ONE*, *16*(8), e0252365. https://doi.org/10.1371/journal.pone.0252365

Werner, B. T., Nasfi, S., Schmitz, M. L., Makhoul, M., Steinbrenner, J., & Schäfer, P. (2025). High Precision Quantification of small RNA Slicing Activity—Native Index Ligation-based Targeted Degradome Sequencing (NIL-TDS). *bioRxiv*, 2025.09.30.679503. https://doi.org/10.1101/2025.09.30.679503

Win, J., Chaparro-Garcia, A., Belhaj, K., Saunders, D. G. O., Yoshida, K., Dong, S., Schornack, S., Zipfel, C., Robatzek, S., Hogenhout, S. A., & Kamoun, S. (2012). Effector Biology of Plant-Associated Organisms: Concepts and Perspectives. *Cold*

Spring Harbor Symposia on Quantitative Biology, *77*, 235–247. https://doi.org/10.1101/sqb.2012.77.015933

Wolf, P. (1967). The Nature and Significance of Platelet Products in Human Plasma. *British Journal of Haematology*, *13*(3), 269–288. https://doi.org/10.1111/j.1365-2141.1967.tb08741.x

World Population Prospects. (2024). Retrieved 20 March 2025, from https://population.un.org/wpp/publications

Wu, F.-H., Shen, S.-C., Lee, L.-Y., Lee, S.-H., Chan, M.-T., & Lin, C.-S. (2009). Tape-Arabidopsis Sandwich—A simpler Arabidopsis protoplast isolation method. *Plant Methods*, *5*(1), 16. https://doi.org/10.1186/1746-4811-5-16

Wu, P., Wu, Y., Liu, C.-C., Liu, L.-W., Ma, F.-F., Wu, X.-Y., Wu, M., Hang, Y.-Y., Chen, J.-Q., Shao, Z.-Q., & Wang, B. (2016). Identification of Arbuscular Mycorrhiza (AM)-Responsive microRNAs in Tomato. *Frontiers in Plant Science*, *7*. https://doi.org/10.3389/fpls.2016.00429

Wu, S., Shan, L., & He, P. (2014). Microbial Signature-Triggered Plant Defense Responses and Early Signaling Mechanisms. *Plant Science : An International Journal of Experimental Plant Biology*, *0*, 118–126. https://doi.org/10.1016/j.plantsci.2014.03.001

Xie, Z., Johansen, L. K., Gustafson, A. M., Kasschau, K. D., Lellis, A. D., Zilberman, D., Jacobsen, S. E., & Carrington, J. C. (2004). Genetic and Functional Diversification of Small RNA Pathways in Plants. *PLoS Biology*, *2*(5). https://doi.org/10.1371/journal.pbio.0020104

Xu, L., Hu, Y., Cao, Y., Li, J., Ma, L., Li, Y., & Qi, Y. (2017). An expression atlas of miRNAs in Arabidopsis thaliana. *Science China Life Sciences*, *61*(2), 178–189. https://doi.org/10.1007/s11427-017-9199-1

Ye, W., Shen, C.-H., Lin, Y., Chen, P.-J., Xu, X., Oelmüller, R., Yeh, K.-W., & Lai, Z. (2014). Growth Promotion-Related miRNAs in Oncidium Orchid Roots Colonized by the Endophytic Fungus Piriformospora indica. *PLOS ONE*, *9*(1), e84920. https://doi.org/10.1371/journal.pone.0084920

Zamioudis, C., & Pieterse, C. M. J. (2012). Modulation of Host Immunity by Beneficial Microbes. *Molecular Plant-Microbe Interactions®*, *25*(2), 139–150. https://doi.org/10.1094/MPMI-06-11-0179

Zand Karimi, H., Baldrich, P., Rutter, B. D., Borniego, L., Zajt, K. K., Meyers, B. C., & Innes, R. W. (2022). Arabidopsis apoplastic fluid contains sRNA- and circular RNA–protein complexes that are located outside extracellular vesicles. *The Plant Cell*, *34*(5), 1863–1881. https://doi.org/10.1093/plcell/koac043

Zand Karimi, H., & Innes, R. W. (2022). Molecular mechanisms underlying host-induced gene silencing. *The Plant Cell*, *34*(9), 3183–3199. https://doi.org/10.1093/plcell/koac165

Zeng, J., Gupta, V. K., Jiang, Y., Yang, B., Gong, L., & Zhu, H. (2019). Cross-Kingdom Small RNAs among Animals, Plants and Microbes. *Cells*, *8*(4), Article 4. https://doi.org/10.3390/cells8040371

Zhang, H., Xia, R., Meyers, B. C., & Walbot, V. (2015). Evolution, functions, and mysteries of plant ARGONAUTE proteins. *Current Opinion in Plant Biology, Cell Signalling and Gene Regulation*, *27*, 84–90. https://doi.org/10.1016/j.pbi.2015.06.011

Zhang, J., Pan, L., Xu, W., Yang, H., He, F., Ma, J., Bai, L., Zhang, Q., Zhou, Q., & Gao, H. (2024a). Extracellular vesicles in plant-microbe interactions: Recent advances and future directions. *Plant Science*, *341*, 111999. https://doi.org/10.1016/j.plantsci.2024.111999

Zhang, T., Zhao, Y.-L., Zhao, J.-H., Wang, S., Jin, Y., Chen, Z.-Q., Fang, Y.-Y., Hua, C.-L., Ding, S.-W., & Guo, H.-S. (2016). Cotton plants export microRNAs to inhibit virulence gene expression in a fungal pathogen. *Nature Plants*, *2*(10), 16153. https://doi.org/10.1038/nplants.2016.153

Zhang, X., Niu, D., Carbonell, A., Wang, A., Lee, A., Tun, V., Wang, Z., Carrington, J. C., Chang, C. A., & Jin, H. (2014). ARGONAUTE PIWI domain and microRNA duplex structure regulate small RNA sorting in Arabidopsis. *Nature Communications*, *5*(1), 5468. https://doi.org/10.1038/ncomms6468

Zhang, X., Zhao, H., Gao, S., Wang, W.-C., Katiyar-Agarwal, S., Huang, H.-D., Raikhel, N., & Jin, H. (2011). Arabidopsis Argonaute 2 Regulates Innate Immunity via miRNA393∗-Mediated Silencing of a Golgi-Localized SNARE Gene, MEMB12. *Molecular Cell*, *42*(3), 356–366. https://doi.org/10.1016/j.molcel.2011.04.010

Zhang, Y., Yang, Z., Yang, Y., Han, A., Rehneke, L., Ding, L., Wei, Y., Liu, Z., Meng, Y., Schäfer, P., & Shan, W. (2024). A symbiont fungal effector relocalizes a plastidic oxidoreductase to nuclei to induce resistance to pathogens and salt stress. *Current Biology*, *34*(13), 2957-2971.e8. https://doi.org/10.1016/j.cub.2024.05.064

Zhao, J.-H., Liu, Q.-Y., Xie, Z.-M., & Guo, H.-S. (2024). Exploring the challenges of RNAi-based strategies for crop protection. *Advanced Biotechnology*, *2*(3), 23. https://doi.org/10.1007/s44307-024-00031-x

Zhao, Z., Yang, S.-J., Yin, X.-X., Yan, X.-L., Hassan, B., Fan, J., Li, Y., & Wang, W.-M. (2023). ARGONAUTE 1: A node coordinating plant disease resistance with growth and development. *Phytopathology Research*, *5*(1), 38. https://doi.org/10.1186/s42483-023-00194-w

Zheng, Y., Moorlach, B., Jakobs-Schönwandt, D., Patel, A., Pastacaldi, C., Jacob, S., Sede, A. R., Heinlein, M., Poranen, M. M., Kogel, K.-H., & Ladera Carmona, M. (2025). Exogenous dsRNA triggers sequence-specific RNAi and fungal stress responses to control Magnaporthe oryzae in Brachypodium distachyon. *Communications Biology*, *8*(1), 1–14. https://doi.org/10.1038/s42003-025-07554-6

Zhou, H., Duan, H., Liu, Y., Sun, X., Zhao, J., & Lin, H. (2019). Patellin protein family functions in plant development and stress response. *Journal of Plant Physiology*, *234–235*, 94–97. https://doi.org/10.1016/j.jplph.2019.01.012

Zhu, H., Hu, F., Wang, R., Zhou, X., Sze, S.-H., Liou, L. W., Barefoot, A., Dickman, M., & Zhang, X. (2011). Arabidopsis Argonaute 10 specifically sequesters miR166/165 to regulate shoot apical meristem development. *Cell*, *145*(2), 242–256. https://doi.org/10.1016/j.cell.2011.03.024

Zipfel, C. (2009). Early molecular events in PAMP-triggered immunity. *Current Opinion in Plant Biology, Biotic Interactions*, *12*(4), 414–420. https://doi.org/10.1016/j.pbi.2009.06.003

Zuccaro, A., Lahrmann, U., Güldener, U., Langen, G., Pfiffi, S., Biedenkopf, D., Wong, P., Samans, B., Grimm, C., Basiewicz, M., Murat, C., Martin, F., & Kogel, K.-H. (2011). Endophytic Life Strategies Decoded by Genome and Transcriptome Analyses of the Mutualistic Root Symbiont Piriformospora indica. *PLOS Pathogens*, *7*(10), e1002290. https://doi.org/10.1371/journal.ppat.1002290

Acknowledgements

First, I would like to express my sincere gratitude to Professor Karl-Heinz Kogel for his continued support throughout my studies and for supervising my doctoral thesis. His guidance and trust were essential to my development as a researcher.

I also extend my sincere thanks to Professor Patrick Schäfer, whose encouragement and support since becoming head of our Phytopathology Institute have been invaluable in ensuring the productive and motivating continuation of this project. His involvement and positive energy have significantly influenced my work. I am also grateful to my third supervisor Professor Volker Wissemann.

I would also like to thank Dr. Jens Steinbrenner for his planning and supervision of this project. The invaluable experience I gained under his guidance contributed significantly to my scientific and personal development, and I am particularly grateful for the trust he placed in me.

I express my warmest thanks to Christina Neuman for her extraordinary assistance, patience, and dedication. I am equally grateful to all the other technicians and members of the Phytopathology Institute for their continuous support, kindness, and willingness to help whenever it was needed. I also extend my sincere appreciation to Dr. Ruth Schäfer for her support and critical thinking, and to all my colleagues whose discussions and encouragement have shaped this journey and provided a motivating work environment.

Beyond the scientific support, I am deeply in debt to my family. I thank my parents for their unconditional love, their sacrifices, and their unwavering belief in me. They have been a source of strength in every phase of my life. I thank my sister and my brother for being such wonderful siblings and for having each other's back, which means more to me than I can put into words.

To my husband, thank you for being my anchor. Your patience, kindness, and endless support and care helped me through every challenge of this journey. You cheered me on when I succeeded, stood by me during tough times and reminded me of my strength when I doubted myself. The small life growing alongside the last phases of this thesis reminds us every day of what truly matters.

Finally, I would like to express my gratitude to the Dr. Ernst Leopold Klipstein Foundation for funding this project from the beginning of my master's thesis in 2020 and throughout the three and a half years of my doctoral research. Their support has made this work possible.

This achievement is a tribute to my grandpa,

whose support quietly opened the path

that brought me to Germany.

Declaration of generative AI and AI-assisted technologies

I declare the use of AI-assisted technologies, such as DeepL and Grammarly, during the writing of this thesis for proofreading and to improve readability and language. I fully reviewed and edited the final version of this thesis.